



**HAL**  
open science

# Structural characterization of bacterial defense complex

Marko Nedeljković

► **To cite this version:**

Marko Nedeljković. Structural characterization of bacterial defense complex. Structural Biology [q-bio.BM]. Université Grenoble Alpes, 2017. English. NNT : 2017GREAV067 . tel-03085778

**HAL Id: tel-03085778**

**<https://theses.hal.science/tel-03085778>**

Submitted on 22 Dec 2020

**HAL** is a multi-disciplinary open access archive for the deposit and dissemination of scientific research documents, whether they are published or not. The documents may come from teaching and research institutions in France or abroad, or from public or private research centers.

L'archive ouverte pluridisciplinaire **HAL**, est destinée au dépôt et à la diffusion de documents scientifiques de niveau recherche, publiés ou non, émanant des établissements d'enseignement et de recherche français ou étrangers, des laboratoires publics ou privés.

## THÈSE

Pour obtenir le grade de

### **DOCTEUR DE LA COMMUNAUTE UNIVERSITE GRENOBLE ALPES**

Spécialité : **Biologie Structurale et Nanobiologie**

Arrêté ministériel : 25 mai 2016

Présentée par

**Marko NEDELJKOVIĆ**

Thèse dirigée par **Andréa DESSEN**

préparée au sein du **Laboratoire Institut de Biologie Structurale**  
dans l'**École Doctorale Chimie et Sciences du Vivant**

## **Caractérisation structurale d'un complexe de défense bactérienne**

## **Structural characterization of a bacterial defense complex**

Thèse soutenue publiquement le **21 décembre 2017**,  
devant le jury composé de :

**Monsieur Herman VAN TILBEURGH**

Professeur, Université Paris Sud, Rapporteur

**Monsieur Laurent TERRADOT**

Directeur de Recherche, Institut de Biologie et Chimie des Protéines,  
Rapporteur

**Monsieur Patrice GOUET**

Professeur, Université Lyon 1, Président

**Madame Montserrat SOLER-LOPEZ**

Chargé de Recherche, European Synchrotron Radiation Facility,  
Examineur

**Madame Andréa DESSEN**

Directeur de Recherche, Institut de Biologie Structurale , Directeur de  
These





## Contents

ABBREVIATIONS .....	5
Summary.....	7
Résumé.....	9
Acknowledgements .....	11
INTRODUCTION.....	13
1.1. Host-pathogen interaction and virulence factors .....	15
1.2. Proteases as virulence factors .....	16
1.3. Protease inhibitors .....	18
1.4. The $\alpha$ 2M subfamily .....	19
1.5. Structure of human $\alpha$ -2-macroglobulin .....	23
1.6. Bacterial $\alpha$ 2Ms .....	24
1.7. The bacterial cell wall .....	27
1.8. Peptidoglycan precursor synthesis .....	28
1.9. Penicillin-Binding Proteins.....	31
1.10. Glycan chain polymerization .....	32
1.11. Cross-linking .....	33
1.12. Class A PBPs .....	35
1.13. Penicillin-binding protein 1c .....	37
AIMS OF THE PROJECT .....	38
MATERIALS AND METHODS .....	41
2.1. PBP1c sequence analysis .....	43
2.2. Cloning.....	43
2.3. Protein expression and purification .....	44
2.4. Electrophoresis.....	47
2.5. Western blotting.....	49
2.6. Mass spectrometry .....	49
2.7. Analytical ultracentrifugation (AUC) and SEC-MALS .....	50

<b>2.8.</b>	<b>Thermal shift assay</b> .....	53
<b>2.9.</b>	<b>The PBP1c activity test</b> .....	55
<b>2.10.</b>	<b>Small-Angle X-ray Scattering (SAXS)</b> .....	56
<b>2.11.</b>	<b>Electron microscopy</b> .....	57
<b>2.12.</b>	<b>Crystallization trials</b> .....	58
<b>RESULTS</b> .....		59
<b>3.1.</b>	<b>Expression and purification of ECAM</b> .....	61
<b>3.2.</b>	<b>Purification and characterization of PBP1c</b> .....	63
<b>3.2.1.</b>	<b>Amino acid sequence analysis</b> .....	63
<b>3.2.2.</b>	<b>Expression and solubilization</b> .....	66
<b>3.2.3.</b>	<b>Purification of PBP1c</b> .....	69
<b>3.2.4.</b>	<b>SEC-MALS analysis of PBP1c</b> .....	72
<b>3.2.5.</b>	<b>Cell-free expression and purification of PBP1c</b> .....	74
<b>3.2.6.</b>	<b>Mass spectrometry of PBP1c</b> .....	75
<b>3.2.7.</b>	<b>Thermal stability analysis</b> .....	76
<b>3.3.</b>	<b>Complex reconstitution and characterization</b> .....	79
<b>3.3.1.</b>	<b>Complex formation</b> .....	79
<b>3.3.2.</b>	<b>AUC analysis</b> .....	80
<b>3.3.3.</b>	<b>Peptidoglycan synthesis assay</b> .....	83
<b>3.3.4.</b>	<b>Crystallization trials of PBP1c in apo form and in the presence of moenomycin</b> .....	87
<b>3.3.5.</b>	<b>Negative staining electron microscopy</b> .....	89
<b>3.3.6.</b>	<b>SAXS</b> .....	92
<b>DISCUSSION AND PERSPECTIVES</b> .....		103
<b>References</b> .....		110
<b>INDEX</b> .....		122
<b>ANNEXES</b> .....		124

## ABBREVIATIONS

<b><math>\alpha</math>2M</b>	$\alpha$ -2-macroglobulin
<b>AMP</b>	Adenosine monophosphate
<b>ATP</b>	Adenosine triphosphate
<b>AUC</b>	Analytical ultracentrifugation
<b>C<sub>55</sub>-PP</b>	Undecaprenyl pyrophosphate
<b>CMC</b>	Critical micellar concentration
<b>CTP</b>	Cytosine triphosphate
<b>DDM</b>	n-dodecyl- $\beta$ -D-maltopyranoside
<b>DM</b>	n-decyl- $\beta$ -D-maltopyranoside
<b>DNA</b>	Deoxyribonucleic acid
<b>DTT</b>	Dithiothreitol
<b>ECAM</b>	<i>E. coli</i> $\alpha$ -2-macroglobulin
<b>EM</b>	Electron microscopy
<b>GlcNAc</b>	N-acetylglucosamine
<b>GT, GTase</b>	Glucosyltransferase
<b>GTP</b>	Guanosine triphosphate
<b>HPLC</b>	High-performance liquid chromatography
<b>LAPAO</b>	3-laurylamido-N,N'-dimethylpropyl amine oxide
<b>MALDI-TOF</b>	Matrix-assisted Laser Desorption/Ionization Time of Flight
<b>meso-A2pm</b>	Meso-diaminopimelic acid
<b>MG</b>	Macroglobulin-like
<b>MurNAc</b>	N-acetylmuramic acid
<b>NAG</b>	N-acetylglucosamine
<b>NAM</b>	N-acetylmuramic acid
<b>PBP</b>	Penicillin-binding protein
<b>PZP</b>	Pregnancy zone protein
<b>RBD</b>	Receptor-binding domain
<b>SAXS</b>	Small angle X-ray scattering
<b>SEC-MALS</b>	Size exclusion chromatography with multi-angle light scattering
<b>SDS-PAGE</b>	Sodium dodecyl sulfate polyacrylamide gel electrophoresis
<b>SST</b>	Sodium silicotungstate

<b>TED</b>	Thioester-binding domain
<b>TEM</b>	Transmission electron microscopy
<b>TEP</b>	Thioester-containing proteins
<b>TP, TPase</b>	Transpeptidase
<b>UB2H</b>	UvrB Domain 2 homolog
<b>UDP</b>	Uridine diphosphate
<b>UTP</b>	Uridine triphosphate

## Summary

The widespread resistance to antibiotics developed by bacterial pathogens calls for the characterization of original, yet unexplored potential targets in bacteria. Alpha2-macroglobulins ( $\alpha$ 2Ms) are broad-spectrum protease inhibitors that play key roles in eukaryotic immunity. They are multi-domain molecules that carry approximately 1,800 residues and harbor a central amino acid sequence, the ‘bait site’, which is recognized and cleaved by a large number of proteases. Upon cleavage, the resulting conformational change exposes a buried thioester bond between a cysteine and a glutamine, which is readily hydrolyzed, allowing the resulting glutamate to associate covalently to the target protease, trapping it within the  $\alpha$ 2M cage-like structure. Recently,  $\alpha$ 2M homologs from pathogenic and colonizing bacteria have also started to be characterized. These findings suggest that bacteria possess a rudimentary immune system that mimics initial key steps of the eukaryotic immune pathway and that could represent a yet unexplored target in pathogen biology.

The genes for two types of  $\alpha$ 2M are present in bacterial genomes: type 1, which contains the thioester bond, and type 2 that does not harbor it. Type 1 bacterial  $\alpha$ 2Ma persistently co-occur within the same operon with a gene that encodes a cell wall biosynthesis enzyme, Penicillin-Binding Protein 1c (PBP1c). This suggests that the association between the two proteins could be highly advantageous for the cell during infection/colonization, when the outer cell wall is targeted by host defenses. In this situation,  $\alpha$ 2M and PBP1c could exert the role of ‘guardians of the periplasm’, with PBP1c repairing damaged peptidoglycan, and  $\alpha$ 2M trapping invading proteases.

The aim of this work was to demonstrate the existence of such complex and characterize this interaction structurally and functionally. For this purpose,  $\alpha$ 2M and PBP1c from *E. coli* were studied. The proteins were expressed and purified separately.  $\alpha$ 2M (also called ECAM in *E. coli*) is a highly soluble, monomeric protein with a mass of 182 kDa, monodisperse and stable during the course of time. PBP1c is a membrane-bound, 87 kDa protein, predominantly present as a dimer. The complex, reconstituted *in vitro* by mixing and incubating the proteins for 2 hours, resulted in formation of a complex, demonstrated by appearance of a new peak in size exclusion chromatography. This result was further confirmed by SDS-PAGE, analytical centrifugation and small-angle x-ray scattering (SAXS) experiments. ECAM and PBP1c associated with 2:2 and 4:4 stoichiometries. The activity test confirmed that PBP1c performs polymerization of glycan chains and that its activity is enhanced in the presence of ECAM.

Crystallization trials yielded crystals of PBP1c in several conditions, while the study of ECAM by electron microscopy proved that this technique could be used for structural studies of the complex. Both approaches are under optimization, and combined, they could be employed for structural characterization of the ECAM-PBP1c complex

## Résumé

De nos jours, la résistance aux antibiotiques développée par des pathogènes bactériens est de plus en plus répandue, et en conséquent il devient primordial de caractériser de nouvelles cibles bactériennes potentielles. Les alpha2-macroglobulines ( $\alpha 2M$ s) sont des inhibiteurs de protéases à large spectre jouant un rôle clé dans l'immunité eucaryote. Ce sont des molécules multi domaines d'environ 1800 résidus qui arborent une séquence en acide nucléique très spécifique appelée « bait site » qui est reconnu et coupé par un très grand nombre de protéases. Durant ce clivage, la nouvelle conformation de la protéine entraîne l'exposition de la liaison thioester entre une cystéine et une glutamine, qui est alors hydrolysée, permettant ainsi au glutamate résultant de s'associer de façon covalente à la protéase cible, et d'être piégé dans la structure en forme de cage de  $\alpha 2M$ . Des homologues de  $\alpha 2M$  provenant de bactéries colonisant et pathogéniques ont récemment été caractérisés. Ces nouvelles recherches suggèrent que la bactérie dispose d'un système immunitaire capable de mimer les étapes clés initiales du système immunitaire eucaryote et que celui-ci pourrait constituer une cible encore inexploitée en biologie bactérienne.

On retrouve dans le génome bactérien deux types de gènes pour  $\alpha 2M$  : celui de type 1 qui contient la liaison thioester et celui de type 2 qui n'en dispose pas. De façon intéressante, le gene  $\alpha 2M$  de type 1 est situé dans le même opéron que le gène codant pour une enzyme de biosynthèse de la paroi cellulaire appelée Penicillin-Binding Protein 1c (PBP1c). Ceci suggère qu'une association étroite entre ces deux protéines pourrait être très avantageuse pour la cellule, en particulier durant l'infection et/ou la colonisation durant laquelle la membrane cellulaire externe est ciblée par des agents de défense de l'hôte. Dans cette situation,  $\alpha 2M$  et PBP1c pourraient exercer les rôles de « gardiens du périplasme » avec PBP1c réparant les dommages causés au niveau du peptidoglycane et  $\alpha 2M$  traquant les protéases invasives.

Le but de ce travail était donc de démontrer l'existence de ce complexe PBP1C/A2M et de caractériser cette interaction de façon structurale et fonctionnelle. Dans ce sens, les deux protéines provenant d'*E. coli* ont été étudiées, ainsi qu'exprimées et purifiées séparément. La protéine  $\alpha 2M$  (également appelé ECAM dans *E. coli*) est très soluble, exprimée de façon monomérique à une taille de 182 kDa, monodisperse et stable dans l'échelle de temps. PBP1c est une protéine se fixant à la membrane, d'une taille de 87 kDa et présente de façon prédominante en tant que dimère. La reconstitution du complexe *in vitro* par incubation et mélange des deux protéines pendant 2 heures a permis d'obtenir un complexe PBP1C/ECAM,

dont la présence a été prouvée par un nouveau pic caractéristique sur chromatographie par exclusion de taille. Ces résultats ont également été appuyés par SDS-PAGE, centrifugation analytique et par diffusion des rayons X aux petits angles (SAXS). ECAM et PBP1c s'associent à des ratios stœchiométriques de 2:2 et 4:4. Enfin, un test d'activité a permis de confirmer tout d'abord le rôle de PBP1c dans la polymérisation des chaînes glycanes mais aussi que cette activité est amplifiée en présence d'ECAM.

Les essais cristallographiques ont permis d'obtenir des cristaux de PBP1c dans différentes conditions. De plus l'étude d'ECAM par microscopie électronique a prouvé que la technique était applicable pour des études structurales du complexe. De ce fait, après optimisation, ces deux approches pourraient être la solution envisagée pour la caractérisation structurale du complexe ECAM/PBP1c.

## Acknowledgements

When I arrived in Grenoble three years ago, I didn't have a clear idea what I was getting into and whether I would succeed. Thankfully, I was entering a community that is very welcoming, knows how to deal with rookies like me and has a guy for everything. All these people helped me to make this project work and get me where I am today. The end of a cycle inevitably calls for a short retrospection and acknowledging each one of them.

Firstly, I would like to express my gratitude to my supervisor Andrea Dessen for giving me the opportunity to experience what science actually is. With a background in computational biology and overly tanned from Barcelonan sun in the middle of my internship, many would doubt if I was a suitable choice for a project starting from the scratch. Yet she didn't, and that may be the first lesson I learned, that sometimes you have to risk with people and projects in order to push limits in science. I also thank her for all the effort she invested to teach me how to think like a scientist and for the endless positive energy she has, no matter how bad the things are.

I would like to say huge thanks to my first two tutors, Alexandre Martins for all the patience he had while training me in protein purification and not killing me during the Covalab order crisis, and Anne-Emmanuelle Foucher for the lessons in molecular biology and proper lab behavior. I would like to thank Charlotte Lombardi for all the advice and answers to so many unnecessary questions (“C'est la tête d'un Serbe qui vient poser une question dont il connaît déjà la réponse”) during my first year in the lab, and apologize for judging her eating habits during pregnancy. Further, I would like to thank Ioulia Nikolaidis for teaching me how to work with membrane proteins and giving me a shelter for three days when I locked myself out of my apartment; Vivian Job for advice on mutagenesis and all the microbiology work on my project she is currently developing which, I hope, we'll present very soon. Even though I didn't succeed in solving any crystal structures, I'm very grateful to Carlos Contreras for the advice on how to proceed and what to try next, and above all, for his bitter Chilean humor that I enjoy so much.

In my work I extensively used the services of different platforms and collaborated with many people. I would like to express my gratitude to Lionel Imbert for the initial tests of the cell-free expression he did, Aline Leroy and Christine Ebel from the AUC platform at the IBS for performing my AUC experiments, Caroline Mas from the Biophysical platform for the SEC-MALS analyses and Elisabetta Boeri from the Mass Spectrometry platform for teaching

me how to do MALDI/TOF experiments and helping me with the interpretation of results. I would like to thank Daphna Fenel for all the electron microscopy work she did and say sorry for emotionally manipulating her to put me on the schedule when there were no time slots available. I am very grateful to Gabriele Giachin for teaching me how to process SAXS data and Orso Subrini for his help in interpreting the results from Prometheus experiments. I would also like to thank Victor Hernandez Rocamora from Dr Waldemar Vollmer's lab at Newcastle University for the work he did testing the activity of PBP1c.

During my studies I had a had two thesis advisory committee meetings during which I discussed my work with Dr Carlo Petosa and Dr Ina Atree. They had greatly contributed to my work with their recommendations, for which I'm very grateful.

The work on this manuscript was long and exhausting, and occasionally needed a fresh insight of a third party. Special thanks to my copy editor Simon Harris and my rédactrice pour la langue française Laura Lemel, for the invaluable help in their respective native languages. I promise I'll return the favor if ever you choose to write your theses in Serbian.

Two additional thanks go to my labmate and flatmate Quentin Bertrand for all the quiches and other French food he made during the course of writing, because cooking was definitely last thing on my mind (and I hope I wasn't a bad flatmate), and Federica Laddomada, a labmate with whom I have been sharing the same fate for the last three months, for frequently being my therapist. We made it.

I would like to thank the Université Grenoble Alpes for providing funds for the duration of my fellowship.

I am also grateful to my family for being emotional support from the beginning and making it clear that no matter what happens, there's always a place to come back.

Pour finir, j'aimerais également mentionner des personnes qui n'ont pas été directement impliquées dans le travail de thèse, mais qui ont entièrement fait partie de ma vie quotidienne à Grenoble. Merci tout d'abord à Julien qui m'a hébergé pendant deux semaines lors de mon arrivée à Grenoble. J'ai été naïf de croire que je trouverai un appartement en trois jours. Et merci à Charles, Muge, Silvia, Tomáš, Charline, Joyce, Vilius, Sonja, Albert et tous les autres pour toutes les fêtes, les apéros, les week-ends et voyages qu'on a pu faire ensemble. Cela va être très difficile de partir, mais surtout de vous quitter.

# **I**

## **INTRODUCTION**



## **1.1. Host-pathogen interaction and virulence factors**

The number of existing prokaryotic species on Earth is estimated to be between 10 and 1,000 million, although it is hard to determine precisely (Curtis et al. 2002; Dykhuizen 2005). This is partly due to the lack of consensus among scientists in what defines species in microorganisms (Cohan 2002), but also because of their presence in virtually every type of environment and the fact that less than 1% of bacteria can be successfully cultivated in laboratory conditions (Pham & Kim 2012). They inhabit soil, fresh and marine waters, as well as specific habitats such as plant leaves and roots, and skin and gastrointestinal tract of mammals (Floyd et al. 2005).

The human microbiome project calculated that more than 10,000 microbial species live in a healthy human individual (NIH 2012). The majority of them are bacteria, although protozoa, archaea, bacteriophages, wormlike helminth parasites and yeast are widely present. In normal conditions they are only found on the skin and mucosal surfaces. Their penetration into the body is prevented by numerous mechanisms that comprise nonspecific and specific immune system of the host (Peterson 1996). However, there are pathogenic species that are able to evade innate immunity and disseminate inside the host, causing diseases (Wilson et al. 2002). Their capacity to cause damage in a host is called virulence (Casadevall & Pirofski 2003). There are around 1,400 human pathogens, which is far less than 1% of the total microbial species, making pathogenicity a rare exception (Diard 2017; Taylor et al. 2001).

Comparisons between commensal and pathogenic species revealed that the increased virulence of pathogens is due to the presence of specific molecules called virulence factors which aid evasion of the host immune system (Diard 2017). Virulence factors are encoded on their chromosomal DNA, plasmids, bacteriophage DNA and transposons (Peterson 1996). They have diverse functions in host-pathogen interaction, such as breaching physical barriers, shielding from host's immune defense and acquiring nutrients during the infection (Diard 2017).

There are several types of virulence factors, depending on the role they exhibit: adhesins, invasins, capsules, endo- and exotoxins and siderophores (Peterson 1996).

## 1.2. Proteases as virulence factors

One class of virulence factors that are found in most thoroughly-studied pathogens are proteases. Proteases are enzymes that digest proteins by hydrolyzing peptide bonds (López-Otín & Bond 2008). Proteases are globally divided in two major groups: exopeptidases, which hydrolyze peptide bonds proximal to the amino or carboxy termini of the substrate, and endopeptidases which cleave internal peptide bonds (Rani et al. 2012). Furthermore, depending on the structure of their active site, they are classified as serine, cysteine, threonine, aspartic, glutamic and metalloproteases (López-Otín & Bond 2008). The first three classes utilize serine, cysteine and threonine respectively for the nucleophilic attack of the peptide bond, while aspartic, glutamic and metalloproteases utilize an activated water molecule.

Pathogen proteases belong to any of the six classes of proteases and they can be secreted or surface-bound (Armstrong 2006). They are efficient virulence factors employed in many stages of infection. The first line of defense in vertebrates is skin and mucosal surfaces of gastrointestinal and respiratory tracts. Epithelial cells produce antimicrobial peptides (AMPs), a diverse group of pore-forming molecules that act against microorganisms by increasing cell membrane permeation, leading to the leakage of cellular content (Diamond et al. 2009; Zasloff 2002). Cationic peptide LL-37 from the cathelicidin family of AMPs has a prominent role in eliminating bacteria in the stage of colonization (Henzler-Wildman et al. 2004). Bacteria, meanwhile, secrete proteases that cleave LL-37, thus evading its lethal effect. Examples include metalloprotease aureolysin (Aur) from *Staphylococcus aureus*, LasB (elastase) of *Pseudomonas aeruginosa*, *Enterococcus faecalis* gelatinase and *Staphylococcus epidermidis* SepA (Schmidtchen et al. 2002; Sieprawska-Lupa et al. 2004).

Keratinocytes from the skin are tightly connected by desmosomes, membrane structures that provide strong cell-to-cell contact and adhesion (Kowalczyk & Green 2013). *S. aureus* is able to rupture the skin using two serine proteases, exfoliative toxins A (ETA) and B (ETB) that digest desmoglein 1, one of the components of desmosomes (Hanakawa et al. 2004).

Extracellular matrix proteins collagen, elastin, fibronectin and laminin are also substrates for various pathogen-produced proteases. LasB from *P. aeruginosa* cleaves human type III and IV collagens, and together with alkaline protease rapidly degrades laminin (Heck, K Morihara, et al. 1986; Heck, K. Morihara, et al. 1986). LasB and Ecp of *S. epidermidis* target fibronectin and elastin (Oleksy et al. 2004; Schmidtchen et al. 2003). Elastin is also proteolysed by SspB of *S. aureus* (Kantyka et al. 2011).

Once pathogens breach the primary protective layers of the host surface, they face the danger of being phagocytized by macrophages and neutrophils. The complement system and antibodies engage in process called opsonization by binding to the surface of the pathogen, marking it for digestion by phagocytes (Janeway et al. 2001). In order to avoid opsonization, pathogens employ different strategies, one of them being proteolytic cleavage of the proteins involved in this process. Complement component 3 (C3) is completely degraded by *S. pyogenes* SpeB while *S. aureus* aureolysin cleaves C3 protein far from the bacterial surface converting it to active C3b that is rapidly processed by host proteases (Laarman et al. 2011; Terao et al. 2008). On the other hand, the cysteine protease IdeS from *S. pyogenes*, as well as the serratial 56-kDa protease are involved in cleavage of immunoglobulin G (Molla et al. 1988; Su et al. 2011).

Coagulation is a process that activates upon rupture of blood vessels creating a clot that closes the opening, maintaining hemostasis and preventing pathogen infiltration (Levi et al. 2004). It is a cascade reaction that activates the host protease thrombin to convert fibrinogen to fibrin. Fibrin polymerizes into a network, creating a fibrin-based clot. Blood clotting can also be activated independently of the vessel injury, triggered by the presence of pathogens in the blood (Wang et al. 2010). In that manner, fibrin clots immobilize pathogens in an attempt to prevent their dissemination (Loof et al. 2011). Nevertheless, pathogen proteases can trigger the destruction of the fibrin clot by converting host protease plasminogen to its active form, plasmin, dissolving the clot. That is the case with Pla protease from *Yersinia pestis*, OmpT of *E. coli* and PgtE of *Salmonella enterica* (Kukkonen & Korhonen 2004; Sodeinde et al. 1992). On the other hand, CpaA of *Acetivobacter baumannii* interferes with clot formation by cleaving factor V (that is part of thrombin activation complex) and fibrinogen (Tilley et al. 2014).

Proteases are also engaged in fulfilling nutritional requirements of pathogens during infection. Blood parasites, such as *Plasmodium falciparum* and *Schistosoma mansoni* use hemoglobin as an amino acid and energy source. Aspartic and cysteine proteases plasmepsins and falcipain of *P. falciparum* and cathepsins L1 and L2 (SmCL1 and 2) and D (SmCD) of *S. mansoni* digest hemoglobin (Caffrey et al. 2004; Francis et al. 1997). Moreover, there are species like *P. gingivalis* that digest host proteins in order to release sequestered iron required for their growth (Carlsson et al. 1984).

### 1.3. Protease inhibitors

Pathogen proteases represent a major weapon during the infection process. Host organisms, on the other hand, responded to this threat by developing different types of protease inhibitors in order to neutralize damaging effects caused by the pathogen proteases. These inhibitors are important components of the vertebrate and arthropod plasma making up 5% of its total content (Laskowski & Kato 1980). The reason for this presumably lies in the fact that blood and hemolymph easily reach all parts of the body and have direct contact with tissues. The mechanism they use to inactivate the target protease classifies them in two groups: active-site inhibitors and alpha-2-macroglobulins ( $\alpha$ 2Ms). The first group inactivates proteases by binding to their active site and completely preventing them from performing further hydrolysis (Armstrong 2006). The second group, the  $\alpha$ 2Ms, consists of proteins that entrap the target protease into a molecular cage (figure 1.1). The members of this group possess a surface-exposed loop recognized by proteases as a substrate and which is cleaved, inducing a conformational rearrangement of the inhibitor in a form of cage around the protease. This cage sterically hinders the protease from the protein substrate. Nonetheless, the protease active site is not affected and it remains active against small substrate that can easily access the cavity inside the cage (Nielsen & Sottrup-Jensen 1993; Quigley et al. 1991).

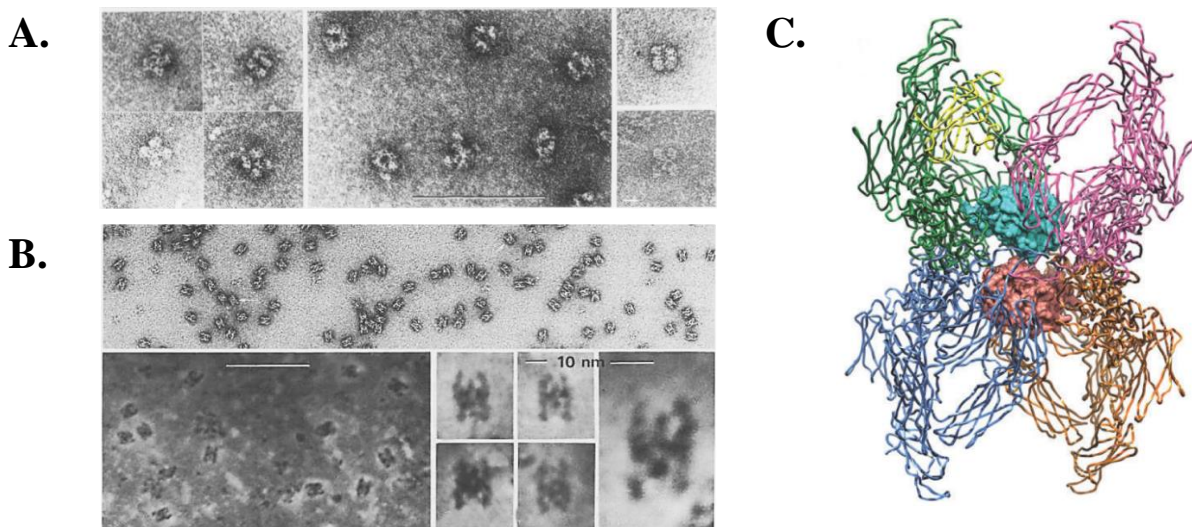


**Figure 1.1.** A and B – Early EM images showing tetrameric structure of native human  $\alpha$ 2M ( $h\alpha$ 2M) with a cavity visible as dense zone in the middle (A) and a  $h\alpha$ 2M-trypsin complex (B). C – Model representing possible protease binding mode in induced  $h\alpha$ 2M based on the crystal structure. (A and B taken from (Tapon-Breaudière et al. 1985), C from (Marrero et al. 2012)).

Alpha-2-macroglobulins belong to the family of thioester-containing proteins (TEPs) that are abundant in human plasma and are engaged in different stages of the innate immune response (Sottrup-Jensen 1989) (Law & Dodds 1997). Based on phylogenetic analyses, this family comprises three subfamilies: 1 –  $\alpha$ 2Ms, with members such as  $\alpha$ 2M, muroglobulin,  $\alpha$ 1I<sub>3</sub> of rats, human pregnancy zone proteins (PZPs) and ovostatin from eggs, 2 – complement factors C3, C4 and C5 and 3 – a recently described subfamily of insect TEPs (Armstrong & Quigley 1999)(Blandin & Levashina 2004). While  $\alpha$ 2Ms act as protease inhibitors, members of the complement subfamily are part of the cascade reaction that results in marking of foreign agents for elimination, either by the innate or the adaptive immune system. Even though insect TEPs show a greater overall similarity with  $\alpha$ 2M, they act as opsonins and in that aspect they are closer to complement system proteins (Shokal & Eleftherianos 2017). Amino acid sequence comparisons and evolutionary studies show that TEPs arose from a common ancestor after gene duplication of an  $\alpha$ 2M-like protein, predating the divergence of proteostomes and deuterostomes (Levashina et al. 2002; Zhu et al. 2005).

All TEPs have several features common features. They are large (over 100 kDa), glycosylated proteins that undergo substantial conformational changes upon proteolytic cleavage of a highly variable, so-called bait region, resulting in transformation to their active forms (figure 1.2) (Williams & Baxter 2014). Most of them also contain a highly reactive thioester bond between a thiol group of a cysteine and a  $\gamma$ -carbonyl group of a glutamine which is readily hydrolyzed by water molecules (Law & Dodds 1997). In the native state, the thioester bond is buried inside the protein where it is protected from water. However, small nucleophiles like methylamine, hydrazine and ammonia can still diffuse inside and inactivate it. Sensitivity of the thioester bond towards nucleophiles is, however, slightly different between proteins since  $\alpha$ 2M can be inhibited by methylamine, while the thioester of C3 can be efficiently inhibited by both methylamine and glycerol (Rehman et al. 2013).

#### **1.4. The $\alpha$ 2M subfamily**

As already mentioned, the  $\alpha$ 2M subfamily contains various protease-binding proteins, including a canonical  $\alpha$ 2M widely present in animals from nematodes to mammals. Additionally,  $\alpha$ 2M homologs such as muroglobulin of mice, alpha-1-macroglobulin ( $\alpha$ 1M) and alpha-1-inhibitor III ( $\alpha$ 1I<sub>3</sub>) of rats,  $\alpha$ 2M-like protein 1 ( $\alpha$ 2ML1) in skin, human pregnancy zone

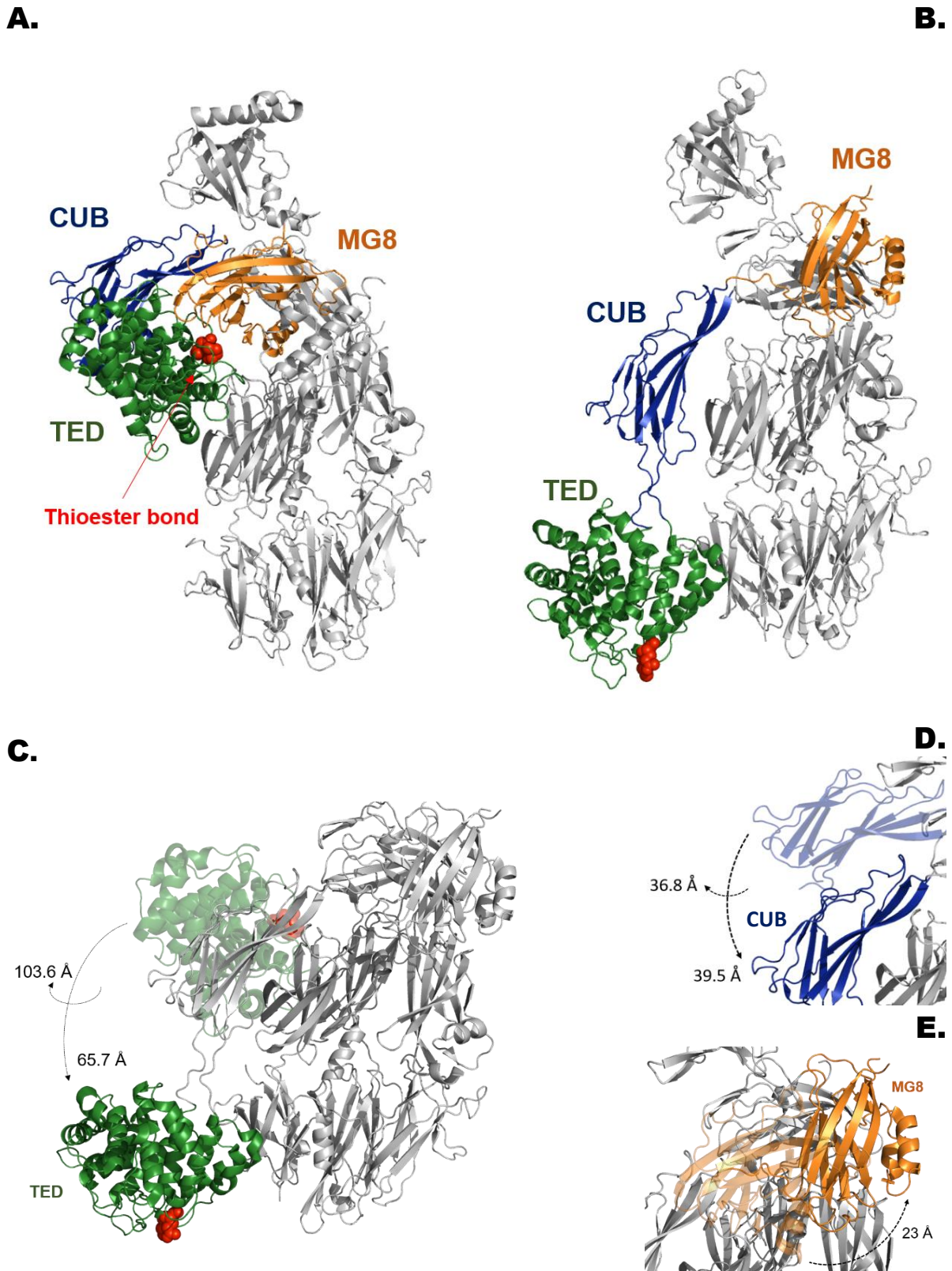


**Figure 1.2.** The conformational change of thioester-containing proteins upon the cleavage of the bait region illustrated on the example of complement protein C3. A – In native C3, TED, CUB and MG8 domains are in close contact (PDB: 2A73); Upon induction by a protease (B), TED moves farther away, exposing previously hidden thioester bond (PDB: 2I07); C, D and E – translational and rotational movements of TED, CUB and MG8 domains, respectively.

protein (PZP), which is highly expressed during pregnancy, and ovostatin of avian and reptile eggs also belong to this subfamily (Armstrong & Quigley 1999).

The size of monomeric forms of these proteins is between 180 and 200 kDa and they are found in different oligomerization states. Human and snail  $\alpha$ 2Ms, for example, form homotetramers, while  $\alpha$ 2Ms from arthropods and PZP are found as homodimers (Bender & Bayne 1996; Sottrup-Jensen 1989; Wyatt et al. 2016). Several of these proteins function as monomers, like  $\alpha$ 2ML1 (Galliano et al. 2006) or murinoglobulin (Overbergh et al. 1994). The sequences of the bait regions of different  $\alpha$ 2Ms are variable suggesting that, despite what appears to be a universally-cleavable sequence, a degree of specialization towards certain proteases exist, depending on the environment in which individual  $\alpha$ 2Ms are expressed (Sottrup-Jensen et al. 1989).

The principle by which  $\alpha$ 2Ms work involves sequestration of the protease in a molecular cage, making it physically inaccessible to their substrate. Each of the subunits in an oligomer has a surface-exposed bait region, that is readily accessible and recognized by a wide range of proteases. The activation of  $\alpha$ 2M occurs upon cleavage of the bait region, triggering a large conformational change that encloses the prey protease into a chamber in a way that resembles the Venus flytrap mechanism. This conformational change uncovers a highly reactive thioester bond that had been previously buried inside the molecule. Now exposed, the bond is hydrolyzed and the  $\gamma$ -carbonyl group of the glutamine forms an isopeptide bond with the  $\epsilon$ -amino group of a lysine on the protease surface (Sottrup-Jensen et al. 1990). Covalent binding to the target protease is, however, not mandatory for efficient inhibitory function. In *Limulus polyphemus*  $\alpha$ 2M for example, a thiol esterified glutamine crosslinks to a lysine residue of the opposite chain of  $\alpha$ 2M dimer rather than to a protease, making the inhibition essentially a non-covalent reaction. Furthermore, there are forms of  $\alpha$ 2Ms like chicken ovomacroglobulin that do not harbor a thioester motif, yet are still able to inhibit proteases by confining them within a molecular cage (Nielsen & Sottrup-Jensen 1993).

Activation of  $\alpha$ 2M by proteases converts it to a more compact form, an effect that is easily observable on SDS-PAGE (Barrett et al. 1979). At the same time, a conformational rearrangement causes the exposure of the receptor binding domains on each monomer, leading the  $\alpha$ 2M-protease complex to bind to the low-density lipoprotein related protein (LRP/ $\alpha$ 2M-R) receptor, resulting in its subsequent clearing (Holtet et al. 1994; Sottrup-Jensen et al. 1986) (Kristensen et al. 1990). The LRP/ $\alpha$ 2M-R receptor is a 600 kDa heterodimer and belongs to the family of low-density lipoproteins (LDLs) found on hepatocytes, fibroblasts, macrophages, syncytiotrophoblasts, adipocytes and astrocytes (Krieger & Herz 1994).

<b>A.</b>	<b>Human <math>\alpha</math>2M</b>	<b>P</b> KM <b>C</b> PQLQQYEMHGPE--GLRVGFYESDVMGRGHARLVHVEE-----PHT <b>E</b> TV <b>R</b> --
	<b>Rat <math>\alpha</math>2M</b>	<b>P</b> KV <b>C</b> ERLRDN-----KGIPAA-----YHLVSQS-HMDAF-LESSESPT <b>E</b> TRRSY
	<b>Muroglobulin</b>	<b>P</b> I <b>I</b> C <b>F</b> FDYGMVPI <b>S</b> APRV <b>E</b> FDLAF <b>T</b> PE <b>I</b> SWSLR <b>T</b> TLSKRPE <b>E</b> PPR <b>K</b> DPSSNDPL <b>T</b> E <b>T</b> IR--
	<b>Limulus <math>\alpha</math>2M</b>	<b>P</b> -- <b>C</b> PQYD <b>V</b> AFA-APQAANRIGGG <b>E</b> -AGGFGGG <b>I</b> RKK-----TNKPV <b>V</b> E <b>I</b> - <b>R</b> --
	<b>PZP</b>	<b>P</b> K <b>S</b> <b>C</b> S <b>V</b> I <b>P</b> SV <b>S</b> AGAV----GQGY <b>I</b> -----GAGL <b>G</b> V <b>V</b> ER <b>P</b> Y
	<b>Ovostatin</b>	<b>P</b> TV <b>C</b> TRET <b>V</b> RPPS---YFLNAG <b>F</b> TAS-----THHV <b>K</b> LSAEVARE-ER <b>G</b> KRH <b>I</b> L <b>E</b> T <b>I</b> REF
<b>B.</b>	<b>Human <math>\alpha</math>2M</b>	SARASVSVLGDILGSAMQNTQNLQMPY <b>G</b> CG <b>E</b> Q <b>N</b> MVLFAPNIYVLDYLN <b>E</b> TQQL <b>T</b> PE <b>I</b> 100.00%
	<b>Rat <math>\alpha</math>2M</b>	SARASVTVLGDILGSAMQNTQDLKMPY <b>G</b> CG <b>E</b> Q <b>N</b> MVLFAPNIYVLDYLN <b>E</b> TQQL <b>T</b> Q <b>E</b> I 93.10%
	<b>Muroglobulin</b>	SARAHFSVMGDILSSAIRNTQNLHMPY <b>G</b> CG <b>E</b> Q <b>N</b> MVLFAPNIYVLKYL <b>N</b> E <b>T</b> Q <b>Q</b> ----- 84.91%
	<b>Limulus <math>\alpha</math>2M</b>	SARGYVSITGDLMGPAIKNLDHLVRLPT <b>G</b> CG <b>E</b> Q <b>N</b> MVLFVFNIFVLDYLTATGSITDS <b>I</b> 55.17%
	<b>C3</b>	QGT <b>P</b> V <b>A</b> Q <b>M</b> T <b>E</b> D--AVDAERL <b>K</b> HL <b>I</b> V <b>T</b> PS <b>G</b> CG <b>E</b> Q <b>N</b> MIG <b>M</b> T <b>P</b> T <b>V</b> I <b>A</b> V <b>H</b> Y <b>L</b> D <b>Q</b> T <b>E</b> Q <b>W</b> E <b>K</b> -- 27.78%
	<b>Ovostatin</b>	SPRPSFSVVGDMGT <b>A</b> I <b>Q</b> N <b>V</b> H <b>Q</b> L <b>L</b> Q <b>M</b> PF <b>G</b> <b>N</b> CG <b>E</b> Q <b>N</b> MVLFAPNIYVLDYLD <b>K</b> T <b>R</b> Q <b>L</b> S <b>E</b> D <b>V</b> 67.24%
	. : * . . . . * : * * * * * : : . * : . : . * * *	
<b>C.</b>	<b>Human <math>\alpha</math>2M</b>	VY <b>L</b> Q <b>T</b> S <b>L</b> K <b>Y</b> N <b>I</b> L <b>P</b> E <b>K</b> E <b>F</b> F <b>A</b> L <b>G</b> V <b>Q</b> T <b>L</b> P <b>Q</b> T <b>C</b> D <b>E</b> P <b>K</b> A <b>H</b> T <b>S</b> F <b>Q</b> I <b>S</b> L <b>S</b> V <b>S</b> Y <b>T</b> G <b>S</b> R <b>S</b> A <b>S</b> N <b>M</b> A <b>I</b> V
	<b>Murinoglobulin</b>	V <b>Y</b> A <b>Q</b> T <b>M</b> L <b>R</b> Y <b>N</b> M <b>H</b> L <b>E</b> K <b>Q</b> L <b>S</b> A <b>F</b> A <b>I</b> W <b>V</b> Q <b>T</b> V <b>P</b> L <b>T</b> C <b>N</b> N <b>P</b> K <b>G</b> H <b>N</b> S <b>F</b> Q <b>I</b> S <b>L</b> E <b>I</b> S <b>Y</b> T <b>G</b> S <b>R</b> P <b>A</b> S <b>N</b> M <b>V</b> I <b>A</b>
	<b>Ovostatin</b>	V <b>L</b> I <b>Q</b> T <b>A</b> L <b>R</b> Y <b>N</b> I <b>H</b> L <b>P</b> E <b>G</b> A <b>F</b> G <b>F</b> S <b>L</b> S <b>V</b> Q <b>T</b> S <b>N</b> A <b>S</b> C <b>P</b> R <b>D</b> Q--P <b>G</b> K <b>F</b> D <b>I</b> V <b>L</b> I <b>S</b> S <b>Y</b> T <b>G</b> K <b>R</b> S <b>S</b> N <b>M</b> V <b>I</b> I
	<b>Limulus <math>\alpha</math>2M</b>	G <b>L</b> V <b>Q</b> T <b>S</b> L <b>R</b> Y <b>N</b> V <b>N</b> T <b>P</b> P <b>R</b> K <b>G</b> F <b>H</b> L <b>E</b> V <b>T</b> V <b>K</b> R <b>G</b> L <b>Y</b> R--D <b>C</b> I <b>N</b> A <b>H</b> I <b>A</b> T <b>C</b> V <b>K</b> Y <b>D</b> G <b>K</b> G <b>V</b> S <b>N</b> M <b>A</b> V <b>L</b>
		** * : * * : * : * . . . * . * * . * * * : :
	<b>Human <math>\alpha</math>2M</b>	D <b>V</b> K <b>M</b> V <b>S</b> G <b>F</b> I <b>P</b> L <b>K</b> P <b>T</b> V <b>K</b> M <b>L</b> E <b>R</b> S <b>N</b> H--V <b>S</b> R <b>T</b> E <b>V</b> S <b>S</b> N <b>H</b> V <b>L</b> I <b>Y</b> L <b>D</b> K <b>V</b> S <b>N</b> --Q <b>T</b> L <b>S</b> L <b>F</b> F <b>T</b> V <b>L</b> Q <b>D</b> V <b>P</b>
	<b>Murinoglobulin</b>	D <b>V</b> K <b>M</b> L <b>S</b> G <b>F</b> I <b>P</b> L <b>K</b> P <b>T</b> V <b>K</b> K <b>L</b> E <b>R</b> L <b>E</b> H--V <b>S</b> R <b>T</b> E <b>V</b> S <b>N</b> N <b>V</b> L <b>I</b> Y <b>L</b> D <b>Q</b> V <b>T</b> N--Q <b>T</b> L <b>A</b> F <b>S</b> F <b>I</b> I <b>Q</b> Q <b>D</b> I <b>P</b>
	<b>Ovostatin</b>	D <b>V</b> K <b>M</b> L <b>S</b> G <b>F</b> V <b>P</b> V <b>K</b> S <b>S</b> L <b>D</b> Q <b>L</b> I <b>D</b> D <b>H</b> T--V <b>M</b> Q <b>V</b> E <b>Y</b> K <b>K</b> N <b>H</b> V <b>L</b> L <b>Y</b> L <b>G</b> N <b>I</b> L <b>Q</b> K <b>R</b> R <b>E</b> V <b>T</b> F <b>S</b> V <b>E</b> Q <b>D</b> F <b>V</b>
	<b>Limulus <math>\alpha</math>2M</b>	E <b>M</b> K <b>M</b> V <b>S</b> G <b>W</b> I <b>P</b> D <b>E</b> E <b>S</b> I <b>K</b> N <b>I</b> V <b>D</b> R <b>E</b> E <b>L</b> N <b>L</b> R <b>R</b> Y <b>E</b> V <b>D</b> G <b>N</b> Q <b>L</b> N <b>L</b> Y <b>F</b> S <b>E</b> L <b>T</b> D--Q <b>N</b> L <b>C</b> F <b>N</b> F <b>W</b> L <b>E</b> Q <b>D</b> I <b>E</b>
		: : * : * : * : * : : : . : : * . * : : * : : : : : . * : * * .
	<b>Human <math>\alpha</math>2M</b>	VR <b>D</b> L <b>K</b> P <b>A</b> I <b>V</b> K <b>V</b> Y <b>D</b> Y <b>E</b> T <b>D</b> E <b>F</b> A <b>I</b> A <b>E</b> Y <b>N</b> A <b>P</b> --C <b>S</b> K <b>D</b> L <b>G</b> N <b>A</b> -- 100.00%
	<b>Murinoglobulin</b>	VR <b>N</b> L <b>Q</b> P <b>A</b> I <b>V</b> K <b>V</b> Y <b>D</b> Y <b>E</b> T <b>D</b> E <b>M</b> A <b>F</b> A <b>E</b> Y <b>S</b> S <b>P</b> --C <b>S</b> T <b>D</b> K <b>Q</b> N <b>V</b> -- 68.63%
<b>Ovostatin</b>	V <b>T</b> H <b>P</b> K <b>P</b> A <b>P</b> V <b>Q</b> I <b>D</b> Y <b>D</b> Y <b>E</b> T <b>E</b> E <b>Y</b> A <b>V</b> A <b>E</b> Y <b>M</b> S <b>L</b> --C <b>R</b> G <b>V</b> V <b>E</b> E <b>M</b> G-- 42.76%	
<b>Limulus <math>\alpha</math>2M</b>	V <b>Q</b> E <b>T</b> K <b>P</b> A <b>T</b> I <b>R</b> L <b>Y</b> D <b>Y</b> E <b>L</b> E <b>Q</b> E <b>V</b> V <b>T</b> S <b>Y</b> S <b>I</b> D <b>E</b> N <b>C</b> E <b>K</b> L <b>P</b> P <b>L</b> P-- 30.67%	
	* . : * * : : * * * * : : . . : * *	

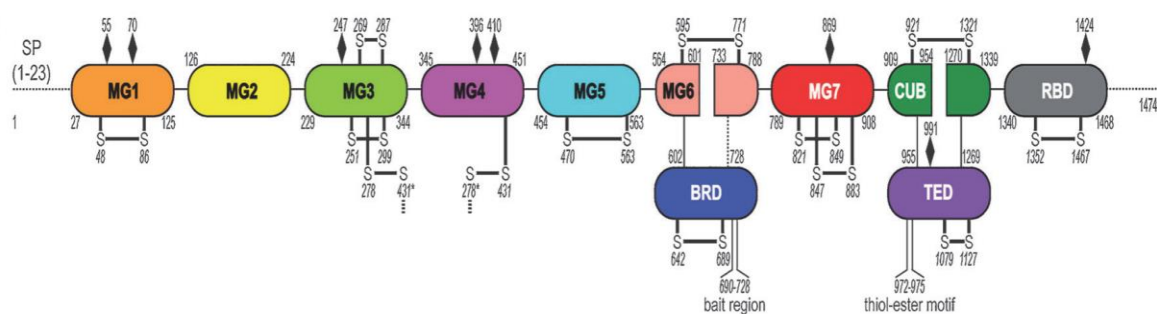
**Figure 1.3.** Sequence alignment of three domains of thioester-containing proteins (TEPs). A – Bait region is highly variable among TEPs, with PxxC and ExxR motifs found at its N- and C-termini; B – Thioester domain (TED) with CGEQ motif; C – Receptor binding domain (RBD). Lysine residues in red are important for the binding of RBD to the receptor (Sottrup-Jensen et al. 1986). The percentages in B and C show the identity of amino acid sequence of  $\alpha$ 2Ms compared to the human form.

Apart from acting like a protease inhibitor,  $\alpha$ 2M has wider role in the innate immune system by binding and promoting clearance of many molecules. So far it is well established that  $\alpha$ 2M binds number of cytokines and growth factors, such as transforming growth factor- $\beta$  (TGF- $\beta$ ), tumor necrosis factor- $\alpha$  (TNF- $\alpha$ ), interleukin 1 $\beta$  (IL-1 $\beta$ ), interleukin 8 (IL-8), platelet-derived growth factor-BB (PDGF-BB), nerve growth factor- $\beta$  (NGF- $\beta$ ) and vascular endothelial growth factor (VEGF) (LaMarre et al. 1991). In these cases,  $\alpha$ 2M is not converted to the activated form and the mode of interaction with these molecules is independent of its protease-inhibiting function.

## 1.5. Structure of human $\alpha$ -2-macroglobulin

The first low-resolution crystal structure of any  $\alpha$ 2M was that of human methylamine-induced  $\alpha$ 2M (h $\alpha$ 2M) reported in 1995 (Andersen et al. 1995). Subsequently, the 4.3 Å resolution structure of h $\alpha$ 2M became available in 2012 (Marrero et al. 2012). Human  $\alpha$ 2M is a 1491 residue molecule made of 11 domains, with 13 disulfide bridges, 11 of them intramolecular and 2 additional ones that participate in the formation of a dimer (Marrero et al. 2012). The first seven domains are termed macroglobulin-like domains (MG) and they are approximately 110-residue antiparallel  $\beta$ -sandwiches of three- and four-stranded  $\beta$ -sheets (figure 1.4). Other regions of note include the thioester domain (TED) which harbors the CxEQ sequence and maintains it at the interior of the molecule to protect it from hydrolysis, and the bait region, 39-residue sequence that is recognized by a large number of proteases (Sottrup-Jensen et al. 1981)(Marrero et al. 2012).

A.



B.

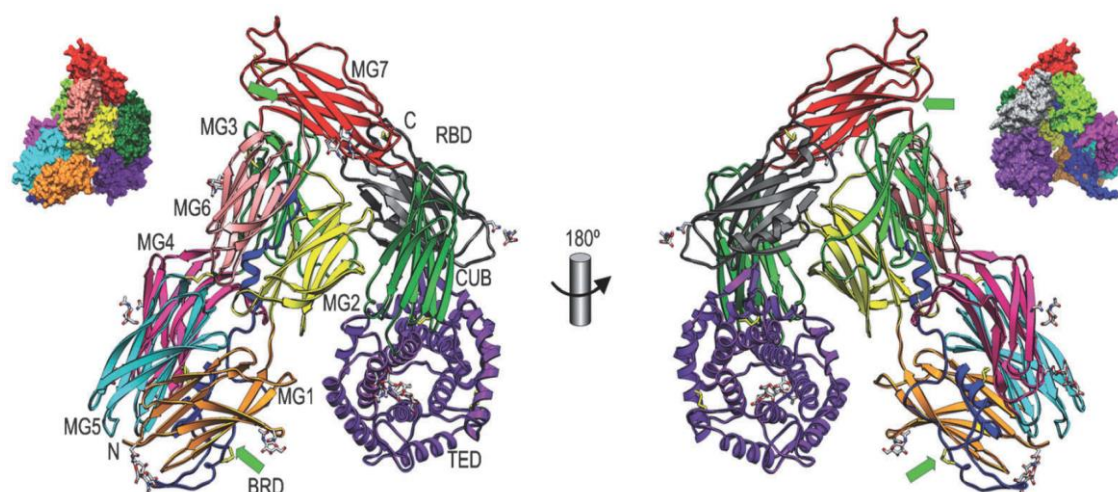


**Figure 1.4.** Structure of the human  $\alpha$ 2M monomer. A – schematic representation of domain organization; B – domain arrangement; (Marrero et al. 2012)

Human  $\alpha$ 2M circulates in the bloodstream as tetramer of approximately 720 kDa in which two subunits (monomers) interact covalently through two disulfide bridges, leading to the association of two dimers through non-covalent interactions. In this way they build a large central cavity at the center of the tetramer, named the prey chamber, which can be large enough to capture up to two proteases of 20-30 kDa (Marrero et al. 2012). This corresponds to the previously determined stoichiometry of 1:2 (Sottrup-Jensen 1989).

## 1.6. Bacterial $\alpha$ 2Ms

Protein sequences related to  $\alpha$ 2M were found in all metazoan groups and for a long time it was believed that  $\alpha$ 2Ms are an exclusively animal characteristic. In 2004, Budd et al. reported that sequences homologous to eukaryotic  $\alpha$ 2M were widely present in the genomes of different bacterial species (Budd et al. 2004). Moreover,  $\alpha$ 2M homologs that did not carry the thioester motif were also identified. In *E. coli* for example, there are two  $\alpha$ 2M homologs: *yfhM*, that has thioester motif, and *yfaS*, a highly divergent homolog that does not carry it. Using *E. coli* as a reference, they classified bacterial  $\alpha$ 2Ms into two types, with the main characteristic being the presence or absence of the thioester. The most plausible explanation of the origin of  $\alpha$ 2M-like genes in bacterial genomes is horizontal gene transfer.

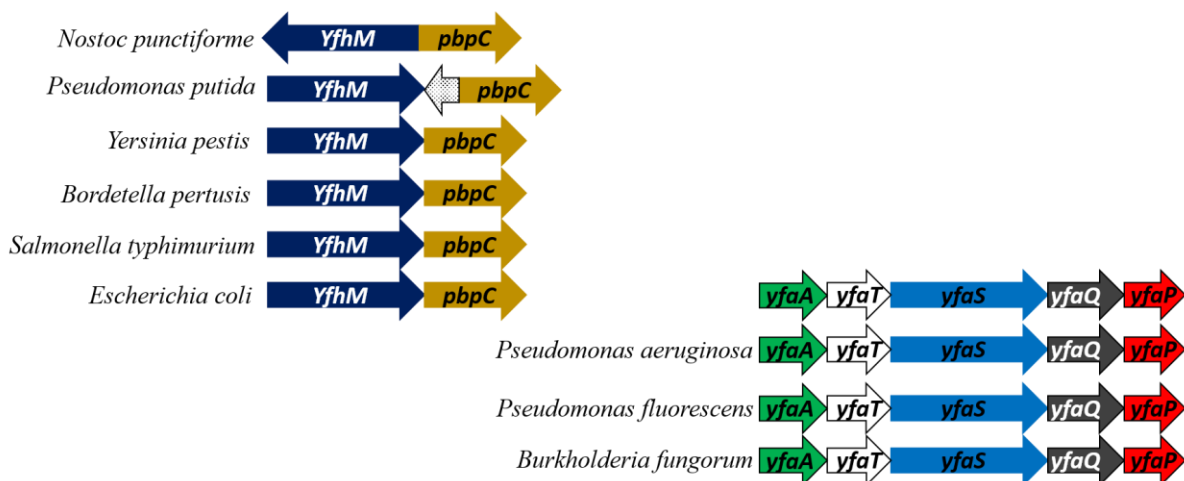


**Figure 1.4.** Genetic localization of  $\alpha$ 2M in some bacterial species.

Notably, Budd et al. noted that these genes were present only in Gram-negative bacteria with colonizing and parasitic lifestyles, while Gram-positive bacteria and archaea lacked  $\alpha$ 2Ms

(Budd et al. 2004). This suggests that  $\alpha$ 2M may provide Gram-negative bacteria with an advantage during colonization and infection events.

Finally, the genetic context in which the two types of bacterial  $\alpha$ 2Ms were found was intriguing. YfhM was always found juxtaposed or in an operon with the gene encoding Penicillin-Binding Protein 1c (*pbpc*), whose protein product, PBP1c, is involved in cell wall formation, while *yfaS* was present in an operon with five other genes whose function has not yet been fully elucidated.

YfhM is a 1653-residue polypeptide containing a characteristic consensus lipobox sequence (LAGC) suggesting that it is a membrane-bound protein (Budd et al. 2004)(Kovacs-Simon et al. 2011). The lipobox cysteine is followed by an aspartic acid from an inner-membrane sorting signal, localizing YfhM in the periplasm (Fukuda et al. 2002). On the other hand, YfaS does not have a lipobox motif indicating that the protein may be secreted (Budd et al. 2004). Biochemical characterization of YfhM (named ECAM, for *E. coli*  $\alpha$ -2-macroglobulin) by Doan and Gettings confirmed that it is expressed as a 180 kDa monomer that is only found in the inner membrane fraction (Doan & Gettings 2008). They also validated the presence of an intact thiol ester between cysteine and glutamine residues within the CxEQ motif that is hydrolyzed by small nucleophiles like methylamine. In addition, they showed that proteases can cleave ECAM in the predicted bait region. Their data also showed that, as in the case of human  $\alpha$ 2M, ECAM becomes more compacted upon incubation with proteases, resulting in increased electrophoretic mobility in SDS-PAGE as compared to the native “slow” form. Structural analyses using small-angle x-ray scattering (SAXS) and electron microscopy confirmed that the induced form of ECAM is more compact than the native one and that the conformational rearrangement that takes place after the interaction with proteases resembles the changes that occur in the transition of eukaryotic C3 from a preactivated to an activated state (Neves et al. 2012).

The first crystal structure of a bacterial  $\alpha$ 2M was obtained by our group in 2014 (Wong & Dessen 2014). This is a 2.95 Å resolution structure of  $\alpha$ 2M from *Salmonella enterica* (Sa-A2M) (PDB-ID: 4U48). Sa-A2M is a 1644-residue protein that shares 82% identity with ECAM. The structure shows high overall similarity with the human form. It consists of 13 domains, 11 of them folding as  $\beta$ -sandwich-like MG domains, as in the case of human  $\alpha$ 2M. Compared to the human form, Sa-A2M has two additional domains, MG1 and MG2, spanning residues 57 to 281. MG1 is believed to associate to the inner membrane by a flexible loop and together they appear to play a role of a linker (Wong & Dessen 2014). From the MG3 domain on, they follow a similar pattern to the domain arrangement in human  $\alpha$ 2M including a highly

flexible bait site from residues 925 to 950 and a helical TED domain with the thioester motif. The polypeptide chain terminates with the MG10 which structurally resembles the receptor-binding domain in human  $\alpha 2M$ ; however, its role remains unclear.

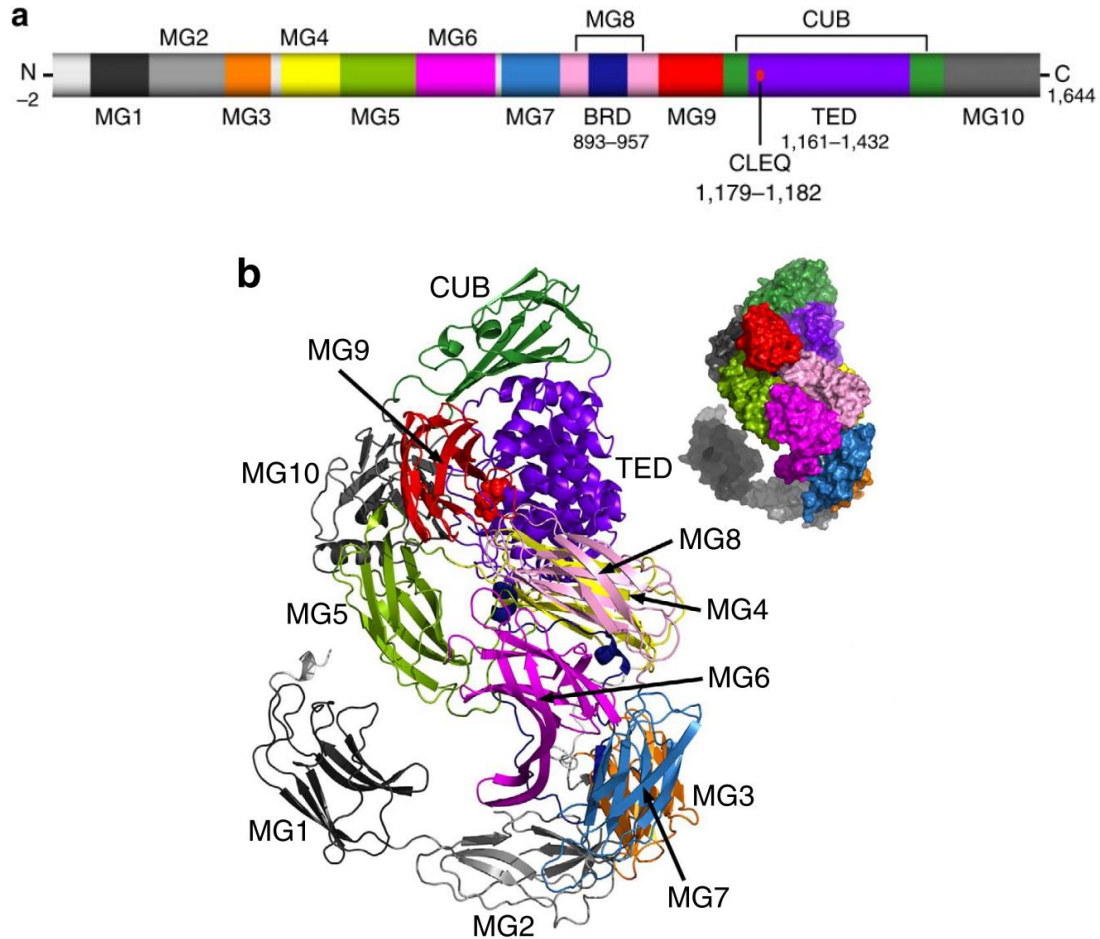


**Figure 1.5.** Structure of *Salmonella enterica*  $\alpha 2M$ . MG 1-10 – macroglobulin-like domains; BDR – bait region domain; TED – thioester domain. From (Wong & Dessen 2014)

Garcia-Ferrer et al. subsequently structurally characterized ECAM in both the presence and absence of a protease, and concluded that it underwent a major conformational change upon protease binding. However, they were not able to trace a trustworthy model for the protease in the complex, and thus the mechanism of this interaction still remains obscure (Garcia-Ferrer et al. 2015).

## 1.7. The bacterial cell wall

The bacterial cell wall is a robust protective layer that ensures integrity and protection from environmental stress (Scheffers & Pinho 2005). The main component of the bacterial cell wall is peptidoglycan (murein), a mesh-like sacculus surrounding the cytoplasmic membrane (Typas et al. 2011). The most important function of the peptidoglycan is to resist internal osmotic pressure and any inhibition of its synthesis or enzymatic degradation leads to cell lysis (Mengin-Lecreulx & Lemaitre 2005). It also maintains the shape of the cells and serves as a scaffold to which numerous proteins and teichoic acids are attached (Dramsı et al. 2008)(Neuhaus & Baddiley 2003).

Gram-positive bacteria have a thick peptidoglycan layer that can constitute up to 95% of their cell wall, with teichoic and lipoteichoic acids embedded within, the latter directly connected to the plasma membrane lipids. On the surface of peptidoglycan there is often a layer of identical proteins attached to it called S-layer, and a capsule of polysaccharides (figure 1.6b). On the other hand, Gram-negative bacteria have inner and outer membranes that enclose a compartment called periplasm in which thin layer of peptidoglycan is located (figure 1.6a) (Vollmer et al. 2008)(Malanovic & Lohner 2016).

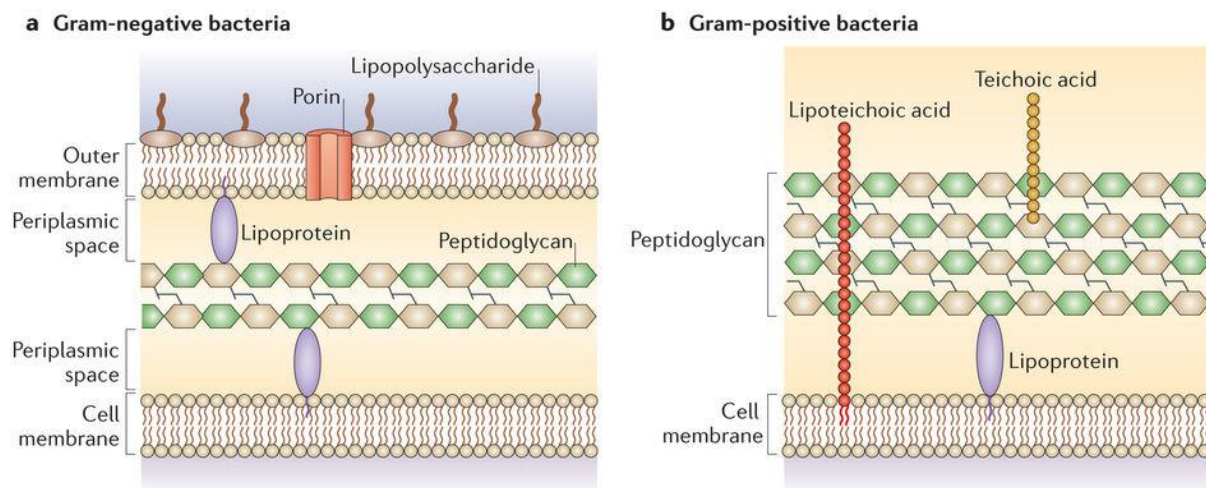


**Figure 1.6.** Differences between the cell walls of Gram-negative and Gram-positive bacteria. Taken from (Brown et al. 2015).

Peptidoglycan is a complex polymer consisting of linear glycan chains cross-linked by short peptides (Rogers et al. 1980). The glycan chains are composed of two alternating amino sugars, N-acetylglucosamine (GlcNAc) and N-acetylmuramic acid (MurNAc) that are linked by a  $\beta$ -(1,4) glycosidic bond (figure 1.7) (Vollmer et al. 2008). The pentapeptide stem is

attached to the lactoyl group of MurNAC. The composition of the pentapeptide varies, though generally it consists of L-Ala- $\gamma$ -D-Glu-meso-A<sub>2</sub>pm (or L-Lys)-D-Ala-D-Ala, A<sub>2</sub>pm being 2,6-diaminopimelic acid. The last D-Ala is trimmed from the mature molecule. The stem peptides are cross-linked between the carboxyl group of D-Ala and the amino group of neighboring diamino acid, either directly or through a peptide bridge (ex. pentaglycine) (Vollmer et al. 2008).

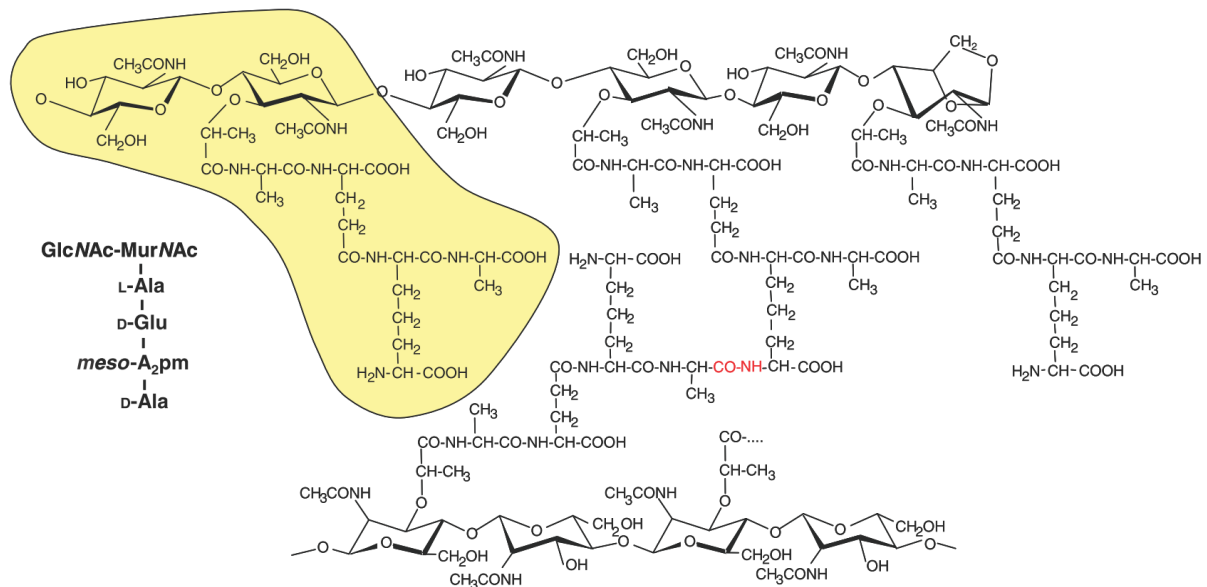


**Figure 1.7.** Structure of the *E. coli* peptidoglycan. The basic building block marked in yellow consists of N-acetylglucosamine (GlcNAc) and N-acetylmuramic acid (MurNAc) connected by a  $\beta$ -(1,4) glycosidic bond, with a L-Ala- $\gamma$ -D-Glu-meso-A<sub>2</sub>pm-D-Ala-D-Ala pentapeptide attached to MurNAc. Glycan chains are cross-linked directly between a meso-A<sub>2</sub>pm residue of one and a D-Ala residue at position 4 of another disaccharide (red). Taken from (Mengin-Lecreulx & Lemaitre 2005)

## 1.8. Peptidoglycan precursor synthesis

Peptidoglycan synthesis involves around 20 cascade reactions that can be grouped in three phases. It starts with the synthesis of precursors in the cytosol, followed by their linkage to an undecaprenyl phosphate group on the membrane to form lipid II. Lipid II is subsequently flipped across the membrane to the periplasm where it will be acted upon by the glycosyltransferase and transpeptidase action of Penicillin-Binding Proteins (PBPs) (Typas et al. 2011).

The first stage involves the synthesis of the soluble nucleotide-bound individual components that will later form the basic building block of peptidoglycan (figure 1.8).

Formation of GlcNAc starts with amination of fructose-6-phosphate to produce glucosamine-6-phosphate (GlcN-6-P), followed by its conversion to GlcN-1-P, addition of the acetyl group and linking to the UDP to create UDP-GlcNAc (Barreteau et al. 2008). The newly created UDP-GlcNAc is a substrate for formation of the second sugar component by transferring enolpyruvate from phosphoenolpyruvate (PEP) and reduction to yield UDP-MurNAc. The final stage is the synthesis of pentapeptide associated to the UDP-MurNAc in a series of reactions catalyzed by a family of enzymes called Mur ligases. This is done in a stepwise fashion where MurC, MurD and MurE add L-Ala, D-Glu and diamino acid respectively, while MurF completes the chain by adding the D-Ala-D-Ala dipeptide. These enzymes are specialized for different substrates but they share the same reaction mechanism and have overall structural similarities (El Zoeiby et al. 2003) (Barreteau et al. 2008).

Subsequent steps of peptidoglycan synthesis are localized on the cytoplasmic side of the cell membrane. Individual components, UDP-GlcNAc and MurNAc-pentapeptide, must be linked, forming a basic disaccharide-pentapeptide building block of peptidoglycan, which is then translocated through the hydrophobic environment of the cellular membrane on the periplasmic side. The key role in the processes is assigned to undecaprenyl pyrophosphate ( $C_{55}$ -PP), also known as bactoprenol, a lipidic molecule embedded in the plasma membrane (Bouhss et al. 2007)(Manat et al. 2014). This molecule is also involved in the biogenesis of other bacterial cell wall carbohydrate polymers such as lipopolysaccharides, the enterobacterial common antigen, capsule polysaccharides and teichoic acids (Touzé & Mengin-Lecreulx 2008).

The first membrane-associated step involves anchoring of MurNAc-peptide to  $C_{55}$ -P. It is a transfer reaction performed by *MraY*, an integral membrane protein, resulting in  $C_{55}$ -PP-MurNAc-pentapeptide with the release of UMP. The newly created  $C_{55}$ -PP-MurNAc-pentapeptide is called Lipid I, an essential intermediate in peptidoglycan biosynthesis (Bouhss et al. 2007).

Formation of Lipid I provides the substrate for *MurG*, a membrane-associated enzyme that attaches GlcNAc to Lipid I producing Lipid II. This molecule is translocated to the outer side of the plasma membrane where it serves as a substrate for PBPs (Heijenoort 2007). The proteins involved in this translocation are called flippases. The first flippases shown to be involved in this process were *FtsW* and its homolog *RodA*, but recently other proteins have also been implicated, such as *MurJ* and *AmiJ* (Mohammadi et al. 2011) (Meeske et al. 2015; Sham et al. 2014).

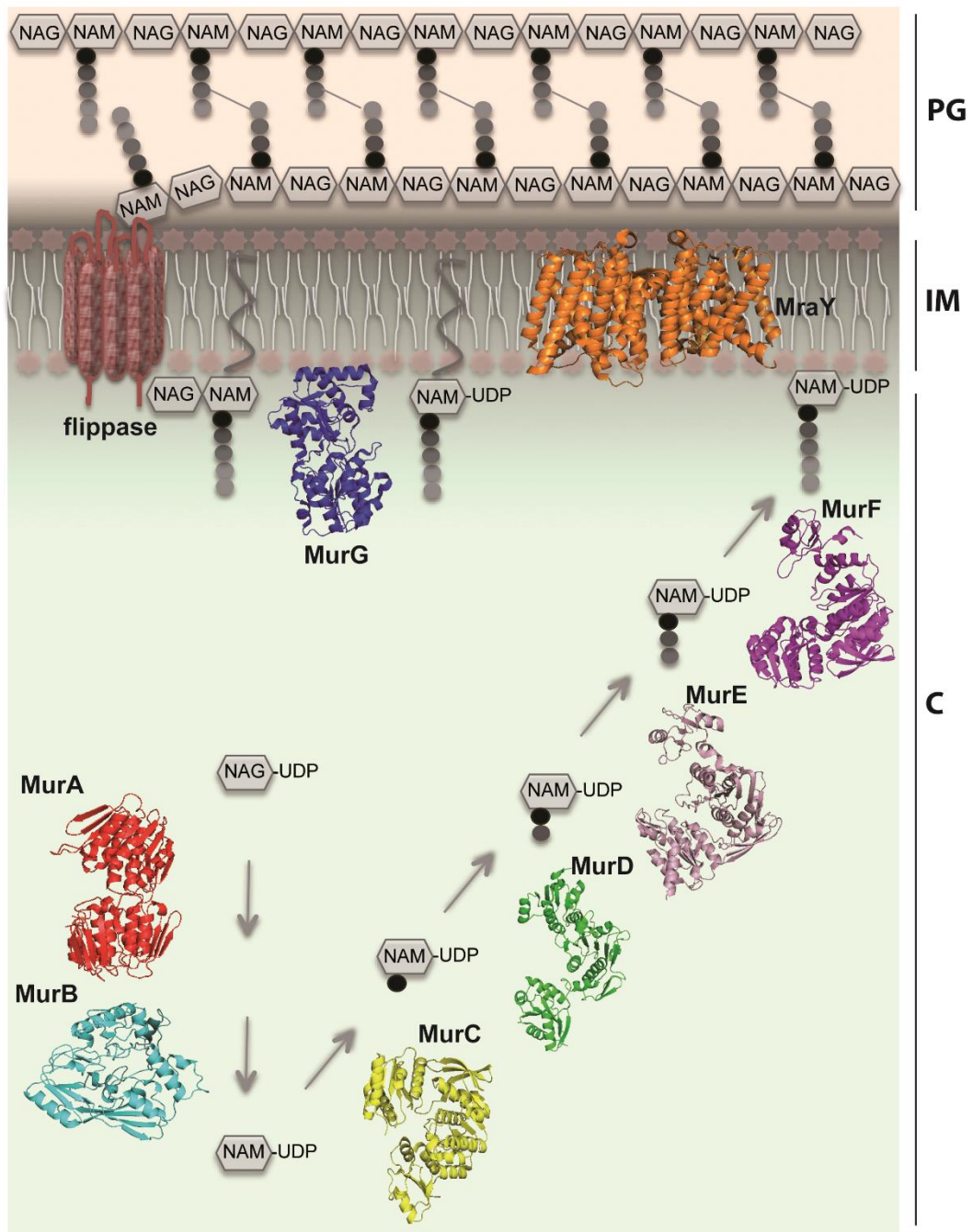


**Figure 1.8.** Synthesis of peptidoglycan precursors in the cytosol. NAG – N-acetylglucosamine; NAM – N-acetylmuramic acid; C – cytosol; IM – inner membrane; PG – peptidoglycan. From (Laddomada et al. 2016).

## 1.9. Penicillin-Binding Proteins

Penicillin-binding proteins (PBPs) are peptidoglycan synthases located in the periplasm where they catalyze the final steps of peptidoglycan synthesis, i. e. glycan chain polymerization and cross-linking of stem peptides (Macheboeuf et al. 2006). PBPs were discovered in the mid-1970s due to their ability to covalently bind  $\beta$ -lactam antibiotics, most notably penicillin and its derivatives. After it was initially established that  $\beta$ -lactams interfere with cell wall formation, leading to the bursting of cells and lysis, it was suspected that they could inhibit enzymes in the late stage of peptidoglycan synthesis by interfering with the transpeptidation reaction (Blumberg & Strominger 1974). Thanks to the different effects of specific  $\beta$ -lactams, numerous Penicillin-Binding Proteins were identified that were capable of catalyzing transpeptidation, carboxypeptidation and endopeptidation reactions (Blumberg & Strominger 1974; Spratt 1975). Initially, 6 PBPs were identified in *E. coli*, named PBP1-6 based on their descending molecular weights on denaturing polyacrylamide gels. Moreover, based on their susceptibilities to different antibiotics, it was demonstrated that they are involved in different processes of peptidoglycan maintenance during the cell cycle, such as shape preservation, elongation or cell division (Spratt 1975). This gradually started to uncover the complexity of cell wall synthesis.

Eventually, 12 PBPs were identified in *E. coli*, 8 of which are anchored to the inner membrane (Sauvage et al. 2008). They are classified in 3 classes based on their size and activity (Goffin & Ghuysen 1998). Class A contains three members of bifunctional enzymes PBP1a, 1b and 1c having both glycosyltransferase (GTase) and transpeptidase (TPase) domains, while class B consists of monofunctional transpeptidases PBP2 and PBP3. Classes A and B are further grouped together as high molecular weight (HMW) PBPs. All of the HMW members are multimodular proteins docked to the inner membrane by an N-terminal transmembrane helix. Lack of any of them results in the formation of aberrant peptidoglycan structure (Denome et al. 1999). Class C comprises low molecular weight (LMW) proteins with carboxypeptidases PBP5, PBP6 and PBP6b, carboxypeptidase/endopeptidase PBP4 and endopeptidases PBP4b, PBP7 and AmpH. With the exception of PBP5, the deletion of any of the class C PBPs has no consequence on the cell phenotype (Denome et al. 1999). PBP5, 6 and 6b are membrane-anchored through a C-terminal amphipathic helix which in case of PBP5 is essential for its function (Nelson et al. 2002). Even though the role of the class C PBPs in peptidoglycan maintenance is not clear and their roles overlap, the reason for their redundancy may be

connected with the activity in different environmental conditions, like the recently demonstrated impact of pH on the function of PBP5 and PBP6b (Peters et al. 2016).

### **1.10. Glycan chain polymerization**

Polymerization of glycan chains in bacterial cell wall is performed mainly by the GTase activity of bifunctional class A PBPs. GTases are a very large group of enzymes that catalyze the transfer of a saccharide moiety from a nucleotide-activated or lipid-linked sugar donor to a nucleophilic acceptor (Rini et al. 2009). Bacteria also have monofunctional GTases, which account for approximately 20% of the total number of GTases, and the role of which is still not completely explained (Sauvage et al. 2008).

Bacterial GTases belong to the GT51 family. To date, several structures of bifunctional bacterial GTases have been solved, such as PBP2 from *S. aureus* (Lovering et al. 2007), the GTase domain of PBP1a from *Aquifex aeolicus* (Yuan et al. 2008), PBP1b from *E. coli* (King et al. 2017; Sung et al. 2009) and one monofunctional Mgt from *S. aureus* (Huang et al. 2012). Unlike other GTases that have variants of Rossmann domains, bacterial GTases fold into a structure that resembles that of phage  $\lambda$ -lysozyme (Lairson et al. 2008; Lovering et al. 2007). Consisting almost entirely of  $\alpha$ -helices, they form two lobes, a small flexible jaw and a globular head with the cleft in between that contains the active site.

Current evidence shows that the GTase reaction is performed in a processive manner, that is the growing glycan strand remains within the enzyme active site until it is fully polymerized and released (Egan et al. 2015). In order to initiate the reaction, two Lipid II molecules are required to be placed in the active site of the GTase, one in the donor and one in the acceptor position. The reaction is initiated by formation of  $\beta$ -(1,4) glycosidic bond between the donor MurNAc and GlcNAc of the acceptor, yielding a tetrasaccharide (Lipid IV) in the acceptor site with the release of undecaprenyl pyrophosphate from the donor site that will be reused for the formation of the new Lipid II (Terrak et al. 2008)(Egan et al. 2015). Lipid IV now moves to the donor site, while new Lipid II arrives on the acceptor position and another transfer occurs yielding a hexasaccharide. The reactions that follow are faster than the initiation step (Egan et al. 2015).

When it comes to the length of the glycan chains, this varies greatly between different species (Vollmer et al. 2008). The average length of the glycan chains can span from between 3 and 10 disaccharide units for *S. aureus* up to 135 for *Bacillus licheniformis* (Boneca et al.

2000; Ward 1973). The average length of *E. coli* strands is 21 disaccharide units (Harz et al. 1990).

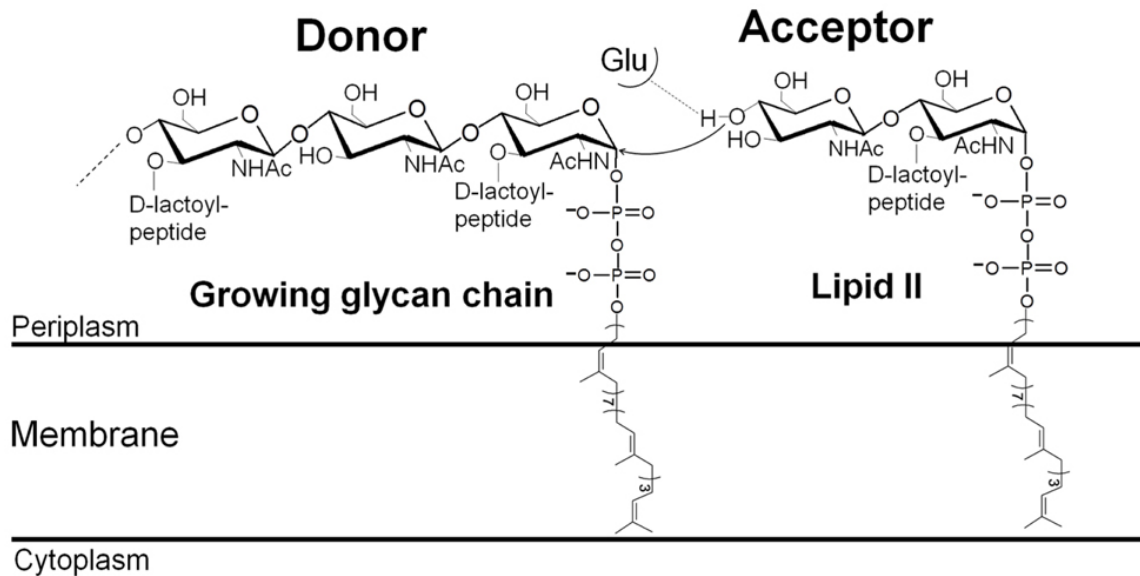


**Figure 1.9.** Schematic representation of the glycosyltransferase reaction. Initially, two Lipid II molecules are placed at a donor and an acceptor site in a GTase domain of Class A PBPs. Formation of a  $\beta$ -(1,4)-glycosidic bond between MurNAc of the donor Lipid II and GlcNAc of the acceptor Lipid II is aided by a catalytic glutamate from the active site, forming Lipid IV with a release of undecaprenyl pyrophosphate. Lipid IV then moves to the donor site and engages in another GTase reaction with a new Lipid II. From (Derouaux et al. 2013).

### 1.11. Cross-linking

Polymerization of glycan chains is coupled with transpeptidation reactions in which peptide moieties of two disaccharide units become cross-linked with the concomitant release of D-alanine (Goffin & Ghuyssen 1998). Transpeptidation is catalyzed by the transpeptidase (TPase) domain of the bifunctional class A PBPs, or by monofunctional TPases of the class B PBPs. The reaction is performed in two steps: acylation and deacylation (Ghuyssen 1991; Goffin & Ghuyssen 1998). Once the donor pentapeptide reaches the active site of TPase, a catalytic serine residue attacks the carbonyl carbon atom of the D-Ala-D-Ala peptide bond forming an acyl-enzyme complex, releasing terminal D-Ala. In the next step, nucleophilic attack of an acceptor peptide will resolve the acyl intermediate creating a peptide bond between donor and acceptor strands. If the acceptor is a water molecule, the ester bond of the intermediate is hydrolyzed and the enzyme releases the shortened peptide. This reaction is called carboxypeptidation and it is catalyzed by various class C PBPs and, under specific conditions, it can be performed by class A PBPs (Egan et al. 2015).

From a structural aspect, TPase domains are made of two subdomains, one entirely  $\alpha$ -helical, and another consisting of  $\beta$ -sheet covered by 3  $\alpha$ -helices (Sauvage et al. 2008). The active site is located at the interface of the two subdomains, carrying 3 motifs that are highly conserved among PBPs. Motif 1, SxxK, consists of an active serine that forms an acyl-intermediate with donor pentapeptide, followed by a lysine that may play an important role in serine deprotonation. The second highly conserved motif, SxN, contains a serine that is believed to be responsible for the deacylation step. The third motif is composed of KTG(T/S), the lysine of which activates the second serine (Goffin & Ghuysen 1998).

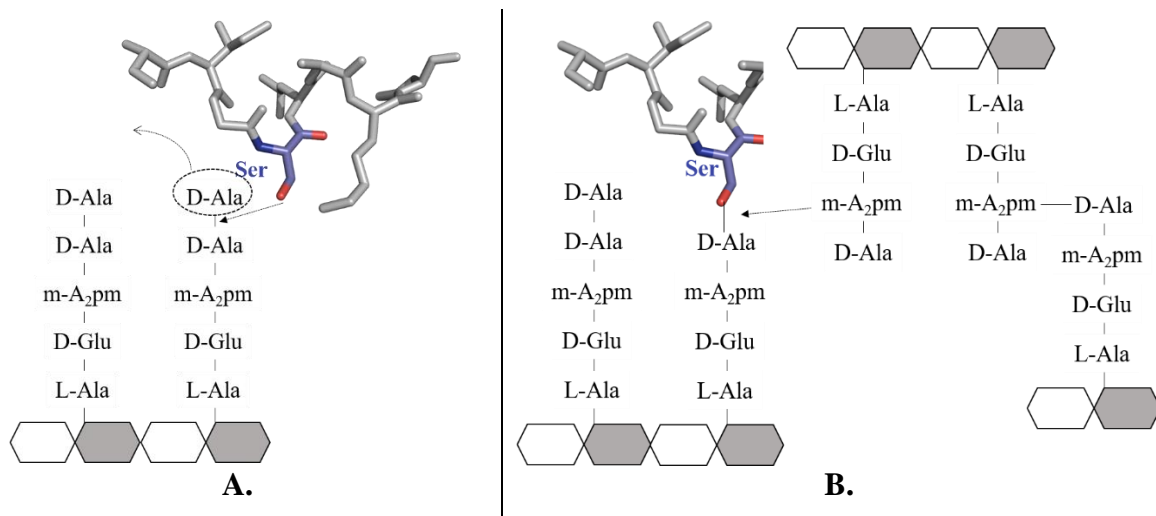


**Figure 1.10.** Transpeptidase reaction in *E. coli*. In the acylation step (A) a catalytic serine of PBPs attacks the bond between two D-Ala residues, forming a covalent acyl-enzyme intermediate, with a release of terminal D-Ala. In the deacylation step (B), the intermediate is resolved by forming a peptide bond between D-Ala of the donor peptide and m-A<sub>2</sub>pm of an acceptor peptide.

In bifunctional PBP1a and PBP1b of *E. coli*, glycan chain polymerization and transpeptidation are coupled although they differ slightly in the time-course. In PBP1b GTase and TPase activities occur almost simultaneously, while PBP1a initially shows only GTase activity with transpeptidation starting to occur after 15 minutes. This suggests that PBP1a may require pre-oligomerized acceptor (Bertsche et al. 2005; Born et al. 2006).

The most common type of cross-linking is the 3-4 cross-link which occurs between the amino group of diamino acid residue at position 3 of the acceptor peptide and the carboxyl group of D-alanine at position 4 of the donor peptide. In most Gram-negative bacteria this occurs directly, whereas in Gram-positive bacteria, this occurs mostly through a peptide bridge. Additionally, 2-3 and 3-3 crosslinks have also been observed (Vollmer et al. 2008).

## 1.12. Class A PBPs

Class A PBPs are multidomain, high molecular weight Penicillin-Binding Proteins that have both glycosyltransferase and transpeptidase activities. In *E. coli*, it was initially thought that class A PBPs were in fact one protein in four isoforms, but it was later discovered that the uppermost band on the SDS-PAGE was a product of separate gene, *ponA*, and its protein product was eventually designated as PBP1a (Tamaki et al. 1977). Three other bands were recognized to be the isoforms  $\alpha$ ,  $\beta$  and  $\gamma$  of the same polypeptide chain, PBP1b, encoded by the *ponB* gene. While  $\beta$ -PBP1b arises from the proteolytic cleavage of the  $\alpha$  form,  $\gamma$ -PBP1b is the product of an alternative ribosome-binding site (Nakagawa & Matsushashi 1982). The third member of the family, PBP1c was not discovered until a few years later since it was not visible in the standard penicillin-binding assays (Schwarz et al. 1981).

PBP1a and PBP1b share several common features. They are both anchored to the inner membrane of *E. coli* through a short transmembrane helix (Egan et al. 2015). In the periplasm they appear as monomers and homodimers (Charpentier et al. 2002). Dimers are catalytically more efficient and more tightly bound to the peptidoglycan compared to monomers (Zijderveld et al. 1995). Their double activities as GTases and TPases were identified early on, together with the fact that their functions are largely interchangeable, meaning that the absence of one does not endanger the formation of fully protective peptidoglycan (Nakagawa et al. 1979)(Ishino et al. 1980)(Suzuki et al. 1978). Furthermore, the presence of at least one of them is essential for cell viability, as a double knock-out is deleterious for the cell, suggesting that their functions are partially overlapping (Denome et al. 1999). However, these proteins are not completely redundant. Inactivation of PBP1a does not result in the same phenotype like inactivation of PBP1b, indicating that PBP1a is involved largely in the cell elongation phase while PBP1b preferentially acts in the formation of the septum during the cell division (Del Portillo & Pedro 1990). PBP1b-knockout cells are more sensitive to  $\beta$ -lactam antibiotics than mutants without PBP1a (Yousif et al. 1985) and, unlike  $\Delta$ PBP1a,  $\Delta$ PBP1b mutants lose cell integrity upon inactivation of PBP2, PBP3, or the cell division protein FtsQ (Del Portillo & Pedro 1990).

PBP1a and PBP1b are part of multi-protein complexes referred to as elongasome and divisome respectively, involved in cell elongation and cell division (Typas et al. 2011). Each of them works closely in tandem with one class B PBP, PBP1a with PBP2 and PBP1b with PBP3. The presence of PBP2 increases Lipid II consumption by PBP1a, decreases the length of glycan chains and almost doubles the insertion of newly synthesized peptidoglycan into the

existing sacculi (Banzhaf et al. 2012). On the other hand, the mid-cell localization of PBP1b and its GTase activity are dependent on the presence of PBP3 (Bertsche et al. 2006; Leclercq et al. 2017). Both PBP1a and PBP1b require additional stimulation from outer-membrane anchored proteins LpoA and LpoB (Paradis-Bleau et al. 2010; Typas et al. 2010). These proteins, except for being attached to the outer membrane, are not related in terms of amino acid sequence. LpoA exhibits elongated structure with dimensions that allow it to span through periplasmic space and penetrate through peptidoglycan pores, coming in direct contact with its cognate PBP1a (Jean et al. 2014). The mechanisms by which they act on PBP1a and PBP1b remain unclear.

PBP1a and PBP1b essentially have four domains: a single-helix transmembrane domain (TM), a glycosyltransferase domain (GT), a transpeptidase domain (TP) and an additional domain that serves for the interaction with other periplasmic proteins (Sung et al. 2009) (Typas et al. 2010).

The first structure of PBP1b solved to 2.16 Å was reported in 2009 by Sung et al. (Sung et al. 2009) and recently complemented by more detailed model of GT domain by King et al. in which previously missing loop region was traced (figure 1.11a) (King et al. 2017). The protein is anchored to the inner membrane by a 30 residue TM domain (residues 66-96). Residues 83-88 are predominantly hydrophobic and situated close to the GT domain, possibly interacting with it.

The GT domain is highly similar to previously reported GT domain structures of *S. aureus* and *Aquifex aeolicus* (Lovering et al. 2007; Yuan et al. 2008). It is predominantly  $\alpha$ -helical and composed of a globular “head” region and smaller “jaw” positioned below the head, in very close contact with the membrane (figure 1.11c). The active site is located in the shallow groove between these two regions. The TP domain has a typical penicilloyl-serine transferase fold of two subdomains, one five-stranded antiparallel  $\beta$ -sheet flanked by three  $\alpha$ -helices on one side and another completely  $\alpha$ -helical. The active site is located at the interface of these two subdomains with three conserved motifs (figure 1.11b) (SxxK, SxN and KTGT) (Sauvage et al. 2008).

Between GT and TP domains there is a smaller, PBP1b-specific domain folded into five-stranded  $\beta$ -sheet with one  $\alpha$ -helix, in close contact with the TP domain. Structurally it is homologous to a domain from UvrB, a component of the nucleotide excision repair (NER) system in DNA damage repairs, which is why it was named UvrB Domain 2 homolog (UB2H). It was later determined that PBP1b and its activator LpoB are in contact through the UB2H domain of PBP1b (Typas et al. 2010).

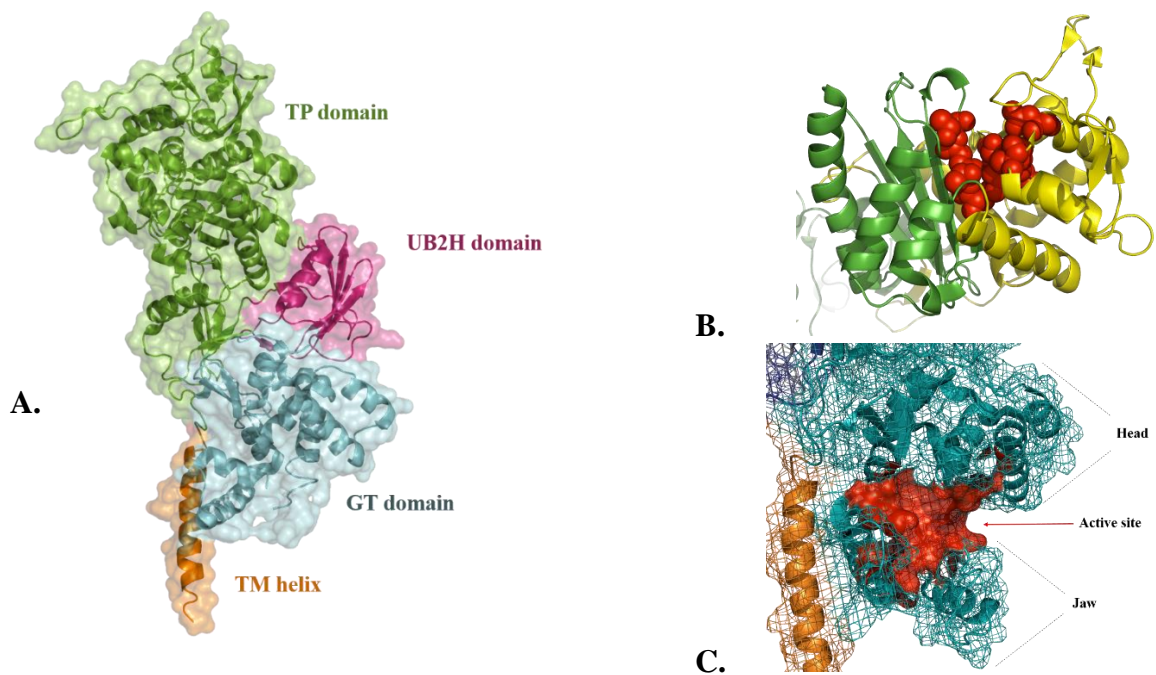


**Figure 1.11.** Structure of PBP1b (PDB: 5HLB). A – Domain organization; B – Catalytic residues of the TP domain (red spheres) are at the interface of the two subdomains (in green and yellow). TP domain. C – Active site of the GT domain is in the cleft between “head” and “jaw” regions.

### 1.13. Penicillin-binding protein 1c

As already mentioned, PBP1c is the third member of the class A PBPs and very little information on its role is available. It was discovered later than the other HMW PBPs as it required special penicillin derivatives to be labeled. Only after application of  $^{125}\text{I}$ -labeled latamoxef or  $^{125}\text{I}$ -labeled Bolton and Hunter derivative of ampicillin, PBP1c was observed as a band between PBP1b and PBP2 (Schwarz et al. 1981)(Labia et al. 1985). This protein, encoded by the *pbpc* gene, is 770-residues long, with 85 kDa, and it is anchored to the inner membrane. In 1999, it shortly drew attention of Holtje et al. after they discovered that PBP1c was specifically eluted from a MltA-Sepharose column together with PBP1b, PBP2 and PBP3 from the crude cell extract (Vollmer et al. 1999). Initial biochemical characterization showed that PBP1c has high glycosyltransferase activity, with no transpeptidase activity reported (Schiffer & Höltje 1999). Deletion of the *pbpc* gene did not show any physiological effect or altered peptidoglycan structure. In addition, in the strains with inactivated PBP1a and PBP1b, overexpression of PBP1c could not compensate for the lack of the other two, eventually leading to cell death.

## AIMS OF THE PROJECT

The discovery of  $\alpha 2M$  in bacteria was a surprising fact that brought plenty of questions. The fact that bacterial genomes conserved the sequence of such a large protein that would be energetically expensive to produce indicates that it provides advantage to bacteria during their life cycle. As a protease inhibitor localized in periplasm, it is reasonable to believe that it protects the periplasmic space from host proteases during infection. Finding the  $\alpha 2M$  gene in an operon juxtaposed to the gene of the poorly characterized, efficient transglycosylase PBP1c led to hypothesis that these two proteins form an uncharacterized defense complex that could protect the integrity of periplasm. During infection or during microbial competition events, the outer membrane could be breached, allowing the molecules of the host defense system to penetrate into the periplasm and damage the peptidoglycan. In such scenario,  $\alpha 2M$  and PBP1c could function as complex in which PBP1c could rapidly repair peptidoglycan, while  $\alpha 2M$  could protect PBP1c and other periplasmic proteins from proteolysis.

The main goal of this project was to demonstrate the existence of such complex and characterize this interaction structurally and functionally. A deeper understanding of the interaction between  $\alpha 2M$  and PBP1c could provide the basis for developing novel strategies to combat bacterial infections.

For this purpose, we chose to work with  $\alpha 2M$  and PBP1c from *E. coli*. Firstly, that required the biophysical characterization of individual proteins. While the protocols for  $\alpha 2M$  studies have largely been established, the study of PBP1c required extensive optimization in the phases of cloning, expression and purification. Once the protocols were set up, the aim was to reconstitute the complex *in vitro* and determine its stoichiometry.

In collaboration with Dr. Waldemar Vollmer's team from Newcastle University, we analyzed the peptidoglycan synthase activity of PBP1c and determined the effects that  $\alpha 2M$  has on its activity.

Finally, for the structural analysis of the complex we employed techniques such as small-angle x-ray scattering (SAXS), electron microscopy and crystallography that were essential for different aspects of the study. This work has allowed for a better understanding of the  $\alpha 2M$ -PBP1c partnership in *E. coli*, which can reflect a yet undescribed link between bacterial immunity and cell wall formation.





## **II**

# **MATERIALS AND METHODS**



## 2.1. PBP1c sequence analysis

The amino acid sequence of PBP1c was obtained from the Uniprot database, entry P76577 (Consortium 2017). The molecular weight, isoelectric point and amino acid composition were determined using the ProtParam tool on the ExPASy server (Gasteiger et al. 2005). The prediction of putative transmembrane helices was done with the TMHMM Server (CBS, Technical University of Denmark), while the search for conserved domains was performed using NCBI's Conserved Domain Database (Krogh et al. 2001; Marchler-Bauer et al. 2015). For the secondary structure prediction, the PSIPRED tool from the Bloomsbury Centre for Bioinformatics was used (Buchan et al. 2013). Multiple sequence alignments were performed with Clustal Omega (Sievers et al. 2011).

## 2.2. Cloning

The genes for ECAM (*yfhM*) and PBP1c (*pbpc*) were cloned from the genome of *E. coli* strain BL21(DE3). The first 18 N-terminal amino acids of ECAM represent the signal peptide for sorting to the inner membrane and the corresponding region on the gene was omitted in the final clone. For the wild-type construct, ECAM<sub>WT</sub>, the fragment of 4911 bp between residues 19-1653 was cloned into the pET15b vector with an N-terminal polyhistidine tag using the restriction cloning method with NdeI and XhoI restriction sites on the N- and C-termini, respectively.

In the case of PBP1c, the full-length 2637 bp *pbpc* gene was amplified using a Biometra thermocycler from Analytik Jena using PfuUltra polymerase. The forward primer 5'-GGGCT CTGCG CATAT GATGC CTCGC TTGTT AACCA AACG-3' had a NdeI restriction site and the reverse primer 5'-GCTCG AATTC GGATC CCTAT TGCAT GACAA ATTTC ACTGT CGCG-3' had a BamHI restriction site. PCR products were cloned using the restriction cloning technique into three different vectors: pET15b with an N-terminal polyhistidine tag, pET30b containing an N-terminal Strep tag and pIVEX 2.4 for cell-free expression with an N-terminal polyhistidine tag.

In the course of the study, numerous additional constructs of the genes originating from *E. coli* and *Salmonella enterica* were tested in the initial phase of the project, all of which were obtained by the restriction cloning approach, with the exception of pGEX4-PBP1c that was purchased from Eurofins Genomics (table 1).

Name of the construct	Source organism	Plasmid	Resistance	Tag
<b><math>\alpha</math>2M constructs</b>				
ECAM <sub>WT</sub>	<i>E. coli</i>	pET15b	amp	His
ECAM <sub>TEV</sub>	<i>E. coli</i>	pET15b	amp	His
SA-A2M <sub>WT</sub>	<i>S. enterica</i>	pET28a	kan	His
SA-A2M <sub>TEV</sub>	<i>S. enterica</i>	pET28a	kan	His
<b>PBP1c constructs</b>				
His-PBP1c	<i>E. coli</i>	pET15b	amp	His
Strep-PBP1c	<i>E. coli</i>	pET30b	kan	Strep
Cf-PBP1c	<i>E. coli</i>	pIVEX2.4	amp	His
PBP1c <sub><math>\Delta</math>TM</sub>	<i>E. coli</i>	pET30b	kan	His
PBP1c <sub><math>\Delta</math>TM</sub>	<i>S. enterica</i>	pGEX-4	amp	GST
PBP1c <sub><math>\Delta</math>TM</sub>	<i>S. enterica</i>	pET30b	kan	Strep
PBP1c <sub><math>\Delta</math>TM/Cter</sub>	<i>S. enterica</i>	pGEX-4	amp	GST
PBP1c <sub><math>\Delta</math>TM/Cter</sub>	<i>S. enterica</i>	pET30b	kan	Strep
PBP1c <sub>PEL</sub>	<i>S. enterica</i>	pET22b	amp	His

WT – wild-type; TEV – Tev bait site; FL – full-length;  $\Delta$ TM – without transmembrane helix;  $\Delta$ TM/Cter – without transmembrane helix and C-terminal domain

**Table 2.1.** List of the constructs of  $\alpha$ 2M and PBP1c created and tested.

### 2.3. Protein expression and purification

**Expression and purification of ECAM.** For the expression of ECAM, *E. coli* strain BL21(DE3) was used. The cells transformed with plasmid pET15b-ECAM<sub>WT</sub> were grown in Terrific Broth at 37 °C and induced with 1 mM IPTG at an OD<sub>600</sub> = 0.8 AU. The cells were further grown at 37 °C for 3 hours after induction, harvested and resuspended in 50 mM Tris pH 8, 300 mM NaCl and 25 mM imidazole buffer containing protease inhibitors.

The cells were lysed using a microfluidizer in three passages applying 15 kpsi of pressure. The lysate was clarified by centrifugation at 18,000 rpm for 1 hour and the supernatant was loaded onto a 5 mL NTA column (Qiagen). The sample was eluted in the same buffer with 500 mM imidazole and dialyzed overnight in a buffer containing 25 mM Tris pH 8. Following dialysis, the sample was applied to Resource Q anion exchange column (GE Healthcare) and eluted with a gradient increase of elution buffer containing 25 mM Tris pH 8 and 1 M NaCl.

The final purification step was size exclusion chromatography on a Superdex 200 (10/300) column (GE Healthcare) in 25 mM Tris pH 8, 500 mM NaCl, 10 mM MgCl<sub>2</sub> and 0.17% n-Decyl-β-D-Maltoside (DM).

***PBP1c expression test:*** For the expression of two full-length PBP1c constructs, His-PBP1c and Strep-PBP1c, three *E. coli* expression strains were tested: BL21(DE3), C41 and C43. Each of them was grown in LB and TB media at 37 °C for 3 hours and at 25 °C overnight in the presence of antibiotics. The expression of PBP1c was detected using Western blotting with HRP-conjugated Anti-His and Anti-Strep antibodies (Covalab).

***PBP1c solubility test:*** A 500 mL culture of *E. coli* C41 cells transformed with the His-PBP1c plasmid and supplemented with 100 µg/ml of ampicillin was grown at 37 °C until OD<sub>600</sub> = 0.9 AU. The expression was induced with 1 mM IPTG and cells were grown at 37 °C for 3 hours. The cells were resuspended in 50 mM Tris pH 8, 300 mM NaCl and 10 mM MgCl<sub>2</sub> and lysed in six passes through a microfluidizer at 15 kpsi.

Cell debris and unbroken cells were removed by a short 10-minute centrifugation at 10,000 rpm and the membranes from the supernatant were pelleted by additional centrifugation in a Beckman ultracentrifuge for 1 hour at 40,000 rpm in a Ti45 rotor. Membranes were resuspended in 110 mL of 50 mM Tris pH 8, 300 mM NaCl and 10 mM MgCl<sub>2</sub>. Resuspended membranes were subsequently divided into 11 Falcon tubes of 10 mL each, and 11 different detergents were added (table 2) at a concentration of 1% and incubated for 2 hours on rotating wheel on 4 °C. Soluble fractions were obtained by another round of ultracentrifugation for 1 hour.

DETERGENT	Critical micellar concentration (CMC) mM (%)	Micellar size (kDa)
<b>CHAPS</b>	8 (0.49)	6
<b>Triton X-100</b>	0.23 (0.015)	49-107
<b>DM</b> ( <i>n-decyl-β-D-maltopyranoside</i> )	1.8 (0.087)	33
<b>DDM</b> ( <i>n-dodecyl-β-D-maltopyranoside</i> )	0.17 (0.0087)	40-76
<b>LAPAO</b> ( <i>3-laurylamido-N,N'-dimethylpropyl amine oxide</i> )	1.56 (0.052)	
<b>LDAO</b> ( <i>lauryldimethylamine-N-Oxide</i> )	2 (0.023)	17-21.5
<b>OG</b> ( <i>n-octyl-β-D-glucopyranoside</i> )	18 (0.53)	23
<b>DMNG</b> ( <i>decyl maltose neopentyl glycol</i> )	0.036 (0.0034)	
<b>LMNG</b> ( <i>lauryl maltose neopentyl glycol</i> )	0.01 (0.001)	
<b>Fos-choline-12</b>	1.5 (0.047)	18-21
<b>Sarkosyl</b>	14.4 (0.42)	

**Table 2.2.** List of detergents used in the solubility test

**Expression and purification of PBP1c.** *E. coli* C41 cells were transformed with pET15b-PBP1c and grown in LB medium supplemented with 100 µg/ml of ampicillin at 37 °C until OD<sub>600</sub> = 0.9 AU. Expression was induced with 1 mM IPTG and cells were grown at 25 °C until OD<sub>600</sub> = 4 AU. The cells were resuspended in 50 mM Tris pH 8, 500 mM NaCl, 10 mM MgCl<sub>2</sub> and 25 mM imidazole and lysed, in the presence of protease inhibitors, by passing through a microfluidizer six times at 15 kpsi.

Cell debris and unbroken cells were removed by a short 10-minute centrifugation step at 10,000 rpm and the membranes from the supernatant were pelleted by additional centrifugation in a Beckman ultracentrifuge for 1 hour at 40,000 rpm using a Ti45 rotor. Membranes were

solubilized in 50 mM Tris pH 8, 500 mM NaCl, 10 mM MgCl<sub>2</sub> and 25 mM imidazole with the addition of 1% of DM for 2 hours at 4 °C. The unsolubilized fraction was removed by another run of ultracentrifugation at 40,000 rpm for 1 hour in a Ti70 rotor. The supernatant was diluted with the solubilization buffer, without detergent in order to decrease the DM concentration to 0.25% and loaded onto NiNTA column (Qiagen) in a loop overnight at 4 °C. The unbound sample was removed by washing the column with 10 column volumes of 50 mM Tris pH 8, 500 mM NaCl, 10 mM MgCl<sub>2</sub>, 25 mM imidazole and 0.17% DM. The sample was subsequently eluted in the same buffer with 250 mM imidazole. The sample was finally purified by gel filtration with a Superdex 200 (10/300) column (GE Healthcare).

***Complex reconstitution.*** Purified ECAM and PBP1c were mixed in a molar ratio of 1:2 and incubated for 2 hours at 4 °C. The sample was injected in a Superdex 200 (10/300) column to separate the complex fraction from unreacted individual proteins.

***Cell-free expression and purification of PBP1c.*** The initial expression and solubilization trials were performed by Lionel Imbert at the cell-free expression platform at the IBS. The expression of His-tagged PBP1c from the pIVEX2.4 vector was tested in a 50 µl batch setup with shaking at 30 °C or 23 °C using an S30 LI12F *E. coli* extract. The cell-free reaction mix was clarified by centrifugation at 14,000 rpm for 20 minutes. The samples for soluble and pellet fractions were loaded on SDS-PAGE, transferred to a nitrocellulose membrane and visualized by Western blotting. For the solubilization trial, three different detergents were tested: Brij 35, DDM and Brij 58, all three of them in concentrations of 10 and 50 x CMC.

For the large-scale purifications, the dialysis method of expression was used in which the 3 mL dialysis tube with the reaction mixture was placed in a Falcon tube containing 30 mL of feeding mix and incubated overnight at room temperature on a rotating wheel. The compositions of the reaction and feeding mixes are shown in table 3.

## **2.4. Electrophoresis**

Sample analyses with denaturing gel electrophoresis were performed with 10% acrylamide (29/1) running gels containing 0.1% SDS. The 5X stock solution of the sample buffer was composed of 250 mM Tris·HCl, pH 6.8, 10% SDS, 30% (v/v) Glycerol, 10 mM DTT, 0.05%

(w/v) Bromophenol Blue. PageRuler Prestained (10-180 kDa) and PageRuler Unstained (10-200 kDa) protein ladders from ThermoFisher were used as references. Gels were stained with Coomassie brilliant blue R-250.

<b>Components</b>	<b>Concentration</b>
water soluble amino acids	1 mM
acid soluble amino acids	1 mM
base soluble amino acids	1 mM
rCTP	0.8 mM
rGTP	0.8 mM
rUTP	0.8 mM
HEPES pH 7.5	55 mM
ATP	1.2 mM
Folinic Acid	68 $\mu$ M
Cyclic AMP	0.64 mM
DTT	3.4 mM
Spermidine	2 mM
NH <sub>4</sub> OAc	27.5 mM
Creatine phosphate	80 mM
KGlu	208 mM
Mg(OAc) <sub>2</sub>	12 mM / 6.4 mM*
tRNA **	0.175 mg/mL
Creatine kinase **	250 $\mu$ g/mL
T7 RNA polymerase **	1/100e
vector **	16 $\mu$ g/mL
Brij 35	0.4%
<b>S30 extract **</b>	1200 $\mu$ L in 3000 $\mu$ L reaction mix

\* Concentrations in the reaction mix / feeding mix

\*\* Components not present in the feeding mix

**Table 2.3.** Components and concentrations of the reaction and feeding mixes for cell-free expression of PBP1c. The volume of the reaction mix was 3 mL, while the volume of the feeding mix was 30 mL.

## 2.5. Western blotting

Proteins were separated by SDS-PAGE, followed by transfer onto a nitrocellulose membrane for 100 minutes at 300 W in transfer buffer containing 25 mM Tris and 190 mM glycine. The membranes were blocked with 3% BSA in PBS buffer pH 7 for 1 hour at 42 °C and subsequently incubated with HRP-conjugated Anti-His antibodies (Covalab) in a PBS buffer supplied with 1% BSA and 0.02% Tween-20. Membranes were developed using SIGMAFAST DAB tablets with metal enhancer.

## 2.6. Mass spectrometry

The quality of the sample was assessed by mass spectrometry using the Matrix-assisted Laser Desorption/Ionization Time of Flight (MALDI-TOF) approach and carried out on the Mass Spectrometry Platform at the IBS with the assistance of Elisabetta Boeri Erba.

In the MALDI approach, an analyte is mixed with a saturated matrix solution that crystallizes after drying, incorporating the analyte into the crystals. The laser beam is directed to the matrix and the energy of the beam is absorbed by the matrix, causing ablation. It is believed that during this process, the matrix transfers a proton charge to the analyte. Charged particles enter the TOF spectrometer where they are accelerated by applying the electrical field and directed to a detector. The time necessary for the particles to reach the detector, i.e. particle velocity depends on the mass-to-charge ratio, enabling ion identification (Hillenkamp & Karas 2007).

The analysis was conducted in an Autoflex MALDI-TOF instrument (Bruker Daltonics) with a mass range up of to 500 kDa in linear mode and resolving power up to 20,000 in reflectron mode. ECAM was prepared in a buffer containing 25 mM Tris pH8 and 50 mM NaCl, while PBP1c was prepared in a buffer with 100 mM Tris pH 8, 150 mM NaCl and 0.17% DM, the protein concentration of both being 10  $\mu$ M.

Thin layers of saturated  $\alpha$ -cyano-4-hydroxycinnamic acid ( $\alpha$ -CHCA) in acetone were spotted on a MALDI-TOF target plate (Bruker Daltonics) to prepare thin layers. Different dilutions of the proteins in 5% formic acid solution were prepared (1:5, 1:4, 1:3 and 1:2) and deposited on the thin layers by application of 0.5  $\mu$ L. Subsequently, the matrix solution was added to the sample. Two different matrices were tested: 1:1 mixture of  $\alpha$ -CHCA and 2,5-

dihydroxybenzoic acid (DHB) solutions and sinapinic acid (SA) solution, making in total 8 spots for each protein (Signor & Erba 2013).

The target plate with dried samples was inserted in the instrument and sample spectra were acquired using the positive-ion mode with pulsed ion extraction. The instrument was calibrated with BSA. Up to 1,000 shots per sample were executed with laser intensity between 30-35%. Data were collected with the Flex Control software.

## **2.7. Analytical ultracentrifugation (AUC) and SEC-MALS**

For characterization of the oligomeric state of ECAM, PBP1c and the ECAM-PBP1c complex samples, samples were analyzed by analytical ultracentrifugation (AUC) and size exclusion chromatography with multi-angle light scattering (SEC-MALS).

**Analytical ultracentrifugation.** This method is based on the principle of redistribution of the mass in a gravitational field until the potential energy of the field balances the chemical potential energy in each radial position (Cole et al. 2008). In ultracentrifugation, an inertial centrifugal force created by rotor spinning accelerates particle sedimentation. The particles form a sedimenting boundary that migrates away from the center of the rotor. Following the velocity of migration of the sedimenting boundary yields the sedimentation coefficient of the particles that is directly connected to their size and shape (Dam & Schuck 2004).

In practice, this is performed in a special rotor for analytical ultracentrifugation with holes for monitoring the sample (figure 2.1). The sample cells that are placed in the rotor contain a centerpiece with the sample sealed between windows that allow the passage of light. The radial concentration distribution (sedimenting boundary) is followed using absorbance and interference detectors at specific time intervals, yielding “scans”, curves that represent concentration distribution as a function of time at specific values of radius. The scans are subtracted in pairs to approximate the time derivative that is thereafter used to obtain the apparent sedimentation coefficient (Cole et al. 2008; Dam & Schuck 2004; Stafford 1992).

The sedimentation velocity experiment was performed on the Analytical Ultracentrifugation Platform at the IBS by Aline Leroy and Christine Ebel.

The samples were analyzed in a buffer containing 25 mM Tris pH 8, 300 mM NaCl, 10 mM MgCl<sub>2</sub> and 0.17% of DM. Two concentrations of both ECAM and PBP1c were analyzed, 1 mg/mL and 2 mg/mL. For the ECAM-PBP1c complex, three samples were prepared in molar ratios of 1:1, 1:2 and 1:3.

The experiment was performed at 35,000 rpm on 4 °C, on an analytical ultracentrifuge XLI in Anti-50 rotor (Beckman Coulter, Palo Alto, USA) with double-sector cells of optical path lengths of 3 and 1.5 mm equipped with sapphire windows (Nanolytics, Potsdam, DE).

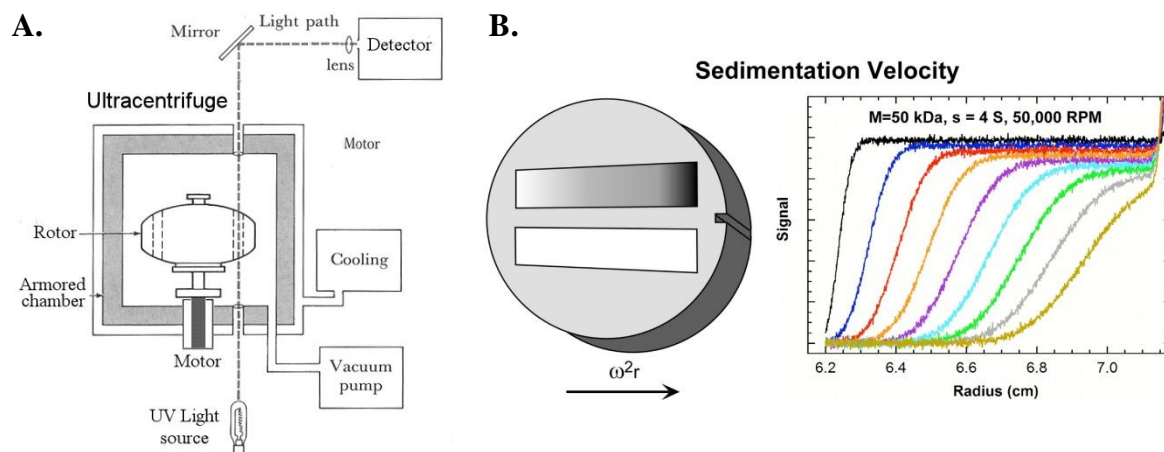


**Figure 2.2.** A – Scheme of an AUC experiment setup. The sample cells are placed in a rotor with holes that allow the passage of the light. The light is recorded by a detector. Adapted from (Freifelder 1983). B – left: a two-sector cell used for sedimentation velocity experiment with a reference solution in white and the analyte in gray; right – the scans recorded at fixed interval during the course of experiment. From (Cole et al. 2008).

For data acquisition, absorbance at 280 nm and optical interference were recorded. The reference was the sample buffer without detergent. Data processing was done with Redate software v0.2.1, while data analysis was performed with SEDFIT version 15.01b and Gussi 1.2.1. The sedimentation coefficient  $S_{20w}$  for the protein-detergent complex was calculated using a mean  $\bar{v}$  value corresponding to 1 g/g of bound detergent.

**SEC-MALS.** In addition to analytical ultracentrifugation, samples were analyzed in a SEC-MALS experiment on the Biophysical Platform at the CIBB, Grenoble by Caroline Mas.

Size-exclusion chromatography coupled with multi-angle light scattering is a technique used to measure the molecular weight of proteins based on the intensity of the light scattered by the molecule. Since proteins are large molecules, a factor called angular dependence affects the intensity of the scattered light, and consequently the calculated molecular weight. In a SEC-MALS experiment, a sample is injected into a gel filtration column that is coupled with a MALS detector (figure 2.3). The MALS detector collects scattered light at many angles and these data are used to model the angular dependence (Striegel et al. 2009).

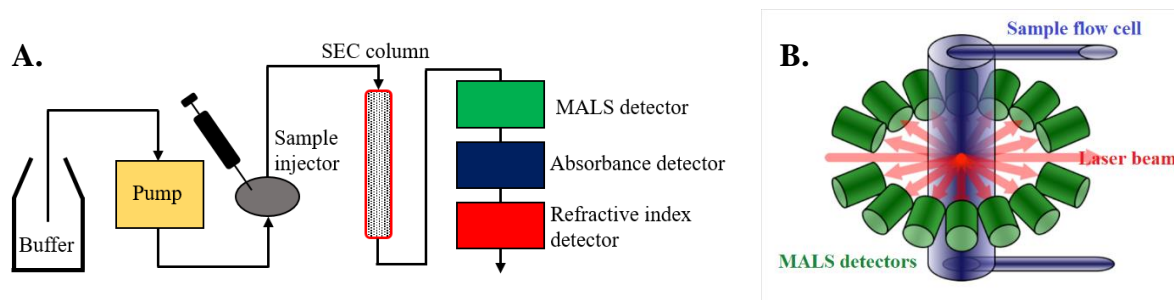


**Figure 2.3.** A – Scheme of a SEC-MALS experiment setup. The sample is injected into a SEC column which is connected to MALS, absorbance and refractive index detectors. B – Inside a MALS detector, sample passes through a flow cell (blue), where it is illuminated by the light beam. The scattered light is recorded at many angles and data are used for molecular weight calculations. B) taken From (Pothecary 2014).

The samples were prepared in the same buffer used for the AUC experiments at a concentration of 3 mg/mL. 55  $\mu$ L of each sample were injected into a Superdex 200 size-exclusion column.

The instrument set-up included Dawn Heleos II MALS detector (Wyatt), Optilab T-rEX differential refractive index (dRI) detector (Wyatt), Hitachi LaChrom L-2400 UV detector and Hitachi LaChrom L-2130 pump. Data were analyzed with the ASTRA 6.0.5.3 software.

Sample	Mw (kDa)	V bar (mL/g)	dn/dc (mL/g)	Eps ( $L \cdot g^{-1} \cdot cm^{-1}$ )
ECAM	182	0.729	0.189	1.292
PBP1c	87.4	0.732	0.191	1.973
DM	0.483	0.82	0.147	
ECAM-DM		0.775		
PBP1c-DM		0.776		
ECAM-PBP1c-DM		0.76		

**Table 2.4.** Parameters of samples used in the sedimentation velocity and SEC-MALS experiments.

## 2.8. Thermal shift assay

Thermal stability of PBP1c was analyzed on a Prometheus NT.48 instrument (NanoTemper Technologies GmbH, DE) using a label-free method in which protein denaturation is followed by changes in tryptophan fluorescence intensity. Tryptophan emission is recorded at two wavelengths, 300 and 350 nm (figure 2.4a). The first derivative of the 300/350 nm ratio is plotted against the temperature yielding a melting curve from which the thermal unfolding transition midpoint  $T_m$  ( $^{\circ}\text{C}$ ) is determined. This is the temperature at which half of the protein population is unfolded. In parallel, the instrument also follows the scattering of light, giving insight into the formation of aggregates during the course of experiment which is used for assessing protein stability (figure 2.4b) (<https://nanotempertech.com/prometheus/>) (Matthias Haffke et al. 2016).

Purified PBP1c was incubated in different buffers (table 2.5) for 30 minutes prior to the experiment. Standard Prometheus NT.48 capillaries were each filled with approximately 20  $\mu\text{L}$  of each sample and loaded onto the instrument. A temperature range between 15  $^{\circ}\text{C}$  and 95  $^{\circ}\text{C}$  was tested with the temperature increasing 1  $^{\circ}\text{C}$  per minute. The data were analyzed using the PR.ThermControl v2.0.4 software.

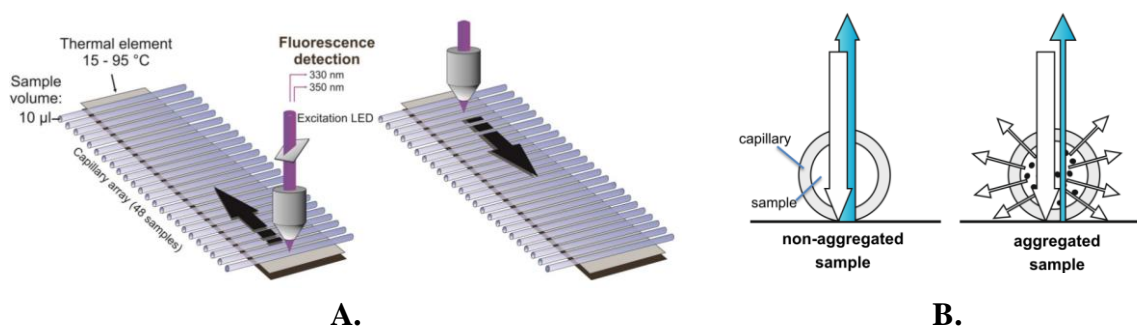


**Figure 2.4.** A – Design of a Prometheus instrument for protein stability assays. Capillaries are filled with samples and placed on a capillary array inside the instrument, where they are illuminated by light. Tryptophan fluorescence is followed at 330 and 350 nm. The first derivative of the 330/350 ratio determines the melting point temperature ( $T_m$ ) of a protein. B – In parallel, back reflection optics monitors scattering that appears when the sample starts to aggregate. This allows the determination of the onset temperature for aggregation.

1	25 mM Tris pH 8, 300 mM NaCl, 10 mM MgCl <sub>2</sub> , 0.17% DM
2	25 mM Tris pH 8, 300 mM NaCl, 10 mM MgCl <sub>2</sub> , 0.5% NM
3	25 mM Tris pH 8, 300 mM NaCl, 10 mM MgCl <sub>2</sub> , 1% OG
4	25 mM Tris pH 8, 300 mM NaCl, 10 mM MgCl <sub>2</sub> , 0.017% DDM
5	25 mM Tris pH 8, 300 mM NaCl, 10 mM MgCl <sub>2</sub> , 0.0065% DMNP
6	25 mM Tris pH 8, 300 mM NaCl, 10 mM MgCl <sub>2</sub> , 0.002% LMNP
7	25 mM Tris pH 8, 300 mM NaCl, 10 mM MgCl <sub>2</sub> , 0.05% LDAO
8	25 mM Tris pH 8, 300 mM NaCl, 10 mM MgCl <sub>2</sub> , 0.1% Fos-choline-12
9	25 mM Tris pH 8, 300 mM NaCl, 10 mM MgCl <sub>2</sub> , 0.15% LAPAO
10	25 mM Tris pH 8, 300 mM NaCl, 10 mM MgCl <sub>2</sub> , no detergent
11	25 mM Tris pH 8, 300 mM NaCl, 10 mM MgCl <sub>2</sub> , 0.17% DM, 5% glycerol
12	25 mM Tris pH 8, 300 mM NaCl, 10 mM MgCl <sub>2</sub> , 0.17% DM, 5 mM β-met
13	25 mM Tris pH 8, 300 mM NaCl, 0.17% DM
14	25 mM Tris pH 8, 500 mM NaCl, 10 mM MgCl <sub>2</sub> , 0.17% DM
15	25 mM Tris pH 8, 1 M NaCl, 10 mM MgCl <sub>2</sub> , 0.17% DM
16	25 mM Tris pH 8, 300 mM KCl, 10 mM MgCl <sub>2</sub> , 0.17% DM
17	100 mM MES pH 6, 300 mM NaCl, 10 mM MgCl <sub>2</sub> , 0.17% DM
18	100 mM HEPES pH 7, 300 mM NaCl, 10 mM MgCl <sub>2</sub> , 0.17% DM
19	100 mM BisTris pH 9, 300 mM NaCl, 10 mM MgCl <sub>2</sub> , 0.17% DM
20	100 mM CAPS pH 10, 300 mM NaCl, 10 mM MgCl <sub>2</sub> , 0.17% DM
21	25 mM Tris pH 8, 500 mM NaCl, 10 mM MgCl <sub>2</sub> , 0.17% DM, 1% glycerol
22	25 mM Tris pH 8, 500 mM NaCl, 10 mM MgCl <sub>2</sub> , 0.17% DM, 5% glycerol
23	25 mM Tris pH 8, 500 mM NaCl, 10 mM MgCl <sub>2</sub> , 0.17% DM, 10% glycerol
24	25 mM Tris pH 8, 500 mM NaCl, 10 mM MgCl <sub>2</sub> , 0.17% DM, 20 mM KCl
25	25 mM Tris pH 8, 500 mM NaCl, 10 mM MgCl <sub>2</sub> , 0.17% DM, 50 mM KCl
26	25 mM Tris pH 8, 500 mM NaCl, 10 mM MgCl <sub>2</sub> , 0.17% DM, 2.5 mM β-met
27	25 mM Tris pH 8, 500 mM NaCl, 10 mM MgCl <sub>2</sub> , 0.17% DM, 5 mM β-met
28	25 mM Tris pH 8, 500 mM NaCl, 10 mM MgCl <sub>2</sub> , 0.17% DM, 100 μM moenomycin
29	25 mM Tris pH 8, 500 mM NaCl, 10 mM MgCl <sub>2</sub> , 0.17% DM, Ni
30	25 mM Tris pH 8, 500 mM NaCl, 10 mM MgCl <sub>2</sub> , 0.17% DM, Zn
31	25 mM Tris pH 8, 500 mM NaCl, 10 mM MgCl <sub>2</sub> , 0.17% DM, Fe

**Table 2.5.** Different buffers used for thermal stability analyses of PBP1c

## 2.9. The PBP1c activity test

The enzymatic activity of PBP1c was tested by Victor Hernandez Rocamora in the laboratory of Dr. Waldemar Vollmer at The Centre for Bacterial Cell Biology, Newcastle University.

First, the  $\beta$ -lactam binding ability of PBP1c was tested by labeling with biotinylated ampicillin and fluorescent Bocillin FL. The protein was incubated with ampicillin or Bocillin FL for 10 minutes at 30 °C and loaded on a denaturing 10% polyacrylamide gel. For visualization of ampicillin-labeled PBP1c the protein was transferred from the gel to a nitrocellulose membrane which was blocked and visualized with a streptavidin-peroxidase conjugate used at 1:10,000 dilution. Visualization of the Bocillin-labeled PBP1c was done by scanning with FluorImager 595 (Molecular Dynamics), with excitation at 488 nm and emission at 530 nm.

The GTase and TPase activities of PBP1c were tested using radioactive and fluorescent Lipid II. PBP1c and ECAM were prepared in 10 mM HEPES pH 7.5, 100-200 mM NaCl, 10 mM MgCl<sub>2</sub> and 0.05% DDM in the concentration of 2  $\mu$ M. For the experiments with radioactive Lipid II, activity was tested in the absence and presence of peptidoglycan. Proteins were incubated with Lipid II alone for 2 hours at 37 °C and with Lipid II in the presence of peptidoglycan for 3 hours at 37 °C, followed by boiling to inactivate PBP1c and cellosyl digestion. Cellosyl is a muramidase that cleaves the  $\beta$ -(1,4) glycosidic bond between MurNAc and GluNAc, producing muropeptides (Bräu et al. 1991). Prior to HPLC analysis, a step of the MurNAc reduction to NAc-muraminitol by sodium borohydride is performed to prevent mutarotation, which could result in double peaks.

Experiments with fluorescent Lipid II-atto550 were performed for PBP1c alone and for the PBP1c-ECAM complex, examining the impact of ampicillin and glycerol on the activity of PBP1c. Samples were incubated with the mixture of 12.5  $\mu$ M Lipid II and 2.5  $\mu$ M fluorescent Lipid II-atto550. In the ampicillin experiment, the samples with 1 mM ampicillin, and samples without ampicillin were incubated for 60 minutes at 37 °C and aliquots were taken at 0, 5, 10, 20, 40 and 60 minutes. In the glycerol experiment, both samples with 2% glycerol, and samples in the absence of glycerol were incubated for 2 hours and aliquots were taken at 0, 5, 10, 20, 40, 60 and 120 minutes. The reaction products were separated on a gel that was scanned and the scans were analyzed with ImageJ.

## 2.10. Small-Angle X-ray Scattering (SAXS)

SAXS is a method used for structural characterization of proteins in solution in which a collimated, monochromatic beam of X-rays illuminates the sample and the intensities of the scattered X-rays are recorded by an X-ray detector (Kikhney & Svergun 2015; Putnam et al. 2007). Scattering of solvent is also measured and subtracted from the sample solution scattering in order to obtain the scattering signal coming only from the randomly oriented particles in solution. This signal is an average of the scattering from all possible orientations. Scattering patterns recorded by two-dimensional detectors are transformed into one-dimensional curves that represent the scattering intensity  $I$  as a function of momentum transfer  $q = 4\pi\sin\frac{\theta}{\lambda}$ , where  $\lambda$  is the beam wavelength and  $2\theta$  is the scattering angle. Depending on the way the scattering data are analyzed, it is possible to obtain important structural information about the protein in the solution, such as radius of gyration ( $R_g$ ), maximum intraparticle distance ( $D_{max}$ ), flexibility, foldedness, molecular mass and overall 3D shape (Kikhney & Svergun 2015; Skou et al. 2014).

The samples were prepared according to the protocol described in 2.1 with the addition of 5% glycerol. Scattering data for PBP1c were collected the samples eluting at the middle and at the rear end of the peak from a size exclusion chromatography column, at the concentrations of 2.64 and 1.1 mg/mL. Samples from each fraction were tested in the presence and absence of 10  $\mu$ M moenomycin. ECAM was prepared at three different concentrations: 0.5, 1.5 and 3 mg/mL. The 4 ECAM-PBP1c complex samples that were tested were obtained from two preparations: one performed as previously described, and the second one to which 10  $\mu$ M moenomycin were added. The buffer in which the complex samples were prepared did not contain glycerol, since it was previously noticed that it interferes with the complex formation.

SAXS measurements were performed at the BM29 beamline of the European Synchrotron Radiation Facility (ESRF), Grenoble. X-ray scattering was recorded on the Pilatus 1M detector. Bovine serum albumin at a concentration of 4 mg/mL was measured for calibration. Ten 1-second exposure frames were collected at 20 °C for each 50  $\mu$ L sample in flow-mode (Pernot et al. 2013). Between measurements, scattering from a buffer sample was recorded, and these data were subsequently subtracted from the sample curves. Data were treated following default parameters of the PRIMUS software package (Konarev et al. 2003). The radius of gyration  $R_g$  and the forward scattering value  $I(0)$  were estimated using the Guinier approximation. Both parameters, as well the maximum particle dimension  $D_{max}$ , were also calculated by the

GNOM software (Svergun 1992). *Ab initio* models of ECAM were generated using Damin (Svergun 1999). A final average model was generated from 15 independent models using DAMAVER through their pairwise superposition (Volkov & Svergun 2003). For the molecule fitting, a model of PBP1c was generated using homology modelling by Robetta server (Song et al. 2013). The region between residues 1 and 622 was modelled using the structure of *E. coli* PBP1b as a template (PDB: 3FWL), while the C-terminal part was modelled using CbhA fibronectin(III)-like module from *Clostridium thermocellum* (PDB: 3PDD).

## 2.11. Electron microscopy

Transmission electron microscopy (TEM) is an imaging method used for visualization of objects smaller than 100  $\mu\text{m}$  by illuminating them with an electron beam. Compared to photons used in light microscopy, the wavelength of electrons is substantially shorter providing an electron microscope with a maximum resolution of 0.2 nm. An electron beam is generated by an electron gun containing a source of electrons, accelerated by an anode, focused by electromagnetic lenses and directed to the sample, where electrons are partially scattered. A transmitted beam passes through objective lenses and it is recorded by a detector. The sample is immobilized on carbon-coated mica grids. In order to increase the contrast between the background and the sample, the negative staining technique is routinely used in which the background is stained with a heavy atom solution, leaving the object of interest untouched (Bozzola & Russell 1991).

Negative-staining TEM was performed at the Electron Microscopy Platform at the IBS by Daphna Fenel. The samples were prepared in two different buffers at a concentration of 0.02 mg/mL: 1 – 25 mM sodium citrate pH 4, 500 mM NaCl, 10 mM MgCl<sub>2</sub>, 0.17% DM and 2 - 25 mM Tris pH 8, 500 mM NaCl, 10 mM MgCl<sub>2</sub> and 0.17% DM. They were subsequently applied to the clean side of carbon on mica (carbon/mica interface) and negatively stained with 1% (w/v) uranyl-acetate. The samples were examined with the FEI Tecnai12 microscope operating at 120 kV with an Orius GATAN camera.

## 2.12. Crystallization trials

Screening assays for crystallization conditions of PBP1c alone and the ECAM-PBP1c complex were performed automatically in a high-throughput manner in the HTX lab at the EMBL, Grenoble and manually, using 24-well plates.

For the high-throughput screens, PBP1c and the ECAM-PBP1c complex were purified by the protocol described in 2.1 and concentrated to 4.93 mg/mL and 4.97 mg/mL respectively. The crystallization experiments were performed with a Cartesian PixSys 4200 crystallization robot (Genomic Solutions, UK) at 4 °C using the sitting drop method. PBP1c was tested in two ratios, mixing 100 nL of sample with 100 nL of precipitant (1:1) and 100 nL of sample with 50 nL of precipitant (2:1), while the complex was mixed in standard, 1:1 ratio with precipitant (100 nL of each). Seven different screens were tested: The Classical Suite (Quiagen/Nextal), PEGs-I (Quiagen/Nextal), Wizard I&II (Rigaku Reagents), MemGold, MemGold2, MemStart and MemSys (Molecular Dimensions), 576 different conditions in total.

For the manual screens, both *E. coli* and cell-free expressed and purified PBP1c were used, concentrated to 5.1 and 1.13 mg/mL, respectively. The MemGold2 screen from Molecular Dimensions was tested using 24-well crystallization plates prepared at 4 °C using the hanging drop method. For each condition, protein and precipitant were mixed in 1:1 ratio (2+2  $\mu$ L), while each well contained 1 mL of precipitant.

# **III**

## **RESULTS**



### 3.1. Expression and purification of ECAM

The construct used for expression of ECAM did not have the lipobox sequence, therefore the protein was expressed in the cytosol. BL21(DE3) cells were grown in TB medium at 37 °C and harvested 3 hours after induction, reaching an optical density of approximately 4.5. After nickel affinity chromatography, the SDS-PAGE analysis showed that, apart from the expected band of ECAM that migrated between 150 and 200 kDa, several additional unexpected bands with lower and higher molecular weights were present in the sample. Western blot analysis with Anti-His antibodies confirmed that the lower bands originated from ECAM degradation, while the higher bands represented oligomers, most likely associated by disulfide bonds. All of the contaminating forms were removed by anion exchange chromatography, as confirmed in a subsequent gel filtration step.

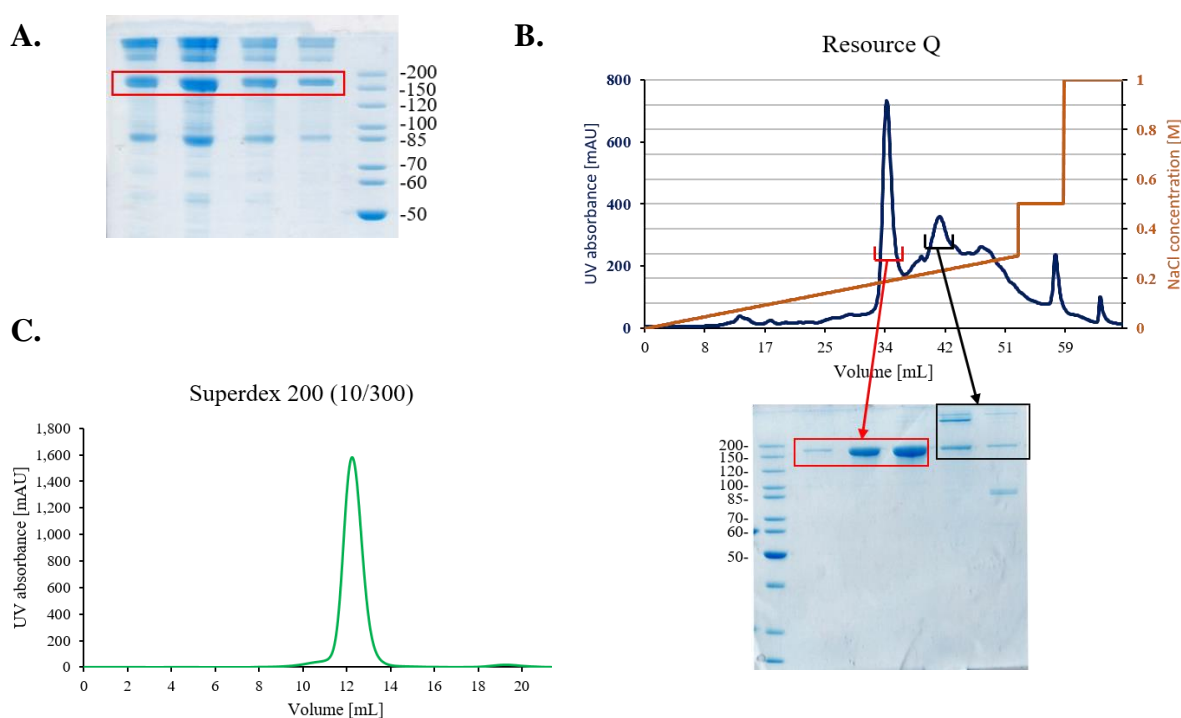


**Figure 3.1.** Purification of ECAM. A – Four elution fractions from nickel affinity column. ECAM form of interest marked in red (full-length); B – Anion exchange chromatography separated monomeric ECAM from other species in the sample. The major peak was pooled and injected into a Superdex 200 (10/300 column) for gel filtration analysis. C – The size-exclusion chromatography profile indicates that ECAM is homogeneous, eluting mostly in a single peak.

SEC-MALS analysis of purified ECAM showed that the sample is monodisperse (figure 3.2). The calculated molecular mass of the protein is  $177.3 \pm 2.2$  kDa, which is in agreement with the theoretical mass (181,62 Da). and it does not bind the detergent. More details regarding these results will be discussed below, in the section describing the ECAM:PBP1c complex.

Analysis of the ECAM sample by MALDI-TOF, performed using the Mass Spectrometry platform at the IBS, determined that the experimental mass of the recombinant protein is equal to 181.45 kDa (histidine-tagged form). The theoretical mass of his<sub>6</sub>-ECAM corresponds to 182.11 kDa (181.98 kDa without the initiator methionine), and thus these results indicate that there is an approximate difference of 665 Da (524 Da without the initiator methionine) between theoretical and measured forms.

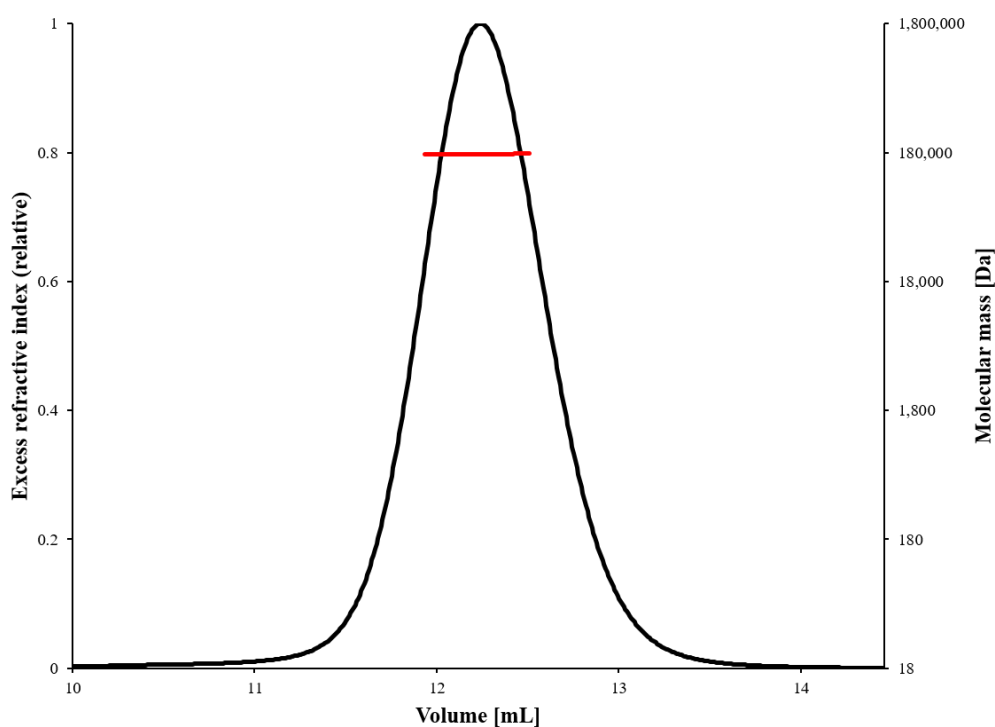


**Figure 3.2.** SEC-MALS analysis of ECAM performed on a Superdex 200 10/30 column. The protein was previously purified by affinity, anion exchange and size exclusion chromatographies. The left ordinate axis represents elution profile monitored by excess refractive index. The calculated molecular mass of the peak was  $177.3 \pm 2.2$  kDa (red bar). The polydispersity index was 1.000 ( $\pm 1.764\%$ ), indicating that the sample was monodisperse.

## 3.2. Purification and characterization of PBP1c

### 3.2.1. Amino acid sequence analysis

The *pbpC* gene encodes a polypeptide chain of PBP1c that is 770 residues long. The predicted molecular mass of the protein is 85 kDa, the third largest among *E. coli* PBPs with theoretical isoelectric point of 9.5, similar to PBP3 and slightly more basic than PBP1b (Table 3.1). It contains 27 tryptophans and 5 cysteines (C10, C586, C600, C645 and C681).

An amino acid sequence alignment of PBP1c with PBP1a showed 184 identical residues and 136 conserved substitutions, while alignment with PBP1b resulted in 168 identical residues and 123 conserved substitutions.

	Gene	Protein	Mw (Da)	pI
<i>Class A</i>	<i>ponA</i>	PBP1a	93,636	6.15
	<i>ponB</i>	PBP1b	94,292	9.10
	<i>pbpC</i>	PBP1c	85,066	9.50
<i>Class B</i>	<i>pbpA</i>	PBP2	70,856	8.80
	<i>ftsI</i>	PBP3	63,877	9.60
<i>Class C</i>	<i>dacB</i>	PBP4	51,798	8.94
	<i>dacA</i>	PBP5	44,443	8.30
	<i>dacC</i>	PBP6	43,608	7.74
	<i>dacD</i>	PBP6b	43,346	6.24
	<i>pbpG</i>	PBP7	33,887	9.94
	<i>Yfew</i>	PBP4b	47,752	7.70
	<i>ampH</i>	AmpH	41,849	9.50

**Table 3.1.** Comparison of molecular weights and isoelectric points of different PBPs from *E. coli*.

Analysis of the PBP1c sequence with the TMHMM server identified a small cytosolic tail containing the first 8 residues and a transmembrane helix between residues 9 and 28, the segment between residues 29 and 770 of the protein being located in the periplasm. A search for putative domains using NCBI's Conserved Domain Database identified 3 domains: a glycosyltransferase (GT) domain (residues 49-226), a transpeptidase (TP) domain (residues 319-560) present in other PBPs, and a third domain at the C-terminus called BiPBP\_C (residues 691-767), which is specific for PBP1c and not present in other PBPs (figure 3.3). Based on the secondary structure prediction using the PSIPRED server, BiPBP\_C is an all- $\beta$  domain composed of 8  $\beta$ -strands.

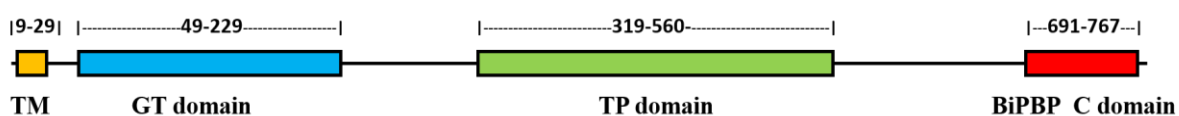


**Figure 3.3.** Domains of PBP1c identified using the TMHMM server and NCBI's Conserved Domain Database (CDD). TM – transmembrane helix; GT – glycosyltransferase; TP – transpeptidase

Individual alignments of the GT and TP domains of PBP1c with the corresponding domains of PBP1a, PBP1b, MgtA and PBP3 revealed significant sequence conservation and the presence of all the signature motifs (figures 3.4 and 3.5). However, the GT domain of PBP1c harbors four mutations in motifs 2, 3 and 5. Most notably, glutamic acid from motif 3, previously demonstrated to be important for the catalytic activity (Terrak et al. 1999), is mutated to glutamine.





**Figure 3.5.** Sequence alignment of transpeptidase domains of PBP1a, PBP1b, PBP1c and PBP3. The residues in red are highly conserved among Penicillin-Binding Proteins (Sauvage et al. 2008).

### 3.2.2. Expression and solubilization

**Expression of PBP1c<sub>ATM</sub>.** The transmembrane helix of PBP1c is a signal sequence for sorting of the protein to the inner membrane (Nilsson et al. 2005; Sakaguchi et al. 1992). The initial approach for the expression and purification of PBP1c was to omit the transmembrane helix in order to overexpress it cytosolically. However, this approach led to the production of highly insoluble protein that could not be solubilized except with the use of strong detergents such as 1% sarkosyl and 1% fos-choline 12. Sarkosyl interfered with the affinity chromatography step and lowering the amount of detergent resulted in heavy precipitation. On the other hand, fos-choline 12 did not show interference with the affinity step, nevertheless it only yielded soluble aggregates. Different tags, cell lines and additives did not increase the solubility of PBP1c. PBP1c has 4 cysteine residues on the C-terminus. The possible effect of inaccurate disulfide bond formation in the reducing cytoplasmic environment was excluded since neither

expression in Shuffle cells, strain engineered to promote correct disulfide bond formation, nor removing the cysteine-containing C-terminus were successful.

The available structures of PBP1b from *E. coli* suggested that the GT domain is embedded in the membrane and that the TM helix may serve to stabilize this interaction (Sung et al. 2009). Since the absence of TM helix caused PBP1c to aggregate in the cytosol, we suspected that the lack of a TM helix destabilized PBP1c and that it is required for proper folding of the protein. For that reason, a full-length gene was cloned in three vectors, His- and Strep-tagged for classical expression in *E. coli* and His-tagged for cell-free expression.

**Expression of PBP1c in *E. coli*.** Two constructs were tested, His-PBP1c (N-terminal His-tagged) and Strep-PBP1c (N-terminal Strep-tagged). In both cases, the protein was not expressed in BL21(DE3) cells under any conditions tested, while it was moderately expressed in C41 and C43 stains (figure 3.6). Furthermore, Strep-PBP1c was expressed only after overnight expression at 25 °C, while His-PBP1c was expressed even after 3 hours at 37 °C. Additionally, the cells that grew overnight in TB medium were lysed, after reaching a plateau in growth.

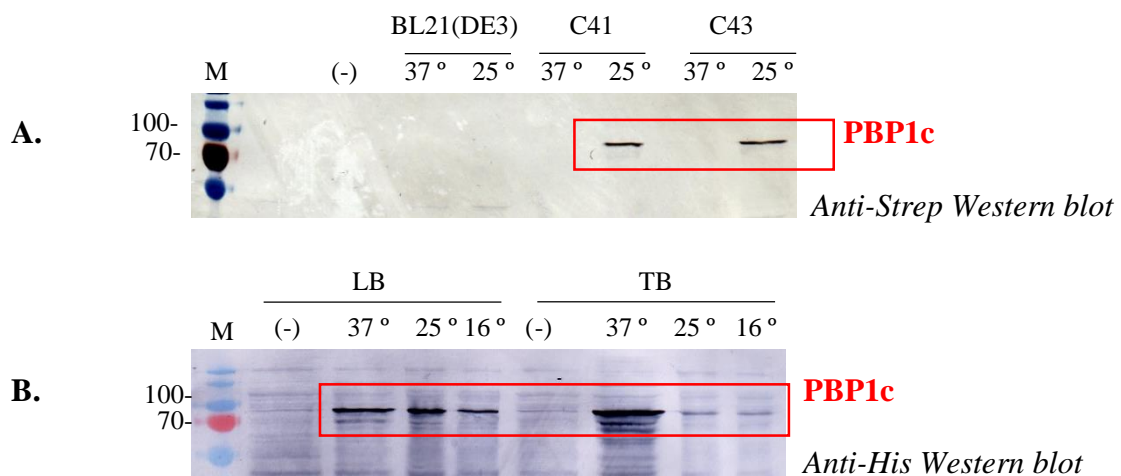


**Figure 3.6. Western blots corresponding to** expression trials of full-length PBP1c. Expression at 37 °C was performed for 3 hours, expression at 25 °C and 16 °C were done overnight. A – blot developed with anti-Strep antibodies indicated that the best conditions were at 25 °C in C41 and C43 cells; B – blot developed with anti-His antibodies indicated that despite the fact that the three temperatures were appropriate while using LB as a medium, only 37 °C could be used for TB. M – molecular ladder (kDa); (-) – uninduced cells; LB – Luria Bertani broth; TB – Terrific broth

**Solubilization of HisPBP1c.** For the solubilization test, 0.5 L of LB culture inoculated with C41 cells transformed with His-PBP1c plasmid were grown on 37 °C for 3 hours after induction with 1 mM IPTG. The cells were harvested, lysed and the membrane fraction was separated from the rest of lysate. Membranes were resuspended in 110 mL of the buffer containing 50 mM Tris pH 8, 300 mM NaCl, 10 mM MgCl<sub>2</sub>. Resuspended membranes were divided in 11 Falcon tubes with 10 mL each, 11 different detergents were added at the concentration of 1% and incubated for 2h. The soluble fractions were subsequently analyzed by Western blotting (figure 3.7).

TritonX-100, DDM and LAPAO were the most efficient when analyzing the total amount of protein in the membranes. On the other hand, in the samples treated with DM, LDAO, OG and sarkosyl, an additional specific high-molecular weight band appeared at around 170 kDa, containing PBP1c (\* in figure 3.7). The band most likely represented dimers of PBP1c that persisted despite denaturing conditions of the SDS-PAGE, since similar observations were for PBP1a and PBP1b (Charpentier et al. 2002; Zijderveld et al. 1991). The studies on PBP1b dimers showed that their formation was not depended on disulfide bonds, since mutants without cysteines were still able to associate (Chalut et al. 1999).

The heterogeneity of TritonX-100 was incompatible with the structural studies planned so its use for purification was ruled out. On the other hand, the efficiency of the nickel affinity column in retention of the protein was impacted by the amount of LAPAO and DDM present in the sample. For that reason, DM was chosen as the solubilizing agent for the large-scale purification of PBP1c.

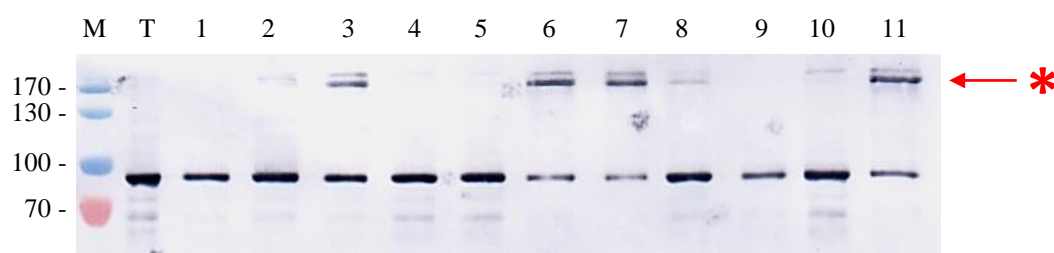


**Figure 3.7.** Western blot corresponding to solubilization trials of PBP1c from *E. coli*, developed with anti-his antibodies. T – total membrane fraction; 1 – CHAPS; 2 – TritonX-100; 3 – DM; 4 – DDM; 5 – LAPAO; 6 – LDAO; 7 – OG; 8 – DMNG; 9 – LMNG; 10 – Fos-choline 12; 11 – Sarkosyl. Detergents were used at a concentration of 1%. Note a higher molecular weight band, indicated with a star, which also lit up and could be suggestive of a dimeric species.

### 3.2.3. Purification of PBP1c

Typically, 4 L of a C41 culture were grown for the large-scale purification, and induction was performed with 1 mM IPTG. Overnight growth resulted in the onset of spontaneous cell lysis that could be due to the high density of the culture or the negative impact of the protein overexpression on the membrane integrity, as suggested by Schiffer and Höltje (Schiffer & Höltje 1999). For that reason, the cells were harvested by centrifugation once they reached the optical density around 4.0, approximately 7-8 hours after induction.

The membrane fraction extracted after the lysis was then treated with a buffer containing DM at a concentration of 1%, which was identified in the experiment described in Figure 3.7. The sample was subsequently loaded onto a nickel affinity column; this step was highly efficient, since little or no PBP1c was present in the flow-through. Elution fractions were highly concentrated, leading to protein precipitation minutes after the elution. Notably, the precipitation of PBP1c was negligible after the removal of imidazole from the sample. Therefore, nickel affinity chromatography was always coupled with immediate preparative gel filtration without previous sample concentration. The purity of the protein on denaturing polyacrylamide gel was high already after the affinity step (figure 3.8 left).

Size-exclusion chromatography yielded a broad peak around the same elution volume as in the case of ECAM (figure 3.8 right). Together with the width of the elution curve, this indicated that the sample may be a mixture of different oligomeric species.

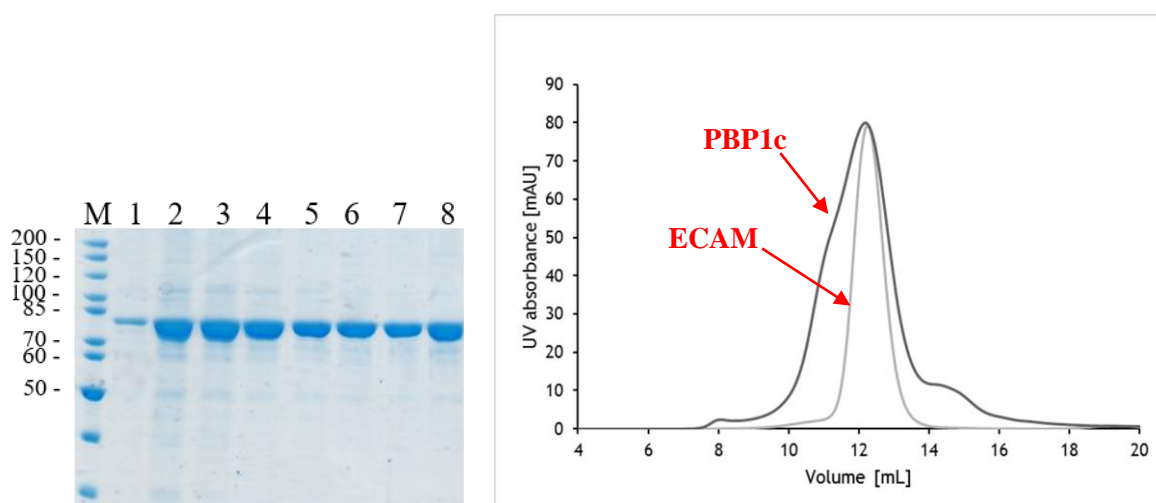


**Figure 3.8.** Left – SDS-PAGE of PBP1c fractions that eluted from a nickel affinity column. Molecular mass markers are shown on the far left. right – comparison of SEC profiles of PBP1c and ECAM. Both proteins eluted at the same peak volume even though the molecular weight of ECAM is approximately twice that of PBP1c. Experiments were performed on a Superdex 200 (10/300) column.

The effects of different buffer components were assessed by analytical gel filtration. As mentioned above, the initial membrane solubilization step was done in a DM concentration of 1%, which is around 11 times its critical micellar concentration (CMC). However, subsequent steps of purification required reduction of the detergent content in the sample. For PBP1c, the concentrations of 4, 2 and 1 CMC were tested. While there was no significant difference in the gel filtration elution profiles when concentrations of 4 and 2 CMC DM were used, decreasing the concentration to 1 CMC clearly resulted in protein aggregation, as the shift of the elution peak towards the void volume of the column showed (figure 3.9a).

When the concentration of NaCl was varied from 300 mM to 1 M, the protein did not show any significant changes in behavior. In the case of a buffer containing 100 mM NaCl, however, PBP1c started to show signs of aggregation since a large peak could be seen near the void volume that is around 1 mL (figure 3.9b). However, the protein precipitation in time was substantially reduced in the presence of 500 mM NaCl. For that reason, all subsequent purifications included 500 mM NaCl in the buffer, instead of initial 300 mM.

Since PBP1c has 4 cysteines, it was conceivable that addition of a reducing agent could aid in its stabilization and prevention of aggregation. However, the addition of  $\beta$ -mercaptoethanol at a concentration of 5 mM did not have any significant effect on the sample (figure 3.9c) and thus further experiments were performed in the absence of this component.

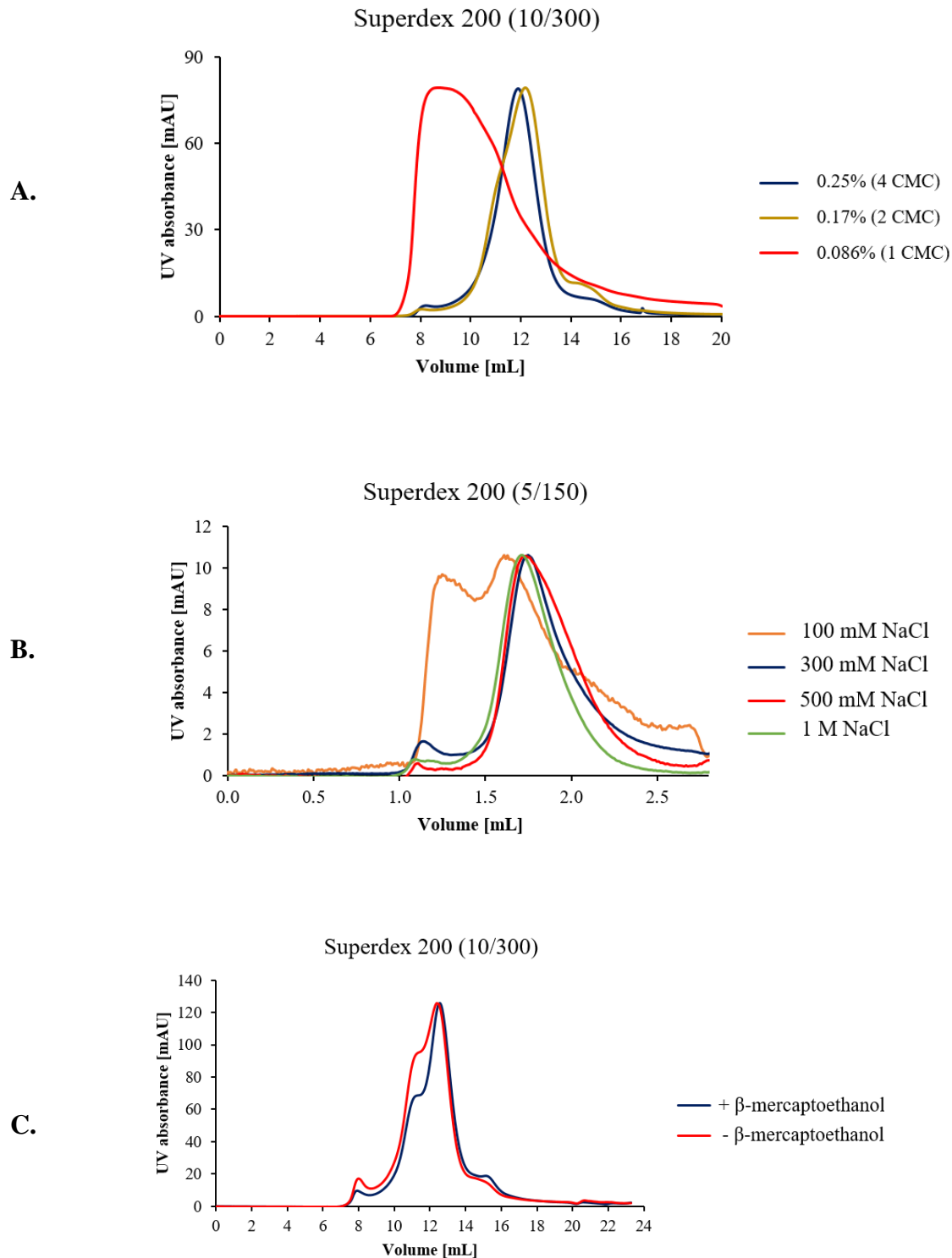


**Figure 3.9.** Elution of PBP1c in size-exclusion chromatography in variable concentrations of additives. The objective of this experiment was to verify which were the optimal conditions for the isolation of a homogeneous form of PBP1c. All experiments were performed in a buffer containing 50 mM Tris pH 8 and 10 mM MgCl<sub>2</sub>, 300 mM NaCl (except in experiment B) and 0.17% DM (except in experiment A). The amount of DM in the buffer proved to be critical as shown in (A). In (B) and (C), DM was maintained at a concentration of 0.17% (2 CMC), and (B) NaCl concentrations and (C) the presence of  $\beta$ -mercaptoethanol at a concentration of 5 mM were tested.

### 3.2.4. SEC-MALS analysis of PBP1c

In order to further characterize PBP1c, a SEC-MALS experiment was performed. This experiment was conducted at a concentration of 3 mg/mL and 55  $\mu$ L were injected onto a Superdex 200 10/300 column. Upon elution, sample was monitored by refractive index, UV and light scattering detectors. The UV absorption profile showed the presence of one peak at 12.5 mL, while the refractive index profile (figure 3.10) indicated a main peak at 12.5 mL and a minor peak at approximately 16 mL, not detected by the UV detector. This peak could correspond to DM micelles, since DM does not absorb UV. The calculated molecular mass was 38 kDa, which is close to the value reported by Anatrace (33 kDa). The difference in sizes may originate from the conditions in which the measurements were performed, which were not reported in the specification.

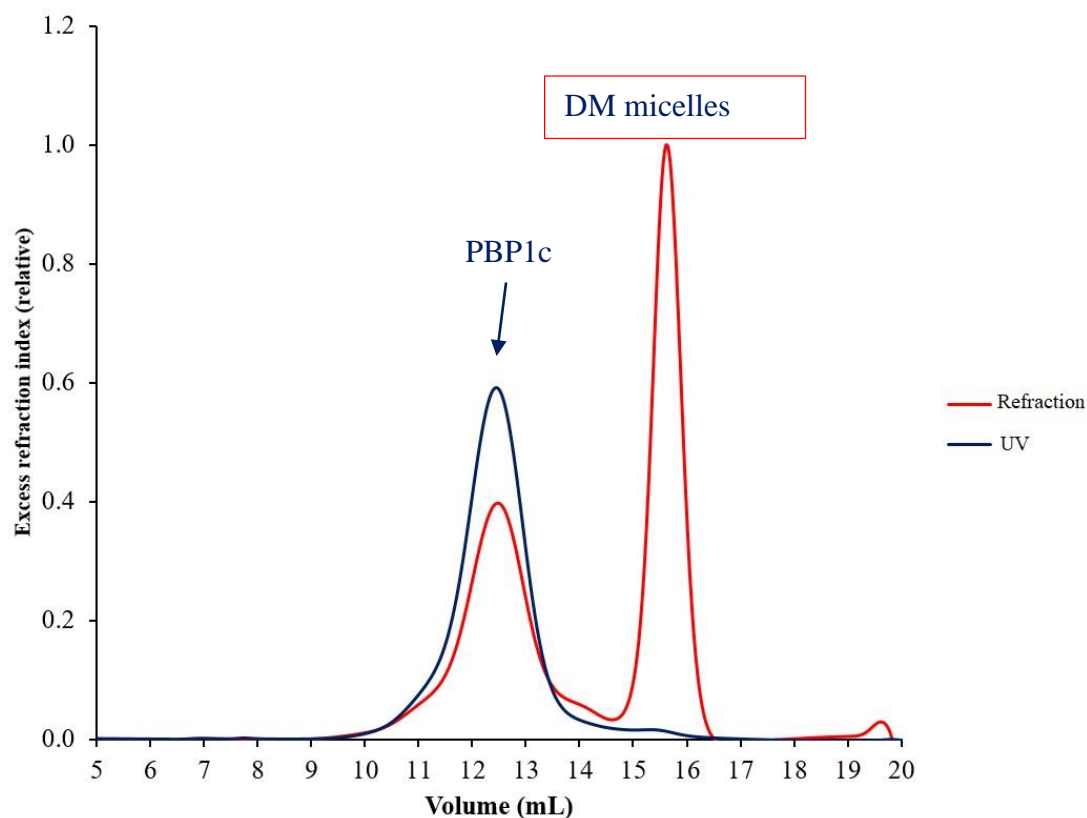


**Figure 3.10.** PBP1c refraction (red curve) and UV absorbance (blue curve) obtained from the SEC-MALS. The sample is purified by a Superdex 200 column and on the exit it passes through a refractive index and UV detectors. The peak for PBP1c elutes at approximately 12 mL and it is detected by both the UV and refractive index detector. DM micelles do not absorb light and they are detectable only in the refraction index curve, eluting at approximately 16 mL. The calculated size of the micelle is 38 kDa, as can be seen below in the table.

Light scattering analyses for the main peak were performed for the front, central and rear part of the peak (figure 3.11). The analyses showed that the front end of the peak contained the protein with a molecular mass of  $199 \pm 1.45$  kDa that could correspond to a dimer of PBP1c (theoretical mass 175 kDa). The molecular weight assigned to the central part of the peak was  $120.3$  kDa  $\pm 1.3$  kDa, a value that is between the masses of a dimer and monomer, while the rear end of the peak contained the protein with molecular weight of  $94.2 \pm 0.9$  kDa. The polydispersity indexes for all three parts show that the analyzed regions were monodisperse. These results suggest that a PBP1c sample contains a mixture of dimers and monomers, with the gradual transition in the size exclusion chromatography.

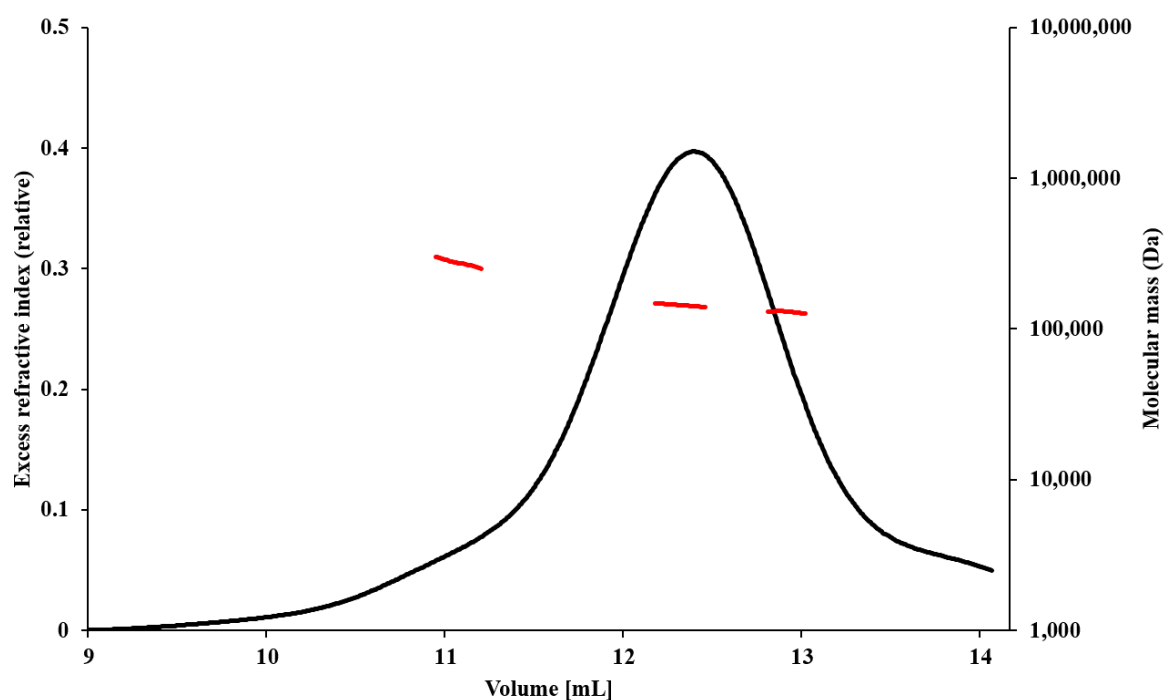


**Figure 3.11.** SEC-MALS analysis of PBP1c. The protein was injected onto a Superdex 200 (10/300) column at the concentration of 3 mg/mL. Separate analyses for the front, central and rear part of the peak were performed and the molecular weights obtained were 199, 120 and 94 kDa, respectively. This suggests that the PBP1c sample is a mixture of monomers and dimers (theoretical weights of 174 and 87 kDa) with the gradual transition between two forms in a size exclusion chromatography. With the polydispersity indexes of  $1.002 (\pm 1.02\%)$ ,  $1.000 (\pm 1.5\%)$  and  $1.000 (\pm 1.4\%)$ , the analyzed regions were characterized as monodisperse.

### 3.2.5. Cell-free expression and purification of PBP1c

**Cell-free expression of PBP1c.** In order to try to obtain homogeneous samples of PBP1c, the cell-free expression technique was attempted. In this technique, also called *in vitro* expression, proteins are expressed using purified components of the *E. coli* translation machinery, but not within a cellular environment. There are several advantages of cell-free protein expression, including the fact that it is much less time-consuming and does not require extensive cell culture experiments. Typical experiments are performed in a batch setup, where a reaction mixture includes *E. coli* lysate, a vector expressing the target DNA, and a mixture that includes purified components such as amino acids, tRNAs, salts, nucleotides, and cofactors.

Initial tests of cell-free expression of PBP1c in a batch set-up showed that the protein could be successfully expressed. The Western blot analysis revealed that the protein was expressed and migrated close to the expected size, and that the most efficient detergent for the solubilization was Brij 35 present in a concentration 50 times its CMC (figure 3.12).

For optimization of the purification, the protein was expressed by the dialysis method in which 3 mL of cell-free reaction mix were incubated overnight at room temperature, constantly supplied by fresh reaction ingredients from the surrounding feeding solution. After overnight incubation, roughly 50% of the protein was precipitated. The protein from the soluble fraction was purified by affinity and SEC. The comparison of the SEC elution profiles between HisPBP1c expressed in *E. coli* and in a cell-free fashion showed that the latter approach resulted in increased homogeneity, and better separation of different species (figure 3.13).

However, further scale-up proved to be challenging and the maximum yield obtained by cell-free expression did not go beyond 100 µg of pure protein.

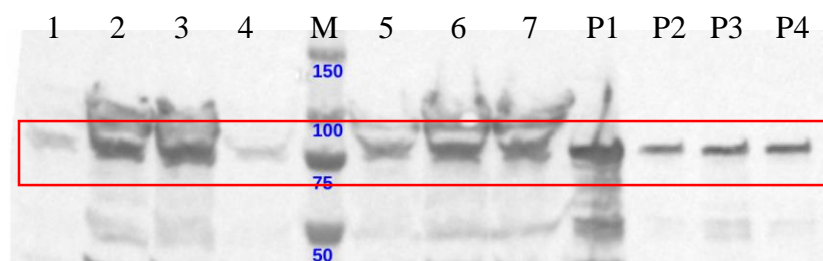


**Figure 3.12.** Western blot analysis of the solubility of PBP1c (red rectangle) expressed in the cell-free system. Soluble fractions: 1 – no detergent; 2 – Brij 35 10 CMC; 3 – Brij 35 50 CMC; 4 – DDM 10 CMC; 5 – DDM 50 CMC; 6 – Brij 58 10 CMC; 7 – Brij 58 50 CMC. P1, P2, P3, P4 – insoluble fractions of the samples 1-4. CMC – critical micellar concentration.

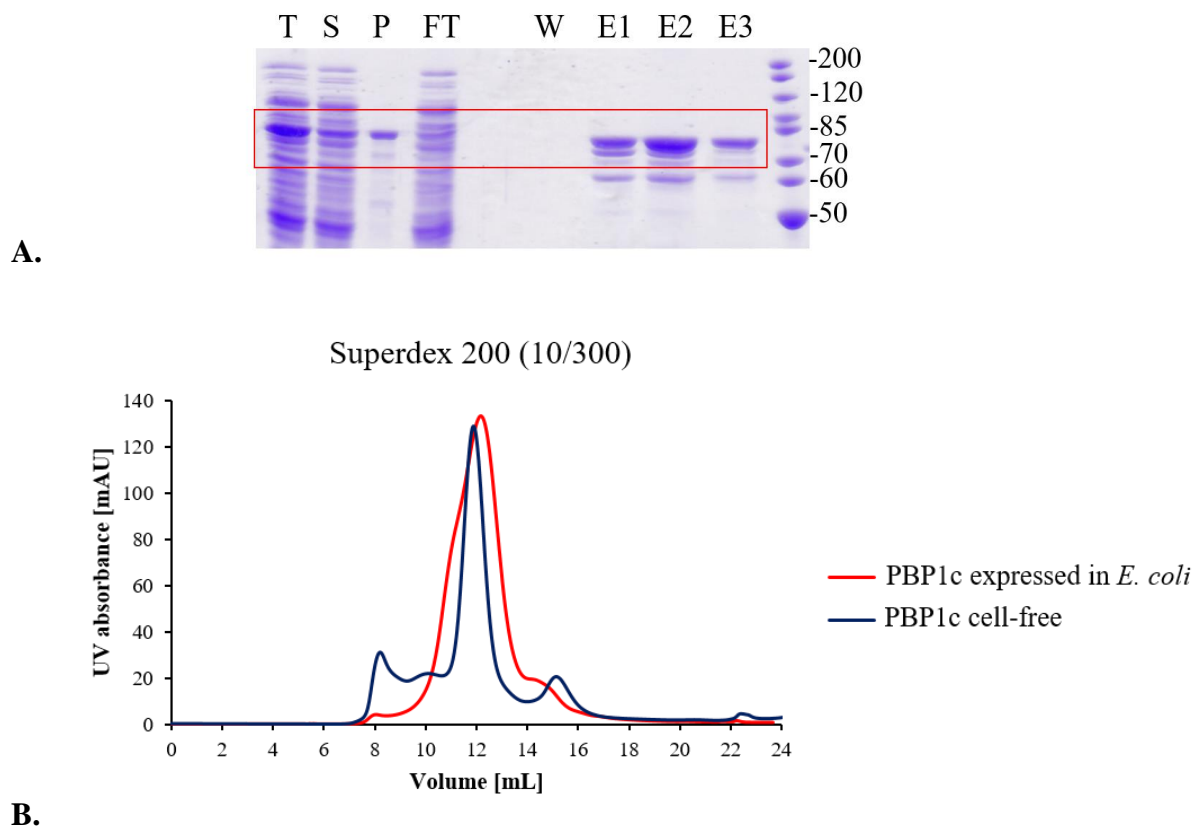


**Figure 3.13. Results for the different steps involved in cell-free expression and purification of PBP1c.** A – SDS-PAGE of the different steps of the experiment. T = totally lysate, S= soluble material, P = pellet, FT = flow through. The lanes on the right side of the gel are indicative of the fractions eluted from nickel affinity purification. W = wash, E1, E2, E3 = elution. The lane on the right is the molecular mass ruler. B – Comparison of gel filtration profiles of cell-free and *E. coli* expressed PBP1c. Protein expressed using the cell-free system eluted mostly in a sharp peak, while that expressed in *E. coli* eluted as a broad peak, suggesting less homogeneity and potentially that it could be a mixture of different species.

### 3.2.6. Mass spectrometry of PBP1c

In order to determine the experimental mass of HisPBP1c, MALDI/TOF analysis was performed. The mass of a singly-charged particle determined in denaturing conditions by MALDI-TOF was 87,077 Da (figure 3.14). An additional doubly-charged particle was also registered with the mass of 43,445 Da, roughly half of the singly-charged ion, confirming that molecular mass of PBP1c is approximately 87 kDa. This value is, however, 284 Da lower compared to the theoretical mass (87,361 Da)

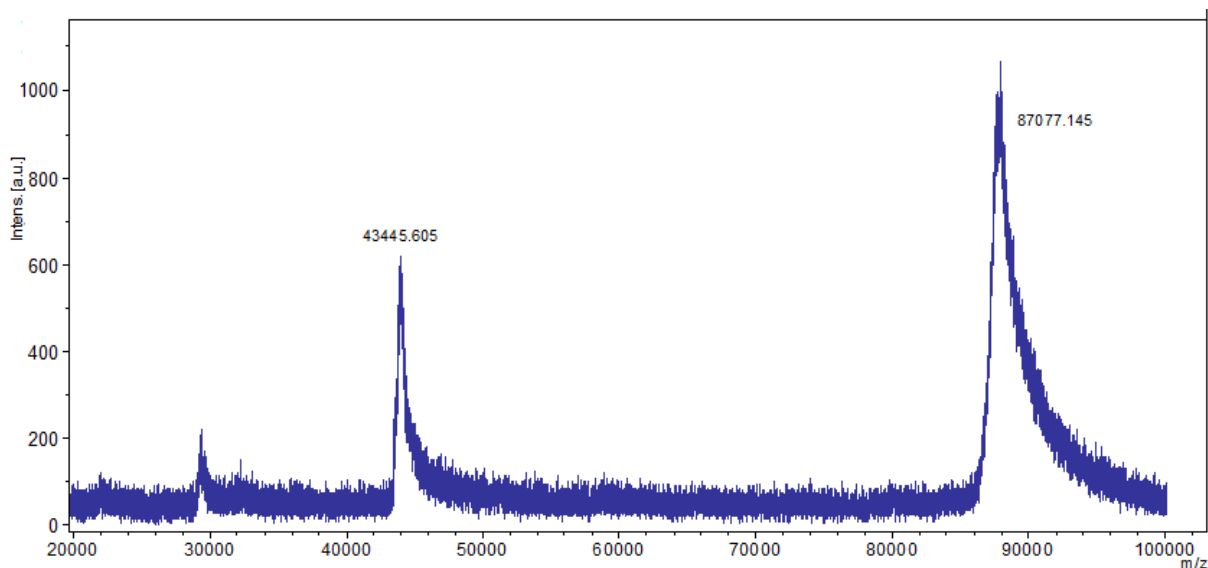


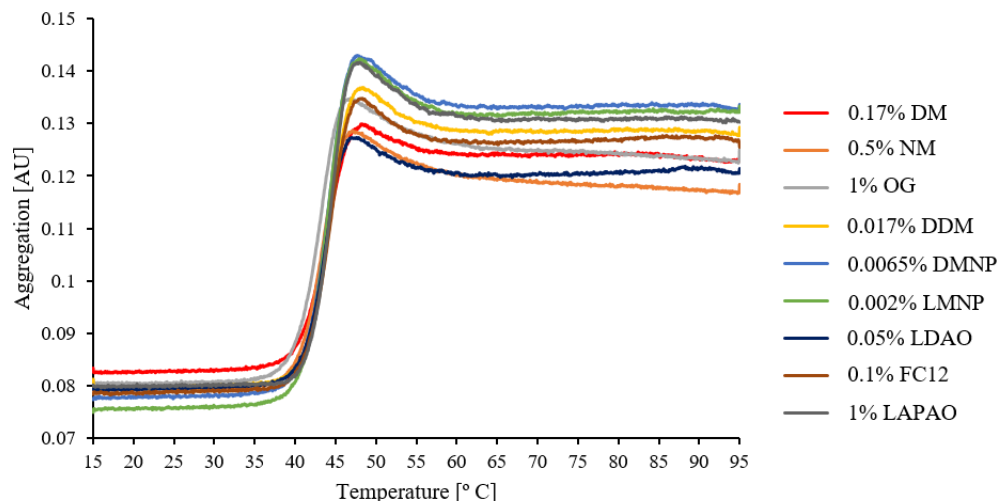
**Figure 3.14.** The mass spectrum of HisPBP1c obtained in MALDI/TOF analysis showed the presence of a singly-charged ion with the mass of 87,077 Da and a doubly-charged ion with a mass of 43,445 Da. Additionally, a triply-charged ion can be detected with a mass around 29 kDa.

### 3.2.7. Thermal stability analysis

The stability of HisPBP1c was assessed using a Prometheus instrument in an experiment in which aggregation onset was monitored for PBP1c while gradually increasing the temperature. In total, 31 different buffers described in Materials and Methods section were tested. The protein was purified as previously described and concentrated to 2.5 mg/mL. For each condition, 40  $\mu$ L of buffer were mixed with 10  $\mu$ L of PBP1c (final concentration 0.5 mg/mL) and incubated for 30 minutes. The samples were transferred to the capillaries that were loaded onto the instrument and the light scattering was followed with the increase of temperature.

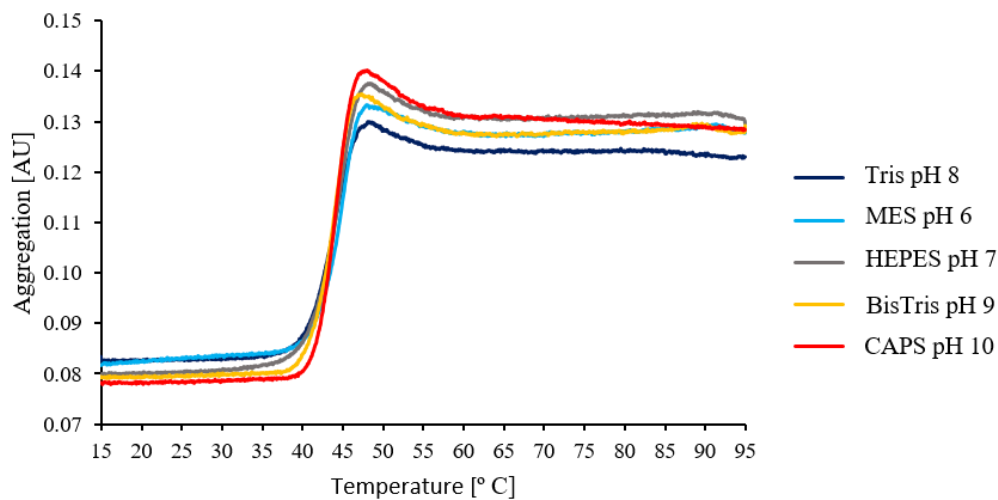
In the conditions used for purification that were used as a reference, the protein started to aggregate around 36  $^{\circ}$ C. From the nine detergents tested, only Fos-choline 12 and LAPAO slightly delayed the onset of aggregation for approximately 1 and 2  $^{\circ}$ C, respectively (figure 3.15a). In the case where the pH of the buffer was varied, the protein showed increased stability in basic conditions, especially in CAPS pH 10, for which the aggregation started at 39  $^{\circ}$ C (figure 3.15b).

**A.**



Detergent	Aggregation onset [°C]	Detergent	Aggregation onset [°C]
DM	36.4	LMNP	35.0
NM	36.2	LDAO	36.1
OG	34.8	FC12	37.6
DDM	36.7	LAPAO	38.9
DMNP	34.6		

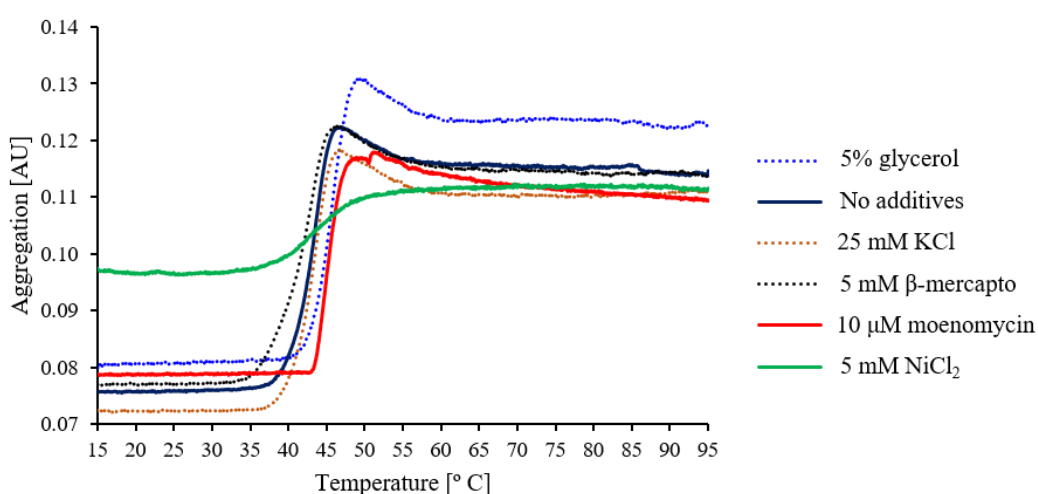
**B.**



Buffer	Aggregation onset [°C]	Buffer	Aggregation onset [°C]
MES pH 6	37.9	BisTris pH 9	38.2
HEPES pH 7	31.1	CAPS pH 10	39.1
Tris pH 8	36.4		

**Figure 3.15.** Light scattering of PBP1c resulting from the aggregation formation following the increase of temperature in different detergents (A) and pH values (B). The purified protein was mixed with buffers in which one of the components was varied compared to the standard purification buffer, incubated for 30 minutes and analyzed in a Prometheus instrument.

The most remarkable differences were observed in the samples where 5% glycerol was added, raising the aggregation onset temperature to 40.4 °C and in the case of moenomycin, whose presence delayed aggregation for 7 °C compared to the reference condition (figure 3.16). Moenomycin is a GTase reaction inhibitor that binds tightly to the active site of the GT domain of the PBPs (Goldman & Gange 2000). The effect of moenomycin on the stability of PBP1c was not surprising as it was previously reported that crystals of its homolog PBP1b could not be obtained without the addition of moenomycin (King et al. 2017; Sung et al. 2009). Based on these results, 5% glycerol was added in the buffer for PBP1c purification, while moenomycin was used in the crystallization trials and SAXS experiments.



Additive	Aggregation onset [° C]	Additive	Aggregation onset [° C]
No additive	36.4	β-mercaptoethanol	33.1
5% glycerol	40.4	moenomycin	43.1
25 mM KCl	36.5	NiCl <sub>2</sub>	32.5

**Figure 3.16.** Aggregation of PBP1c following the increase of temperature in the presence of different additives.

### 3.3. Complex reconstitution and characterization

#### 3.3.1. Complex formation

For the reconstitution of the complex *in vitro*, purified ECAM and PBP1c were mixed in a 1:2 molar ratio, incubated for 2 hours at 4 °C and subjected to gel filtration. The appearance of a new peak of higher molecular weight not present in the elution of individual proteins was recorded (figure 3.17a). The SDS-PAGE showed the presence of both proteins in the new peak, leading to the conclusion that the new species is the complex formed between ECAM and PBP1c (figure 3.17b).

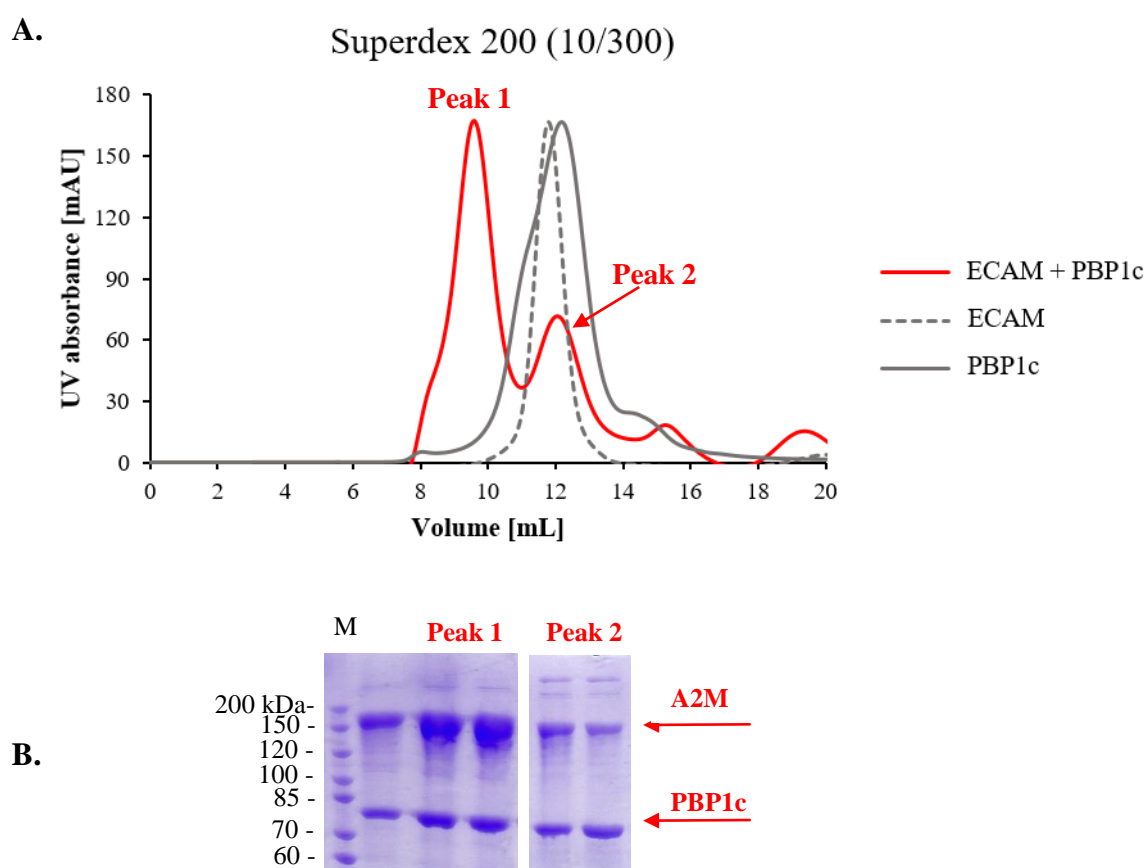


**Figure 3.17.** A – The comparison of elution profiles of ECAM and PBP1c alone and after the mixture. ECAM and PBP1c were mixed in 1:2 ratio, incubated and injected in the gel filtration column. Peak 2 corresponds to the co-elution of individual, unbound proteins. Peak 1 represents the elution of new, high-molecular weight species formed upon incubation. B – SDS-PAGE showing the presence of both proteins in peak 1.

### 3.3.2. AUC analysis

In order to investigate the stoichiometry of the complex, samples were examined by analytical ultracentrifugation using the sedimentation velocity method. In the experiment, the sedimentation of individual proteins and the mixture of ECAM and PBP1c were studied in parallel. Individual proteins were analyzed at two different concentrations, 1 mg/mL and 2 mg/mL, while the ECAM-PBP1c complex samples were prepared in 3 molar ratios: 1:1, 1:2 and 1:3. The samples were centrifuged at 35,000 rpm at 4 °C, monitoring interference and absorbance at 280 nm. The scans were recorded at regular intervals and analyzed with Sedfit using the continuous size distribution  $c(s)$  analysis method to determine sedimentation coefficients.

In all samples a contribution at  $1.6 \pm 0.02$  S ( $s_{20w} = 2.7 \pm 0.03$  S) was observed only in interference. Combined with the optical parameters of the proteins and detergent, it was established that this corresponded to the micelle of DM with the molecular weight of 41 kDa.

In the case of ECAM alone, the majority of protein ( $91 \pm 3\%$  of the total signal) sedimented as a monomer at an  $s$  value of  $4.8 \pm 0.1\%$  S, corresponding to a molecular weight of 159 kDa (figure 3.18, table 3.2). This sedimentation coefficient was in agreement with the theoretical  $s$  of 4.87 calculated from the crystal structure of monomeric ECAM with the molecular weight of 182 kDa (Garcia-Ferrer et al. 2015). Analysis of interference and absorption signals, and optical parameters of ECAM and DM determined that ECAM did not bind any detergent. A small contribution was observed at  $6.7 \pm 0.25$  S ( $s_{20w} = 11.4 \pm 0.4$  S) for approximately 4% of the total signal, which corresponded to a potential dimer. Comparison of the results recorded for ECAM at concentrations of 1 mg/mL and 2 mg/mL showed that there was no effect of the concentration on oligomeric state.

<i>s</i> -value	Fitted mass (kDa)	% of the signal	Molecule	Theoretical mass (kDa)
$4.8 \pm 0.1$ S	159	$91 \pm 3$	monomer	182
$6.7 \pm 0.25$ S	280	4	dimer	364

**Table 3.2.** Sedimentation coefficients for different species of ECAM obtained from analytical centrifugation and attributed masses.

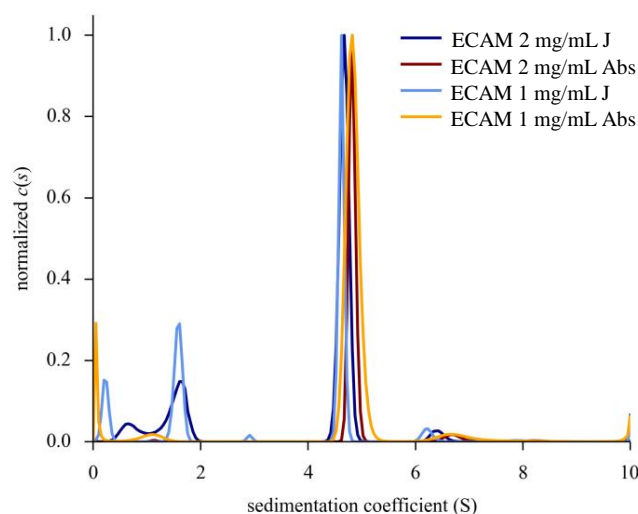


**Figure 3.18.** Sedimentation velocity profiles of ECAM. Experiments were performed at two different concentrations. Results for both interference (J) and absorbance (Abs) are shown.

For PBP1c, a broad peak between 2.5 and 10 S was observed accounting for  $74 \pm 3\%$  of the total signal at 1 mg/mL with  $s_{mean} = 5.1 \pm 0.15$  S and  $s_{max} = 4.4$  S, and approximately 70% at 2 mg/mL with  $s_{mean} = 5.9 \pm 0.30$  S (figure 3.19). The theoretical sedimentation coefficient for monomeric PBP1b, the closest homolog of PBP1c whose structure is known, was calculated to be  $s = 3.05$  S. Comparison with the experimental  $s_{max}$  suggested that PBP1c is present in the sample as an elongated dimer of 130 kDa (theoretical Mw = 174.7 kDa). The amount of DM bound to PBP1c was assessed to be  $0.5 \pm 0.2$  g per gram of protein. In addition, approximately 30% of the signal was attributed to larger oligomers or aggregates. There was no significant effect of the concentration observed.

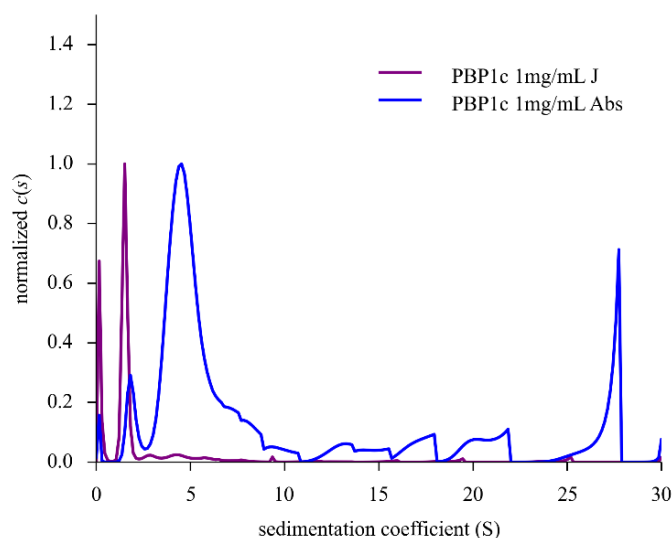


**Figure 3.19.** Results of the  $c(s)$  analysis for PBP1c. J – interference signal. The peak at 1.5 S corresponds to the DM micelle; Abs – signal of absorbance at 280 nm. The  $s_{max}$  value at 4.4 S corresponds to PBP1c dimers.

The samples of the ECAM-PBP1c complex showed the same main features in all three ratios analyzed. Three large peaks were obtained (table 3.3). The first peak was between 2.5 and 6S with  $s_{mean} = 4.8 \pm 0.1S$  and  $s_{max} = 4.2 \pm 0.3S$  that accounted for approximately 40% of the signal. Comparison with the  $s$  values obtained for ECAM and PBP1c alone (4.8 S and 4.4 S) lead to the conclusion that this peak corresponded to co-sedimentation of each protein alone.

Two other peaks resulted from the sedimentation of higher molecular species not present in the analyses of individual proteins and they were assigned to the ECAM-PBP1c complex. The peak between 6 and 13 S, representing 35% of total signal, with  $s_{mean} = 11S$  and  $s_{max} = 10 S$  corresponded to molecular weight of 450 kDa. Taking into account the masses of individual proteins determined in this experiment, the complex of 450 kDa would comprise of 2 molecules of ECAM and 2 molecules of PBP1c.

The second complex peak comprised particles sedimenting between 13 and 27 S, with  $s_{mean} = 20 S$  and  $s_{max} = 16 S$ . The molecular weight assigned was 900 kDa, double the size of the particles from peak 2. This suggested the presence of larger ECAM-PBP1c complex consisting of 4 molecules of each partner.

$S_{max}$ value	Fitted mass (kDa)	% of the signal	Molecule	Theoretical mass (kDa)
$4.2 \pm 0.3S$	120	40	Co-sedimentation of individual proteins	182
10S	450	35	2+2 complex	560
16S	900	20	4+4 complex	1120

**Table 3.3.** Sedimentation coefficients for different species present in the ECAM-PBP1c sample obtained from analytical centrifugation and attributed masses.

### 3.3.3. Peptidoglycan synthesis assay

These assays were performed by Victor Hernandez Rocamora in the laboratory of Dr. Waldemar Vollmer, Newcastle University.

#### $\beta$ -lactam binding

The ability of PBP1c to bind  $\beta$ -lactam antibiotics was tested using biotinylated ampicillin and a fluorescent penicillin V derivate, bocillin FL. PBP1c was incubated with 1 mM ampicillin or 1.5  $\mu$ M bocillin for 10 minutes and loaded onto SDS-PAGE. Ampicillin-bound PBP1c was visualized with a streptavidin-peroxidase conjugate, while the PBP1c-bocillin complex was visualized by laser scanning. In both cases, binding of  $\beta$ -lactam to PBP1c was detected in the presence and absence of glycerol, as well as in the presence of ECAM, confirming that the TPase domain of PBP1c is well folded (figure 3.20). The presence of glycerol does not interfere with the  $\beta$ -lactam binding, even when it is bound to ECAM, PBP1c still binds ampicillin, indicating that its active site is not ‘masked’.

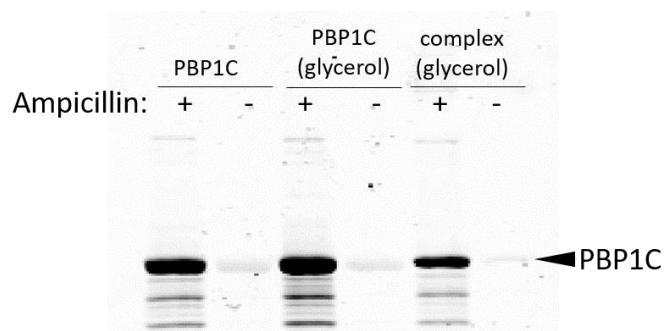


**Figure 3.20.** Western blot analysis of PBP1c-binding of biotinylated ampicillin. The activity of PBP1c was tested in the presence and absence of glycerol. The membrane was visualized with a streptavidin-peroxidase conjugate. (+) – samples incubated with 1 mM biotinylated ampicillin; (-) – samples not incubated with ampicillin

### Measurement of glycosyltransferase activity

The peptidoglycan synthesis activity of PBP1c was examined in an assay in which 2  $\mu$ M PBP1c were incubated with radiolabeled Lipid II (figure 3.21). In this assay, radiolabeled Lipid II is polymerized by both GTase and TPase activities of an active PBP, producing peptidoglycan chains that can subsequently be detected by HPLC.

In terms of the GTase activity tested with this assay, an active PBP is expected to generate dephosphorylated muropeptides that are incorporated into peptidoglycan chains and elute later in time (figure 3.21, peak 2). If the sample does not display GTase activity, only phosphorylated disaccharide pentapeptides can be detected, eluting earlier in the profile (Figure 3.21, peak 1). As can be seen in figure 3.22, PBP1c is capable of generating dephosphorylated muropeptides (peak at approx. 35 mins), both when it is purified in the absence or presence of glycerol. However, ECAM, as expected, does not present GTase activity, and thus only the phosphorylated forms of the disaccharide pentapeptides could be detected (peak at approx. 25 mins).

### Measurement of transpeptidase activity

This assay was also employed to test the transpeptidase activity of both PBP1c and ECAM. This assay did not reveal any peaks in the expected region in the elution profile (after 35 mins), indicating that neither protein could catalyze the formation of bis-disaccharide

tetrapentapeptide or tris-disaccharide tetrapentapeptides, the expected products of the peptidoglycan transpeptidation reaction.

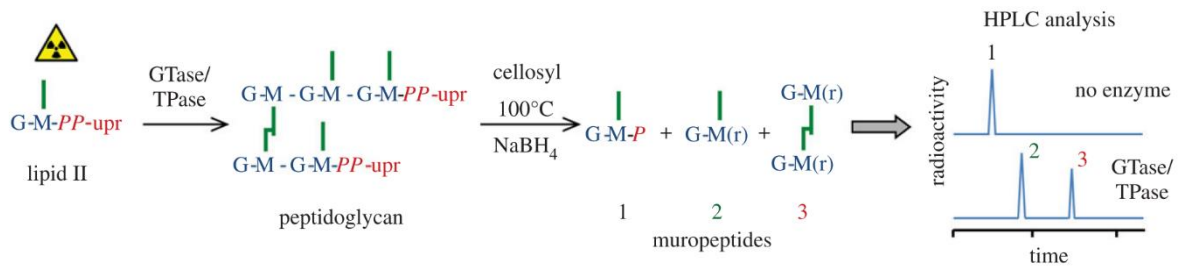


**Figure 3.21.** Schematic representation of the peptidoglycan synthesis assay with radiolabeled Lipid II. Synthesized peptidoglycan chains are digested with cellosyl, yielding muropeptides of different sizes. In the absence of GTase reaction, only phosphorylated disaccharide pentapeptides are registered in an HPLC analysis (peak 1). Muropeptides that are incorporated into peptidoglycan chains elute later in time (taken from (Egan et al. 2015)).

Both GTase and TPase activities were also tested after co-incubation of PBP1c and ECAM, using the same assay described above. As can be seen in figure 3.22, the presence of ECAM does not modify the activity profile for PBP1c, which is still able to catalyze the GTase activity but not transpeptidation in the presence of ECAM.

These results were confirmed by additional assay in which we incubated fluorescently labeled Lipid II with PBP1c and PBP1c + ECAM, and the reactions were followed in time. Furthermore, ECAM seemed to stimulate the GTase activity of PBP1c, since longer disaccharide chains (and in greater quantity) could be observed at earlier times. This suggests that ECAM may act as an enhancer of the GTase activity of PBP1c. However, these results should be confirmed by additional tests.

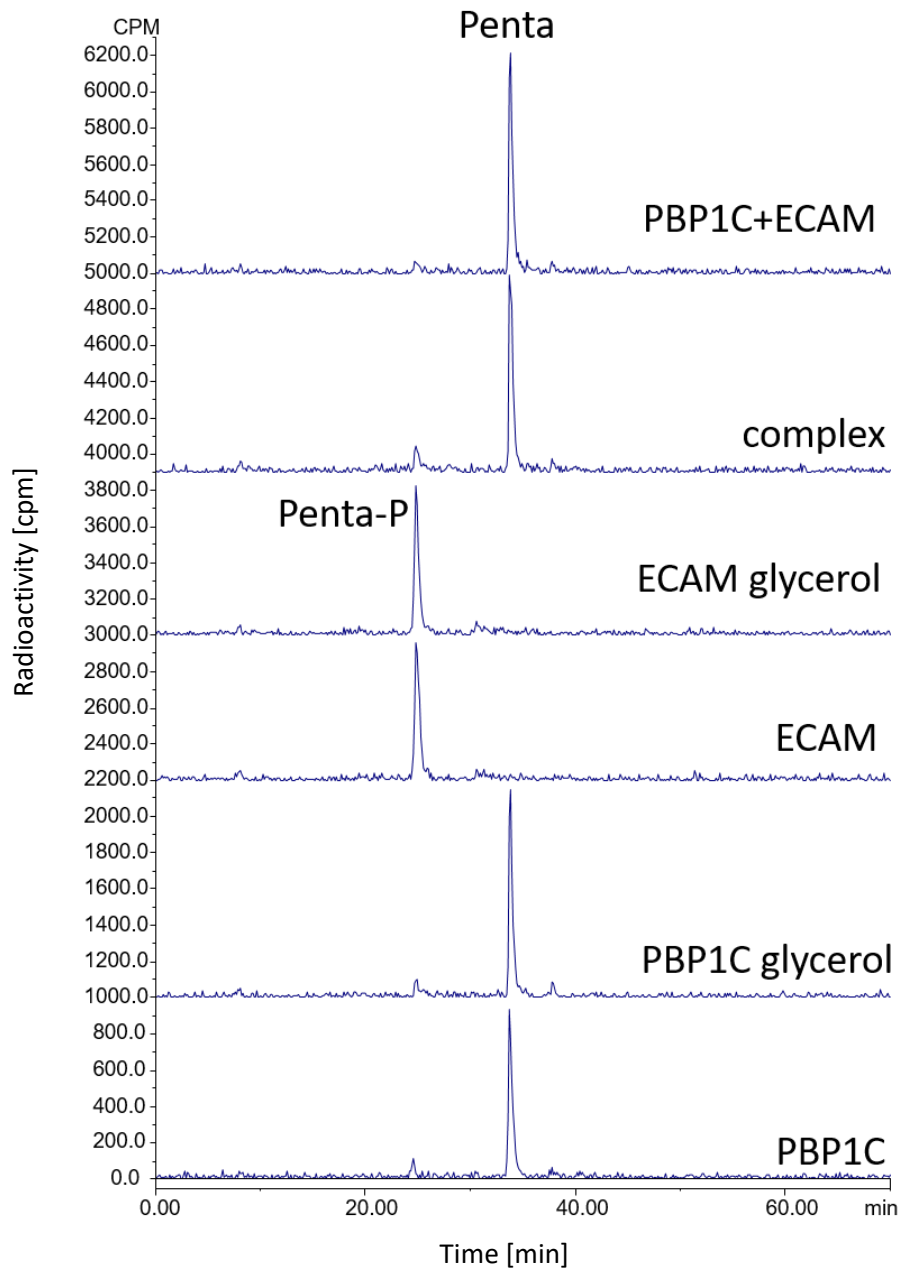


**Figure 3.22.** Analysis of mucopeptides by HPLC. Penta-P – phosphorylated disaccharide pentapeptides; Penta – disaccharide pentapeptides (products of GTase reaction). ECAM alone has no GTase activity. PBP1c alone or in complex with ECAM shows GTase, but no TPase activity, since no radiolabeled reaction products were detected after 35 minutes.

### **3.3.4. Crystallization trials of PBP1c in apo form and in the presence of moenomycin**

In order to characterize both PBP1c and the ECAM-PBP1c complex at an atomic level, we performed crystallization trials of the samples. We used both the HTX platform (PSB Grenoble) for high-throughput screening and also performed screens manually.

In the crystallization trials performed at the HTX facility, PBP1c was tested in the absence and presence of the GT-specific antibiotic moenomycin. The crystallization plates were prepared at 4 °C. In both cases, PBP1c at the concentration of 4.95 mg/mL was mixed with crystallization buffers in two ratios, 1:1 and 2:1. The PBP1c sample used for these tests was expressed and purified from *E. coli*, and was subsequently mixed with ECAM at a 2:1 ratio prior to crystallization. Samples were screened against 576 different conditions, but no crystals were obtained.

In parallel, manual trials were performed for PBP1c that had been expressed and purified using both *E. coli* and the cell-free approach. In several conditions, amorphous crystals were observed for the PBP1c form that had been expressed using the cell-free system. Interestingly, two conditions resulted in the formation of small cuboid protein crystals (figure 3.23). In both cases, they were grown in a sodium citrate buffer at pH 5.5 with PEG 4000 as the precipitant, and either lithium chloride (figure 3.23a and 3.23b) or ammonium sulfate (figure 3.23c) as salts. Interestingly, the appearance of crystals required the inclusion of moenomycin in the samples.

It is of interest that there were two key requirements for the crystallization of PBP1c. One was the expression of protein using the cell-free system. The sample prepared using this system showed higher homogeneity than the one obtained after expression in *Escherichia coli*, as discussed in this manuscript. The superior quality of samples prepared from cell-free expression has already been observed for other proteins in the laboratory, notably for samples that are either membrane-associated or membrane-embedded. Unfortunately, as mentioned above, these expression trials were very difficult to reproduce, and since the amount of protein obtained was very small, it was not possible to proceed with this strategy. However, this approach is being continued in the laboratory.

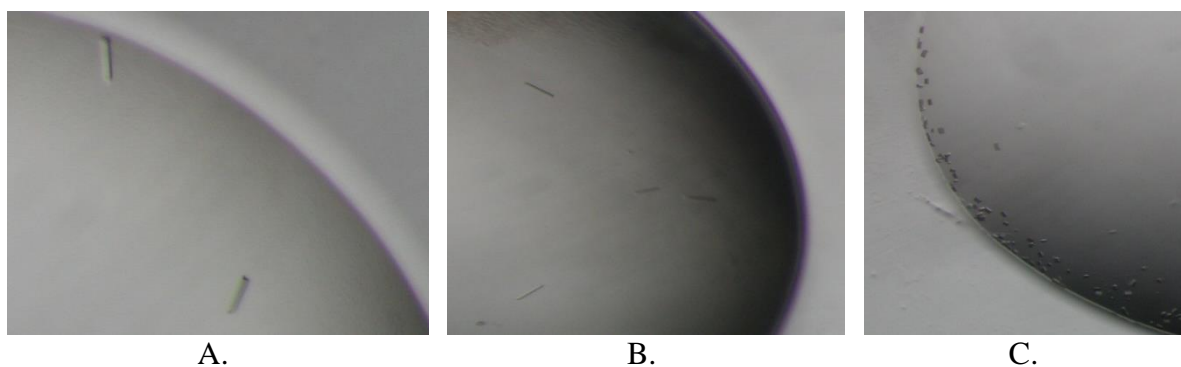


**Figure 3.23.** Crystals of PBP1c obtained using the hanging-drop method. Crystals were grown at 4 °C in 0.1 M sodium citrate pH 5.5, 12% PEG 4000, 0.32 M lithium chloride (A and B) or 0.34 M ammonium sulfate. Crystals were only obtained when the protein was expressed using the cell-free system, and when moenomycin, a specific inhibitor of the GT domain of PBPs, was used in the crystallization trials. Similar results have also been observed for crystallization trials of PBP1b from *E. coli*, a close counterpart (King et al. 2016, JBC)

Another notable point regarding the crystallization of PBP1c is that the appearance of crystals absolutely required the employment of the GT-specific antibiotic moenomycin. Moenomycin was employed to stabilize class A PBPs since the solution of the first crystal structure of PBP2 from *S. aureus* by the Strynadka group (Lovering et al. 2007) and has been employed for this purpose since. Moenomycin, a multi-ring molecule, binds in an extended conformation within the GT domain, forming an extended plane within the active site cleft (Lovering et al., 2007). In the future, attempts to obtain crystals of the ECAM:PBP1c complex will require the fulfillment of both conditions: expression of PBP1c using the cell-free system, and employment of moenomycin viewing stabilization of the GT domain of the molecule.

### 3.3.5. Negative staining electron microscopy

In addition to the fact that electron microscopy is one of the techniques of choice for the study of a large protein complex such as ECAM-PBP1c, there were two reasons that encouraged us to explore EM studies for this project. One of them was the large number of crystallization trials that were performed for the complex, to no avail. A second reason was directly linked to the fact that ECAM is a large, multi-domain molecule, that displays inherent flexibility in the first two N-terminal domains (Garcia-Ferrer et al., 2015). This flexibility could hinder crystallization of the complex. Given the fact that our objective was to characterize the complex structurally, we thus decided to initiate tests to characterize the proteins using electron microscopy, with the goal of eventually obtaining a homogeneous, well-behaved sample that could be tested in cryo-EM.

In order to increase our chances of achieving this goal, we performed an extensive optimization phase using negative staining TEM. For that reason, we started the optimization process using ECAM alone as a reference (despite the fact that its structure has already been described in Garcia-Ferrer et al., 2015).

The sample analyses were performed by Daphna Fenel at the EM platform at the IBS. ECAM was purified using the strategies described above. Prior to negative staining experimentation, samples were gel filtered in 25 mM Tris pH 8.0 and 25 mM sodium citrate pH 4.0 buffers supplemented with 500 mM NaCl, 10 mM MgCl<sub>2</sub> and 0.17% DM, at 0.05, 0.03 and 0.02 mg/mL. The choice of buffers with acidic and basic pHs was made in order to examine if the effects on the grid quality originate from the stain itself or the pH of the staining solution. The pH of uranyl acetate is 4.5, while the pH of SST is pH 7.5. Although ECAM does not require any detergent, it is required for PBP1c and consequently, for the complex reconstitution. As it could greatly influence the process of grid preparation and quality of imaging, it was important to include DM in the optimization process from the beginning. The samples were applied to the clean side of carbon on mica (carbon/mica interface) and treated with either uranyl acetate or SST stains. After drying, the grids were introduced into the FEI Tecnai12 microscope. As can be seen in figure 3.22, in the case of the samples treated with SST, the particles showed great variation in sizes, suggesting that in the conditions tested, ECAM was prone to aggregation.

On the other hand, using uranyl acetate as a stain repeatedly resulted in images with better contrast, that could not be achieved with SST (figure 3.24a). Samples were homogenous, independent of the pH or protein concentration (figure 3.24a). In order to gain insight into the actual shape of ECAM under these conditions, we compared the images obtained in uranyl acetate to a surface model generated from the crystal structure of the  $\alpha$ 2M from *S. enterica* (Sa-A2M) (figure 3.24b) (Wong & Dessen 2014). Dimensions of Sa-A2M range between 8.5 and 12 nm. As can be seen in figure 3.24, the particles are comparable in size and shape.

After the conditions were established, further tests were focused on the ECAM-PBP1c complex. The samples were prepared from the complex fraction eluted in gel filtration. The complex was tested in 25 mM Tris pH 8.0, 500 mM NaCl, 10 mM MgCl<sub>2</sub> and 0.17% DM at 0.02 mg/mL, using uranyl acetate, SST and ammonium molybdate as stains in a negative staining EM experiment. However, in all of the conditions, the samples showed high heterogeneity. The reason for this may be the presence of the complexes of different stoichiometries, as well as dissociation of the proteins during the adsorption to the carbon grids or the process of staining. It is also conceivable that the dyes destabilize and disrupt the complex, leading to heterogenous images. The optimization thus continues in the direction of decreasing heterogeneity of the samples, and one of the approaches could be cross-linking the complex subunits and separation of the complexes of different sizes, possibly using the GraFix technique (Stark 2010).

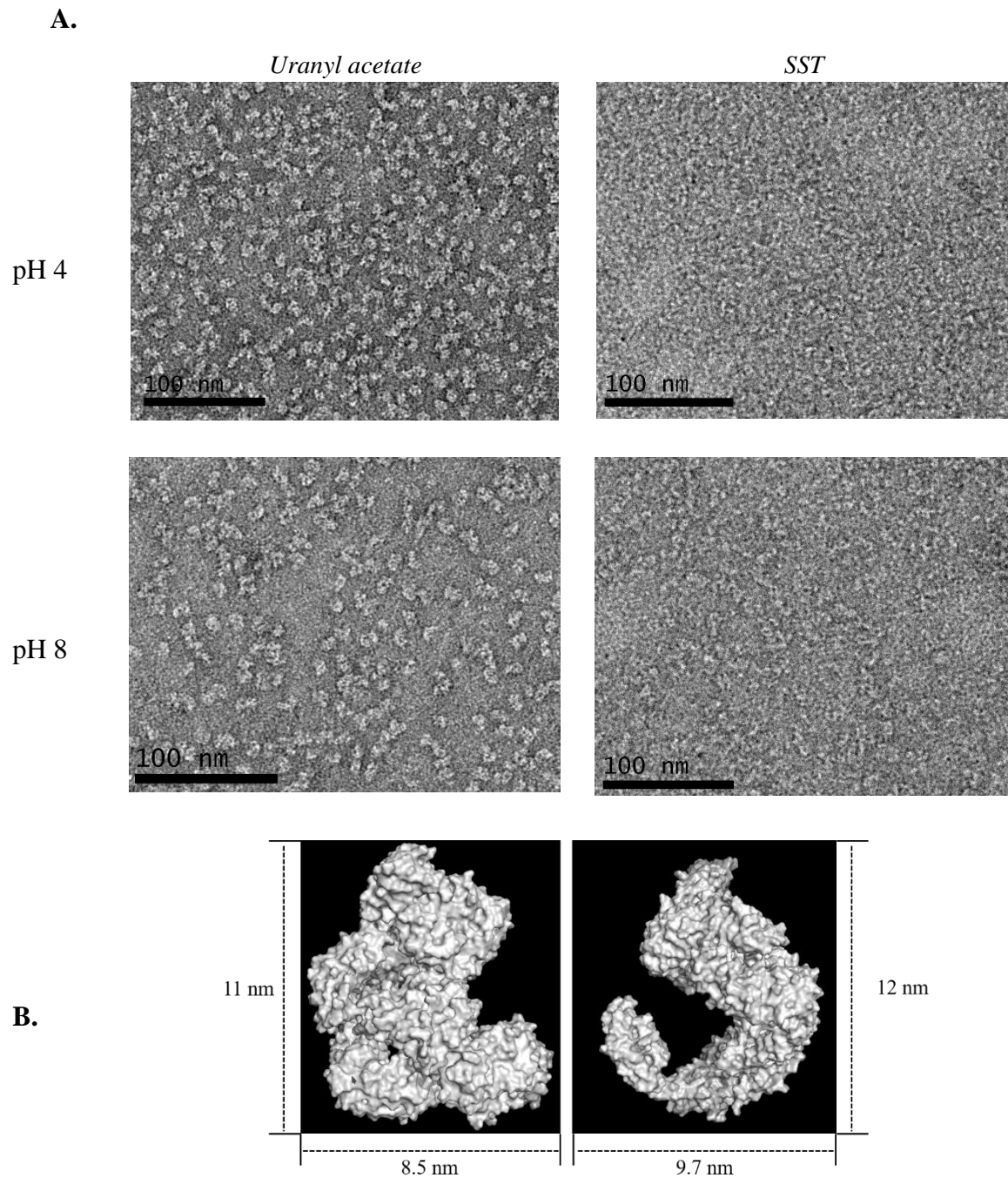


**Figure 3.24.** A – Electron microscopy of ECAM in uranyl acetate and SST in different pHs. Uranyl acetate provides better contrast compared to SST-stained samples in which isolated particles are difficult to visualize. B – Two different views of the surface model of SA-A2M ( $\alpha$ 2M from *S. enterica* (PDB: 4U48)). Particles in this orientation can be identified in the EM images above.

### 3.3.6. SAXS

In order to structurally characterize ECAM, PBP1c and the ECAM-PBP1c complex in solution, we employed the small angle X-ray scattering (SAXS) technique. Data were collected at the BM29 beamline of the ESRF synchrotron in Grenoble.

The individual proteins were prepared in the buffer containing 25 mM Tris pH 8.0, 500 mM NaCl, 10 mM MgCl<sub>2</sub>, 5% glycerol and 0.17% DM, and subjected to size exclusion chromatography in a Superdex200 10/30 experiment prior to the SAXS. The ECAM:PBP1c complex sample was prepared in the same manner; however, glycerol was omitted from the buffer since it was previously noticed that it interfered with complex formation.

In the experiment, the scattering intensities of samples and the buffer in which the samples were prepared were collected. The scattering of the buffer was subtracted from the scattering of the sample in order to obtain the scattering of the solute only. As mentioned above, in each case, the buffer contained 0.17% of DM. Micelles in the sample could also contribute to the scattering and influence the correct interpretation of the data. However, in the SEC-MALS experiments shown above (figure 3.10), by following the refractive index and UV absorption it was demonstrated that the excess of micelles was eliminated during gel filtration, eluting as peak 2. Thus, we could assume that the only detergent signal that could contribute to the scattering profiles of the samples would be that from detergent bound directly to PBP1c, since ECAM does not bind any detergent.

#### **SAXS experiments with ECAM**

The intensity of scattering of the ECAM sample was recorded at 0.6, 1.5 and 3 mg/mL. Data were plotted by using the program PRIMUS (Konarev et al. 2003) in the form of  $I(q)$  versus  $q$  (nm<sup>-1</sup>), where  $I$  is the measured intensity and  $q$  is the momentum transfer determined by a scattering angle and the wavelength of the incoming X-ray beam. The absence of a steep slope in the low  $q$  range of the scattering curve showed that concentration increase did not have an effect on the oligomerization or aggregation states of the sample (figure 3.25).

Data quality was analyzed by performing a Guinier analysis, which evaluates scattering data at small scattering angles. A Guinier analysis plots the logarithm of the scattering intensity versus the square of the amplitude of the scattering vector, and the linearity of the result is indicative of good data quality (including lack of aggregation). As can be observed from the analysis below, the radius of gyration ( $R_g$ ) and  $I_0$  value for monomeric ECAM obtained from the Guinier plot were 4.6 nm and 132.9, which are in agreement with the values from pair distribution analysis performed by GNOM ( $R_g = 4.6$ ,  $I_0 = 132.4$ ).  $R_g$  represents the volume of distribution of the sample, and refers to the rms distance of all of the particles from the axis of rotation.  $I_0$ , on the other hand, refers to the molecular weight. The shape of the pair distribution function corresponds to a globular protein with a maximum particle dimension ( $D_{max}$ ) of 16.1 nm (figure 3.26, table 3.4).

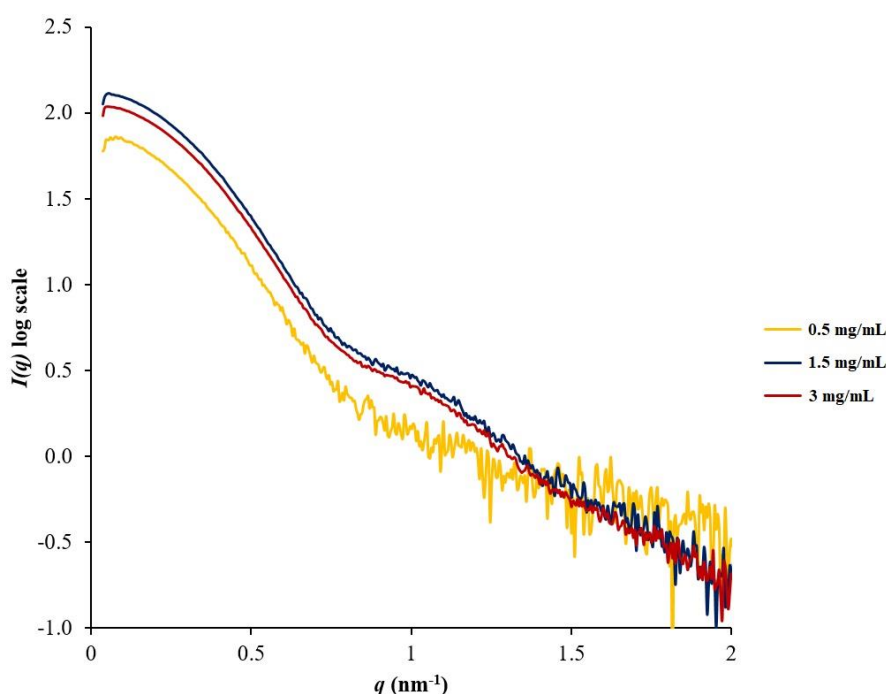
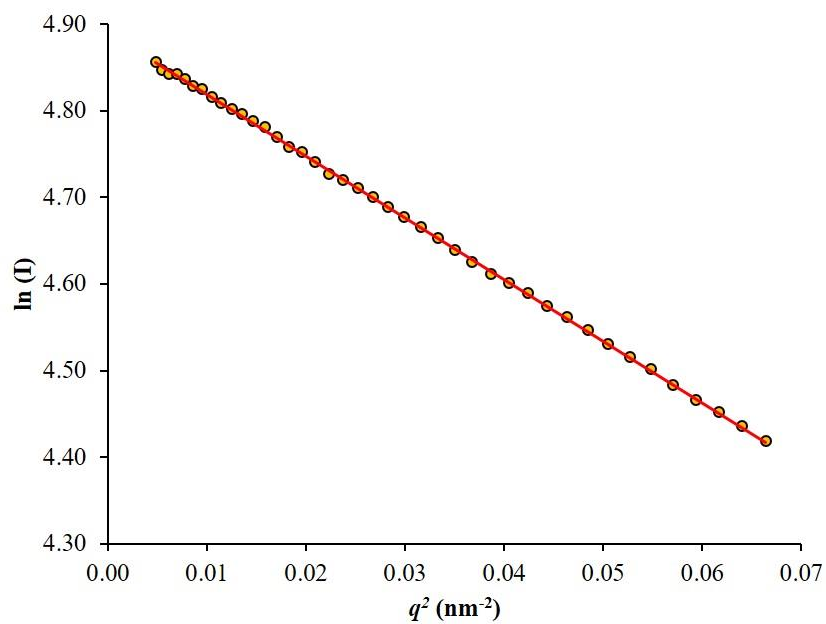


**Figure 3.25.** Scattering curves for the different concentrations of ECAM, plotted in the form of scattered X-ray intensity ( $I$ ) as a function of momentum transfer  $q$ . The shape of the curves in the low  $q$  range shows that the samples are not prone to aggregation with the increase of concentration.

Sample	Guinier analysis		GNOM analysis		
	$R_g$ (nm)	$I(0)$	$R_g$ (nm)	$I(0)$	$D_{max}$ (nm)
ECAM	4.6	132.9	4.6	132.4	16.1
PBP1c	4.2	174.4	4.5	176.7	17.4
PBP1c	5.1	173.5	5.4	176.6	21.4
Complex	8.3	93.2	8.3	92.6	24.6

**Table 3.4.** Properties of different samples tested by SAXS



B —

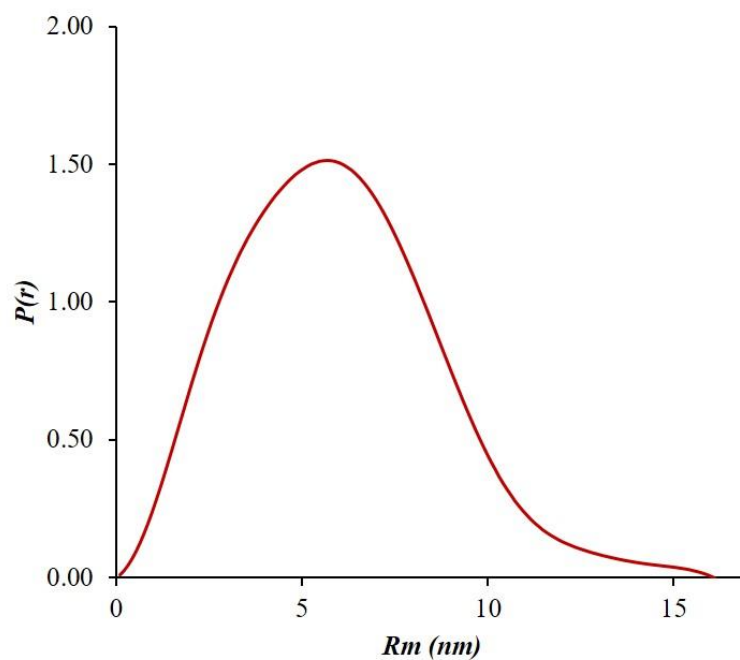


**Figure 3.26.** A - Guinier plot for the sample at 3 mg/mL, indicating a linear dependence of the logarithm of the scattering intensity  $I(S)$  versus the square of the amplitude of the scattering vector. B - Pair distribution function  $p(r)$  for ECAM obtained from the GNOM analysis. The curve is bell-shaped, suggesting the protein displays a globular shape. Maximum particle dimension ( $D_{\max}$ ) is 16.1 nm.

## SAXS experiments with PBP1c

Due to greater heterogeneity of PBP1c suggested by SEC-MALS (please see results on figure 3.11 above), the protein peak was studied by performing SAXS analyses on different sections of the peak that eluted from gel filtration. Two individual fractions were tested: a central fraction at 2.64 mg/mL, and a later fraction at 1.1 mg/mL (figure 3.27).

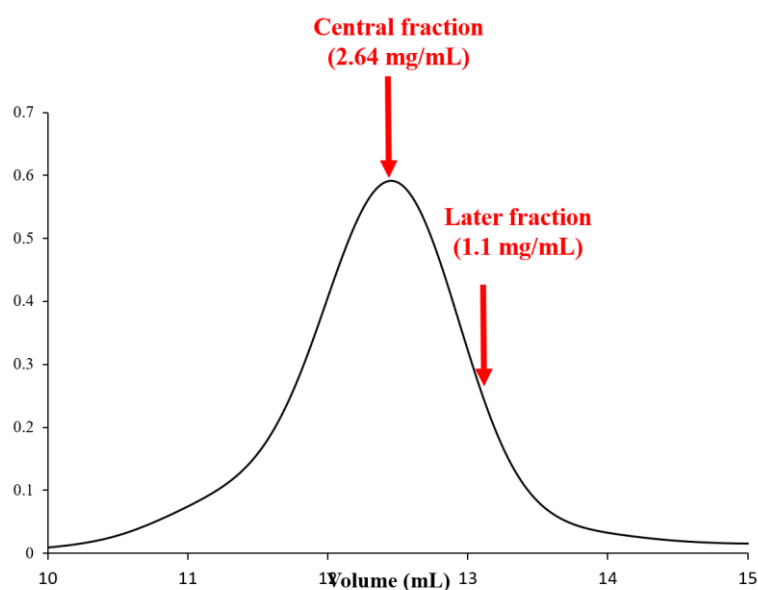


**Figure 3.27.** The position of two fractions of PBP1c in the elution profile from the Superdex 200 column that were tested in the SAXS experiment.

Analysis of scattering curves of the later fraction and subsequent Guinier analysis showed that samples did not display aggregation, as shown by the linearity of the result (figures 3.28 and 3.29a and b). If aggregation had been seen, the points would have appeared above the best fit line, creating a smiley Guinier effect. The Guinier plot-calculated  $R_g$  for the later fraction was 4.2 nm and  $I_0 = 174.4$  (figure 3.29a). The pair distribution function, calculated with GNOM, displayed a shape characteristic for an elongated molecule containing long tail and multiple peaks with the maximum particle dimension  $D_{\max} = 17.4$  nm. Based on the scattering data, the excluded volume calculated according to the Porod law was  $199.8 \text{ nm}^3$  (figure 3.27c).

The protein from the central fraction had  $R_g = 5.1$  nm and  $I_0 = 173.5$  (figure 3.29b). The pair distribution function also showed that it is an elongated molecule with  $D_{\max} = 21.4$

nm and a volume of  $369.5 \text{ nm}^3$  (figure 3.29d). These results suggested that the later fraction could correspond to monomers, while the central fraction could correspond to dimers.

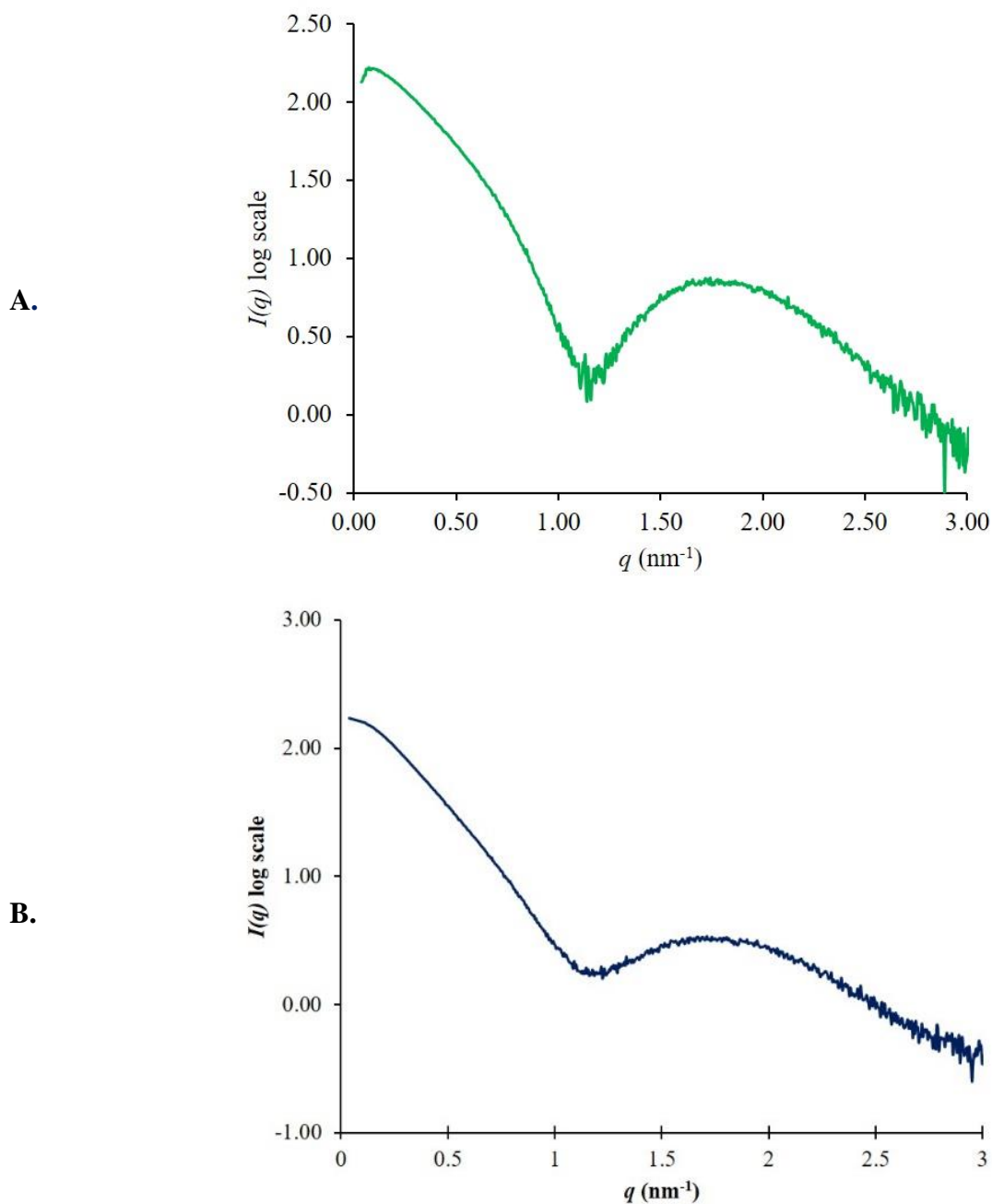


**Figure 3.28.** Scattering intensities for later (A) and central (B) fractions of PBP1c. Prior to SAXS measurements, PBP1c was subjected to a size exclusion chromatography and two different fractions originating from the elution peak were analyzed at concentrations of 1.1 (A) and 2.64 (B) mg/mL.

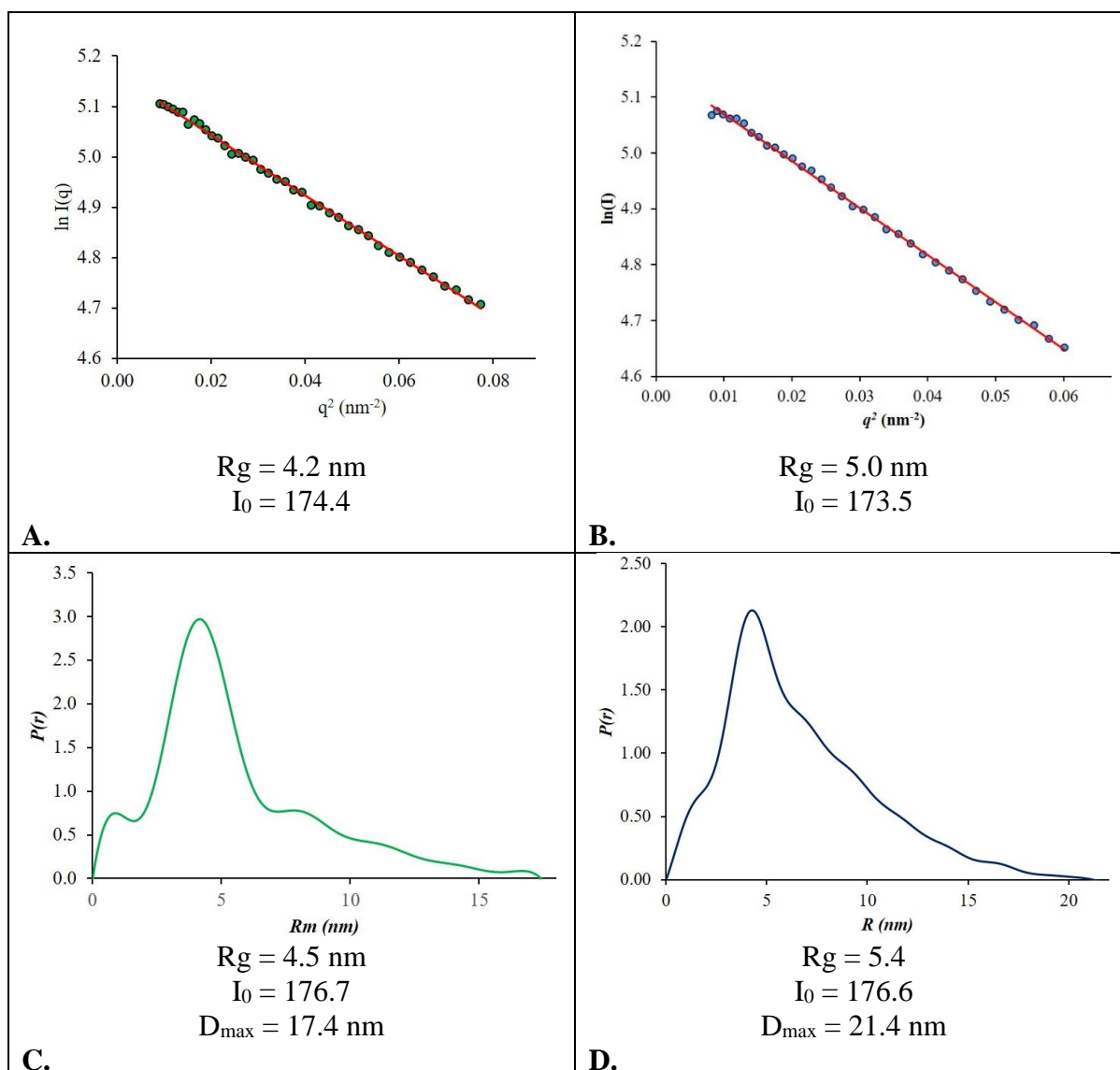
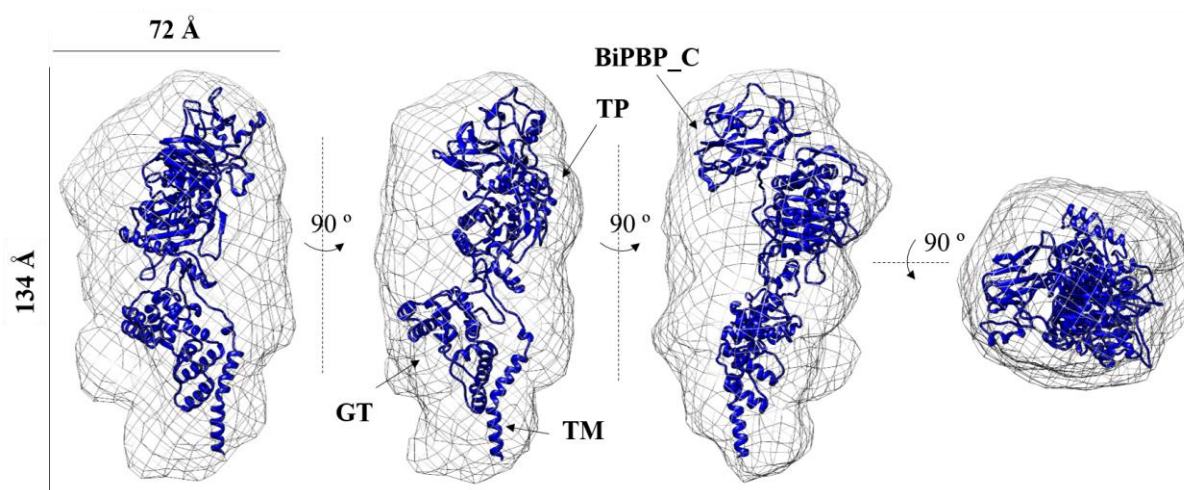


**Figure 3.29.** Guinier plots and pair distribution function for the latter fraction (A and C) and the central fraction of PBP1c from gel filtration (B and D) with  $R_g$ ,  $I_0$  and  $D_{\max}$  calculated using respective methods. Differences in sizes suggest that the later fraction corresponds to monomer, while the central fraction represents a dimeric form of PBP1c. In both cases, there was no aggregation observed.

The *ab initio* shape reconstitution of the monomer and dimer was performed using DAMMIN. In this procedure, 10 models for each sample were created from the pair distribution function, and these models were then analyzed and averaged by DAMAVER. This procedure yielded low-resolution models for both forms of PBP1c (figure 3.30). In the absence of the atomic structure of PBP1c, a model was created by the Robetta server by homology modeling. The region spanning residues 1-622 was modeled using the PBP1b structure from *E. coli* (PDB:

3FWL) as a reference, while the C-terminal domain of PBP1c, which lies between residues 623-770 and that does not display a homologous region in the structure of any PBP solved to date, was generated by the Robetta server using to the CbhA fibronectin(III)-like module from *Clostridium thermocellum* (PDB: 3PDD). This PBP1c model was subsequently used for manual fitting inside the two different envelopes obtained by DAMAVER (figure 3.30).

A.



B.

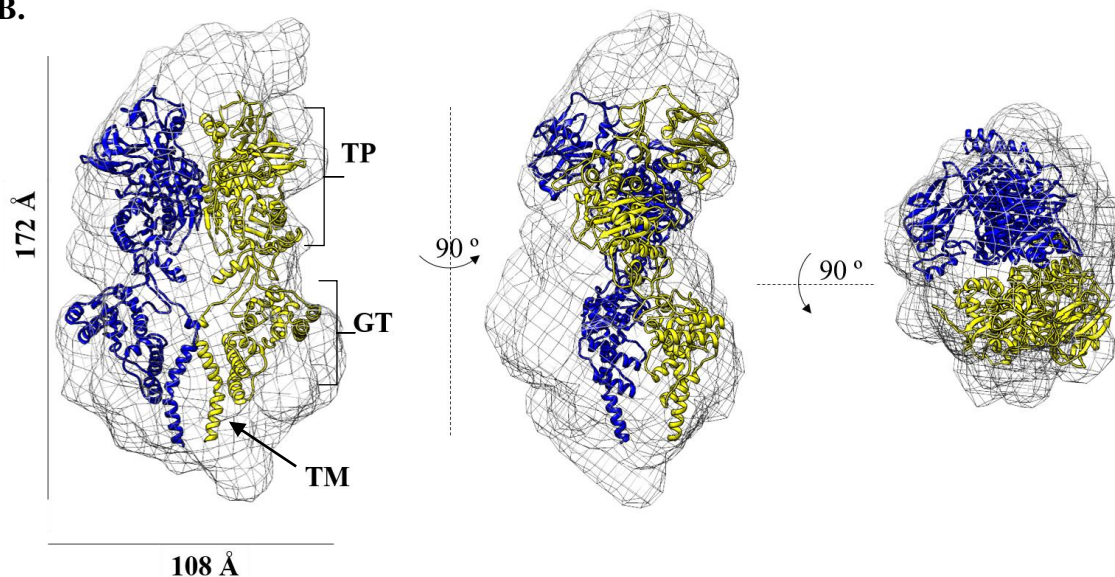


**Figure 3.30.** Low-resolution models for PBP1c monomer (A) and dimer (B) generated from the scattering data collected by SAXS. Ten models were created by DAMMIN for both monomer and dimer and subsequently averaged by DAMAVER. In the absence of the 3D structure of PBP1c, a model was created by Robetta server in a combination of homology and *ab initio* modelling. This model was fitted inside the envelopes. Fitting of the models, performed manually, provided additional evidence that the analyzed fractions corresponded to the monomer and dimer of PBP1c. TM – transmembrane domain; GT – glycosyltransferase domain; TP – transpeptidase domain.

In the envelope generated from data collected from the later fraction, it was possible to fit only one molecule of PBP1c, while the volume of the central fraction envelope allowed fitting of two PBP1c molecules. These results provide additional evidence that we identified two forms of PBP1c present in solution, monomer and dimer. So far, the presence of dimers and monomers of other class A PBPs has been shown using microbiological and biophysical methods, including surface plasmon resonance as well as cross-linking and Western blotting directly on bacterial membranes (Bertsche et al. 2005, Charpentier et al 2002) . However, to our knowledge, this is the first time that both forms of a class A PBP have been structurally characterized.

### **SAXS experiments performed with the ECAM-PBP1c complex**

The measurements of SAXS scattering data for the sample corresponding to the ECAM:PBP1c complex, isolated by size exclusion chromatography, were performed at the concentration of 0.3 mg/mL (figure 3.31a). As performed previously for PBP1c and ECAM, data were plotted by using the program PRIMUS (Konarev et al. 2003) in the form of  $I(q)$  versus  $q$  ( $\text{nm}^{-1}$ ), and the pair distribution analysis was performed with GNOM (Svergun, 1992). PRIMUS allowed the calculation of the Porod volume. The obtained values of  $R_g = 8.28$  nm,  $D_{\text{max}} = 24.65$  nm and volume of  $1220$  nm<sup>3</sup> were larger than those of the individual proteins (figure 3.31b and c). The calculated molecular mass based on the Porod volume was in a range between 610 and 813 kDa. Considering the individual masses of 182 and 87 kDa for ECAM and PBP1c, and the detergent bound to PBP1c, this indicates that the complex could be composed of 2 ECAM and 2 PBP1c molecules, confirming the results obtained by analytical ultracentrifugation.

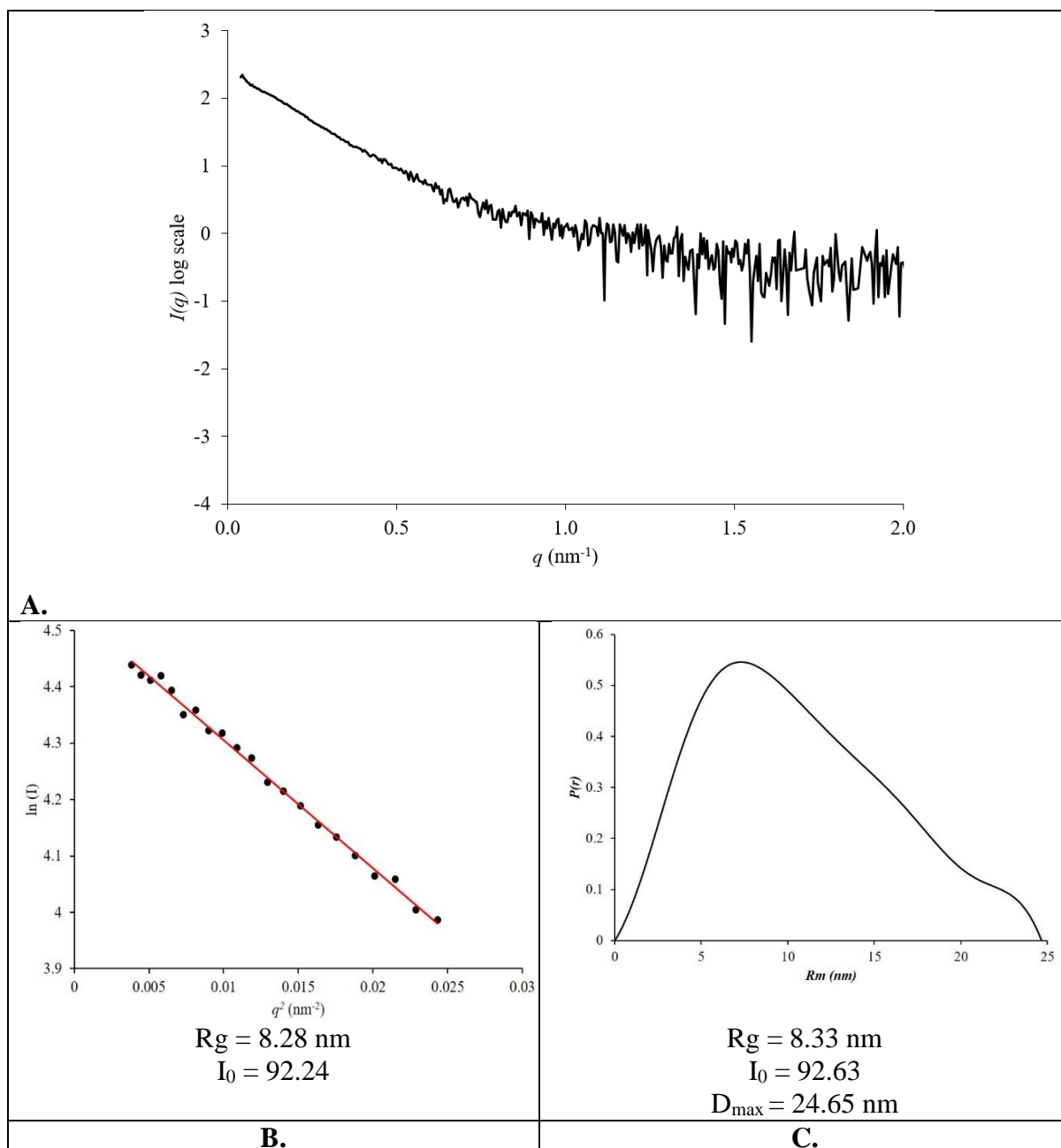


**Figure 3.31.** Scattering intensities (A), Guinier analysis (B) and pair distribution function (C) for the ECAM-PBP1c complex. Data were collected at beamline BM29 at the ESRF, and the sample was gel filtered before analysis.

The low-resolution model of the complex was generated by DAMMIN and DAMAVER, as performed above for the different forms of PBP1c. Subsequently, the structure of Sa-A2M ( $\alpha$ 2M from *S. enterica*) and the Robetta-derived PBP1c model were manually fitted into the envelopes. Interestingly, this allowed the inclusion two molecules of Sa-A2M and two of PBP1c, suggesting that the envelopes could indeed correspond to the 2:2 complex suggested by AUC measurements, discussed above. .

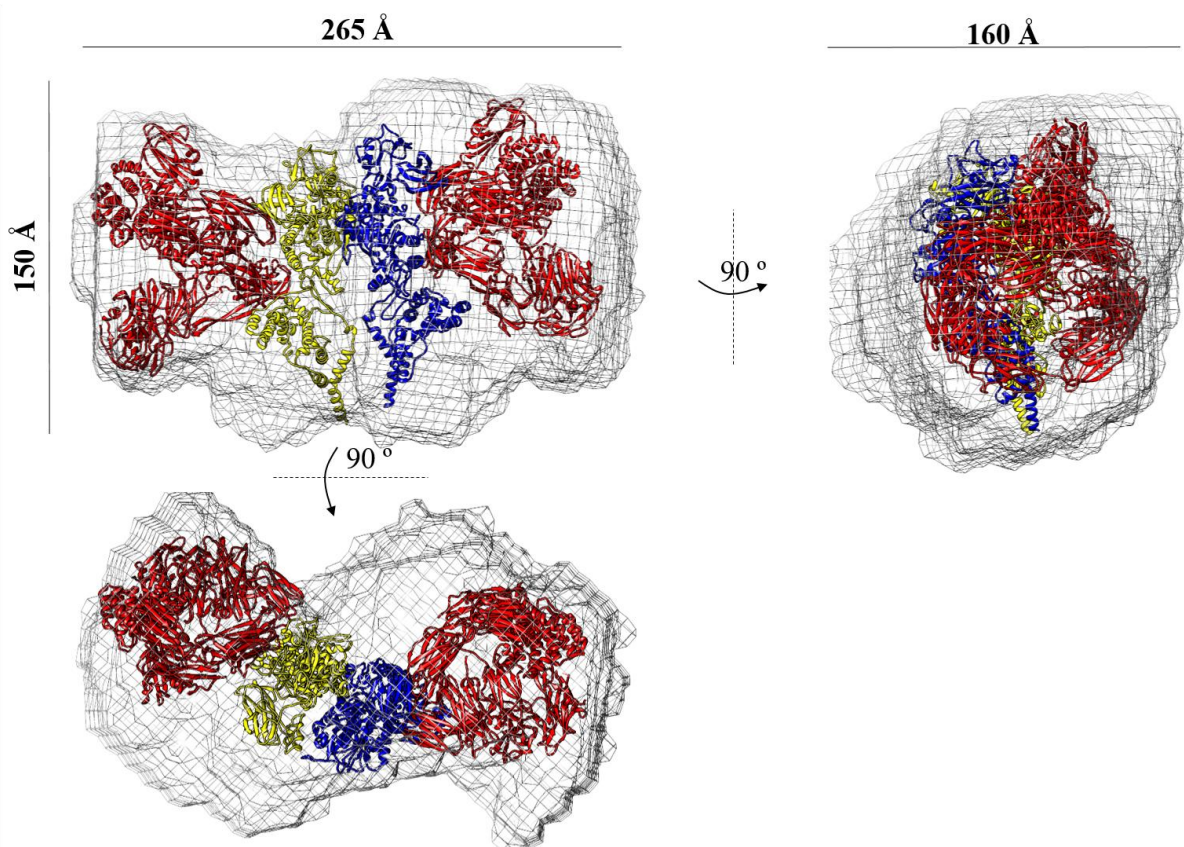


**Figure 3.32.** Low-resolution envelopes for the ECAM-PBP1c complex generated by DAMMIN and DAMAVER based on the scattering intensities obtained by SAXS. For the fitting, the structure of  $\alpha 2M$  from *S. enterica* (Sa-A2M, PDB: 4U48) and the model of PBP1c obtained from Robetta server, described above, were employed. Fitting was performed manually. The volume of the envelope allowed fitting of 2  $\alpha 2M$  and 2 PBP1c molecules, further confirming the previously established stoichiometry of ECAM:PBP1c=2:2



## **IV**

# **DISCUSSION AND PERSPECTIVES**



The bacterial cell wall is the main protective layer of bacterial cells and it is under a constant pressure from the host immune system during colonization and infection (Höltje 1998). In Gram-negative bacteria, the outer membrane can be breached, allowing various bactericidal agents entry to the periplasmic space. Agents such as lysozyme can hydrolyze peptidoglycan, while proteases eliminate proteins engaged in peptidoglycan synthesis and remodeling, leaving cells without any protection against osmotic pressure, which could result in cell lysis (Ellison & Giehl 1991; Reeves et al. 2002). The gene coding for a broad-range protease inhibitor,  $\alpha 2M$  (also known as ECAM in *E. coli*), the most abundant protease inhibitor in metazoans, is also present in genomes of Gram-negative bacteria (Budd et al. 2004). It is located in an operon that also expresses a gene encoding for PBP1c, a poorly characterized peptidoglycan synthase. Given their periplasmic localization and the fact that their transcription is under control of the same promoter, it is reasonable to believe that  $\alpha 2M$  and PBP1c could associate, forming a complex in order to maintain the integrity of the periplasmic space. To date, however, the nature of their interaction had not yet been investigated. This study focused on the biophysical and structural characterization of PBP1c from *E. coli*, as well as exploring the potential complex formation between PBP1c and ECAM.

PBP1c belongs to the class A Penicillin-Binding Proteins (PBPs), along with PBP1a and PBP1b (Schiffer & Höltje 1999). Class A PBPs are bifunctional enzymes that act in peptidoglycan synthesis, performing both glycan chain polymerization and peptide cross-linking (Goffin & Ghuysen 1998). Analysis of the PBP1c amino acid sequence showed that the protein has four potential domains: a 20-residue transmembrane helix (TM), a glycosyltransferase (GT) domain, a transpeptidase (TP) domain and PBP1c-specific Bi\_PBPC domain at its C-terminus, predicted to consist entirely of  $\beta$ -strands. The function of the Bi\_PBPC domain is not known. The crystal structure of PBP1b, on the other hand, showed that apart from TM, GT and TP domains, PBP1b has an additional non-catalytic domain, UB2H, that plays a role in interaction with its outer-membrane activator, LpoB (Sung et al. 2009) (Typas et al. 2010). Thus, it is possible that the Bi\_PBPC domain plays a similar role in PBP1c.

In the initial expression and purification trials, the PBP1c construct without the TM domain was tested. The protein was highly expressed in the BL21(DE3) strain of *E. coli*. However, none of the attempts to obtain the protein in soluble form were successful. The reason for that was not due to the presence of incorrectly formed disulfide bonds, since neither

expression in Shuffle cells engineered for correct folding of disulfide bond containing proteins, nor expression of truncated constructs lacking cysteine residues prevented the aggregation of PBP1c.

On the other hand, the full-length PBP1c construct containing TM was soluble and readily purified from the inner membranes of C41 cells. The most plausible explanation would be that TM helix stabilizes the GT domain at the domain-membrane interface, as in the case of PBP1b. The crystal structure of *E. coli* PBP1b showed that several hydrophobic residues of the TM helix are localized in close vicinity to the hydrophobic residues of the GT domain (Sung et al. 2009). Furthermore, the lack of the TM helix impacts the binding affinity of a GTase inhibitor moenomycin to the GT domain of PBP1b (Cheng et al. 2008). The conservation of aforementioned hydrophobic residues suggests that the similar interaction could also be present in PBP1c.

During the solubility trials, a Western blot analysis showed that, apart from the expected band of PBP1c at around 90 kDa, a PBP1c-specific band, displaying twice the expected molecular mass of PBP1c, could also be identified. Similar results had been previously observed for the other class A PBPs and subsequent studies identified that this band corresponded to the dimeric forms of the proteins (Zijderveld et al. 1991; Zijderveld et al. 1995). In the case of the work developed here, the existence of the PBP1c dimers was confirmed by analytical ultracentrifugation and SEC-MALS experiments, and dimers were the predominant species in solution. The SAXS analysis further identified the presence of both monomers and dimers in different fractions from the gel filtration elution profile. Scattering data also allowed us to obtain low-resolution models for both.

Notably, it was possible to perform a manual fit of the PBP1c model, obtained by Robetta, into the envelopes obtained through the SAXS experiments. Interestingly, upon analysis of the model of the dimer (figure 3.30), the suggested fit places both TM helices in close proximity, which would be the expected conformation upon interaction with the membrane. Both C-terminal regions of PBP1c would be positioned 'away' from the membrane, being available for recognition of partner molecules, for example.

PBP1c showed a tendency to precipitate in solution. Thus, numerous conditions were tested in aggregation assays to increase stability of the protein. The increase in NaCl

concentration from 300 to 500 mM and the addition of 5% glycerol in the samples substantially decreased the amount of precipitation and increased the aggregation onset temperature by 5 °C. The addition of 10 µM moenomycin, a specific inhibitor of the GTase activity, exhibited the greatest impact on PBP1c, delaying aggregation by 7 °C. This is in accordance with observations made during the crystallization trials for *E. coli* PBP1b, in which the addition of moenomycin was essential to obtain protein crystals (King et al. 2017).

ECAM had already been well characterized (Neves et al. 2012). The protein is overexpressed and highly soluble. The appearance of the short form of ECAM in the eluate from the nickel affinity column suggested that the protein was cleaved by intracellular proteases. However, forms that were larger than the monomer were also observed on SDS-PAGE. These were most likely dimers that associated upon cleavage, an observation already made by Garcia-Ferrer et al. (Garcia-Ferrer et al. 2015). Both the cleaved form and the oligomers were easily removed from the sample by anion exchange chromatography, resulting in a homogenous, monodisperse sample.

Mixing previously purified ECAM and PBP1c resulted in formation of a complex containing both proteins, as confirmed by SDS-PAGE, and it could be clearly separated from the individual proteins in gel filtration. Thus, for the first time, we demonstrated that ECAM and PBP1c physically interact and form a stable complex. Analytical ultracentrifugation analyses showed the presence of two complex species that sedimented as particles of 450 and 900 kDa, suggesting that the proteins could associate in ratios of 2:2 and 4:4. SAXS confirmed the presence of a 2:2 complex, with higher  $R_g$  and  $D_{max}$  values as compared to the individual proteins. Moreover, SAXS data were used to obtain a low-resolution envelope of the complex in solution in which it was possible to fit 2 copies of ECAM and a model of PBP1c generated by the program Robetta.

Despite the fact that generating a reasonable fit of four proteins into an envelope calculated from SAXS data can be very challenging, one possibility could be the one that is suggested in the figure above. In this fit, the PBP1c dimer is maintained, with each monomer associated to an individual ECAM molecule. If this architecture were to represent the association between ECAM and PBP1c on the bacterial cell, this would allow the bacterium to maintain PBP1c in dimeric form, and at the same time allow a fruitful association with ECAM monomers.

The peptidoglycan synthase activity of PBP1c tested in assays with radioactive and fluorescent Lipid II showed that, despite the presence of mutations in the catalytic site of the GT domain, the glycosyltransferase activity was unaffected. The presence of mutations within the GT domain of PBP1c was first described by Schiffer & Holtje (1999), who performed a sequence analysis between class A PBPs from *E. coli* and noticed that the highly conserved residues Arg136, Glu140, and Arg218 were replaced by Gly, Gln and Ala, respectively. In this paper, the authors employed two different assays to measure the GT activity of PBP1c, both involving the membrane-associated enzyme. In both cases, GT activity could be measured, and this activity was sensitive to moenomycin. Thus, PBP1c is an unusual GTase, and its structural characterization in atomic detail will provide key information regarding glycan chain polymerization without the well-studied and conserved amino acids.

No transpeptidase activity for PBP1c could be detected using the assay described above, despite the fact that a sequence analysis showed that the catalytic residues of the TP domain were all conserved and PBP1c bound some labeled  $\beta$ -lactams. Interestingly, the unusual aspect of the TP domain had also been suggested by Schiffer and Holtje (Schiffer & Holtje, 1999), who had pointed out the fact that the TP domain PBP1c must be distinct from that of its *E. coli* counterparts, PBP1a and PBP1b. At the time, the authors suggested that PBP1c could function in the bacterial cell as a monofunctional GTase, and that its TP domain could be used primarily for interacting with partner molecules. Our results provide some indication that this could indeed be the case since preliminary experiments have suggested that in the presence of ECAM, PBP1c produced longer glycan chains. Even though these results are yet to be confirmed by additional assays, they open the exciting perspective that one of the functions of ECAM could be to enhance the GTase activity of PBP1c, thus playing a key role in periplasm protection upon breaching of the outer membrane.

If this were to be the case, this would explain an aspect that has to date been unexplained: the need for *E. coli* to maintain three class A PBPs, especially considering that PBP1c is non-essential. If PBP1c acts indeed uniquely as a glycosyltransferase in moments when the outer membrane is breached, this suggests that it could play a role of ‘guardian of the periplasm’. This possibility is currently being investigated in the laboratory.

This work established the basis for the future studies of the interaction between ECAM and PBP1c. The stability of the complex should be confirmed by determining the dissociation constant, using techniques such as isothermal titration calorimetry (ITC) or surface plasmon resonance (SPR). The regions of interaction could be initially be identified by testing C-terminal truncated variants of PBP1c. Furthermore, testing the behavior of the complex in the presence of different proteases could give an insight in the nature of association and dissociation of the partners in physiologically relevant conditions and its effect on the activity of PBP1c. The lack of transpeptidase activity of PBP1c suggests that it may require additional activation in the same way as LpoA and LpoB stimulate the activity of PBP1a and PBP1b from *E. coli* (Paradis-Bleau et al. 2010; Typas et al. 2010). This could be investigated by expression of PBP1c and cross-linking in the periplasm or by a pull-down assay.

For the in-depth structural studies, different approaches could be integrated. We showed that PBP1c is able to crystallize. Further efforts should be directed to the optimization of the crystallization conditions with the goal of obtaining a high-resolution structure of PBP1c. For the structure of the complex, cryo-EM could be the technique of choice. In order to obtain homogenous samples for single-particle cryo-EM experiments, the GraFix method could be employed, in which samples are cross-linked in an ultracentrifugation gradient and the particles of different sizes are separated in different layers of glycerol (Stark 2010).

Finally, microbiological studies should offer an answer on the conditions that trigger the expression of  $\alpha$ 2M and PBP1c and examine the effects of this defense complex for bacterial cell survival during infectious or bacterial competition tests. These assays are currently under development in the laboratory.

## References

- Andersen, G.R. et al., 1995. Low resolution X-ray structure of human methylamine-treated  $\alpha$ 2-macroglobulin. *Journal of Biological Chemistry*, 270(42), pp.25133–25141.
- Armstrong, P.B., 2006. Proteases and protease inhibitors: a balance of activities in host–pathogen interaction. *Immunobiology*, 211(4), pp.263–281.
- Armstrong, P.B. & Quigley, J.P., 1999.  $\alpha$ 2 -macroglobulin: an evolutionarily conserved arm of the innate immune system. *Developmental and Comparative Immunology*, 23, pp.375–390.
- Banzhaf, M. et al., 2012. Cooperativity of peptidoglycan synthases active in bacterial cell elongation. *Molecular microbiology*, 85(1), pp.179–194.
- Barreteau, H. et al., 2008. Cytoplasmic steps of peptidoglycan biosynthesis. *FEMS microbiology reviews*, 32(2), pp.168–207.
- Barrett, A., Brown, M. & Sayers, C., 1979. The electrophoretically 'slow' and 'fast' forms of the alpha 2-macroglobulin molecule. *Biochem J*, 181, pp.401–418.
- Bender, R. & Bayne, C., 1996. Purification and characterization of a tetrameric  $\alpha$ -macroglobulin protease inhibitor from the gastropod mollusc, *Biomphalaria glabrata*. *Biochem J*, 316, pp.893–900.
- Bertsche, U. et al., 2005. In vitro murein peptidoglycan synthesis by dimers of the bifunctional transglycosylase-transpeptidase PBP1B from *Escherichia coli*. *J Biol Chem*, 280, pp.38096–38101.
- Bertsche, U. et al., 2006. Interaction between two murein (peptidoglycan) synthases, PBP3 and PBP1B, in *Escherichia coli*. *Molecular Microbiology*, 61(3), pp.675–690.
- Blandin, S. & Levashina, E., 2004. Thioester-containing proteins and insect immunity. *Molecular Immunology*, 40(12), pp.903–908.
- Blumberg, P. & Strominger, J., 1974. Interaction of penicillin with the bacterial cell: penicillin-binding proteins and penicillin-sensitive enzymes. *Bacteriol Rev*, 38(3), pp.291–335.
- Boneca, I. et al., 2000. Characterization of *Staphylococcus aureus* cell wall glycan strands, evidence for a new beta-N-acetylglucosaminidase activity. *Journal of Biological Chemistry*, 275, pp.9910–9918.
- Born, P., Breukink, E. & Vollmer, W., 2006. In vitro synthesis of cross-linked murein and its attachment to sacculi by PBP1A from *Escherichia coli*. *J Biol Chem*, 281, pp.26985–26993.
- Bouhss, A. et al., 2007. The biosynthesis of peptidoglycan lipid-linked intermediates. *FEMS microbiology reviews*, 32(2), pp.208–233.

- Bozzola, J. & Russell, L., 1991. *Electron Microscopy: Principles and Techniques for Biologists* First edition., Jones & Bartlett Pub.
- Bräu, B. et al., 1991. Increased yield of a lysozyme after self-cloning of the gene in *Streptomyces coelicolor* "Müller. *Appl Microbiol Biotechnol*, 34(4), pp.481–487.
- Brown, L. et al., 2015. Through the wall: extracellular vesicles in Gram-positive bacteria, mycobacteria and fungi. *Nat Rev Microbiol*, 13(10), pp.620–630.
- Buchan, D. et al., 2013. Scalable web services for the PSIPRED Protein Analysis Workbench. *Nucleic Acids Research*, 41(W1), pp.W340–W348.
- Budd, A. et al., 2004. Bacterial  $\alpha$ 2-macroglobulins: colonization factors acquired by horizontal gene transfer from the metazoan genome? *Genome biology*, 5(6), p.R38.
- Caffrey, C. et al., 2004. Blood 'n' guts: an update on schistosome digestive peptidases. *Trends Parasitol*, 20(5), pp.241–248.
- Carlsson, J., Höfling, J. & Sundqvist, G., 1984. Degradation of albumin, haemopexin, haptoglobin and transferrin, by black-pigmented *Bacteroides* species. *J Med Microbiol*, 18, pp.39–46.
- Casadevall, A. & Pirofski, L., 2003. The damage-response framework of microbial pathogenesis. *Nat Rev Microbiol*, 1(1), pp.17–24.
- Chalut, C., Remy, M. & Masson, J., 1999. Disulfide bridges are not involved in penicillin-binding protein 1b dimerization in *Escherichia coli*. *J Bacteriol*, 181(9), pp.2970–2972.
- Charpentier, X. et al., 2002. Penicillin-Binding Proteins 1a and 1b Form Independent Dimers in *Escherichia coli*. *Jurnal of Bacteriology*, 184, pp.3749–3752.
- Cheng, T. et al., 2008. Domain requirement of moenomycin binding to bifunctional transglycosylases and development of high-throughput discovery of antibiotics. *PNAS*, 105(2), pp.431–436.
- Cohan, F., 2002. What are bacterial species? *Annu Rev Microbiol*, 56, pp.457–487.
- Cole, J.L. et al., 2008. Analytical ultracentrifugation: sedimentation velocity and sedimentation equilibrium. *Methods in cell biology*, 84, pp.143–179.
- Consortium, T.U., 2017. UniProt: the universal protein knowledgebase. *Nucleic Acids Research*, 45(D1), pp.D158–D169.
- Curtis, T., Sloan, W. & Scannell, J., 2002. Estimating prokaryotic diversity and its limits. *PNAS*, 99(16), pp.10494–10499.
- Dam, J. & Schuck, P., 2004. Calculating Sedimentation Coefficient Distributions by Direct Modeling of Sedimentation Velocity Concentration Profiles. *Methods in Enzymology*, 384, pp.185–212.

- Denome, S. et al., 1999. Escherichia coli mutants lacking all possible combinations of eight penicillin binding proteins: viability, characteristics, and implications for peptidoglycan synthesis. *Journal of Bacteriology*, 181(13), pp.3981–3993.
- Derouaux, A., Sauvage, E. & Terrak, M., 2013. Peptidoglycan glycosyltransferase substrate mimics as templates for the design of new antibacterial drugs. *Front Immunol*, 4, p.78.
- Diamond, G. et al., 2009. The Roles of Antimicrobial Peptides in Innate Host Defense. *Curr Pharm Des*, 15(21), pp.2377–2392.
- Diard, W. M an Hardt, 2017. Evolution of bacterial virulence. *FEMS Microbiol Rev*, 41(5), pp.679–697.
- Doan, N. & Gettins, P.G., 2008.  $\alpha$ -Macroglobulins Are Present in Some Gram-negative Bacteria: characterization  $\alpha$ 2-macroglobulin from Escherichia coli. *Journal of Biological Chemistry*, 283(42), pp.28747–28756.
- Dramsı, S. et al., 2008. Covalent attachment of proteins to peptidoglycan. *FEMS microbiology reviews*, 32(2), pp.307–320.
- Dykhuisen, D., 2005. Species Numbers in Bacteria. *Proc Calif Acad Sci*, 56(6), pp.62–71.
- Egan, A.J. et al., 2015. Activities and regulation of peptidoglycan synthases. *Phil. Trans. R. Soc. B*, 370(1679), p.20150031.
- El Zoeiby, A., Sanschagrın, F. & Levesque, R., 2003. Structure and function of the Mur enzymes: development of novel inhibitors. *Molecular Microbiology*, 47(1), pp.1–12.
- Ellison, R. & Giehl, T., 1991. Killing of gram-negative bacteria by lactoferrin and lysozyme. *J Clin Invest*, 88(4), pp.1080–1091.
- Floyd, M. et al., 2005. Captured diversity in a culture collection: case study of the geographic and habitat distributions of environmental isolates held at the american type culture collection. *Appl Environ Microbiol*, 71(6), pp.2813–2823.
- Francis, S., Sullivan, D. & Goldberg, D., 1997. Hemoglobin metabolism in the malaria parasite Plasmodium falciparum. *Annu Rev Microbiol*, 51, pp.97–123.
- Freifelder, D., 1983. *Physical Biochemistry: Applications to Biochemistry and Molecular Biology*, W.H.Freeman & Co Ltd.
- Fukuda, A. et al., 2002. Aminoacylation of the N-terminal cysteine is essential for Lol-dependent release of lipoproteins from membranes but does not depend on lipoprotein sorting signals. *Journal of Biological Chemistry*, 277(45), pp.43512–43518.
- Galliano, M.-F. et al., 2006. A novel protease inhibitor of the  $\alpha$ 2-macroglobulin family expressed in the human epidermis. *Journal of Biological Chemistry*, 281(9), pp.5780–5789.
- Garcia-Ferrer, I. et al., 2015. Structural and functional insights into Escherichia coli  $\alpha$ 2-macroglobulin endopeptidase snap-trap inhibition. *Proceedings of the National Academy of Sciences*, 112(27), pp.8290–8295.

- Gasteiger, E. et al., 2005. Protein Identification and Analysis Tools on the ExPASy Server. In J. Walker, ed. *The Proteomics Protocols Handbook*. Humana Press.
- Ghuysen, J., 1991. Serine beta-lactamases and penicillin-binding proteins. *Annu Rev Microbiol*, 45, pp.37–67.
- Goffin, C. & Ghuysen, J., 1998. Multimodular penicillin-binding proteins: an enigmatic family of orthologs and paralogs. *Microbiol Mol Biol Rev*, 62, pp.1079–1093.
- Goldman, R. & Gange, D., 2000. Inhibition of transglycosylation involved in bacterial peptidoglycan synthesis. *Curr Med Chem*, 7(8), pp.801–820.
- Hanakawa, Y. et al., 2004. Enzymatic and molecular characteristics of the efficiency and specificity of exfoliative toxin cleavage of desmoglein 1. *The Journal of Biological Chemistry*, 279(7), pp.5268–5277.
- Harz, H., Burgdorf, K. & Höltje, J., 1990. Isolation and separation of the glycan strands from murein of *Escherichia coli* by reversed-phase high-performance liquid chromatography. *Anal Biochem*, 190, pp.120–128.
- Heck, L., Morihara, K., et al., 1986. Specific cleavage of human type III and IV collagens by *Pseudomonas aeruginosa* elastase. *Infect Immun*, 51, pp.115–118.
- Heck, L., Morihara, K. & Abrahamson, D., 1986. Degradation of soluble laminin and depletion of tissue-associated basement membrane laminin by *Pseudomonas aeruginosa* elastase and alkaline protease. *Infect Immun*, 54, pp.149–153.
- Heijenoort, J. van, 2007. Lipid Intermediates in the Biosynthesis of Bacterial Peptidoglycan. *Microbiol Mol Biol Rev*, 71(4), pp.620–635.
- Henzler-Wildman, K.A. et al., 2004. Perturbation of the Hydrophobic Core of Lipid Bilayers by the Human Antimicrobial Peptide LL-37. *Biochemistry*, 43, pp.8459–8469.
- Hillenkamp, F. & Karas, M., 2007. The MALDI Process and Method. In F. Hillenkamp & J. Peter-Katalinić, eds. *MALDI MS: A Practical Guide to Instrumentation, Methods and Applications*. Wiley-VCH Verlag GmbH & Co. KGaA, Weinheim, Germany.
- Holtet, T. et al., 1994. Recombinant a2M receptor binding domain binds to the a2M receptor with high affinity. *Ann N Y Acad Sci*, 737, pp.480–482.
- Höltje, J., 1998. Growth of the stress-bearing and shape-maintaining murein sacculus of *Escherichia coli*. *Microbiol Mol Biol Rev*, 62(1), pp.181–203.
- Huang, C.-Y. et al., 2012. Crystal structure of *Staphylococcus aureus* transglycosylase in complex with a lipid II analog and elucidation of peptidoglycan synthesis mechanism. *Proceedings of the National Academy of Sciences*, 109(17), pp.6496–6501.
- Ishino, F. et al., 1980. Dual enzyme activities of cell wall peptidoglycan synthesis, peptidoglycan transglycosylase and penicillin-sensitive transpeptidase, in purified preparations of *Escherichia coli* penicillin-binding protein 1A. *Biochemical and biophysical research communications*, 97(1), pp.287–293.

- Janeway, C.J. et al., 2001. The complement system and innate immunity. In *The Immune System in Health and Disease*. Garland Science, New York.
- Jean, N. et al., 2014. Elongated structure of the outer-membrane activator of peptidoglycan synthesis LpoA: implications for PBP1A stimulation. *Structure*, 22(7), pp.1047–1054.
- Kantyka, T., Shaw, L. & Potempa, J., 2011. Papain-like proteases of *Staphylococcus aureus*. *Adv Exp Med Biol*, 712, pp.1–14.
- Kikhney, A. & Svergun, D., 2015. A practical guide to small angle X-ray scattering (SAXS) of flexible and intrinsically disordered proteins. *FEBS Letters*, 589, pp.2570–2577.
- King, D.T. et al., 2017. Structural Insights into Inhibition of *Escherichia coli* Penicillin-binding Protein 1B. *Journal of Biological Chemistry*, 292(3), pp.979–993.
- Konarev, P. et al., 2003. PRIMUS - a Windows-PC based system for small-angle scattering data analysis. *J Appl Cryst*, 36, pp.1277–1282.
- Kovacs-Simon, A., Titball, R. & Michell, S.L., 2011. Lipoproteins of bacterial pathogens. *Infection and immunity*, 79(2), pp.548–561.
- Kowalczyk, A.P. & Green, K.J., 2013. Structure, Function and Regulation of Desmosomes. *Prog Mol Biol Transl Sci*, 116, pp.95–118.
- Krieger, M. & Herz, J., 1994. Structures and functions of multiligand lipoprotein receptors: macrophage scavenger receptors and LDL-receptor-related protein (LRP). *Annu Rev Biochem*, 63, pp.601–637.
- Kristensen, T. et al., 1990. Evidence that the newly cloned low-density-lipoprotein receptor related protein (LRP) is the a 2 -macroglobulin receptor. *FEBS Lett*, 276, pp.151–155.
- Krogh, A. et al., 2001. Predicting transmembrane protein topology with a hidden Markov model: Application to complete genomes. *Journal of Molecular Biology*, 305(3), pp.567–580.
- Kukkonen, M. & Korhonen, T., 2004. The omptin family of enterobacterial surface proteases/adhesins: from housekeeping in *Escherichia coli* to systemic spread of *Yersinia pestis*. *Int J Med Microbiol*, 294(1), pp.7–14.
- Laarman, A. et al., 2011. *Staphylococcus aureus* Metalloprotease Aureolysin Cleaves Complement C3 To Mediate Immune Evasion. *The Journal of Immunology*, 186, pp.6445–6453.
- Labia, R., Baron, P. & Masson, J.-M., 1985. Binding of latamoxef (moxalactam) and its decarboxylated derivative to *Escherichia coli* and *Pseudomonas aeruginosa* penicillin-binding proteins. *Journal of Antimicrobial Chemotherapy*, 15(1), pp.9–15.
- Laddomada, F., Miyachiro, M. & Dessen, A., 2016. Structural Insights into Protein-Protein Interactions Involved in Bacterial Cell Wall Biogenesis. *Antibiotics*, 5(2), p.E14.
- Lairson, L. et al., 2008. Glycosyltransferases: structures, functions, and mechanisms. *Annu Rev Biochem*, 77, pp.521–555.

- LaMarre, J. et al., 1991. Cytokine binding and clearance properties of proteinase-activated alpha 2-macroglobulins. *Lab Invest*, 65(1), pp.3–14.
- Laskowski, M. & Kato, I., 1980. Protein inhibitors of proteinases. *Annu Rev Biochem*, 49, pp.593–626.
- Law, S. & Dodds, A., 1997. The internal thioester and the covalent binding properties of the complement proteins C3 and C4. *Protein Science*, 6(2), pp.263–274.
- Leclercq, S. et al., 2017. Interplay between Penicillin-binding proteins and SEDS proteins promotes bacterial cell wall synthesis. *Scientific Reports*, 7, p.43306.
- Levashina, E. et al., 2002. Thioester-containing proteins of protostomes. In R. Ezekowitz & J. Hoffmann, eds. Humana Press Inc, Totowa, NJ, pp. 155–173.
- Levi, M., Poll, T. van der & Büller, H.R., 2004. Bidirectional Relation Between Inflammation and Coagulation. *Circulation*, 109(22), pp.2698–2704.
- Loof, T. et al., 2011. Coagulation, an ancestral serine protease cascade, exerts a novel function in early immune defense. *Blood*, 118, pp.2589–2598.
- López-Otín, C. & Bond, J.S., 2008. Proteases: Multifunctional Enzymes in Life and Disease. *The Journal of Biological Chemistry*, 283, pp.30433–30437.
- Lovering, A.L. et al., 2007. Structural insight into the transglycosylation step of bacterial cell-wall biosynthesis. *Science*, 315(5817), pp.1402–1405.
- Macheboeuf, P. et al., 2006. Penicillin binding proteins: key players in bacterial cell cycle and drug resistance processes. *FEMS Microbiol Rev*, 30(5), pp.673–691.
- Malanovic, N. & Lohner, K., 2016. Gram-positive bacterial cell envelopes: The impact on the activity of antimicrobial peptides. *Biochimica et Biophysica Acta*, 1858(5), pp.936–946.
- Manat, G. et al., 2014. Deciphering the metabolism of undecaprenyl-phosphate: the bacterial cell-wall unit carrier at the membrane frontier. *Microbial Drug Resistance*, 20(3), pp.199–214.
- Marchler-Bauer, A. et al., 2015. CDD: NCBI’s conserved domain database. *Nucleic Acids Research*, 43, pp.222–226.
- Marrero, A. et al., 2012. The crystal structure of human  $\alpha$ 2-macroglobulin reveals a unique molecular cage. *Angewandte Chemie International Edition*, 51(14), pp.3340–3344.
- Matthias Haffke, M. et al., 2016. *nanoDSF: Label-free Thermal Unfolding Assay of G Protein Coupled Receptors for Compound Screening and Buffer Composition Optimization*, Center for Proteomic Chemistry, Novartis Institutes for Biomedical Research, Basel, Switzerland and NanoTemper Technologies GmbH Munich, Germany.
- Meeske, A. et al., 2015. MurJ and a novel lipid II flippase are required for cell wall biogenesis in *Bacillus subtilis*. *PNAS*, 112(20), pp.6437–6442.

- Mengin-Lecreux, D. & Lemaitre, B., 2005. Structure and metabolism of peptidoglycan and molecular requirements allowing its detection by the *Drosophila* innate immune system. *Journal of endotoxin research*, 11(2), pp.105–111.
- Mohammadi, T. et al., 2011. Identification of FtsW as a transporter of lipid-linked cell wall precursors across the membrane. *The EMBO journal*, 30(8), pp.1425–1432.
- Molla, A., Kagimoto, T. & Maeda, H., 1988. Cleavage of immunoglobulin G (IgG) and IgA around the hinge region by proteases from *Serratia marcescens*. *Infect Immun*, 56, pp.916–920.
- Nakagawa, J. & Matsushashi, M., 1982. Molecular divergence of a major peptidoglycan synthetase with transglycosylase-transpeptidase activities in *Escherichia coli*: penicillin-binding proteins 1Bs. *Biochem Biophys Res Commun*, 105, pp.1546–1553.
- Nakagawa, J., Tamaki, S. & Matsushashi, M., 1979. Purified penicillin binding proteins 1Bs from *Escherichia coli* membrane showing activities of both peptidoglycan polymerase and peptidoglycan crosslinking enzyme. *Agricultural and Biological Chemistry*, 43(6), pp.1379–1380.
- Nelson, D.E. et al., 2002. Contribution of membrane-binding and enzymatic domains of penicillin binding protein 5 to maintenance of uniform cellular morphology of *Escherichia coli*. *Journal of bacteriology*, 184(13), pp.3630–3639.
- Neuhaus, F.C. & Baddiley, J., 2003. A continuum of anionic charge: structures and functions of D-alanyl-teichoic acids in gram-positive bacteria. *Microbiology and Molecular Biology Reviews*, 67(4), pp.686–723.
- Neves, D. et al., 2012. Conformational states of a bacterial  $\alpha$ 2-macroglobulin resemble those of human complement C3. *PLoS One*, 7(4), p.e35384.
- Nielsen, K. & Sottrup-Jensen, L., 1993. Evidence from sequence analysis that hen egg-white ovomacroglobulin (ovostatin) is devoid of an internal beta-Cys-gamma-Glu thiol ester. *Biochim Biophys Acta*, 1162, pp.230–232.
- NIH, 2012. NIH Human Microbiome Project defines normal bacterial makeup of the body. Available at: <https://www.nih.gov/news-events/news-releases/nih-human-microbiome-project-defines-normal-bacterial-make-up-body>.
- Nilsson, J., Persson, B. & Heijne G, 2005. Comparative analysis of amino acid distributions in integral membrane proteins from 107 genomes. *Proteins*, 60(4), pp.606–616.
- Oleksy, A. et al., 2004. Growth phase-dependent production of a cell wall-associated elastolytic cysteine proteinase by *Staphylococcus epidermidis*. *Biol Chem*, 385, pp.525–535.
- Overbergh, L. et al., 1994. Identification of Four Genes Coding for Isoforms of Murinoglobulin, the Monomeric Mouse  $\alpha$  2-Macroglobulin: Characterization of the Exons Coding for the Bait Region. *Genomics*, 22(3), pp.530–539.
- Paradis-Bleau, C. et al., 2010. Lipoprotein cofactors located in the outer membrane activate bacterial cell wall polymerases. *Cell*, 143(7), pp.1110–1120.

- Pernot, P. et al., 2013. Upgraded ESRF BM29 beamline for SAXS on macromolecules in solution. *Journal of synchrotron radiation*, 20(4), pp.660–664.
- Peters, K. et al., 2016. The Redundancy of Peptidoglycan Carboxypeptidases Ensures Robust Cell Shape Maintenance in *Escherichia coli*. *MBio*, 7(3), pp.819–16.
- Peterson, J., 1996. Bacterial Pathogenesis. In S. Baron, ed. *Medical Microbiology*. Galveston (TX): University of Texas Medical Branch at Galveston.
- Pham, V. & Kim, J., 2012. Cultivation of unculturable soil bacteria. *Trends Biotechnol*, 30(9), pp.475–484.
- Del Portillo, F.G. & Pedro, M.A. de, 1990. Differential effect of mutational impairment of penicillin-binding proteins 1A and 1B on *Escherichia coli* strains harboring thermosensitive mutations in the cell division genes *ftsA*, *ftsQ*, *ftsZ*, and *pbpB*. *Journal of bacteriology*, 172(10), pp.5863–5870.
- Pothecary, M., 2014. When only a MALS detector will do. *The Analytical Scientist*, 0514, p.CC001.
- Putnam, C. et al., 2007. X-ray solution scattering (SAXS) combined with crystallography and computation: defining accurate macromolecular structures, conformations and assemblies in solution. *Q Rev Biophys*, 40(3), pp.191–285.
- Quigley, J. et al., 1991. Reaction of proteinases with alpha 2-macroglobulin from the American horseshoe crab, *Limulus*. *Journal of Biological Chemistry*, 266, pp.19426–19431.
- Rani, K., Rana, R. & Datt, S., 2012. Review on latest overview of proteases. *International Journal of Current Life Sciences*, 2, pp.12–18.
- Reeves, E. et al., 2002. Killing activity of neutrophils is mediated through activation of proteases by K<sup>+</sup> flux. *Nature*, 416(6878), pp.291–297.
- Rehman, A., Ahsan, H. & Khan, F., 2013.  $\alpha$ -2-Macroglobulin: a physiological guardian. *J Cell Physiol*, 228(8), pp.1665–1675.
- Rini, J., Esko, J. & Varki, A., 2009. Glycosyltransferases and Glycan-processing Enzymes. In A. Varki et al., eds. *Essentials of Glycobiology*. Cold Spring Harbor (NY).
- Rogers, H., Perkins, H. & Ward, J., 1980. *Microbial Cell Walls and Membranes*, Springer Netherlands.
- Sakaguchi, M. et al., 1992. Functions of signal and signal-anchor sequences are determined by the balance between the hydrophobic segment and the N-terminal charge. *PNAS*, 89(1), pp.16–19.
- Sauvage, E. et al., 2008. The penicillin-binding proteins: structure and role in peptidoglycan biosynthesis. *FEMS microbiology reviews*, 32(2), pp.234–258.
- Scheffers, D. & Pinho, M., 2005. Bacterial cell wall synthesis: new insights from localization studies. *Microbiol Mol Biol Rev*, 69(4), pp.585–607.

- Schiffer, G. & Höltje, J.-V., 1999. Cloning and characterization of PBP 1C, a third member of the multimodular class A penicillin-binding proteins of *Escherichia coli*. *Journal of Biological Chemistry*, 274(45), pp.32031–32039.
- Schmidtchen, A. et al., 2003. Elastase-producing *Pseudomonas aeruginosa* degrade plasma proteins and extracellular products of human skin and fibroblasts, and inhibit fibroblast growth. *Microb Pathog*, 34, pp.47–55.
- Schmidtchen, A. et al., 2002. Proteinases of common pathogenic bacteria degrade and inactivate the antibacterial peptide LL-37. *Mol Microbiol*, 46, pp.157–168.
- Schwarz, U. et al., 1981. Penicillin-binding proteins of *Escherichia coli* identified with a 125I-derivative of ampicillin. *FEMS Microbiology Letters*, 10(2), pp.107–109.
- Sham, L. et al., 2014. Bacterial cell wall. MurJ is the flippase of lipid-linked precursors for peptidoglycan biogenesis. *Science*, 345(6193), pp.220–222.
- Shokal, U. & Eleftherianos, I., 2017. Evolution and Function of Thioester-Containing Proteins and the Complement System in the Innate Immune Response. *Front Immunol*, 8, p.759.
- Sieprawska-Lupa, M. et al., 2004. Degradation of human antimicrobial peptide LL-37 by *Staphylococcus aureus*-derived proteinases. *Antimicrob Agents Chemother*, 48, pp.4673–4679.
- Sievers, F. et al., 2011. Fast, scalable generation of high-quality protein multiple sequence alignments using Clustal Omega. *Mol Syst Biol*, 7, p.539.
- Signor, L. & Erba, E.B., 2013. Matrix-assisted laser desorption/ionization time of flight (MALDI-TOF) mass spectrometric analysis of intact proteins larger than 100 kDa. *Journal of visualized experiments: JoVE*, (79).
- Skou, S., Gillilan, R. & Ando, N., 2014. Synchrotron-based small-angle X-ray scattering of proteins in solution. *Nature Protocols*, 9(7), pp.1727–1739.
- Sodeinde, O. et al., 1992. A surface protease and the invasive character of plague. *Science*, 258(5084), pp.1004–1007.
- Song, Y. et al., 2013. High-resolution comparative modeling with RosettaCM. *Structure*, 21(10), pp.1735–1742.
- Sottrup-Jensen, L., 1989. Alpha-macroglobulins: structure, shape, and mechanism of proteinase complex formation. *Journal of Biological Chemistry*, 264(20), pp.11539–11542.
- Sottrup-Jensen, L. et al., 1990. Localization of epsilon-lysyl-gamma-glutamyl cross-links in five human alpha 2-macroglobulin-proteinase complexes. Nature of the high molecular weight cross-linked products. *Journal of Biological Chemistry*, 265(29), pp.17727–17737.
- Sottrup-Jensen, L. et al., 1981. Primary structure of the 'bait' region for proteinases in alpha 2-macroglobulin. Nature of the complex. *FEBS Lett*, 127(2), pp.167–173.

- Sottrup-Jensen, L. et al., 1989. Sequence diversity and localization of cleavage sites for proteinases in five mammalian alpha-macroglobulins. *J Biol Chem*, 264, pp.15781–15789.
- Sottrup-Jensen, L., Gliemann, J. & Van Leuven, F., 1986. Domain structure of human alpha 2-macroglobulin. Characterization of a receptor-binding domain obtained by digestion with papain. *FEBS Lett*, 205, pp.20–24.
- Spratt, B., 1975. Distinct penicillin binding proteins involved in the division, elongation, and shape of Escherichia coli K12. *PNAS*, 72(8), pp.2999–3003.
- Stafford, W.F., 1992. Boundary analysis in sedimentation transport experiments: a procedure for obtaining sedimentation coefficient distributions using the time derivative of the concentration profile. *Analytical Biochemistry*, 203(2), pp.295–301.
- Stark, H., 2010. GraFix: stabilization of fragile macromolecular complexes for single particle cryo-EM. *Methods Enzymol*, 481, pp.109–126.
- Striegel, A. et al., 2009. *Modern Size-Exclusion Liquid Chromatography: Practice of Gel Permeation and Gel Filtration Chromatography*, John Wiley & Sons.
- Su, Y. et al., 2011. The deficient cleavage of M protein-bound IgG by IdeS: insight into the escape of Streptococcus pyogenes from antibody-mediated immunity. *Molecular Immunology*, 49, pp.134–142.
- Sung, M.-T. et al., 2009. Crystal structure of the membrane-bound bifunctional transglycosylase PBP1b from Escherichia coli. *Proceedings of the National Academy of Sciences*, 106(22), pp.8824–8829.
- Suzuki, H., Nishimura, Y. & Hirota, Y., 1978. On the process of cellular division in Escherichia coli: a series of mutants of E. coli altered in the penicillin-binding proteins. *PNAS*, 75(2), pp.664–668.
- Svergun, D., 1992. Determination of the regularization parameter in indirect-transform methods using perceptual criteria. *J Appl Crystallogr*, 25, pp.495–503.
- Svergun, D., 1999. Restoring low resolution structure of biological macromolecules from solution scattering using simulated annealing. *Biophys J*, 76(6), pp.2879–2886.
- Tamaki, S., Nakajima, S. & Matsushashi, M., 1977. Thermosensitive mutation in Escherichia coli simultaneously causing defects in penicillin-binding protein-1Bs and in enzyme activity for peptidoglycan synthesis in vitro. *Proceedings of the National Academy of Sciences*, 74(12), pp.5472–5476.
- Tapon-Bretonnière, J. et al., 1985. Electron microscopy of the conformational changes of alpha 2-macroglobulin from human plasma. *The EMBO journal*, 4(1), pp.85–89.
- Taylor, L., Latham, S. & Woolhouse, M., 2001. Risk factors for human disease emergence. *Philos Trans R Soc Lond B Biol Sci*, 356(1411), pp.983–989.

- Terao, Y. et al., 2008. Group A Streptococcal Cysteine Protease Degrades C3 (C3b) and Contributes to Evasion of Innate Immunity. *Journal of Biological Chemistry*, 283, pp.6253–6260.
- Terrak, M. et al., 2008. Importance of the conserved residues in the peptidoglycan glycosyltransferase module of the class A penicillin-binding protein 1b of *Escherichia coli*. *Journal of biological chemistry*, 283(42), pp.28464–28470.
- Terrak, M. et al., 1999. The catalytic, glycosyl transferase and acyl transferase modules of the cell wall peptidoglycan-polymerizing penicillin-binding protein 1b of *Escherichia coli*. *Molecular Microbiology*, 34(2), pp.350–364.
- Tilley, D. et al., 2014. CpaA a novel protease from *Acinetobacter baumannii* clinical isolates deregulates blood coagulation. *FEMS Microbiol Lett*, 356, pp.53–61.
- Touzé, T. & Mengin-Lecreulx, D., 2008. Undecaprenyl Phosphate Synthesis. *EcoSal Plus*.
- Typas, A. et al., 2011. From the regulation of peptidoglycan synthesis to bacterial growth and morphology. *Nature reviews. Microbiology*, 10(2), p.123.
- Typas, A. et al., 2010. Regulation of peptidoglycan synthesis by outer-membrane proteins. *Cell*, 143(7), pp.1097–1109.
- Volkov, V. & Svergun, D., 2003. Uniqueness of ab-initio shape determination in small-angle scattering. *J Appl Cryst*, 36, pp.860–864.
- Vollmer, W., Blanot, D. & De Pedro, M.A., 2008. Peptidoglycan structure and architecture. *FEMS microbiology reviews*, 32(2), pp.149–167.
- Vollmer, W., Rechenberg, M. von & Höltje, J.-V., 1999. Demonstration of molecular interactions between the murein polymerase PBP1B, the lytic transglycosylase MltA, and the scaffolding protein MipA of *Escherichia coli*. *Journal of Biological Chemistry*, 274(10), pp.6726–6734.
- Wang, Z. et al., 2010. Pathogen entrapment by transglutaminase – a conserved early innate immune mechanism. *PLoS Pathog*, 6(2), p.e1000763.
- Ward, J., 1973. The chain length of the glycans in bacterial cell walls. *Biochem J*, 133, pp.395–398.
- Williams, M. & Baxter, R., 2014. The structure and function of thioester-containing proteins in arthropods. *Biophys Rev*, 6, pp.261–272.
- Wilson, J. et al., 2002. Mechanisms of bacterial pathogenicity. *Postgrad Med J*, 78(918), pp.216–224.
- Wong, S. & Dessen, A., 2014. Structure of a bacterial alpha-2-macroglobulin reveals mimicry of eukaryotic innate immunity. *Nature Communications*, 5, p.4917.
- Wyatt, A.R., Cater, J.H. & Ranson, M., 2016. PZP and PAI-2: Structurally-diverse, functionally similar pregnancy proteins? *The international journal of biochemistry & cell biology*, 79, pp.113–117.

- Yousif, S.Y., Broome-Smith, J.K. & Spratt, B.G., 1985. Lysis of *Escherichia coli* by  $\beta$ -Lactam Antibiotics: Deletion Analysis of the Role of Penicillin-binding Proteins 1A and 1B. *Microbiology*, 131(10), pp.2839–2845.
- Yuan, Y. et al., 2008. Structural analysis of the contacts anchoring moenomycin to peptidoglycan glycosyltransferases and implications for antibiotic design. *ACS chemical biology*, 3(7), pp.429–436.
- Zaslhoff, M., 2002. Antimicrobial peptides of multicellular organisms. *Nature*, 415, pp.389–395.
- Zhu, Y. et al., 2005. The ancient origin of the complement system. *EMBO J*, 24, pp.382–394.
- Zijderveld, C. et al., 1991. Penicillin-Binding Protein 1B of *Escherichia coli* Exists in Dimeric Forms. *Jurnal of Bacteriology*, 173, pp.5740–5746.
- Zijderveld, C., Aarsman, M. & Nanninga, N., 1995. Differences between inner membrane and peptidoglycan-associated PBP1B dimers of *Escherichia coli*. *J Bacteriol*, 177(7), pp.1860–1863.

## INDEX

- 2,5-dihydroxybenzoic acid (DHB), 45  
AmJ, 27  
analytical ultracentrifugation, 46, 47, 72, 82, 88  
angular dependence, 47  
antimicrobial peptides (AMPs), 13  
bait region, 16, 17, 18, 20, 22, 23  
bifunctional PBPs, 28, 29, 30, 31, 87, 92, 93, 101  
biotinylated ampicillin, 51, 75  
BiPBP\_C, 59  
Bocillin FL, 51  
Brij 35, 43, 44, 66, 67  
carboxypeptidation, 28, 30  
cell-free expression, 7, 39, 43, 44, 62, 66, 78  
Cellosyl, 51  
Class A PBPs, 28, 30, 32, 58, 87  
class B PBPs, 28, 30, 32  
Class C PBPs, 28, 58  
Coagulation, 14, 97  
cross-linking, 28, 31, 79, 87, 91  
crystallization, 54, 69, 78, 88, 91  
DDM, 42, 43, 50, 51, 63, 67, 69  
disaccharide-pentapeptide, 26  
divisome, 32  
DM, 41, 42, 43, 45, 46, 48, 50, 53, 63, 64, 66, 69, 72, 73, 81  
ECAM, 3, 4, 5, 6, 22, 23, 39, 40, 43, 45, 46, 48, 51, 52, 53, 54, 56, 57, 64, 71, 72, 73, 74, 76, 77, 78, 79, 80, 81, 82, 83, 84, 87, 89  
electron microscopy, 4, 8, 22, 35, 79  
elongosome, 32  
endopeptidation, 28  
**expression test**, 41  
fibrin clot, 14  
flippases, 26  
fos-choline 12, 61  
FtsW, 26, 97  
glycan chain polymerization, 28, 31, 87  
glycosyltransferase, 25, 30, 32, 33, 34, 59, 60, 75, 87, 89, 91, 93, 101  
GraFix, 79, 91, 101  
Gram-negative bacteria, 21, 24, 31, 87, 91  
Gram-positive bacteria, 21, 24, 31, 93  
GT domain, 33, 34, 59, 62, 69, 88, 89  
hemoglobin, 14  
high molecular weight (HMW) PBPs, 28  
LAPAO, 42, 50, 63, 68, 69  
Lipid I, 26  
Lipid II, 25, 26, 29, 30, 32, 51, 89  
Lipid IV, 29, 30  
low molecular weight (LMW), 28  
low-density lipoprotein related protein (LRP/ $\alpha$ 2M-R) receptor, 18  
macroglobulin-like domains, 20, 23  
MALDI-TOF, 45, 100  
MALS (Multi-angle light scattering), 7, 46, 47, 48, 57, 66, 81, 88, 99  
methylamine, 16, 20, 22, 92  
moenomycin, 50, 52, 69, 70, 78, 88, 93, 102  
monofunctional GTases, 29  
MraY, 26  
Mur ligases, 26  
MurC, 26  
MurD, 26  
MurE, 26  
MurJ, 27, 97, 100  
muroglobulin, 16  
N-acetylglucosamine (GlcNAc), 24  
N-acetylmuramic acid (MurNAc), 24, 25  
opsonization, 14  
ovostatin, 16, 18, 98  
PBP1a, 28, 29, 31, 32, 34, 58, 59, 60, 61, 63, 87, 91  
PBP1b, 29, 31, 32, 33, 34, 58, 59, 60, 61, 62, 63, 69, 73, 87, 88, 89, 91, 101  
PBP1c, 3, 4, 5, 6, 8, 22, 32, 34, 35, 39, 40, 41, 42, 43, 44, 45, 46, 48, 49, 50, 51, 52, 54, 58, 59, 60, 61, 62, 63, 64, 66, 67, 68, 69, 70, 71, 72, 73, 74, 75, 76, 77, 78, 79, 81, 82, 83, 84, 87, 88, 89, 91  
PBP2, 28, 29, 32, 34, 58  
PBP3, 28, 32, 58, 59, 61, 92  
penicillin, 28, 32, 34, 75, 92, 93, 94, 95, 96, 98, 99, 100, 101

Penicillin-Binding Protein 1c, 3, 22  
 Penicillin-Binding Proteins, 25, 28, 61, 87, 93  
 Pentapeptide, 25  
 peptidoglycan, 3, 24, 25, 26, 27, 28, 32, 34, 35, 51, 75, 76, 87, 89, 91, 92, 93, 94, 95, 97, 98, 99, 100, 101, 102, 103  
 pregnancy zone proteins, 16  
 protease inhibitor, 19, 35, 87, 92, 94  
 protease inhibitors, 3, 15, 16, 40, 42, 92  
 proteases, 3, 13, 14, 15, 18, 20, 21, 22, 35, 87, 89, 91, 95, 96, 97, 99  
 radius of gyration, 52, 53, 81  
 receptor-binding domain, 23, 100  
 RodA, 26  
 sarkosyl, 61, 63  
 SAXS (Small-angle X-ray scattering), 3, 6, 8, 22, 35, 52, 69, 81, 82, 83, 84, 88, 89, 95, 98, 99  
 sedimentation velocity, 46, 47, 48, 72, 93  
 sinapinic acid, 45  
 solubilization trial, 43, 61, 63, 66  
 SST, 79, 80  
 The complement system, 14, 95  
 Thermal stability, 49, 68  
 thioester bond, 3, 16, 18  
 thioester-containing proteins, 16, 17, 19, 102  
 TM helix, 62, 88  
 TP domain, 33, 34, 89  
 transmembrane helix, 28, 32, 40, 59, 61, 87  
 Transmission electron microscopy, 53  
 transpeptidation, 28, 30, 31, 76  
 TritonX-100, 63  
 tryptophan fluorescence, 49  
 UB2H domain, 33  
 undecaprenyl pyrophosphate, 26, 29, 30  
 uranyl acetate, 79, 80  
 Virulence factors, 12  
 yfaS, 21, 22  
 yfhM, 21, 22, 39  
 $\alpha_1I_3$ , 16  
 $\alpha_2Ms$ , 3, 5, 15, 16, 18, 19, 21, 22, 91  
 $\alpha$ -cyano-4-hydroxycinnamic acid, 45  
 $\beta$ -lactam antibiotics, 28, 32, 75

**V**  
**ANNEXES**

During my studies, two articles were published in which I am one of the authors. One of them entitled “New strategies for targeting and treatment of multi-drug resistant *Staphylococcus aureus*” is a review article written for Drug Resistance Update. For this article I authored the section on antimicrobial peptides, contributed to the introduction and created the figures.

In the last three years, apart from my main project, I was working in parallel on the type 2  $\alpha$ 2M from *P. aeruginosa* that I briefly mentioned in the introduction of this manuscript. This molecule, known as MagD in the literature, is also intensively studied in our lab in a collaboration with Ina Attrée’s group at the CEA’s Institut de Biosciences et Biotechnologies de Grenoble (BIG). My work was mainly focused on the structure solving using crystallography approach and on the protease cleavage studies. The second article presented here, “Assembly of an atypical  $\alpha$ -macroglobulin complex from *Pseudomonas aeruginosa*” reports, among other results, the part of my work concerning protease cleavage of MagD.



# New strategies for targeting and treatment of multi-drug resistant *Staphylococcus aureus*



L. Mayrink Assis<sup>a</sup>, M. Nedeljković<sup>b</sup>, A. Dessen<sup>a,b,\*</sup>

<sup>a</sup> Brazilian National Laboratory for Biosciences (LNBio), CNPEM, Campinas, São Paulo, Brazil

<sup>b</sup> Institut de Biologie Structurale (IBS), Univ Grenoble Alpes, CEA, CNRS, Bacterial Pathogenesis Group, 38044 Grenoble, France

## ARTICLE INFO

### Article history:

Received 29 September 2016

Received in revised form 7 February 2017

Accepted 23 March 2017

### Keywords:

Bacterial infection

Antibiotic

Resistance mechanism

Staphylococcus

## ABSTRACT

*Staphylococcus aureus* is a major cause of bacterial infection in humans, and has been notoriously able to acquire resistance to a variety of antibiotics. An example is methicillin-resistant *S. aureus* (MRSA), which despite having been initially associated with clinical settings, now is one of the key causative agents of community-acquired infections. Antibiotic resistance in *S. aureus* involves mechanisms ranging from drug efflux to increased expression or mutation of target proteins, and this has required innovative approaches to develop novel treatment methodologies. This review provides an overview of the major mechanisms of antibiotic resistance developed by *S. aureus*, and describes the emerging alternatives being sought to circumvent infection and proliferation, including new generations of classic antibiotics, synergistic approaches, antibodies, and targeting of virulence factors.

© 2017 Elsevier Ltd. All rights reserved.

## 1. Introduction

*Staphylococcus aureus* is the leading cause of bacterial infection in humans. Despite being an asymptomatic colonizer of skin and anterior nares of healthy individuals, it can also cause a large range of diseases with varying severity, ranging from soft tissue infections to pneumonia, septicemia, and septic shock syndrome (Diekema et al., 2001; Lowy, 1998). Penetration into deeper tissue often occurs through invasive procedures in healthcare settings, such as the introduction of catheters or artificial prostheses (von Eiff et al., 2005). The lethality of *S. aureus* is also linked to the fact that it is able to invade and survive within mammalian cells, notably neutrophils and macrophages, leading to its incomplete clearance even in the presence of high levels of antibiotics (Garzoni and Kelley, 2011; Gresham et al., 2000). Intracellular *S. aureus* strains have been linked to a number of chronic infectious processes including osteomyelitis and endocarditis (Bosse et al., 2005; Que et al., 2005), and have also been reported to induce programmed necrosis of neutrophils (Greenlee-Wacker et al., 2014; Kobayashi et al., 2010).

*S. aureus* infections have been treated with penicillin since its introduction in the 1940s, but the appearance and rapid spread

of methicillin-resistant *S. aureus* (MRSA) strains have all but eliminated the use of  $\beta$ -lactams as a treatment option (DeLeo and Chambers, 2009). The subsequent appearance of vancomycin-resistant (VRSA) and vancomycin intermediate (VISA) strains, as well as lineages that display decreased susceptibility to glycopeptides, daptomycin, and linezolid, pose notable threats for these second-line treatments for MRSA (Nannini et al., 2010; Perichon and Courvalin, 2009). The spread of such strains has called for a concerted effort towards the development of novel treatment methodologies. However, despite the few notable breakthroughs that have been made in the area of novel antibiotic development, effective treatments for MRSA are still very much needed (Bettiol et al., 2015).

The introduction of the Generating Antibiotic Incentives Now (GAIN) act in 2012 by the FDA, the 10 X '20 initiative of the IDSA, the initiation of the Innovative Medicines Initiative (IMI) as well as the New Drugs 4 Bad Bugs (ND4BB) programs in Europe have facilitated the creation of networks for clinical trials as well as the registration of novel antibacterial agents. Thus, despite the dearth of novel *S. aureus* treatment possibilities for numerous years, recent developments are showing much promise. This review will examine the biochemical reasons behind the appearance of antibiotic-resistant *S. aureus* strains, as well as discuss new strategies for the control of *S. aureus* infections with emphasis on cell wall inhibitors, both from the viewpoint of revisited molecules as well as totally novel approaches. New ideas for potential targets of future antibiotic development are also discussed.

\* Corresponding author at: Institut de Biologie Structurale (IBS), Univ. Grenoble Alpes, CEA, CNRS, Bacterial Pathogenesis Group, 38044 Grenoble, France.

E-mail address: [andrea.dessen@ibs.fr](mailto:andrea.dessen@ibs.fr) (A. Dessen).

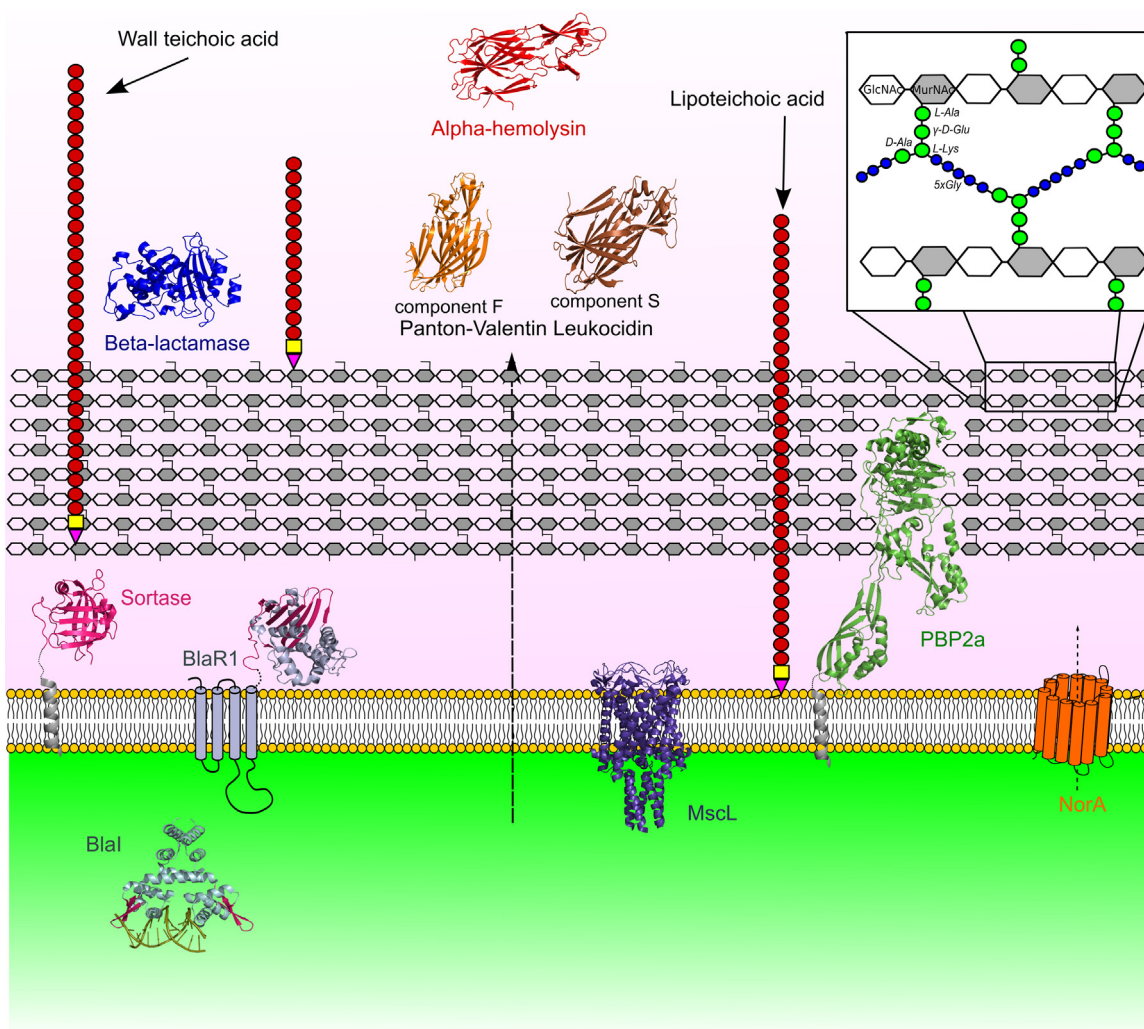


**Fig. 1.** Schematic diagram of the *S. aureus* cell wall. Molecules that are displayed include sortase A (1T2P),  $\beta$ -lactamase PC1 (3BLM), BlaR1 (3Q82), Blal (1SD4),  $\alpha$ -hemolysin (4IDJ), leukotoxin F (1PVL), leukotoxin S (1T5R), PBP2a (1VQQ), and MscL (2OAR). All structures are from *S. aureus*, with the exception of MscL (*M. tuberculosis*). Secreted molecules are shown outside the peptidoglycan (gray and white mesh, with inset).

## 2. Resistance to cell wall-targeting antibiotics

Penicillin and other  $\beta$ -lactam antibiotics target Penicillin-Binding Proteins (PBPs), which employ Lipid II as substrate in the catalysis of the last two steps in the biosynthesis of peptidoglycan, a major component of the bacterial cell wall (Mattei et al., 2010). Peptidoglycan is a cross-linked polymer formed by polymerized glycan chains (*N*-acetylglucosamine and *N*-acetylmuramic acid) and cross-linked short (stem) peptides, generating a mesh that surrounds and protects the entire bacterium (Vollmer et al., 2008); Fig. 1). In Gram-positive organisms the peptidoglycan is several nm thick (Vollmer and Seligman, 2010) and the role it plays in bacterial growth and survival is crucial, ranging from protection of the cell from differences in osmotic pressure to serving as attachment site for surface-exposed virulence factors and secretion systems. Its weakening or disruption often leads to rapid bacterial lysis (Vollmer et al., 2008). Peptidoglycan stem peptide sequences can vary slightly, but are generally *L*-Ala-*g*-*D*-Glu-(*A*<sub>2</sub>pm/*L*-Lys)-*D*-Ala-*D*-Ala in nascent peptidoglycan, with the last *D*-Ala being lost during the transpeptidation reaction catalyzed by PBPs (serine transpeptidases) (Frère et al., 1976; Vollmer et al., 2008). *A*<sub>2</sub>pm, diaminopimelic acid, is often found in the third position of stem peptides of most Gram-negative bacteria, Mycobacteria, and Bacilli, while *L*-Lys is carried by most Gram-positive organisms (Vollmer

et al., 2008). Interestingly, the structure of *D*-Ala-*D*-Ala is similar to that of penicillin; in normal growth conditions, the antibiotic is thought to act by mimicking the stem peptide substrate, being recognized by the active site of PBPs. The covalent interaction between  $\beta$ -lactams and the nucleophilic PBP active site irreversibly blocks transpeptidation, eventually weakening the peptidoglycan structure (Walsh, 2003).

*S. aureus* displays two primary resistance mechanisms against  $\beta$ -lactam antibiotics (Table 1). One general mechanism involves the secretion of high levels of the PC1  $\beta$ -lactamase when a  $\beta$ -lactam antibiotic is sensed in the immediate environment of the cell.  $\beta$ -lactamases are ubiquitous enzymes that can rapidly hydrolyze the  $\beta$ -lactam ring, and have been classified into four classes (A to D) based on sequence homologies. Classes A, C and D are structurally reminiscent of PBPs (Frère et al., 2016; Fuda et al., 2005; Nikolaidis et al., 2014) (Fig. 2), and it is generally accepted that they may have evolved from PBPs secreted by soil organisms (Ghuysen, 1994). PC1 (a class A enzyme) can hydrolyze target  $\beta$ -lactams at a rate that is significantly faster than that displayed by wild type PBPs, leading to a drastic decrease in antibiotic concentrations even before they have the chance to reach their target enzymes (Drawz and Bonomo, 2010; Frère et al., 2016; Nikolaidis et al., 2014). It is of note that over 95% of staphylococcal isolates display  $\beta$ -lactamase-dependent resistance (Lowy, 1998).

**Table 1**  
Mechanisms of resistance to antibiotics employed for the treatment of *S. aureus* infections.

Antibiotic	Class	Mechanism of action	Mechanism of resistance
penicillin	$\beta$ -lactam	Covalent link with PBPs	Acquisition of <i>mecA</i> , expression of low affinity PBP2a
ceftaroline	$\beta$ -lactam (5th generation cephalosporin)	Covalent link with PBPs, including PBP2a	Hydrolysis by $\beta$ -lactamases
vancomycin	glycopeptide	Binding to D-Ala-D-Ala stem peptides	Introduction of mutations in PBP2a
linezolid	oxazolidinone	Prevention of formation of the initiation complex on ribosome	Acquisition of <i>vanA</i> ; downregulation of PBP4 expression
Doxycycline, minocycline	tetracycline	Protein synthesis inhibition through binding to 30S subunit	Methylation of 23S rRNA ribosomal gene
gentamicin	aminoglycoside	Protein synthesis inhibition through binding to 30S subunit	Action of efflux pumps and ribosomal protection through RPPs
			Methylation and mutation of 30S rRNA

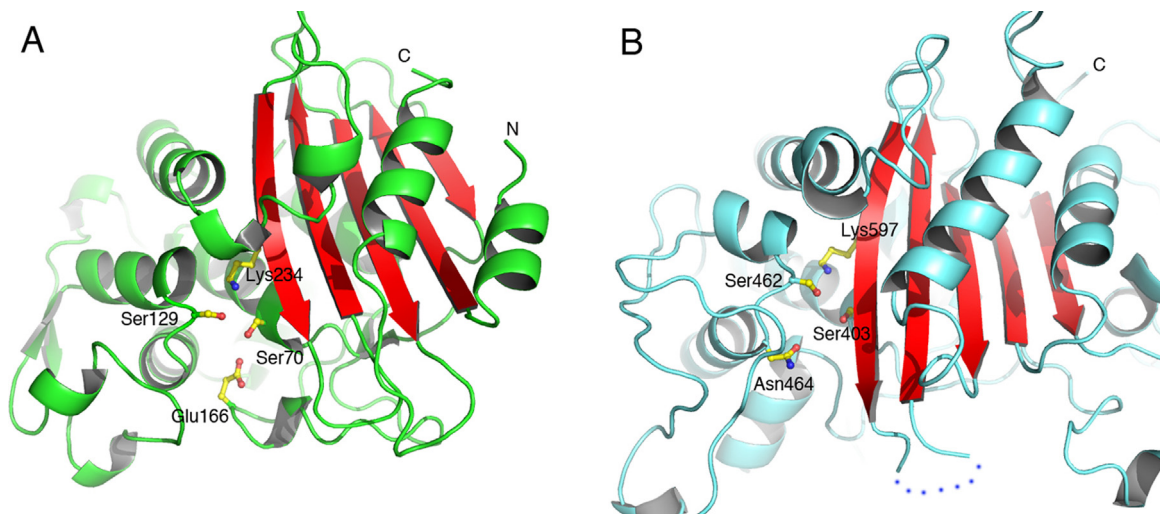


**Fig. 2.**  $\beta$ -lactamases and Penicillin-Binding Proteins show clear structural similarities. (A)  $\beta$ -lactamase PC1 from *S. aureus* (PDB 3BLM) displays Ser70 and Glu166 as its main active site residues; (B) Penicillin-Binding Protein PBP2a from *S. aureus* (PDB 1MWR) carries Ser403 as its nucleophilic residue. The loop between  $\beta$ 3 and  $\beta$ 4, which limits access to the active site, is flexible, as is the case for many PBPs.

Secretion of PC1 into the immediate surrounding of the cell involves a complex signaling mechanism. The gene encoding PC1, *blaZ*, is located on a transposable element of a large plasmid and is linked to two adjacent regulatory genes: *blaR1*, which encodes an integral membrane receptor, and *blaI*, that codes for a cytoplasmic DNA-binding repressor (Hackbarth and Chambers, 1993)(Fig. 1). Induction of PC1 expression has been studied extensively and involves the stepwise acylation of the extracytoplasmic domain of BlaR by the  $\beta$ -lactam antibiotic, followed by the production of a peptidoglycan degradation fragment. This then generates a cytoplasmic signal and the eventual inactivation of the repressor BlaI, leading to expression of the  $\beta$ -lactamase (Amoroso et al., 2012; Fuda et al., 2005).

Higher-level  $\beta$ -lactam resistance by *S. aureus*, as is the case for MRSA, involves the expression of a modified PBP. MRSA strains carry a mobile genetic element (the Staphylococcal Cassette Chromosome *mec*, or SCC*mec*) that is believed to have been acquired through horizontal gene transfer from strains related to *S. sciuri* (Goffin and Ghuyssen, 1998). One of the genes present in the cassette is *mecA*, which is highly conserved within MRSA clinical isolates and encodes PBP2a. PBP2a is much less sensitive to  $\beta$ -lactam antibiotics than the other PBPs that are normally expressed from the *S. aureus* genome (PBPs 1–4). PBP2a displays low affinity towards several  $\beta$ -lactam antibiotics, and thus confers broad-spectrum resistance to a number of clinically employed drugs (de Jonge and Tomasz,

1993; de Lencastre et al., 1994; Hiramatsu et al., 2001; Pinho et al., 2001). Interestingly, the crystal structure of PBP2a sheds light on the resistance mechanism: a distorted active site leads to the inefficient formation of the covalent complex between the antibiotic and the active site serine, a step which is crucial for the capacity of  $\beta$ -lactams to block the transpeptidation reaction (Lim and Strynadka, 2002). Thus, PBP2a remains active at high concentrations of  $\beta$ -lactams, guaranteeing that bacteria can survive even in antibiotic concentrations that are lethal to sensitive organisms (Pinho et al., 2001).

The appearance of MRSA led to an increase in the use of the glycopeptide vancomycin (Fig. 3) for treatment. The mode of action of vancomycin and other glycopeptides involves binding to the D-Ala-D-Ala C-terminal peptide of Lipid II, physically blocking its recognition, and eventual cross-linking, by PBPs (Walsh and Howe, 2002). After the extensive use of vancomycin, two types of resistant strains inevitably appeared: (1) Intermediate-resistant *S. aureus* (VISA) strains which display a poorly linked cell wall, with an accumulation of D-Ala-D-Ala targets in the periphery of the cell that eventually sequester vancomycin, and (2) vancomycin-resistant *S. aureus* (VRSA), which display a high level of resistance (Table 1). VISA strains generally emerge as a consequence of prolonged treatment with vancomycin due to invasive infections, and often lead to poor clinical outcomes. The appearance of VISA strains has been linked to the mutations in loci that play key roles in cell wall

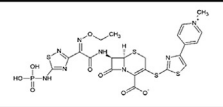
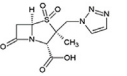
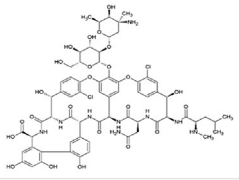
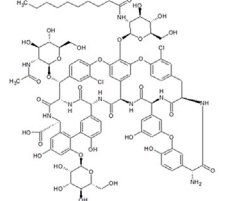
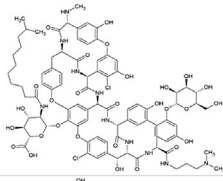
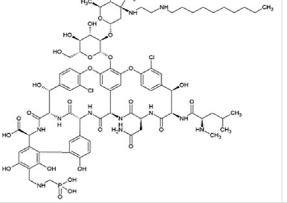
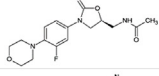
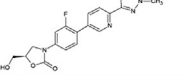
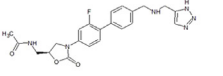
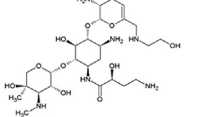
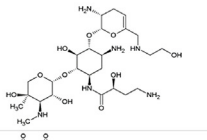
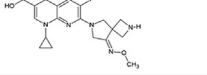
Antibiotic	Chemical structure	Class
Ceftaroline fosamil		$\beta$ -lactam
Tazobactam		$\beta$ -lactam
Vancomycin		Glycopeptide
Teicoplanin		Glycopeptide
Dalbavacin		Lipoglycopeptide
Telavancin		Lipoglycopeptide
Linezolid		Oxazolidinone
Tedizolid		Oxazolidinone
Radezolid		Oxazolidinone
Plazomicin		Aminoglycoside
WCK-771 (nadifloxacin)		Quinolone
Zabofloxacin		Quinolone

Fig. 3. Structures of main molecules in use and being developed against *S. aureus*.

metabolism, including the down-regulation of PBP4 (Katayama et al., 2016; Sieradzki et al., 1999), resulting in the accumulation of mucopeptide monomers that can sequester a larger amount of vancomycin. Recently, the activation of the WalRK two-component system, which leads to impaired cell wall turnover, has also been linked to the development of the VISA phenotype (Cameron et al., 2016).

The appearance of VRSA strains has been directly linked to the acquisition of the *vanA* operon from *Enterococcus* spp (Perichon and Courvalin, 2009). The *vanA* operon is responsible for synthesizing modified peptidoglycan precursors ending in *D*-Lac instead of *D*-Ala, a substitution that dramatically decreases the affinity of peptidoglycan precursors for glycopeptides. VRSA isolates often belong to a MRSA lineage and are linked to prior patient histories of colonization with vancomycin-resistant enterococci and continuous exposure to vancomycin (Sievert et al., 2008). Despite the great malleability shown by *S. aureus* to develop resistance to cell wall biosynthesis inhibitors, analogs of well-known molecules, as well as the employment of totally novel strategies, show promise for the treatment of such infections. The most recently tested molecules, as well as strategies that are being targeted for new inhibitor development, will be described below.

### 3. The bacterial cell wall: still an excellent target for new antibiotic development

#### 3.1. Old backbones, new molecules

Targeting the cell wall formation machinery has been a strategy of choice since the development of penicillin, and the glycopeptide vancomycin has been the drug of choice for MRSA treatment for numerous years. Despite its vast applicability, reports of resistance and high dose requirements are now common (Bassetti and Righi, 2015; Hidayat et al., 2006). Most of the recently approved antibiotics utilized in treatments of *S. aureus* infections are based on the same biological principles of action of well-known antibiotics. Cephalosporins are broad-spectrum  $\beta$ -lactams that present good bioavailability and safety, and 5th generation molecules such as ceftaroline and ceftobiprole are efficient against MRSA and VRSA (Bassetti and Righi, 2015).

Ceftobiprole is the first molecule from a new class of cephalosporins that was developed to bind specifically to mutant PBPs in MRSA. This injectable drug is also active against other Gram-positive organisms, and has been approved for the treatment of complicated skin and skin structure infection (cSSSI) in Canada (Hamad, 2010). Ceftaroline recognizes all *S. aureus* PBPs, displaying particularly high affinity for PBP2a (Acebrón et al., 2015; Saravolatz et al., 2015), with which it generates a covalent complex by recognizing the active site serine (Lovering et al., 2012). Notably, the N-phosphono version of the molecule, ceftaroline fosamil (Fig. 3), has been approved for the treatment of acute bacterial skin and skin structure infections (ABSSSI), as well as community-acquired bacterial pneumonia (www.fda.gov). Importantly, ceftobiprole resists the action of class A (TEM-1) and class C (AmpC)  $\beta$ -lactamases (Queenan et al., 2007) and is presently in Phase 3 clinical trials (Bassetti and Righi, 2015).

Glycopeptides such as vancomycin and teicoplanin (Fig. 3) are mostly effective against Gram-positive organisms. The newest derivatives are lipoglycopeptides such as dalbavancin, oritavancin and telavancin, which carry lipophilic groups linked to their glycopeptidic structures and display good activities against *Staphylococci* (Bassetti and Righi, 2015) (Fig. 3). Phase 3 clinical trials are ongoing to evaluate the efficiency of telavancin for the treatment of bacteremia caused by *S. aureus*, and it has been registered for use in skin structure infections as well as hospital-acquired and

ventilator-assisted pneumonia in cases when other treatments are not appropriate. The FDA has already approved oritavancin, a long-acting, single dose lipoglycopeptide for acute bacterial SSSIs (Corey et al., 2014), and dalbavancin for skin infections caused by MRSA (Bassetti and Righi, 2015; Boucher et al., 2014).

### 3.2. Cell wall synthesis inhibitors

The development of molecules that inhibit transpeptidation efficiently but are structurally distinct from penicillin and its analogs (i.e., that do not carry the  $\beta$ -lactam ring) has been a strategy of choice for curbing *S. aureus* growth. Functionalized boronic acids have been studied with this objective due to the fact that they can inhibit nucleophilic enzymes, including  $\beta$ -lactamases, through the formation of a reversible covalent complex that mimics the tetrahedral catalytic intermediate of a PBP-catalyzed reaction (Crompton et al., 1988). Contreras-Martel and coworkers used a crystallography-guided approach to identify boronic acid analogs that bound reversibly to the active site of the PBP and showed antibacterial activity. One of the analogs was shown to specifically bind to the low affinity PBP2a, isolated from the membranes of *S. aureus*, and to inhibit growth of MRSA (Contreras-Martel et al., 2011). Notably, *D*-Ala-*D*-Ala ligases, which participate at an early, cytoplasmic step of peptidoglycan biosynthesis, have also been shown to be the targets of *d*-boro-Ala analogs that show some specificity towards MRSA (Putty et al., 2011).

PBP2a from MRSA has also been the specific target of other site-directed studies for the development of non- $\beta$ -lactam inhibitors. Oxadizoles, for example, were identified through the *in silico* screening of the ZINC database using the structure of PBP2a, and were shown to efficiently slow down growth of several Gram-positive organisms, including vancomycin- and linezolid-resistant MRSA (O'Daniel et al., 2014; Spink et al., 2015). The same strategy was also the starting point for the identification of a quinazolinone that inhibits *S. aureus* cell wall synthesis and interacts with both PBP1 and PBP2a; interestingly, this molecule binds both at the active site and at a secondary site within the N-terminal region of the PBP (Bouley et al., 2015). It is of note that the active site of PBPs can also be targeted by non-covalent inhibitors with structures derived from that of anthranilic acid, opening the way to the development of molecules that block transpeptidation without having to generate the acyl-enzyme intermediate required for classic PBP inhibitors (Turk et al., 2011). Despite the fact that the inhibitors mentioned above are nowhere near a developmental status, they show considerable promise notably as adjuvants of other molecules employed in therapy.

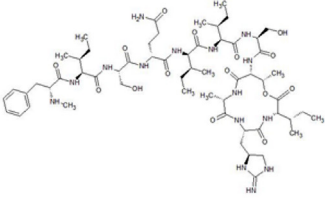
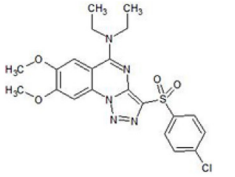
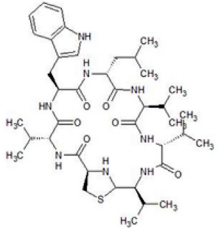
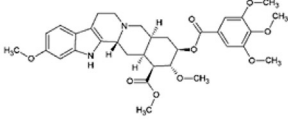
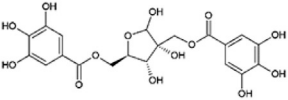
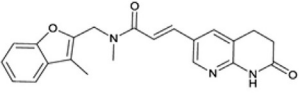
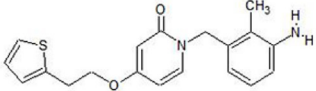
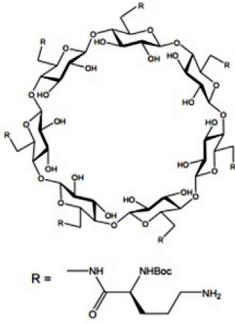
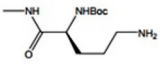
One of the most promising strategies for the identification of novel antibiotics involves tapping into natural product sources. Recently, this methodology has led to the identification of new inhibitors of *S. aureus* growth and infectivity, notably by targeting the bacterial cell wall. Ling and co-workers developed a miniaturized high throughput device called the iChip to cultivate rare soil microorganisms. By screening the resulting extracts for the ability to block *S. aureus* growth, they were able to identify teixobactin (Fig. 4), which exerts its effects by blocking the peptidoglycan synthesis precursor molecule Lipid II. Teixobactin was shown to be active against vancomycin-resistant species by being able to bind to both Lipid II-*D*-Ala-*D*-Lac and Lipid II-*D*-Ala-*D*-Ser. In addition, teixobactin also recognized Lipid III, the building block for the formation of teichoic acids, key components of the staphylococcal cell wall (described below). Strikingly, attempts to generate teixobactin-resistant *S. aureus* mutants were not successful (Ling et al., 2015), pointing to a new class of molecules (presently at a pre-development stage) that could help undermine certain antibiotic-resistance phenomena in Gram-positive bacteria.

### 3.3. Synergy and potentiation of cell wall-targeting inhibitors

The employment of existing antibiotics in combination as drug cocktails has attracted great interest, and the synergistic activity between different existing molecules has been explored as a possible alternative for the treatment of MRSA and VRSA infections. Here, two strategies have been envisioned: targeting different biochemical processes with totally distinct inhibitors, or targeting different proteins involved in the same biochemical pathway. In an example of the latter strategy,  $\beta$ -lactamase inhibitors such as clavulanic acid, tazobactam, and sulbactam, which independently perform weakly as antibiotics, have been shown to be excellent potentiating agents of other  $\beta$ -lactams towards the treatment of resistant infections. The most successful example has been the development of Augmentin, an agent that associates amoxicillin, a  $\beta$ -lactam PBP inhibitor, and the  $\beta$ -lactamase inhibitor clavulanic acid. Augmentin has been shown to be particularly successful for the treatment of soft tissue and skin infections, notably caused by MRSA (Drawz and Bonomo, 2010; White et al., 2004). Despite the fact that resistance to this combination has not been widespread, the appearance of strains expressing mutated forms of  $\beta$ -lactamase TEM-1 have generated lower sensitivity to clavulanate. It is of note that since the number of identified  $\beta$ -lactamases has increased 100-fold in the past four decades, the exploitation of  $\beta$ -lactamases as targets for novel inhibitor development may be limited in the future (Brown, 2015; Coates and Hu, 2014).

In addition to the combination of  $\beta$ -lactam antibiotics, the synergistic activity of glycopeptides and  $\beta$ -lactams has also shown much promise towards the control of methicillin-resistant *S. aureus* infections. Oxacillin, a penicillinase-resistant  $\beta$ -lactam, when provided simultaneously with either vancomycin or teicoplanin at concentrations that are acceptable clinically, displays a synergistic effect against VRSA both *in vitro* and in animal models (Fox et al., 2006; Perichon and Courvalin, 2006). The dual effect involves: (1) inactivation of all native PBPs in *S. aureus*, with the exception of PBP2a, by oxacillin; and (2) synthesis of modified peptidoglycan precursors ending in *D*-Ala-*D*-Lac or *D*-Ala-*D*-Ser in the presence of glycopeptides. The latter molecules are not substrates for the transpeptidation reaction that could be catalyzed by PBP2a, the only PBP not inhibited by the  $\beta$ -lactam. In the absence of peptidoglycan cross-linking, the cell wall collapses, resulting in bacterial death (Perichon and Courvalin, 2009). In a rabbit model of endocarditis involving animals infected with VRSA strains, combination therapy significantly reduced bacterial load when compared to monotherapies (Fox et al., 2006).

Wall teichoic acids (WTA) are glycoposphate polymers that although not being essential for bacterial survival (D'Elia et al., 2006a), play key roles in virulence, as well as cell growth and morphology (Campbell et al., 2011; D'Elia et al., 2009; Weidenmaier and Peschel, 2008). Importantly, WTAs serve as anchoring sites for autolysins, preventing self-hydrolysis of peptidoglycan (Bierbaum and Sahl, 1985). In addition, blocking of their biosynthetic steps is lethal for the cell, due to accumulation of toxic intermediate molecules (D'Elia et al., 2006b). *S. aureus* strains lacking WTAs have a diminished capability to colonize tissues as well as to establish infections in animal mouse models (Weidenmaier and Peschel, 2008). The application of a screening technique for conditionally essential enzymes of the WTA pathway led to the identification of an inhibitor of TarG, a membrane-associated component of an ABC transporter that exports WTAs to the bacterial cell surface (Swoboda et al., 2009). This molecule (later named targocil) (Fig. 4) showed a clear bacteriostatic effect, and was subsequently optimized for potency (Lee et al., 2010; Suzuki et al., 2011). However, frequency of resistance to targocil was high, but could be diminished if application was performed in the presence of oxacillin (Campbell et al., 2011). It was later shown that  $\beta$ -lactams suppress

Molecule	Chemical structure	Class
Teixobactin		Depsipeptide
Targocil		TarG inhibitor
Lugdunin		Cyclic peptide
Reserpine		Alkaloid
Hamamelitannin		Polyphenol
Debio 1450		FabI inhibitor
CG400549		FabI inhibitor
β-cyclodextrin	 <p data-bbox="703 1725 900 1789">R = </p>	Cyclodextrin

**Fig. 4.** Structures and classification of a number of adjuvant and novel molecules described in the text as acting against virulence mechanisms and cell wall biosynthesis targets in *S. aureus*.

the frequency of resistance to targocil and other TarG inhibitors, and their combination is successful in an animal model of MRSA infection (Wang et al., 2013). This exciting work underlines the interest of combining efforts on revisited inhibitors and new screening technologies in the search for novel agents to control MRSA.

Lastly, transposon-based screens have been used to identify auxiliary genes that, when inactivated, increase the susceptibility of MRSA to  $\beta$ -lactams. Thus, identification of inhibitors that target these factors could restore the activity of  $\beta$ -lactams, when employed in combination. Huber and co-workers performed a high-throughput screen of a library of synthetic compounds using a MRSA clinical isolate grown in a sub-MIC of  $\beta$ -lactam erapenem (Huber et al., 2009). This allowed the identification of two compounds that block peptidoglycan biosynthesis by targeting a molecule with sequence similarity to MurJ of *E. coli*, which has been suggested as playing the role of Lipid II flippase. A genetic approach was also employed in the determination of FtsZ, FtsW, and FtsA, involved in cell division, as  $\beta$ -lactam susceptibility determinants in MRSA. Tan and co-workers showed that the specific FtsZ inhibitor PC190723 acts synergistically with  $\beta$ -lactams, and its effect is measurable in a murine model of MRSA infection (Tan et al., 2012). These results highlight the power of genetic approaches towards the identification of new treatments of MRSA that could also be employed in the search for strategies to develop treatments for other Gram-positive or Gram-negative organisms.

### 3.4. Reversal of resistance

Recently, Gonzalez and co-workers have highlighted a particular case of synergy that could be characterized as ‘reversal of resistance’. The combination of tazobactam (Fig. 3), meropenem, and piperacillin has recently been shown to efficiently kill MRSA *in vitro* (Gonzales et al., 2015). These compounds synergistically act upon different targets: meropenem targets both PBP1 and PBP2a, piperacillin inhibits PBP2, and tazobactam acts as a class A  $\beta$ -lactamase inhibitor. Since piperacillin is a target of  $\beta$ -lactamases, tazobactam protects piperacillin, allowing efficient inhibition of PBP2. This 1:1:1 combination of clinically approved antibiotics was effective in a mouse model infected with MRSA, clearing infection. Since numerous antibiotics given at high concentrations can engender toxicity, the employment of a combination of antimicrobials at lower doses with the objective of disrupting the infection process through synergy represents a promising approach (Gonzales et al., 2015). It is of note, however, that the employment of a combination of multiple antibiotics can also lead to the selection in favor of resistance to individual components of the cocktail (Chait et al., 2007). Thus, despite the attractiveness of the synergistic approach, this strategy can also present notable drawbacks.

## 4. Classic targets: the ribosome, topoisomerases, and gyrases

### 4.1. Inhibition of protein synthesis

Oxazolidinones are a relatively new class of antibiotics that display broad-spectrum activity against a number of pathogens, including MRSA. They act by binding to the 23S rRNA of the 50S ribosomal subunit, preventing the formation of the initiation complex, and bringing protein biosynthesis to a standstill (Kloss et al., 1999). Linezolid (Fig. 3) was the first member of its class, and was introduced into the market in 2000 after a long hiatus in the development of novel antibacterial classes (Walsh, 2003). Despite its wide applicability for the treatment of severe Gram-positive infections (especially skin and soft tissue), resistance has arisen

due to the expression of a plasmid-encoded methyltransferase that methylates A2503 of the 23S rRNA gene, which results in resistance not only to linezolid but also to chloramphenicol and clindamycin (Locke et al., 2009; Mendes et al., 2008). Nevertheless, second generation oxazolidinones such as tedizolid (Fig. 3), whose efficacy is superior to that of linezolid (Urbina et al., 2013) and radezolid, which is active even against linezolid-resistant strains (Mendes et al., 2014), are now being actively pursued. Tedizolid, now called Sivextro, has been registered for use against acute SSSIs, while radezolid has shown high activity against strains that are susceptible to linezolid (Bassetti and Righi, 2015). These two oxazolidinones represent a major *tour de force* by pharmaceutical laboratories towards the development of inhibitors against MRSA and other Gram-positive pathogens.

Pleuromutilins are natural products that were identified as *S. aureus* inhibitors in the 1950s (Kavanagh et al., 1951). Their antibacterial activity is mediated by binding to the A- and P- sites of the peptidyl transferase center (PTC) of the ribosome. Resistance mechanisms have been well studied, and involve the methylation of the 23S ribosomal RNA, as well as mutations in the ribosomal rProtein, which is located close to the PTC (Gentry et al., 2007). Lefamulin (Nabriva Therapeutics) is a semi-synthetic pleuromutilin that has succeeded in Phase 2 trails for ABSSSI. It displays higher potency than other pleuromutilins, a fact which can be explained by the induction of an induced fit rearrangement within the PTC (Eyal et al., 2016). Lefamulin is currently undergoing Phase 3 clinical trials for the treatment of community-acquired pneumonia (CAP).

Tetracyclines, such as doxycycline and minocycline, are a group on broad-spectrum antibiotics that inhibit protein synthesis by targeting the 30S ribosomal subunit. As is the case for many other antimicrobials, tetracyclines are natural products from actinomycetes soil bacteria, but have encountered resistance problems, notably related to efflux pumps and the action of RPPs, bacterial elongation factors that weaken the interaction between the antibiotics and the 30S ribosomal subunit (Bassetti and Righi, 2014; Roberts, 2005) (Table 1). Eravacycline (Fig. 3) is a synthetic fluorocycline that presents excellent activity against staphylococci and streptococci, even in strains that express efflux pumps that are well-known for conferring antibiotic resistance to other tetracyclines (such as MepA (Sutcliffe et al., 2013)). The clinical efficacy of eravacycline points to applications in treatments of complicated urinary tract and intra-abdominal infections, and Phase 3 clinical trials are currently ongoing (Zhanet et al., 2016).

Aminoglycosides block bacterial protein synthesis by inducing codon misreading and interrupting translocation of the complex between tRNA and mRNA, interacting directly with the 30S rRNA (Carter et al., 2000). Several mechanisms of resistance have been identified, including methylation or mutation of the 30S subunit, direct deactivation of the antibiotic, decreasing membrane permeability, and efflux (Matt et al., 2010; Pfister et al., 2003; Recht et al., 1999) (Table 1). In addition, the therapeutic employment of aminoglycosides can cause high levels of toxicity (in particular ototoxicity, which can result in severe hearing damage (Duggal and Sarkar, 2007)). There has been thus a renewed interest in the development of new aminoglycosides that are able to not only circumvent resistance but that are also less toxic. An example of a novel, promising aminoglycoside is plazomicin (Fig. 3), which showed potent activity against both methicillin-resistant and -sensitive strains of *S. aureus* when tested against a large collection of clinical isolates. Interestingly, plazomicin displayed synergism *in vitro* with daptomycin and cefotibiprole against MRSA, VRSA and VISA (Zhanet et al., 2012). Another exciting development is that of paromomycin and its analogs, some of which not only target MRSA but also offer considerable selectivity towards bacterial ribosomes, leading to decreased ototoxicity in an animal model (Duscha et al., 2014). This is in sharp contrast to gentamicin, which is linked to signif-

icant decreases in auditory levels (Forge and Schacht, 2000). These results could eventually lead to a much-needed renewal of interest in this class of antibacterials to combat MRSA infections.

#### 4.2. DNA gyrase and topoisomerase inhibition

Quinolones target both bacterial DNA topoisomerase IV and DNA gyrase, and it is not surprising that resistance to these molecules is mediated through the acquisition of mutations in genes encoding these enzymes or by efflux through the NorA/B/C efflux pump (Kaatz et al., 1991) (Table 1). Despite the fact that they were originally developed to combat infections by Gram-negative organisms, new generation quinolones such as delafloxacin and fleroxacin show excellent results against *S. aureus* strains and specifically, MRSA. Interestingly, a quinolone in Phase 2 clinical trials, zafloxacin (Fig. 3), inhibits both DNA gyrase and topoisomerase IV with high potency (Park et al., 2010; Park et al., 2006). This mechanism of action is shared by the new compound JNJ-Q2 (acorfloxacin), which does not seem to be affected by efflux pumps and whose Phase 2 clinical trials have been completed (Biedenbach et al., 2012). Lastly, besifloxacin is a topical ophthalmic fluoroquinolone, approved in 2009 against bacterial conjunctivitis (Chang and Fung, 2010).

Resistance to standard fluoroquinolones like levofloxacin, occurs in *S. aureus* in stepwise fashion; mutations occur first in topoisomerase IV, followed by mutations in DNA gyrase. This is due to the fact that quinolones that are currently in use preferentially act upon topoisomerase IV. WCK 771, however, differs from other quinolones in that it preferentially targets DNA gyrase. It is a broad-spectrum intravenous quinolone that has shown activity against both quinolone-sensitive and -resistant MRSA, VISA, and VRSA strains. It is currently in Phase 2 clinical trials, and its pharmacodynamics properties are starkly different from that of other quinolones, which can be either dual target drugs, as mentioned above, or those that preferentially topoisomerase IV (Bhagwat et al., 2006). WCK 771 (now called nadifloxacin) is already in use topically against skin infections (Kumar and Chopra, 2013) and is in trials for systemic use (Vuong et al., 2016).

### 5. Antimicrobial peptides

Antimicrobial peptides (AMPs) have been investigated as potential inhibitors of *S. aureus* infections for numerous years. However, they have yet to be validated for use in the clinic. AMPs are natural products of practically every group of organism that fights pathogenic species, being members of their innate immunity system (Ortega and van der Donk, 2016). They range in size between 15 and 100 residues, and most are highly cationic, amphipathic compounds that can harbor several post-translational modifications (Peschel and Sahl, 2006). AMPs act by interacting with the bacterial cell membrane, altering its structure and subsequently causing lysis and cell death (Zasloff, 2002). However, many exhibit cytotoxic effects resulting from their interactions with membranes, while others have been reported to be degraded *in vivo* by proteases, decreasing their efficacy (Ruiz et al., 2014). Nevertheless, synthetic stable variants incorporating unnatural amino acids (peptidomimetics) have been developed in order to overcome these shortcomings (Citterio et al., 2016).

One promising development has been the use of lanthipeptides (also known as lantibiotics) against MRSA. Lanthipeptides are ribosomally-synthesized molecules produced by Firmicutes strains, and to a lesser extent, Actinobacteria. The peptides are post-translationally modified, normally by dehydration, cyclization, and proteolysis reactions, to generate lanthionine and methyl-lanthionine containing intramolecular rings (Barbosa et al., 2015).

The structural and chemical diversity of lantibiotics has led to their classification in two main groups: type A, such as nisin, are elongated, flexible and amphipathic and show pore-forming activities. Type B lantibiotics such as mersacidin are globular and either negatively charged or carry no charge (Münch et al., 2014). The mode of action of lantibiotics involves the recognition of Lipid II and the subsequent disruption of peptidoglycan biosynthesis (Breukink and de Kruijff, 2006).

Subtilin is a potent lantibiotic produced by *Bacillus* spp. that shows antimicrobial activity at a nanomolar range against a number of Gram-positive species. However, its close structural analog, entianin, displays the highest activity against both sensitive and methicillin-resistant *S. aureus* strains (Barbosa et al., 2015; Fuchs et al., 2011). Other promising lanthipeptides for the treatment of MRSA have been purified from interesting sources: subtilomycin, from a *B. subtilis* strain isolated from a marine sponge (Phelan et al., 2013); amylolysin, from a *B. amyloliquefaciens* strain isolated from strawberries (Halimi et al., 2010), and lichenicidin, produced by *B. licheniformis* strains isolated from hot springs (Mendo et al., 2004; Shenkarev et al., 2010). Amylolysin (3318 Da) is of particular interest, since it displays an MIC of 0.4 mM towards MRSA (Arguelles Arias et al., 2013). Amylolysin contains three thioether bridges and two unusual didehydrobutyrine residues, as well as two free cysteines, an original feature for lanthipeptides. Amylolysin is heat and pH stable, and has been shown to interact directly with Lipid II and to form pores within the bacterial membrane, thus possibly displaying a dual mode of action (Arguelles Arias et al., 2013). It is of interest that microbisporicin (also called NAI-107), an analog of the glycolipopeptide ramoplanin, also displays high affinity binding to Lipid I and Lipid II, as well as the capacity to insert and disrupt the cytoplasmic membrane. These multi-targeting strategies are at the basis of the excellent activity that these molecules display against Gram-positive bacteria including vancomycin-resistant enterococci and MRSA (Münch et al., 2014). Microbisporicin, for example, is in late preclinical development, having displayed efficacy in animal models that is superior to that of isolated antibiotics such as linezolid and vancomycin (Sandiford, 2015).

Despite these encouraging developments, the main drawbacks of the employment of antimicrobial peptides are still their broad-spectrum character and their cytotoxicity, both linked to their capacity to disrupt membranes non-specifically, as well as their instability. However, while AMPs are not yet being used systematically for treatment of infections, two examples are worth mentioning. Pexiganan is a 22-amino acid AMP derived from magainin, a peptide isolated from the skin of the African clawed frog *Xenopus laevis* (Ge et al., 1999). Its mechanism of action involves the formation of toroidal pores in the bacterial membrane (Gottler and Ramamoorthy, 2009). Pexiganan is broadly active against a number of Gram-positive and Gram-negative bacteria, including MRSA and multi-drug resistant pathogens. Pexiganan is being commercialized as a cream under the name Locilex, with applications for mild or moderate skin infections (<http://www.dipexiumpharmaceuticals.com/locilex/overview>).

Brilacidin is an AMP with a strained, planar scaffold that causes a high level of membrane depolarization in *S. aureus*. In addition, it also generates cell wall stress and the accumulation of misfolded proteins (Mensa et al., 2014). Brilacidin is presently undergoing Phase 2 clinical trials for ABSSSI and oral mucositis in patients who have received chemoradiation (Cellceutix).

Lastly, one notable peptidic antibiotic has recently been identified from an unexpected source: the human microbiota. By screening a collection of nasal *Staphylococcus* isolates, Zipperer and colleagues identified one strain, *S. lugdunensis*, that specifically killed a growing culture of *S. aureus* cells (Zipperer et al., 2016). The mechanism involves the secretion of lugdunin, a non-ribosomally-

synthesized peptide that is able to clear MRSA and Enterococcus infections without the development of resistance. Interestingly, the analysis of hospitalized patients indicated that there was over a five-fold higher prevalence for colonization by *S. aureus* in the noses of those not carrying *S. lugdunensis* than those where the latter bacterium could be identified. Since lugdunin inhibits major biosynthetic pathways (protein, DNA, peptidoglycan synthesis), it is conceivable that its mechanism of action is generalized and involves membrane disruption, which indicates that it would not be a first choice for future therapeutic development, since such compounds also tend to disrupt membranes of eukaryotic organisms. However, this seminal paper indicates that the human microbiota may be a yet unexplored source of totally novel treatment options for MRSA infections.

## 6. New targets and approaches

There are a number of new, alternative strategies that are worthy of mention. As suggested by Czapleski and coworkers, novel, alternative approaches should be carefully monitored in order to minimize the time spent on molecules that show early telltale signs indicating potential failure (Czaplewski et al., 2016). However, despite the fact that most approaches described below are at early stages of investigation, some are already in clinical trials.

### 6.1. Quorum sensing control

The establishment of *S. aureus* infections generally involves two distinct phases. In the early exponential phase of growth, most of the virulence factors expressed are surface molecules, which enable the attachment of bacteria to host tissues and the subsequent beginning of the colonization (Arya and Princy, 2013; Foster et al., 2014; Kong et al., 2016). In the post-exponential phase of growth, the expression of surface molecules is suppressed and the production of exoproteins, such as toxins, proteases, and lipases is initiated, leading to the dissemination of bacteria (tissue penetration) and allowing the evasion of host defense systems. From a genetic point of view, the temporal control of the expression of virulence determinants is regulated, principally, by two-component signal transduction auto-inducible systems and their respective ligands (Kong et al., 2016).

Two-component systems are formed by a sensor, whose primary functions include the detection and processing of signals from the external environment, and by a regulator that drives the expression of genes that encode virulence factors. In *S. aureus*, the most extensively studied system is the accessory gene regulator (Agr), which is directly responsible for the activation of the expression of exoproteins and the down-regulation of surface protein expression (Kong et al., 2016). The Agr system, a highly explored target for the development of anti-virulence therapies, is an auto-inducible (or quorum-sensing) system that generates population-wide responses in a cell-density dependent manner. The *agr* locus, located within the *S. aureus* core genome, is composed of two promoters (P2 and P3), which are responsible for driving the expression of two divergent operons (RNAII and RNAIII). The core machinery of the Agr system is encoded by the RNAII operon, which expresses AgrB, AgrD, AgrC and AgrA, while RNAIII is a regulatory RNA of the system (Kong et al., 2016; Lyon and Novick, 2004).

Since RNAIII is the effector that controls the expression of numerous virulence factors, its inhibition has been a strategy of choice. Interestingly, RNAIII can be inhibited by auto-inducing peptides (AIP), such as the RNAIII-inhibiting heptapeptide (RIP; (Gov et al., 2001; Lyon and Novick, 2004). RIP-based treatment of *S. aureus* pathologies has been demonstrated to decrease infection levels in osteomyelitis and keratitis (tested in rabbits) (Balaban

et al., 2000), cellulitis and septic arthritis (tested in mice) (Balaban et al., 2000; Giacometti et al., 2005), and mastitis (tested in cows) (Balaban et al., 2000). Furthermore, the use of RIP in combination with vancomycin in a mouse sepsis model led to lower lethality rates, indicating that it could be employed synergistically with current antibiotherapies (Giacometti et al., 2005).

Solonomamide B is a non-ribosomal peptide from a marine organism that has been found to antagonize the Agr quorum sensing system (Kong et al., 2016). Its action involves competing with AIPs for binding to AgrC, compromising its activation in a number of strains, especially community-acquired MRSA strain USA300 (Nielsen et al., 2014). Solonomamide B has been shown to reduce *S. aureus* killing of human neutrophils, and novel analog molecules have been reported to not interfere with immune cell activity (Baldry et al., 2016). This suggests that interference with the signaling pathways that regulate bacterial virulence processes can be an interesting strategy for the control of *S. aureus* infections.

### 6.2. Blocking efflux pumps

Efflux pump-mediated resistance is caused either by an increased expression of membrane-embedded pumps, or the acquisition of mutations that enable increased extrusion of antibiotics (Schindler et al., 2013). To date, more than 20 efflux pumps have been identified in the *S. aureus* chromosome (Schindler et al., 2015), and the ones that play the most notable roles in drug resistance are from the major facilitator superfamily (MFS). Typically, these transporters make use of an electrochemical gradient as a source of energy in order to decrease the effective antibiotic concentration within the cytoplasm of *S. aureus*-resistant strains. Within the *S. aureus* MFS superfamily, the NorA efflux pump confers resistance to a wide spectrum of unrelated molecules, including key fluoroquinolones such as norfloxacin and ciprofloxacin (Kaatz et al., 2005; Truong-Bolduc et al., 2003).

Due to its key importance in the drug resistance problem, NorA inhibition has been studied extensively (Schindler et al., 2013), and numerous inhibitors that show effectiveness *in vitro* have been developed. A classic example is reserpine (Fig. 4), a plant alkaloid that is effective at inhibiting NorA action *in vitro* (Neyfakh et al., 1993), but which cannot be employed in the clinic due to neurotoxicity; however, it is commonly used as a reference control for new efflux pump inhibitors.

A particularly interesting molecule is capsaicin (a natural compound produced by plants that are popularly known as 'chili peppers'). Capsaicin is an inhibitor of ATP-binding cassette (ABC) transporters; in spite of the absence of structural similarity between P-glycoproteins and NorA efflux pumps, there seems to be substrate overlap between the two proteins (Brincat et al., 2012; Zhang and Ma, 2010). The efficacy of capsaicin in *S. aureus*-related pathologies occurs via NorA and/or  $\alpha$ -toxin inhibition. When tested in combination with ciprofloxacin on a macrophage cell line, capsaicin not only reduced the MIC of the latter antibiotic but also decreased the invasiveness potential of *S. aureus*. Furthermore, capsaicin was able to decrease the efflux of ethidium bromide via NorA in a model assay to infer bacterial efflux pump inhibition. The employment of capsaicin as a ciprofloxacin adjuvant could increase the effective concentration of the antibiotic, thus promoting an improvement of its pharmacokinetic characteristics and enabling a lower concentration to be employed for treatment, leading to decreased toxicity (Kalia et al., 2012). Other molecules, such as heterocyclic boronic acids, have also been shown to be effective NorA inhibitors in the presence of ciprofloxacin (Fontaine et al., 2014). Although inactive when tested on its own, 6-benzoyloxypyridine-3-boronic acid was shown to potentiate the activity of ciprofloxacin, with little or no cytotoxicity to eukaryotic cells. Interestingly, the presence of the boron atom was essential for biological activity

(Fontaine et al., 2014). To date, however, no efflux pump inhibitors have been approved for clinical use against *S. aureus* infections (Jang, 2016).

Another prominent target for drug development is the mechanosensitive ion channel of large conductance (MscL), a highly conserved integral membrane protein that has a vital function in the maintenance of bacterial homeostasis and also serves as an entry point for small molecules into cells (Liu et al., 2009; Walton et al., 2015). By employing an *in silico* design strategy that involved the identification of ligands that could hydrogen bond to residues lining the gate of the MscL channel, Iscla and co-workers identified a p-carboethoxyl-tristyryl benzene derivative which is able to specifically inhibit MscL activity (Iscla et al., 2015). Interestingly, upon treatment with the derivative, *S. aureus* cells displayed a clear change in morphology that suggested that the compound acts by activating MscL, leading to solute loss and modification in cell size. Importantly, the compound was effective in the treatment of the nematode *C. elegans* infected with MRSA in a therapeutic window that is better than that observed for a number of FDA-approved antibiotics (Iscla et al., 2015). Despite these promising results, experiments that determine the rate of resistance development as well as further cytotoxicity trials still await finalization.

### 6.3. Control of biofilm formation and intracellular infection

*S. aureus* often forms biofilms at the site of infections, including those associated with implanted medical devices, which are difficult to treat since long-term exposure to antibiotics is required and recurrent infections are not rare (Götz, 2002; Kiedrowski and Horswill, 2011). An alternative approach viewing the eradication of *S. aureus* biofilm formation has been the employment of hamamelitannin (HAM, Fig. 4). This molecule was originally identified as a polyphenol analog of RIP (Kiran et al., 2008), and Brackman and co-workers confirmed that it is active against *S. aureus* strains with different *agr* types (Brackman et al., 2016). Notably, HAM increases the susceptibility of *S. aureus* biofilms to different classes of antibiotics, including vancomycin, by affecting genes that lead to modification in cell wall thickness and amounts of extracellular DNA (eDNA) in the biofilm matrix. Since eDNA is a structural adhesin in *S. aureus* biofilms (Fischer et al., 2014) and it can bind vancomycin before it penetrates the cell (Doroshenko et al., 2014), HAM probably has a dual effect in the development of *S. aureus* susceptibility to antibiotic treatment. HAM's efficacy was demonstrated in polyurethane catheter segments in mouse foreign body infection models (Kiran et al., 2008), in rat graft models tested with MRSA (Cobrado et al., 2012) and was shown to increase the susceptibility of *S. aureus* towards cefalexin in a murine model of infection (Brackman et al., 2016).

Invasive *S. aureus* infection can also be exemplified by the fact that it is able to survive within mammalian cells. This fact often undermines the response of the innate immune system, and is a challenge for treatments that involve classical antibiotics. In order to address this issue, Lehar and co-workers designed an elegant strategy involving an antibody-antibiotic conjugate employing an analog of rifampicin (a 'rifalogue') (Lehar et al., 2015). Upon opsonization of the pro-drug into *S. aureus* and eventual bacterial penetration into host cells, intracellular proteases cleave the linker between the antibody and the rifalogue, thus allowing the free antibiotic to rapidly clear non-dividing MRSA that accumulated within mammalian cells (Lehar et al., 2015). This is a totally novel, exciting strategy that could be emulated in the future with other antibiotic conjugates in order to eradicate intracellular *S. aureus* infections.

### 6.4. Anti-virulence through toxin targeting

*S. aureus* is a versatile pathogen that produces a large arsenal of virulence factors. These factors are responsible, in general, for cytolytic processes directed against the host immune system and/or processes that culminate in tissue penetration with subsequent colonization and growth in host cells (Kong et al., 2016). Two groups of *S. aureus* toxins have been suggested as potential targets for anti-virulence therapies: hemolysins and leukotoxins.

The most well characterized *S. aureus* hemolysin is  $\alpha$ -hemolysin (HIA, also known as  $\alpha$ -toxin), a pore-forming toxin (Fig. 1) that lyses erythrocytes and leukocytes through a disruption of homeostasis, causing an influx of  $\text{Ca}^{2+}$  and an efflux of  $\text{K}^{+}$  ions. This 33-kDa protein is secreted in monomeric form, binds ADAM10 (a zinc metalloprotease receptor) on cell membranes and oligomerizes to form a heptameric transmembrane pore that engenders cell lysis (Inoshima et al., 2011; Song et al., 1996). Hla is particularly detrimental for lung epithelium, and thus strains carrying the toxin play important roles in staphylococcal pneumonia; strains that lack Hla are avirulent in a mouse model of infection (Bubeck Wardenburg et al., 2007). Anti-HIA antibodies have received substantial attention as inhibitors of the mechanism of action of the toxin, since a number of them confer a high degree of protection against lethal infection in experimental models.

LC10/MED14893\* is an anti-Hla antibody that displays an extended half-life and high affinity, and which is under development for prevention of pneumonia caused by *S. aureus* in high-risk patients (Hua et al., 2015). Interestingly, this MAb displays an additive effect when employed in conjunction with linezolid or vancomycin (Foletti et al., 2013), and its earliest anticipated registration is in 2021 (Czaplewski et al., 2016). Other anti-HIA MAbs have also shown promising results. MAb 2A3.1 displayed effectiveness in a mouse model tested with three different *S. aureus* clinical isolates (Tkaczyk et al., 2012). MAbs 7B8 and 1A9, which bind to the N-terminal epitope of HIA and prevent its oligomerization, block the cell lysing ability of HIA and prevent mortality in a mouse model of infection after active vaccination (Ragle and Bubeck Wardenburg, 2009).

The action of HIA on cells can also be blocked by small molecule inhibitors.  $\beta$ -cyclodextrins are small molecules whose chemical structure displays seven-fold-symmetry, thus mimicking the architecture of the oligomeric HIA. These molecules have been reported to block ion conductance through the assembled hemolysin pore, and their derivatives have been shown to prevent alveolar cell lysis and to afford protection from infection in both murine and rabbit models of infection (Karginov et al., 2007; McCormick et al., 2009; Ragle et al., 2010). In addition, Hla can also be inhibited by capsaicin, a molecule described above as an efflux pump inhibitor. By using a community-associated methicillin-resistant *S. aureus* (CA-MRSA) strain, Qiu and co-workers showed that capsaicin inhibits the production/secretion of  $\alpha$ -toxin, and has a direct effect on the hemolytic activity of the strain. In addition, capsaicin conferred significant protection from  $\alpha$ -toxin-caused injury to alveolar epithelial cells, and offered significant protection to mice infected with CA-MRSA. It is of note that the authors also noted that  $\alpha$ -toxin production was substantially blocked at the transcription level, since transcription of the *agr* locus, responsible for the production of  $\alpha$ -toxin, was inhibited in a dose-dependent manner (Qiu et al., 2012). This result suggests a multi-targeted role for capsaicin in inhibition of *S. aureus* infectivity.

Leukotoxins are pore-forming molecules that also play an important role in the process of immune evasion in staphylococci. Most of the anti-virulence approaches targeting leukotoxins have been specifically directed against Pantone-Valentine leukocidins (Luk-PV) (Kong et al., 2016). Luk-PV consists of two components (LukS-PV and LukF-PV) which are secreted separately (Fig. 1) and

form a pore-forming octameric complex upon interaction (Miles et al., 2002). Leukocidins target and lyse neutrophils, inducing the release of several different mediators, such as interleukin 8, leukotrienes, among others proinflammatory substances (König et al., 1995). The resulting signaling cascades cause tissue injury and promote necrosis, especially in lung tissue (Francis et al., 2005; Kong et al., 2016). A human intravenous polyclonal immunoglobulin preparation (IVIg) was successfully employed as adjuvant therapy during antibiotic treatment of *S. aureus* infections involving strains expressing Luk-PV, one of which was methicillin-resistant, indicating that rapid administration of anti-PVL antibodies in combination with clindamycin/linezolid could be a successful strategy in difficult cases (Rouzić et al., 2010). However, the employment of single MAbs to circumvent the complex *S. aureus* pathogenicity profile has presented many challenges. With this in mind, Rouha and co-workers isolated MAbs that displayed high affinity for both a hemolysin and bi-component leukotoxins due to the recognition of a common conformational epitope. Interestingly, this single cross-reactive antibody prevented lysis of cells targeted by these toxins *in vitro* (phagocytes, red blood cells, epithelial cells), and provided high levels of protection against *S. aureus* infection in a murine model (Rouha et al., 2015).

In addition to hemolysins and leukotoxins, 90% of all *S. aureus* human clinical isolates also express staphyloxanthin, a carotenoid pigment that protects cell membrane lipids from oxidative stress generated by the host (Clauditz et al., 2006). Chen and co-workers demonstrated that naftifine, an FDA-approved antifungal, inhibits CtrN, a diaphophytoene desaturase involved in staphyloxanthin production. Since CtrN is essential for full virulence of *S. aureus* in a mouse model, naftifine attenuates the virulence potential of a number of *S. aureus* isolates, including MRSA, by blocking staphyloxanthin biosynthesis at low micromolar concentrations (Chen et al., 2016). The fact that naftifine is an antifungal with a well-established safety profile in humans (Koning et al., 2012) not only highlights its potential use in anti-MRSA cocktails but also underlines the fact that the carotenoid biosynthetic pathway may be an interesting, druggable anti-MRSA target.

### 6.5. Lipid biosynthesis

The last step in the biosynthesis of fatty acids is the reduction in the double bond of the enoyl-ACP (acyl carrier protein) molecule, a reaction catalyzed by the ACP reductase FabI. In *S. aureus*, FabI is an essential enzyme (Balemans et al., 2010), and is thus an attractive target for potential inhibitor development. The experimental agent CG400549, shown to be more potent than linezolid or vancomycin, is a FabI inhibitor presently being tested in Phase 2 trials for the treatment of ABSSSI (Park et al., 2007). In addition, Debio 1452 and its pro-drug, Debio 1450 (Debiopharm Group) are FabI inhibitors presently undergoing Phase 2 trials for staphylococcus-specific ABSSSI (Renwick et al., 2016).

## 7. Concluding remarks

In addition to the strategies outlined here, other alternative methods for the treatment of MRSA infections, including lysis therapy, are ongoing and display a number of products on pre-Phase 1 trials. The earliest product registration date for many of these therapies, however, is expected to lie between 2021 and 2022 (Czaplewski et al., 2016). Anti-MRSA vaccination is also a strategy of choice, and Pfizer's 4-antigen vaccine (SA4G) has initiated Phase 2 trials (Scully et al., 2014). Given an appropriate amount of funding, the portfolio of ongoing and alternative strategies to treat MRSA infections should expand rapidly in the near future.

## Acknowledgements

Work on new antibiotic development in our laboratory is supported by the Laboratoire International Associé BACWALL (CNRS), ANR-13-BSV8-0015-01 (Agence Nationale pour la Recherche) and by grant 11/52067-6 from FAPESP (Fundação de Amparo à Pesquisa do Estado de São Paulo) to AD. LMA is supported by fellowship 2013/22681-0 from FAPESP, and M.N. is supported by a doctoral fellowship from Université Grenoble Alpes.

## References

- Acebrón, I., Chang, M., Mobashery, S., Hermoso, J., 2015. The allosteric site for the nascent cell wall in Penicillin-Binding Protein 2a: an achilles' heel of methicillin-resistant *Staphylococcus aureus*. *Curr. Med. Chem.* 22, 1678–1686.
- Amoroso, A., Boudet, J., Berzigotti, S., Duval, V., Teller, N., Mengin-Lecreulx, D., Luxen, A., Simorre, J.P., Joris, B., 2012. A peptidoglycan fragment triggers  $\beta$ -lactam resistance in *Bacillus licheniformis*. *PLoS Pathog.* 8, e1002571.
- Arguelles Arias, A., Ongena, M., Devreese, B., Terrak, M., Joris, B., Fickers, P., 2013. Characterization of amylolysin, a novel lantibiotic from *Bacillus amyloliquefaciens* GA1. *PLoS One* 8, e83037.
- Arya, R., Princy, A., 2013. An insight into pleiotropic regulators Agr and Sar: molecular probes paving the new way for antiviral therapy. *Future Microbiol.* 8, 1339–1353.
- Balaban, N., Collins, L.V., Cullor, J.S., Hume, E.B., Medina-Acosta, E., Vieira da Motta, O., O'Callaghan, R., Rossitto, P.V., Shirliff, M.E., Serafim da Silveira, L., et al., 2000. Prevention of diseases caused by *Staphylococcus aureus* using the peptide RIP. *Peptides* 21, 1301–1311.
- Baldry, M., Kitić, B., Frokier, H., Christensen, S.B., Taverne, N., Meijerink, M., Franzky, H., Olsen, C.A., Wells, J.M., Ingmer, H., 2016. The agr inhibitors solonamide B and analogues alter immune responses to *Staphylococcus aureus* but do not exhibit adverse effects on immune cell functions. *PLoS One* 11, e0145618.
- Balemans, W., Lounis, N., Gilissen, R., et al., 2010. Essentiality of FASII pathway for *Staphylococcus aureus*. *Nature* 463, E3.
- Barbosa, J., Caetano, T., Mendo, S., 2015. Class I and class II lanthipeptides produced by *Bacillus* spp. *J. Natural Prod.* 78, 2850–2866.
- Basseti, M., Righi, E., 2014. Eravacycline for the treatment of intra-abdominal infections. *Expert Opin. Investig. Drugs* 23, 1575–1584.
- Basseti, M., Righi, E., 2015. Development of novel antibacterial drugs to combat multiple resistant organisms. *Langenbecks Arch. Surg.* 400, 153–165.
- Bettiol, E., Wetherington, J.D., Schmitt, N., Harbarth, S., Consortium, C., 2015. Challenges and solutions for clinical development of new antibacterial agents: results of a survey among pharmaceutical industry professionals. *Antimicrob. Agents Chemother.* 59, 3695–3699.
- Bhagwat, S.S., Mundkur, L.A., Gupta, S.V., Patel, M.V., Khorakiwala, H.F., 2006. The anti-methicillin-resistant *Staphylococcus aureus* quinolone WCK 771 has potent activity against sequentially selected mutants, has a narrow mutant selection window against quinolone-resistant *Staphylococcus aureus*, and preferentially targets DNA gyrase. *Antimicrob. Agents Chemother.* 50, 3568–3579.
- Biedenbach, D.J., Farrel, D.J., Flamm, R.K., Liverman, L.C., McIntyre, G., Jones, R.N., 2012. Activity of JNJ-Q2, a new fluoroquinolone, tested against contemporary pathogens isolated from patients with community-acquired bacterial pneumonia. *Int. J. Antimicrob. Agents* 39, 321–325.
- Bierbaum, G., Sahl, H.G., 1985. Induction of autolysis of staphylococci by the basic peptide antibiotics Pep 5 and nisin and their influence on the activity of autolytic enzymes. *Arch. Microbiol.* 141, 249–254.
- Bosse, M.J., Gruber, H.E., Ramp, W.K., 2005. Internalization of bacteria by osteoblasts in a patient with recurrent, long-term osteomyelitis. A case report. *J. Bone Joint Surg. Am.* 87, 1343–1347.
- Boucher, H.W., Wilcox, M., Talbot, G.H., Puttagunta, S., Das, A.F., Dunne, M.W., 2014. Once-weekly dalbavancin versus daily conventional therapy for skin infection. *N. Engl. J. Med.* 370, 2169–2179.
- Bouley, R., Kumarasiri, M., Peng, Z., Otero, L.H., Song, W., Suckow, M.A., Schroeder, V.A., Wolter, W.R., Lastochkin, E., Antunes, N.T., et al., 2015. Discovery of antibiotic (E)-3-(3-carboxyphenyl)-2-(4-cyanostyryl)quinazolin-4(3H)-one. *J. Am. Chem. Soc.* 137, 1738–1741.
- Brackman, G., Breyne, K., De Rycke, R., Vermote, A., Van Nieuwerburgh, F., Meyer, E., Van Calenbergh, S., Coeyne, T., 2016. The quorum sensing inhibitor hamamelitannin increases antibiotic susceptibility of *Staphylococcus aureus* biofilms by affecting peptidoglycan biosynthesis and eDNA release. *Sci. Rep.* 6, 20321.
- Breukink, E., de Kruijff, B., 2006. Lipid II as a target for antibiotics. *Nat. Rev. Drug Discov.* 5, 321–332.
- Brincat, J.P., Broccatelli, F., Sabatini, S., Frosini, M., Neri, A., Kaatz, G.W., Cruciani, G., Carosati, E., 2012. Ligand promiscuity between the efflux pumps human p-glycoprotein and *S. aureus* NorA. *ACS Med. Chem. Lett.* 3, 248–251.
- Brown, D., 2015. Antibiotic resistance breakers: can repurposed drugs fill the antibiotic discovery void? *Nat. Rev. Drug Discov.* 14, 821–832.
- Bubeck Wardenburg, J., Patel, R.J., Schneewind, O., 2007. Surface proteins and exotoxins are required for the pathogenesis of *Staphylococcus aureus* pneumonia. *Infect. Immun.* 75, 1040–1044.

- Cameron, D.R., Jiang, J.H., Kostoulias, X., Foxwell, D.J., Peleg, A.Y., 2016. Vancomycin susceptibility in methicillin-resistant *Staphylococcus aureus* is mediated by YycH1 activation of the WalRK essential two-component regulatory system. *Sci. Rep.* 6, 30823.
- Campbell, J., Singh, A.K., Santa Maria, J.P., Kim, Y., Brown, S., Swoboda, J.G., Mylonakis, E., Wilkinson, B.J., Walker, S., 2011. Synthetic lethal compound combinations reveal a fundamental connection between wall teichoic acid and peptidoglycan biosyntheses in *Staphylococcus aureus*. *ACS Chem. Biol.* 6, 106–116.
- Carter, A.P., Clemons, W.M., Brodersen, D.E., Morgan-Warren, R.J., Wimberly, B.T., Ramakrishnan, V., 2000. Functional insights from the structure of the 30S ribosomal subunit and its interactions with antibiotics. *Nature* 407, 340–348.
- Chait, R., Craney, A., Kishony, R., 2007. Antibiotic interactions that select against resistance. *Nature* 446, 668–671.
- Chang, M.H., Fung, H.B., 2010. Besifloxacin: a topical fluoroquinolone for the treatment of bacterial conjunctivitis. *Clin. Ther.* 32, 454–471.
- Chen, F., Di, H., Wang, Y., Cao, Q., Xu, B., Zhang, X., Yang, N., Liu, G., Yang, C.-G., Xu, Y., et al., 2016. Small-molecule targeting of a diaphytoene desaturase inhibits *S. aureus* virulence. *Nat. Chem. Biol.* 12, 174–179.
- Clauditz, A., Resch, A., Wieland, K.P., Peschel, A., Götz, F., 2006. Staphyloxanthin plays a role in the fitness of *Staphylococcus aureus* and its ability to cope with oxidative stress. *Infect. Immun.* 74, 4950–4953.
- Coates, A., Hu, Y., 2014. In: Phoenix, D.A., Harris, F., Dennison, S.R. (Eds.), *Novel Antimicrobial Agents and Strategies*. Wiley.
- Cobrado, L., Azevedo, M.M., Silva-Dias, A., Ramos, J.P., Pina-Vaz, C., Rodrigues, A.G., 2012. Cerium, chitosan and hamamelitannin as novel biofilm inhibitors? *J. Antimicrob. Chemother.* 67, 1159–1162.
- Conteras-Martel, C., Amoroso, A., Woon, E.C.Y., Zervosen, A., Inglis, S., Martins, A., Verlaque, O., Rydzik, A.M., Job, V., Luxen, A., et al., 2011. Structure-guided design of cell wall biosynthesis inhibitors that overcome  $\beta$ -lactam resistance in *Staphylococcus aureus* (MRSA). *ACS Chem. Biol.* 6, 943–951.
- Corey, G.R., Kabler, H., Mehra, P., Gupta, S., Overcash, J.S., Porwal, A., Giordano, P., Lucasti, C., Perez, A., Good, S., et al., 2014. Single-dose oritavancin in the treatment of acute bacterial skin infections. *N. Engl. J. Med.* 370, 2180–2190.
- Crompton, I.E., Cuthbert, B.K., Lowe, G., Waley, S.G., 1988. The inhibition of serine  $\beta$ -lactamases by specific boronic acids. *Biochem. J.* 251, 453–459.
- Czaplewski, L., Bax, R., Clokie, M., Dawson, M., Fairhead, H., Fischetti, V.A., Foster, S., Gilmore, B.F., Hancock, R.E.W., Harper, D., et al., 2016. Alternatives to antibiotics -- a pipeline portfolio review. *Lancet* 16, 239–251.
- D'Elia, M.A., Millar, K.E., Beveridge, T.J., Brown, E.D., 2006a. Wall teichoic acid polymers are dispensable for cell viability in *Bacillus subtilis*. *J. Bacteriol.* 188, 8313–8316.
- D'Elia, M.A., Pereira, M.P., Chung, Y.S., Zhao, W., Chau, A., Kenney, T.J., Sulavik, M.C., Black, T.A., Brown, E.D., 2006b. Lesions in teichoic acid biosynthesis in *Staphylococcus aureus* lead to a lethal gain of function in the otherwise dispensable pathway. *J. Bacteriol.* 188, 4183–4189.
- D'Elia, M.A., Millar, K.E., Bhavsar, A.P., Tomljenovic, A.M., Hutter, B., Schaab, C., Moreno-Hagelsieb, G., Brown, E.D., 2009. Probing teichoic acid genetics with bioactive molecules reveals new interactions among diverse processes in bacterial cell wall biogenesis. *Chem. Biol.* 16, 548–556.
- de Jonge, B.L.M., Tomasz, A., 1993. Abnormal peptidoglycan produced in a methicillin-resistant strain of *Staphylococcus aureus* grown in the presence of methicillin: functional role for penicillin-binding protein 2A in cell wall synthesis. *Antimicrob. Agents Chemother.* 37, 342–346.
- de Lencastre, H., de Jonge, B.L.M., Matthews, P.R., Tomasz, A., 1994. Molecular aspects of methicillin resistance in *Staphylococcus aureus*. *J. Antimicrob. Chemother.* 33, 7–24.
- DeLeo, F.R., Chambers, H.F., 2009. Reemergence of antibiotic-resistant *Staphylococcus aureus* in the genomics era. *J. Clin. Invest.* 119, 2464–2474.
- Diekema, D.J., Pfaller, M.A., Schmitz, F.J., Smayevsky, J., Bell, J., Jones, R.N., Beach, M., Group, S.P., 2001. Survey of infections due to *Staphylococcus* species: frequency of occurrence and antimicrobial susceptibility of isolates collected in the United States, Canada, Latin America, Europe, and the Western Pacific region for the SENTRY Antimicrobial Surveillance Program, 1997–1999. *Clin. Infect. Dis.* 32 (Suppl. 2), S114–S132.
- Doroshenko, N., Tseng, B.S., Howlin, R.P., Deacon, J., Wharton, J.A., Thurner, P.J., Gilmore, B.F., Parsek, M.R., Stoodley, P., 2014. Extracellular DNA impedes the transport of vancomycin in *Staphylococcus epidermidis* biofilms preexposed to subinhibitory concentrations of vancomycin. *Antimicrob. Agents Chemother.* 58, 7273–7282.
- Drawz, S.M., Bonomo, R.A., 2010. Three decades of  $\beta$ -lactamase inhibitors. *Clin. Microbiol. Rev.* 23, 160–201.
- Duggal, P., Sarkar, M., 2007. Audiologic monitoring of multi-drug resistant tuberculosis patients on aminoglycoside treatment with long term follow-up. *BMC Ear Nose Throat Disord.* 7, 5.
- Duscha, S., Boukari, H., Shcherbakov, D., Salian, S., Sliva, S., Kendall, A., Kato, T., Akbergenov, R., Perez-Fernandez, D., Bernet, B., et al., 2014. Identification and evaluation of improved 4'-O-(Alkyl) 4,5-disubstituted 2-deoxystreptamides as next-generation aminoglycoside antibiotics. *MBio* 5 (e01814-e01827).
- Eyal, Z., Matzov, D., Krupkin, M., Paukner, S., Riedl, R., Rozenberg, H., Zimmerman, E., Bashan, A., Yonath, A., 2016. A novel peluromutilin antibacterial compound, its binding mode and selectivity mechanism. *Sci. Rep.* 6, 39004.
- Fischer, A., Kambara, K., Meyer, H., Stenz, L., Bonetti, E.J., Girard, M., Lalk, M., Francois, P., Schrenzel, J., 2014. GdpS contributes to *Staphylococcus aureus* biofilm formation by regulation of eDNA release. *Int. J. Med. Microbiol.* 304, 284–299.
- Foletti, D., Strop, P., Shaughnessy, L., Hasa-Moreno, A., Casas, M.G., Russell, M., Bee, C., Wu, S., Pham, A., Zeng, Z., et al., 2013. Mechanism of action and *in vivo* efficacy of a human-derived antibody against *Staphylococcus aureus*  $\alpha$ -hemolysin. *J. Mol. Biol.* 425, 1641–1654.
- Fontaine, F., Hequet, A., Voisin-Chiret, A.-S., Bouillon, A., Lesnard, A., Cresteil, T., Jolival, C., Rault, S., 2014. First identification of boronic species as novel potential inhibitors of the *Staphylococcus aureus* NorA efflux pump. *J. Med. Chem.* 57, 2536–2548.
- Forge, A., Schacht, J., 2000. Aminoglycoside antibiotics. *Audio Neurootol.* 5, 3–22.
- Foster, T.J., Geoghegan, J.A., Ganesh, V.K., Höök, M., 2014. Adhesion, invasion and evasion: the many functions of the surface proteins of *Staphylococcus aureus*. *Nat. Rev. Microbiol.* 12, 49–62.
- Fox, P.M., Lampert, R.J., Stumpf, K.S., Archer, G.L., Climo, M.W., 2006. Successful therapy of experimental endocarditis caused by vancomycin-resistant *Staphylococcus aureus* with a combination of vancomycin and beta-lactam antibiotics. *Antimicrob. Agents Chemother.* 50, 2951–2956.
- Frère, J.M., Duez, C., Ghuyesen, J.M., Vanderkerkhove, J., 1976. Occurrence of a serine residue in the penicillin-binding site of the exocellular DD-carboxy-peptidase-transpeptidase from *Streptomyces* R61. *FEBS Lett.* 70, 257–260.
- Frère, J.M., Sauvage, E., Kerff, F., 2016. From An enzyme able to destroy penicillin to carbenapenams: 70 years of beta-lactamase misbehaviour. *Curr. Drug Targets* 17, 974–982.
- Francis, J.S., Doherty, M.C., Lopatin, U., Johnston, C.P., Sinha, G., Ross, T., Cai, M., Hansel, N.N., Perl, T., Ticehurst, J.R., et al., 2005. Severe community-onset pneumonia in healthy adults caused by methicillin-resistant *Staphylococcus aureus* carrying the Panton-Valentine leukocidin genes. *Clin. Infect. Dis.* 40, 100–107.
- Fuchs, S.W., Jaskolla, T.W., Bochmann, S., Kotter, P., Wichelhaus, T., Karas, M., Stein, T., Entian, K.-D., 2011. Entianin, a novel subtilin-like lantibiotic from *Bacillus subtilis* subsp. *spizizenii* DSM 15029T with high antimicrobial activity. *App. Environ. Microbiol.* 77, 1698–1707.
- Fuda, C.C.S., Fisher, J.F., Mobashery, S., 2005.  $\beta$ -lactam resistance in *Staphylococcus aureus*: the adaptive resistance of a plastic genome. *Cell. Mol. Life Sci.* 62, 2617–2633.
- Götz, F., 2002. *Staphylococcus* and biofilms. *Mol. Microbiol.* 43, 1367–1378.
- Garzoni, C., Kelley, W.L., 2011. Return of the Trojan horse: intracellular phenotype switching and immune evasion by *Staphylococcus aureus*. *EMBO Mol. Med.* 3, 115–117.
- Ge, Y., MacDonald, D.L., Holroyd, K.H., Thornsberrry, C., Wexler, H., Zasloff, M., 1999. *In vitro* antibacterial properties of pexiganan, an analog of magainin. *Antimicrob. Agents Chemother.* 43, 782–788.
- Gentry, D.R., Rittenhouse, S.F., McCloskey, L., Holmes, D.J., 2007. Stepwise exposure of *Staphylococcus aureus* to pleuromutilins is associated with stepwise acquisition of mutations in *rplC* and minimally affects susceptibility to retapamulin. *Antimicrob. Agents Chemother.* 51, 2048–2052.
- Ghuysen, J.M., 1994. Molecular structures of penicillin-binding proteins and  $\beta$ -lactamases. *Trends Microbiol.* 2, 372–380.
- Giacometti, A., Cirioni, O., Ghiselli, R., Dell'Acqua, G., Orlando, F., D'Amato, G., Mocchegiani, F., Silvestri, C., Del Prete, M.S., Rocchi, M., et al., 2005. RNAIII-inhibiting peptide improves efficacy of clinically used antibiotics in a murine model of staphylococcal sepsis. *Peptides* 26, 169–175.
- Goffin, C., Ghuyesen, J.M., 1998. Multimodular penicillin-binding proteins: an enigmatic family of orthologs and paralogs. *Microbiol. Mol. Biol. Rev.* 62, 1079–1093.
- Gottler, L.M., Ramamoorthy, A., 2009. Structure, membrane orientation, mechanism, and function of pexiganan—a highly potent antimicrobial peptide designed from magainin. *Biochim. Biophys. Acta* 1788, 1680–1686.
- Gov, Y., Bitler, A., Dell'Acqua, G., Torres, J.V., Balaban, N., 2001. RNAIII inhibiting peptide (RIP), a global inhibitor of *Staphylococcus aureus* pathogenesis: structure and function analysis. *Peptides* 22, 1609–1620.
- Greenlee-Wacker, M.C., Rigby, K.M., Kobayashi, S.D., Porter, A.R., DeLeo, F.R., Nauseef, W.M., 2014. Phagocytosis of *Staphylococcus aureus* by human neutrophils prevents macrophage efferocytosis and induces programmed necrosis. *J. Immunol.* 192, 4709–4717.
- Gresham, H.D., Lowrance, J.H., Caver, T.E., Wilson, B.S., Cheung, A.L., Lindberg, F.P., 2000. Survival of *Staphylococcus aureus* inside neutrophils contributes to infection. *J. Immunol.* 164, 3713–3722.
- Hackbarth, C.J., Chambers, H.F., 1993. *blaI* and *blaR1* regulate  $\beta$ -lactamase and PBP2a production in methicillin-resistant *Staphylococcus aureus*. *Antimicrob. Agents Chemother.* 37, 1144–1149.
- Halimi, B., Dortu, C., Arguelles-Arias, A., Thonart, P., Joris, B., Fickers, P., 2010. Antilisterial activity on poultry meat of amylolysin, a bacteriocin from *Bacillus amyloliquefaciens* GA1. *Probiotics Antimicrob. Proteins* 2, 120–125.
- Hamad, B., 2010. The antibiotics market. *Nat. Rev. Drug Discov.* 9, 675–676.
- Hidayat, L.K., Hsu, D.L., Quist, R., Shriner, K.A., Wong-Beringer, A., 2006. High-dose vancomycin therapy for methicillin-resistant *Staphylococcus aureus* infections: efficacy and toxicity. *Arch. Intern. Med.* 166, 2138–2144.
- Hiramatsu, K., Cui, L., Kuroda, M., Ito, T., 2001. The emergence and evolution of methicillin-resistant *Staphylococcus aureus*. *Trends Microbiol.* 9, 486–493.
- Hua, L., Cohen, T.S., Shi, Y., Datta, V., Hilliard, J.J., Tkaczyk, C., Suzich, J., Stover, C.K., Sellman, B.R., 2015. MEDI4893 promotes survival and extends the antibiotic treatment window in a *Staphylococcus aureus* immunocompromised pneumonia model. *Antimicrob. Agents Chemother.* 59, 4526–4532.
- Huber, J., Donald, R.G.K., Lee, S.H., Jarantow, L.W., Salvatore, M.J., Meng, X., Painter, R., Onishi, R.H., Occi, J., Dorson, K., Young, K., Park, Y.W., Skwish, S., Szymonifka,

- M.J., Waddell, T.S., Miesel, L., Philips, J.W., Roemer, T., 2009. Chemical genetic identification of peptidoglycan inhibitors potentiating carabapenem activity against methicillin-resistant *Staphylococcus aureus*. *Chem. Biol.* 16, 837–848.
- Inoshima, I., Inoshima, N., Wilke, G.A., Powers, M.E., Frank, K.M., Wang, Y., Bubeck Wardenburg, J., 2011. A *Staphylococcus aureus* pore-forming toxin subverts the activity of ADAM10 to cause lethal infection in mice. *Nat. Med.* 17, 1310–1314.
- Iscla, I., Wray, R., Blount, P., Larkins-Ford, J., Conery, A.L., Ausubel, F.M., Ramu, S., Kavanagh, A., Huang, J.X., Blaskovich, M.A., et al., 2015. A new antibiotic with potent activity targets MscL. *J. Antibiotics* 68, 453–462.
- Jang, S., 2016. Multidrug efflux pumps in *Staphylococcus aureus* and their clinical implications. *J. Microbiol.* 54, 1–8.
- König, B., Prevost, G., Piemont, Y., König, W., 1995. Effects of *Staphylococcus aureus* leukocidins on inflammatory mediator release from human granulocytes. *J. Infect. Dis.* 171, 607–613.
- Kaatz, G.W., Seo, S.M., Ruble, C.A., 1991. Mechanisms of fluoroquinolone resistance in *Staphylococcus aureus*. *J. Infect. Dis.* 163, 1080–1086.
- Kaatz, G.W., Thyagarajan, R.V., Seo, S.M., 2005. Effect of promoter region mutations and MgrA overexpression on transcription of *norA*, which encodes a *Staphylococcus aureus* multidrug efflux transporter. *Antimicrob. Agents Chemother.* 49, 161–169.
- Kalia, N.P., Mahajan, P., Mehra, R., Nargotra, A., Sharma, J.P., Koul, S., Khan, I.A., 2012. Capsaicin, a novel inhibitor of the NorA efflux pump, reduces the intracellular invasion of *Staphylococcus aureus*. *J. Antimicrob. Chemother.* 67, 2401–2408.
- Karginov, V.A., Nestorovich, E.M., Schmidtman, F., Robinson, T.M., Yohannes, A., Fahmi, N.E., Bezrukov, S.M., Hecht, S.M., 2007. Inhibition of *S. aureus* alpha-hemolysin and *B. anthracis* lethal toxin by beta-cyclodextrin derivatives. *Bioorg. Med. Chem.* 15, 5424–5431.
- Katayama, Y., Sekine, M., Hishinuma, T., Aiba, Y., Hiramatsu, K., 2016. Complete reconstitution of the vancomycin-intermediate *Staphylococcus aureus* phenotype of strain Mu50 in vancomycin-susceptible *S. aureus*. *Antimicrob. Agents Chemother.* 60, 3730–3742.
- Kavanagh, F., Herve, A., Robbins, W.J., 1951. Antibiotic substances from basidiomycetes: VIII. pleurotus multilus (Fr.) sacc. and pleurotus passeckerianus pilat. *PNAS* 37, 570.
- Kiedrowski, M.R., Horswill, A.R., 2011. New approaches for treating staphylococcal biofilm infections. *Ann. N. Y. Acad. Sci.* 1241, 104–121.
- Kiran, M.D., Adikesavan, N.V., Cirioni, O., Giacometti, A., Silvestri, C., Scalise, G., Ghiselli, R., Saba, V., Orlando, F., Shoham, M., et al., 2008. Discovery of a quorum-sensing inhibitor of drug-resistant *Staphylococcal* infections by structure-based virtual screening. *Mol. Pharmacol.* 73, 1578–1586.
- Kloss, P., Xiong, L., Shinabarger, D.L., Mankin, A.S., 1999. Resistance mutations in 23S rRNA identify the site of action of the protein synthesis inhibitor linezolid in the ribosomal peptidyl transferase center. *J. Mol. Biol.* 294, 93–101.
- Kobayashi, S.D., Braughton, K.R., Palazzolo-Ballance, A.M., Kennedy, A.D., Sampaio, E., Kristosturyan, E., Whitney, A.R., Sturdevant, D.E., Dorward, D.W., Holland, S.M., et al., 2010. Rapid neutrophil destruction following phagocytosis of *Staphylococcus aureus*. *J. Innate Immun.* 2, 560–575.
- Kong, C., Neoh, H., Nathan, S., 2016. Targeting *Staphylococcus aureus* toxins: a potential form of anti-virulence therapy. *Toxins (Basel)* 8, E72.
- Koning, S., van der Sande, R., Verhagen, A.P., van Suijlekom-Smit, L.W., Morris, A.D., Butler, C.C., Berger, M., van der Wouden, J.C., 2012. Interventions for impetigo. *Cochrane Database Syst. Rev.* 1 (CD003261).
- Kumar, K., Chopra, S., 2013. New drugs for methicillin-resistant *Staphylococcus aureus*: an update. *J. Antimicrob. Chemother.* 68, 1465–1470.
- Lee, K., Campbell, J., Swoboda, J.G., Cuny, G.D., Walker, S., 2010. Development of improved inhibitors of wall teichoic acid biosynthesis with potent activity against *Staphylococcus aureus*. *Bioorg. Med. Chem. Lett.* 20, 1767–1770.
- Lehar, S.M., Pillow, T., Xu, M., Staben, L., Kajihara, K.K., Vandlen, R., DePalatis, L., Raab, H., Hazenbos, W.L., Morisaki, J.H., et al., 2015. Novel antibody-antibiotic conjugate eliminates intracellular *S. aureus*. *Nature* 527, 323–328.
- Lim, D., Strynadka, N.C., 2002. Structural basis for the beta lactam resistance of PBP2a from methicillin-resistant *Staphylococcus aureus*. *Nat. Struct. Biol.* 9, 870–876.
- Ling, L.L., Schneider, T., Peoples, A.J., Spoering, A.L., Engels, I., Conlon, B.P., Mueller, A., Schäberle, T.F., Hughes, D.E., Epstein, S., et al., 2015. A new antibiotic kills pathogens without detectable resistance. *Nature* 517, 455–459.
- Liu, Z., Gandhi, C.S., Rees, D.C., 2009. Structure of a tetrameric MscL in an expanded intermediate state. *Nature* 461, 120–124.
- Locke, J.B., Hilgers, M., Shaw, K.J., 2009. Novel ribosomal mutations in *Staphylococcus aureus* strains identified through selection with the oxazolidinones linezolid and terezolid (TR-700). *Antimicrob. Agents Chemother.* 53, 5265–5274.
- Lovering, A.L., Gretes, M.C., Safadi, S.S., Danel, F., de Castro, L., Page, M.G.P., Strynadka, N.C.J., 2012. Structural insights into the anti-methicillin-resistant *Staphylococcus aureus* (MRSA) activity of ceftobiprole. *J. Biol. Chem.* 287, 32096–32102.
- Lowy, F.D., 1998. *Staphylococcus aureus* infections. *N. Engl. J. Med.* 339, 520–532.
- Lyon, J.G., Novick, R.P., 2004. Peptide signaling in *Staphylococcus aureus* and other Gram-positive bacteria. *Peptides* 25, 1389–1403.
- Münch, D., Müller, A., Schneider, T., Kohl, B., Wenzel, M., Bandow, J.E., Maffioli, S., Sosio, M., Donadio, S., Wimmer, R., et al., 2014. The lantibiotic NAI-107 binds to bactoprenol-bound cell wall precursors and impairs membrane functions. *J. Biol. Chem.* 289, 12063–12076.
- Matt, T., Akbergenov, R., Shcherbakov, D., Bottger, E.C., 2010. The ribosomal A-site: decoding, drug target, and disease. *Isr. J. Chem.* 50, 60–70.
- Mattei, P.-J., Neves, D., Dessen, A., 2010. Bridging cell wall biosynthesis and bacterial morphogenesis. *Curr. Opin. Struct. Biol.* 20, 749–755.
- McCormick, C.C., Caballero, A.R., Balzli, C.L., Tang, A., O'Callaghan, R.J., 2009. Chemical inhibition of alpha-toxin, a key corneal virulence factor of *Staphylococcus aureus*. *Invest. Ophthalmol. Vis. Sci.* 50, 2848–2854.
- Mendes, R.E., Deshpande, L.M., Castanheira, M., DiPersio, J., Saubolle, M.A., Jones, R.N., 2008. First report of cfr-mediated resistance to linezolid in human staphylococcal clinical isolates recovered in the United States. *Antimicrob. Agents Chemother.* 52, 2244–2246.
- Mendes, R.E., Deshpande, L.M., Jones, R.N., 2014. Linezolid update: stable in vitro activity following more than a decade of clinical use and summary of associated resistance mechanisms. *Drug Resist. Updat.* 17, 1–12.
- Mendo, S., Faustino, N.A., Sarmento, A.C., Amado, F., Moir, A.J., 2004. Purification and characterization of a new peptide antibiotic produced by a thermotolerant *Bacillus licheniformis* strain. *Biotechnol. Lett.* 26, 115–119.
- Mensa, B., Howell, G.L., Scott, R., DeGrado, W.F., 2014. Comparative mechanistic studies of brlacidin, daptomycin, and the antimicrobial peptide LL16. *Antimicrob. Agents Chemother.* 58, 5136–5145.
- Miles, G., Movileanu, L., Bayley, H., 2002. Subunit composition of a bicomponent toxin: staphylococcal leukocidin forms an octameric transmembrane pore. *Protein Sci.* 11, 894–902.
- Nannini, E., Murray, B.E., Arias, C.A., 2010. Resistance or decreased susceptibility to glycopeptides, daptomycin, and linezolid in methicillin-resistant *Staphylococcus aureus*. *Curr. Opin. Pharmacol.* 10, 516–521.
- Neyfakh, A.A., Borsch, C.M., Kaatz, G.W., 1993. Fluoroquinolone resistance protein NorA of *Staphylococcus aureus* is a multidrug efflux transporter. *Antimicrob. Agents Chemother.* 37, 128–129.
- Nielsen, A., Mansson, M., Bojer, M.S., Gram, L., Larsen, T.O., Novick, R.P., Frees, D., Frokiaer, H., Ingmer, H., 2014. Solonamide B inhibits quorum sensing and reduces *Staphylococcus aureus* mediated killing of human neutrophils. *PLoS One* 9, e84992.
- Nikolaidis, I., Favini-Stabile, S., Dessen, A., 2014. Resistance to antibiotics targeted to the bacterial cell wall. *Protein Sci.* 23, 243–259.
- O'Daniel, P.I., Peng, Z., Pi, H., Testero, S.A., Ding, D., Spink, E., Leemans, E., Boudreau, M.A., Yamaguchi, T., Schroeder, V.A., et al., 2014. Discovery of a new class of non-β-lactam inhibitors of penicillin-binding proteins with Gram-positive antibacterial activity. *J. Am. Chem. Soc.* 136, 3664–3672.
- Ortega, M.A., van der Donk, W.A., 2016. New insights into the biosynthetic logic of ribosomally synthesized and post-translationally modified peptide natural products. *Cell Chem. Biol.* 23, 31–44.
- Park, H.S., Kim, H.J., Seol, M.J., Choi, D.R., Choi, E.C., Kwak, J.H., 2006. In vitro and in vivo antibacterial activities of DW-224a, a new fluoronaphthyridone. *Antimicrob. Agents Chemother.* 50, 2261–2264.
- Park, H.S., Jung, S.J., Kwak, J.H., Choi, D.R., Choi, E.C., 2010. DNA gyrase and topoisomerase IV are dual targets of zafloxacin in *Streptococcus pneumoniae*. *Int. J. Antimicrob. Agents* 36, 97–98.
- Perichon, B., Courvalin, P., 2006. Synergism between beta-lactams and glycopeptides against VanA-type methicillin-resistant *Staphylococcus aureus* and heterologous expression of the vanA operon. *Antimicrob. Agents Chemother.* 50, 3622–3630.
- Perichon, B., Courvalin, P., 2009. VanA-type vancomycin-resistant *Staphylococcus aureus*. *Antimicrob. Agents Chemother.* 53, 4580–4587.
- Peschel, A., Sahl, H.-G., 2006. The co-evolution of host cationic antimicrobial peptides and microbial resistance. *Nat. Rev. Microbiol.* 4, 529–536.
- Pfister, P., Hobbie, S., Vicens, Q., Bottger, E.C., Westhof, E., 2003. The molecular basis for A-site mutations conferring aminoglycoside resistance: relationship between ribosomal susceptibility and X-ray crystal structures. *ChemBiochem* 4, 1078–1088.
- Phelan, R.W., Barret, M., Cotter, P.D., O'Connor, P.M., Chen, R., Morrissey, J.P., Dobson, A.D., O'Gara, F., Barbosa, T.M., 2013. Subtilomycin: a new lantibiotic from *Bacillus subtilis* strain MMA7 isolated from the marine sponge *Haliclona simulans*. *Mar. Drugs* 11, 1878–1898.
- Pinho, M.G., Filipe, S.R., de Lancastre, H., Tomasz, A., 2001. Complementation of the essential peptidoglycan transpeptidase function of Penicillin-Binding Protein 2 (PBP2) by the drug resistance protein PBP2a in *Staphylococcus aureus*. *J. Bacteriol.* 183, 6525–6531.
- Putty, S., Rai, A., Jamindar, D., Pagano, P., Quinn, C.L., Mima, T., Schweizer, H.P., Guthel, W.G., 2011. Characterization of d-boroAla as a novel broad-spectrum antibacterial agent targeting d-Ala-d-Ala ligase. *Chem. Biol. Drug Des.* 78, 757–763.
- Qiu, J., Niu, X., Wang, J., Xing, Y., Leng, B., Dong, J., Li, H., Luo, M., Zhang, Y., Dai, X., et al., 2012. Capsaicin protects mice from Community-Associated Methicillin-Resistant *Staphylococcus aureus* pneumonia. *PLoS One* 7, e33032.
- Que, Y.A., Haefliger, J.A., Piroth, L., Francois, P., Widmer, E., Entenza, J.M., Sinha, B., Herrmann, M., Francioli, P., Vaudaux, P., et al., 2005. Fibrinogen and fibronectin binding cooperate for valve infection and invasion in *Staphylococcus aureus* experimental endocarditis. *J. Exp. Med.* 201, 1627–1635.
- Queenan, A.M., Shang, W., Kania, M., Page, M.G., Bush, K., 2007. Interactions of ceftobiprole with beta-lactamases from molecular classes A to D. *Antimicrob. Agents Chemother.* 51, 3089–3095.
- Ragle, B.E., Bubeck Wardenburg, J., 2009. Anti alpha-hemolysis monoclonal antibodies mediate protection against *Staphylococcus aureus* pneumonia. *Infect. Immun.* 77, 2712–2718.
- Ragle, B.E., Karginov, V.A., Bubeck Wardenburg, J., 2010. Prevention and treatment of *Staphylococcus aureus* pneumonia with a β-cyclodextrin derivative. *Antimicrob. Agents Chemother.* 54, 298–304.

- Recht, M.I., Douthwaite, S., Puglisi, J.D., 1999. Basis for prokaryotic specificity of action of aminoglycoside antibiotics. *EMBO J.* 18, 3133–3138.
- Renwick, M.J., Simpkin, V., Mossialos, E., 2016. International and European initiatives targeting innovation in antibiotic drug discovery and development. In: Report Forth 2016 Dutch Presidency of the European Union.
- Roberts, M.C., 2005. Update on acquired tetracycline resistance genes. *FEMS Microbiol. Lett.* 245, 195–203.
- Rouha, H., Badarau, A., Visram, Z.C., Battles, M.B., Prinz, B., Magyarcis, Z., Nagy, G., Mirkina, I., Stulik, L., Zerbs, M., et al., 2015. Five birds, one stone: neutralization of  $\alpha$ -hemolysin and 4 bi-component leukocidins of *Staphylococcus aureus* with a single human monoclonal antibody. *MAbs* 7, 243–254.
- Rouzic, N., Janvier, F., Libert, N., Javouhey, E., Lina, G., Nizou, J.-Y., Pasquier, P., Stamm, D., Brinquin, L., Pelletier, C., et al., 2010. Prompt and successful toxin-targeting treatment of three patients with necrotizing pneumonia due to *Staphylococcus aureus* strains carrying the Pantone-Valentine leukocidin genes. *J. Clin. Microbiol.* 48, 1952–1955.
- Ruiz, J., Calderon, J., Rondón-Villarreal, P., Torres, R., 2014. Analysis of structure and hemolytic activity relationships of antimicrobial peptides (AMPs). In: Castillo, L.F. (Ed.), *Advances in Computational Biology*, vol. 232. Springer International Publishing, Switzerland, pp. 253–258.
- Sandiford, S.K., 2015. Perspectives on antibiotic discovery — where have we failed and what improvements are required? *Expert Opin. Drug Discov.* 10, 315–320.
- Saravolatz, L.D., Stein, G.E., Johnson, L.B., 2015. Ceftaroline: a novel cephalosporin with activity against methicillin-resistant *Staphylococcus aureus*. *Clin. Infect. Dis.* 52, 1156–1163.
- Schindler, B.D., Jacinto, P., Kaatz, G.W., 2013. Inhibition of drug efflux pumps in *Staphylococcus aureus*: current status of potentiating existing antibiotics. *Future Microbiol.* 8, 491–507.
- Schindler, B.D., Frempong-Manso, E., DeMarco, C.E., Kosmidis, C., Matta, V., Seo, S.M., Kaatz, G.W., 2015. Analyses of multidrug efflux pump-like proteins encoded on the *Staphylococcus aureus* chromosome. *Antimicrob. Agents Chemother.* 59, 747–748.
- Scully, L.L., Liberator, P.A., Jansen, K.U., Anderson, A.S., 2014. Covering all the bases: preclinical development of an effective *Staphylococcus aureus* vaccine. *Front. Immunol.* 5, 109.
- Shenkarev, Z.O., Finkina, E.I., Nurmukhamedova, E.K., Balandin, S.V., Mineev, K.S., Nadezhdin, K.D., Yakimenko, Z.A., Tagaev, A.A., Temirov, Y.V., Arseniev, A.S., et al., 2010. Isolation, structure elucidation, and synergistic antibacterial activity of a novel two-component lantibiotic lichenicidin from *Bacillus licheniformis* VK21. *Biochemistry* 49, 6462–6472.
- Sieradzki, K., Pinho, M.G., Tomasz, A., 1999. Inactivated PBP4 in highly glycopeptide-resistant laboratory mutants of *Staphylococcus aureus*. *J. Biol. Chem.* 274, 18942–18946.
- Sievert, D.M., Rudrik, J.T., Patel, J.B., McDonald, L.C., Wilkins, M.J., Hageman, J.C., 2008. Vancomycin-resistant *Staphylococcus aureus* in the United States, 2002–2006. *Clin. Infect. Dis.* 46, 668–674.
- Song, L., Hobaugh, M.R., Shustak, C., Cheley, S., Bayley, H., Gouaux, J.E., 1996. Structure of staphylococcal  $\alpha$ -hemolysin, a heptameric transmembrane pore. *Science* 274, 1859–1866.
- Spink, E., Ding, D., Peng, Z., Boudreau, M.A., Leemans, E., Lastochkin, E., Song, W., Lichtenwalter, K., O'Daniel, P.I., Testero, S.A., et al., 2015. Structure-activity relationship for the oxadiazole class of antibiotics. *J. Med. Chem.* 58, 1380–1389.
- Sutcliffe, J.A., O'Brien, W., Fyfe, C.D., Grossman, T.H., 2013. Antibacterial activity of eravacycline (TP-434), a novel fluorocycline, against hospital and community pathogens. *Antimicrob. Agents Chemother.* 57, 5548–5558.
- Suzuki, T., Swoboda, J.G., Campbell, J., Walker, S., Gilmore, M.S., 2011. In vitro antimicrobial activity of wall teichoic acid biosynthesis inhibitors against *Staphylococcus aureus* isolates. *Antimicrob. Agents Chemother.* 55, 767–774.
- Swoboda, J.G., Meredith, T.C., Campbell, J., Brown, S., Suzuki, T., Bollenbach, T., Malhowski, A.J., Kishony, R., Gilmore, M.S., Walker, S., 2009. Discovery of a small molecule that blocks wall teichoic acid biosynthesis in *Staphylococcus aureus*. *ACS Chem. Biol.* 4, 875–883.
- Tan, C., Therien, A.G., Lu, J., et al., 2012. Restoring methicillin-resistant *Staphylococcus aureus* susceptibility to  $\beta$ -lactam antibiotics. *Sci. Transl. Med.* 4 (126ra35).
- Tkaczyk, C., Hua, L., Varkey, R., Shi, Y., Dettinger, L., Woods, R., Barnes, A., MacGill, R.S., Wilson, S., Chowdhury, P., et al., 2012. Identification of anti- $\alpha$  toxin monoclonal antibodies that reduce the severity of *Staphylococcus aureus* dermonecrosis and exhibit a correlation between affinity and potency. *Clin. Vacc. Immun.* 19, 377–385.
- Truong-Bolduc, Q.C., Zhang, X., Hooper, D.C., 2003. Characterization of NorR protein, a multifunctional regulator of NorA expression in *Staphylococcus aureus*. *J. Bacteriol.* 147, 305–312.
- Turk, S., Verlaine, O., Gerards, T., Zivec, M., Humljan, J., Sosic, I., Amoroso, A., Zervosen, A., Luxen, A., Joris, B., et al., 2011. New noncovalent inhibitors of Penicillin-Binding Proteins from penicillin-resistant bacteria. *PLoS One* 6, e19418.
- Urbina, O., Ferrandez, O., Espona, M., Salas, E., Ferrandez, I., Grau, S., 2013. Potential role of tedizolid phosphate in the treatment of acute bacterial skin infections. *Drug Des. Devel. Ther.* 7, 243–265.
- Vollmer, W., Seligman, S.J., 2010. Architecture of peptidoglycan: more data and more models. *Trends Microbiol.* 18, 59–66.
- Vollmer, W., Blanot, D., de Pedro, M.A., 2008. Peptidoglycan structure and architecture. *FEMS Microbiol. Rev.* 32, 149–167.
- von Eiff, C., Jansen, B., Kohnen, W., Becker, K., 2005. Infections associated with medical devices: pathogenesis, management and prophylaxis. *Drugs* 65, 179–214.
- Vuong, C., Yeh, A.J., Cheung, G.Y., Otto, M., 2016. Investigational drugs to treat methicillin-resistant *Staphylococcus aureus*. *Expert Opin. Investig. Drugs* 25, 73–93.
- Walsh, T.R., Howe, R.A., 2002. The prevalence and mechanisms of vancomycin resistance in *Staphylococcus aureus*. *Ann. Rev. Microbiol.* 56, 657–675.
- Walsh, C., 2003. Where will new antibiotics come from? *Nat. Rev. Microbiol.* 1, 65–70.
- Walton, T.A., Idigo, C.A., Herrera, N., Rees, D.C., 2015. Mscl: channeling membrane tension. *Pflügers Arch.* 467, 15–25.
- Wang, H., Gill, C.J., Lee, S.H., Mann, P., Zuck, P., Meredith, T.C., Murgolo, N., She, X., Kales, S., Liang, L., et al., 2013. Discovery of wall teichoic acid inhibitors as potential anti-MRSA  $\beta$ -lactam combination agents. *Chem. Biol.* 20, 272–284.
- Weidenmaier, C., Peschel, A., 2008. Teichoic acids and related cell wall glycopolymers in Gram-positive physiology and host interactions. *Nat. Rev. Microbiol.* 6, 276–287.
- White, A.R., Kaye, C., Poupard, J., Pypstra, R., Woodnutt, G., Wynne, B., 2004. Augmentin (amoxicillin/clavulanate) in the treatment of community-acquired respiratory tract infection: a review of the continuing development of an innovative antimicrobial agent. *J. Antimicrob. Chemother.* 53 (Suppl. 1), i3–i20.
- Zaslloff, M., 2002. Antimicrobial peptides of multicellular organisms. *Nature* 415, 389–395.
- Zhanel, G.G., Lawson, C.D., Zelenitsky, S., Findlay, B., Schweizer, F., Adam, H., Walkty, A., Rubinstein, E., Gin, A.S., Hoban, D.J., et al., 2012. Comparison of the next-generation aminoglycoside plazomicin to gentamicin, tobramycin and amikacin. *Expert Rev. Anti-Infect Ther.* 10, 459–473.
- Zhanel, G.G., Cheung, D., Adam, H., Zelenitsky, S., Golden, A., Schweizer, F., Gorityala, B., Lagacé-Wiens, P.R., Walkty, A., Gin, A.S., et al., 2016. Review of eravacycline, a novel fluorocycline antibacterial agent. *Drugs* 76, 567–588.
- Zhang, L., Ma, S., 2010. Efflux pump inhibitors: a strategy to combat p-glycoprotein and the NorA multidrug resistance pump. *ChemMedChem* 5, 811–822.
- Zipperer, A., Konnerth, M.C., Laux, C., Berscheid, A., Janek, D., Weidenmaier, C., Burian, M., Schilling, N.A., Slavetinsky, C., Marschal, M., et al., 2016. Human commensals producing a novel antibiotic impair pathogen colonization. *Nature* 535, 511–516.

**Assembly of an atypical  $\alpha$ -macroglobulin complex from  
*Pseudomonas aeruginosa***

Samira Zouhir <sup>1</sup>, Mylène Robert-Genthon <sup>2</sup>, Daniel Maragno Trindade <sup>1</sup>, Viviana Job <sup>3</sup>, Marko Nedeljković <sup>3</sup>, Cécile Breyton <sup>3</sup>, Christine Ebel <sup>3</sup>, Ina Attrée <sup>2</sup>, and Andréa Dessen <sup>1,3\*</sup>

<sup>1</sup> Brazilian Biosciences National Laboratory (LNBio), CNPEM, Campinas,  
São Paulo, Brazil

<sup>2</sup> Univ. Grenoble Alpes, Bacterial Pathogenesis and Cellular Responses Group, Institut de  
Biosciences et Biotechnologies de Grenoble (BIG), France

<sup>3</sup> Univ Grenoble Alpes, CNRS, CEA, Institut de Biologie Structurale (IBS), F-38000 Grenoble, France

Running head: Macroglobulin complex from *P. aeruginosa*

\* to whom correspondence should be addressed: [andrea.dessen@ibs.fr](mailto:andrea.dessen@ibs.fr)

## ABSTRACT

Alpha-2-macroglobulins (A2Ms) are large spectrum protease inhibitors that are major components of the eukaryotic immune system. Pathogenic and colonizing bacteria, such as the opportunistic pathogen *Pseudomonas aeruginosa*, also carry structural homologs of eukaryotic A2Ms. Two types of bacterial A2Ms have been identified: Type I, much like the eukaryotic form, displays a conserved thioester that is essential for protease targeting, and Type II, which lacks the thioester and to date has been poorly studied despite its ubiquitous presence in Gram-negatives. Here we show that MagD, the Type II A2M from *P. aeruginosa* that is expressed within the six-gene *mag* operon, specifically traps a target protease despite the absence of the thioester motif, comforting its role in protease inhibition. In addition, analytical ultracentrifugation and small angle scattering show that MagD forms higher order complexes with proteins expressed in the same operon (MagA, MagB, and MagF), with MagB playing the key stabilization role. A *P. aeruginosa* strain lacking *magB* cannot stably maintain MagD in the bacterial periplasm, engendering complex disruption. This suggests a regulated mechanism of Mag complex formation and stabilization that is potentially common to numerous Gram-negative organisms, and that plays a role in periplasm protection from proteases during infection or colonization.

## INTRODUCTION

Alpha-2-macroglobulins (A2Ms) are broad-spectrum protease inhibitors present in all metazoans ranging from insects to humans, and play key roles in host defense <sup>1</sup>. A2Ms are essential for trapping proteases secreted by invading microorganisms, thwarting the infectious process <sup>2</sup>. Eukaryotic A2Ms also recognize 'self' proteases, thus regulating inflammatory and blood clotting events. Their ubiquitous action derives from the fact that they are characterized by a highly reactive thioester bond (the CXEQ motif), as well as a bait region whose sequence is recognizable by a large number of proteases <sup>3</sup>.

Upon recognition and cleavage of the bait region by an attacking protease, the thioester bond becomes exposed and subsequently cross-linked to the enzyme, causing the A2M to trap the attacking protease in a cage-like structure <sup>4, 5</sup>. This mechanism ensures that proteases that are secreted by infecting microorganisms are cleared effectively, and is thought to be part of an innate immune system that predates the immunoglobulin-based system <sup>3</sup>. A2Ms are members of a superfamily of proteins involved in other defense mechanisms, such as the complement cascade (i.e., C3/C5 convertases <sup>3,6</sup>).

In spite of the fact that molecules of the A2M/complement superfamily were believed to be limited to metazoans, genomic analyses revealed that genes for A2M-like proteins also exist in several bacterial species, many of which are pathogenic or are common colonizers of higher eukaryotes <sup>7</sup>. This calls into question the reason for the existence of molecules that resemble eukaryotic innate immunity proteins in prokaryotes. Two forms of A2M-like proteins were

identified, only one of which contains the hallmark CXEQ thioester motif. Some bacteria, such as *Escherichia coli*, carry both forms of A2M, while others, such as *Salmonella enterica* or *Pseudomonas aeruginosa*, carry only one form (Fig. 1a) <sup>7</sup>. In a number of bacteria, the gene for the thioester-containing A2M (Type I) is adjacent to that encoding Penicillin Binding Protein 1c (PBP1c) <sup>8</sup>, a membrane-associated protein involved in cell wall synthesis. PBPs are involved in the biosynthesis of peptidoglycan (PG), a three-dimensional cross-linked mesh that surrounds the bacterium, giving it its shape and protecting it from differences in osmotic pressure <sup>9</sup>. PBPs are responsible for the two last reactions in PG biosynthesis, and thus play a key role in its stabilization <sup>10</sup>. The observation of the juxtaposition of *a2m* and *pbpC* genes led to the hypothesis that the two encoded proteins could work conjunctively as a periplasmic defense system. Thus, in the event of a cell wall breach, A2M would inhibit proteases and endopeptidases that penetrate the periplasm while PBP1c would act by repairing damage done to PG destroyed by lysozyme or other PG-targeting factors <sup>7</sup>.

We recently reported the crystal structure of a Type I A2M in three forms <sup>11</sup>, which revealed a fold and activation mechanism that are similar to those of eukaryotic complement proteins <sup>12</sup>. *S. enterica* A2M, a 180 kDa molecule consisting of 13 domains whose overall structure is reminiscent of that of eukaryotic C3, displays an exposed bait region and an entrenched CXEQ motif. Protease recognition occurs through specific targeting of the bait region, as is the case for eukaryotic forms. Garcia-Ferrer and co-workers <sup>13</sup> and Fyfe and co-workers <sup>14</sup> investigated protease recognition of the *E. coli* Type I A2M using electron microscopy and X-ray crystallography, and identified that upon protease binding, the macroglobulin undergoes a major conformational change; details of protease entrapment, however, could not be obtained since the

target protease could not be visualized in electron density maps. The atomic details that describe a complex between a bacterial A2M and a protease are thus still an open question.

The second class of bacterial A2M (Type II), expressed by pathogens such as *P. aeruginosa*, lacks the CXEQ motif (but still carries the bait region) and is encoded within a six-gene operon (Fig. 1b). Recently, we showed that *P. aeruginosa* A2M (MagD) is a periplasmic protein associated preferentially with the inner membrane, and it is expressed by a majority of clinical strains <sup>15</sup>. MagD was shown, using immunoprecipitation pull-down assays in *P. aeruginosa*, to be associated to at least three other proteins from the *mag* operon (Fig. 1c): MagA, MagB and MagF. MagB is of particular interest, since it was predicted to carry a transmembrane helix <sup>15</sup>. Notably, the *magABCDEF* operon is co-expressed with operons encoding the Type VI secretion system as well those involved in exopolysaccharide biosynthesis, required for biofilm formation <sup>16,17</sup>. Moreover, strains lacking MagD display less virulence in an animal model of chronic infection <sup>18</sup>. These findings indicate that bacteria could employ Type II A2Ms to inhibit host proteases during infection, facilitating colonization of eukaryotic hosts, or block other bacterial proteases during microbial warfare, allowing survival in conditions where resources are scarce. How Type II A2Ms, which lack the thioester motif, can still entrap proteases, and what are the roles played by the other proteins expressed in the same operon are still unclear.

In this work we have addressed the structural and functional characterization of MagD as the central member of a multi-partite complex formed with other proteins encoded within the *mag* operon. We show that MagD can be actively recognized and cleaved by a specific protease within its bait region, an event which traps the protease in a stable complex, attesting to the

ability of Type II A2Ms to display macroglobulin-like activity even in the absence of the classical thioester motif. In addition, we show by analytical ultracentrifugation (AUC) and small angle scattering (SAXS) that MagD is able to bind directly to MagA, MagB, and MagF with 1:1 stoichiometry. Furthermore, the formation of higher order complexes *in vitro* (MagD-MagA-MagB; MagD-MagF-MagB) requires the presence of MagB, the only protein predicted to carry a transmembrane domain. Notably, the absence of *magB* in *P. aeruginosa* results in the degradation of MagD in the bacterial periplasm, pointing to the key role MagB plays in complex formation. Type II A2Ms are thus atypical members of a rudimentary bacterial immune system that protects the periplasm by employing a multi-partite complex whose central member structurally mimics eukaryotic immune proteins.

## RESULTS

### MagD can entrap a specific protease non covalently

Although MagD does not carry the CXEQ thioester motif involved in the covalent association to target proteases (Fig. 1) <sup>11,13,14</sup>, we reasoned that if its biological role is linked to protection of the cell from protease attack, it should be targeted by different proteases as shown for Type I A2Ms <sup>19</sup>. We initially performed proteolysis tests of MagD using chymotrypsin, trypsin and papain, and analyzed results by SDS-PAGE, N-terminal sequencing and mass spectrometry (Fig. S1). In all three cases, the bait region was cleaved, generating two species that remained associated to each other and migrated together as a single peak in gel filtration. Notably, the first 198 amino acids, which are presumably flexible, were also proteolyzed.

In order to study MagD targeting by protease that would only recognize the bait region, we designed a mutant form by introducing a recognition sequence for the TEV protease onto the predicted MagD bait region, as previously done for the study of the A2M from *Salmonella enterica*<sup>11</sup>; we called this mutant MagD-TB (for ‘TEV Bait’). The MagD bait sequence ANRSERG (amino acids 847-853) was substituted by ENLYFQG, which if recognized and cleaved by TEV would generate two distinct fragments of 93 kDa (N-term) and 74 kDa (C-term). Apo MagD-TB was incubated overnight with an excess of TEV and subsequently subjected to SEC analysis (Fig. 2). SDS-PAGE analysis of the resulting elution peak indicated 4 bands: uncleaved (full-length) MagD-TB, TEV, and two intermediary forms which were shown by N-terminal sequencing and mass spectrometry to correspond to the expected 91.2 kDa and 74.0 kDa fragments of cleaved MagD-TB (Table 1). These results thus confirmed that despite the absence of the CXEQ motif, MagD is still able to trap target proteases following a bait region-cleaving mechanism in which the protease remains non-covalently associated to MagD. This is a unique characteristic of Type II A2Ms, which leads to the suggestion that protease entrapment occurs through a mechanism that is distinct from what has been proposed to date for most eukaryotic or prokaryotic macroglobulins.

### **MagD interacts individually with MagA, MagB, and MagF forming 1:1 complexes**

Previously, we had shown that MagA, MagB, MagD and MagF co-immunoprecipitate from inner membrane of *P. aeruginosa*<sup>15</sup>. MagA, MagB, and MagF are considerably smaller than MagD (26-60 kDa *versus* 165 kDa) and carry signal peptides at their N-termini (except for MagB; Fig 1c). In order to initiate the characterization of this multi-partite complex, we expressed MagA, MagB, MagD and MagF in the *E. coli* cytoplasm, but all proteins, with the exception of MagD, were expressed as inclusion bodies. We thus tested co-expression of MagD with MagA, MagB or MagF,

and this strategy allowed the co-purification of soluble binary complexes, indicating that MagD is able to interact individually with the three Mag proteins in stable form (Fig. S2). We employed the same strategy to test binary complex formation between MagD and MagC and MagE, but could not show stable complexes by gel filtration chromatography.

To investigate the stoichiometry of the binary Mag complexes, samples were studied by analytical ultracentrifugation using the sedimentation velocity method. After analytical gel filtration, MagA:MagD, MagB:MagD, and MagF:MagD samples were centrifuged at 35,000 rpm using a Beckman ultracentrifuge at 20°C with absorbance monitoring at 280nm. Consecutive scans were automatically recorded at regular intervals and analyzed with Sedfit using the continuous size distribution  $c(s)$  analysis method to determine sedimentation coefficients<sup>20</sup>. Purified MagD and Mag complexes were analyzed at three different concentrations: 0.25 mg/mL, 0.5 mg/mL and 1 mg/mL (Fig. 3). MagD sediments as two species (at all three concentrations): a major form with a mean  $s_{20,w}$  value of 7.8 S +/- 0.5 S, compatible with a monomer, and a minor form presenting a mean  $s_{20,w}$  value of 10.3 S +/- 0.6 S, which is compatible with a dimer (Table 2). The MagA:MagD, MagB:MagD, and MagF:MagD complexes sediment with mean  $s_{20,w}$  values of 8.7 S, 8.4 S and 8.3 S, that are slightly higher than that of MagD and which indicate stoichiometries of 1:1 for the complexes (Table 2). Notably, the MagB:MagD and MagF:MagD sedimentation peaks were sharp, indicating rather homogeneous complexes, but the MagA:MagD peak displayed a clear shoulder indicating the presence of a mixture of higher order species (Fig. 3c). Nevertheless, these data clearly indicate that MagD can form stable 1:1 complexes with these three specific Mag partners.

We then sought to further characterize the binary MagD complexes by using small angle X-ray scattering (SAXS). Experiments were performed with MagD, MagA:MagD, MagF:MagD, and MagB:MagD that had been purified by size exclusion chromatography prior to experimentation. Data were collected at the D01B-SAXS1 beamline at the LCLS light source in Brazil (Figs. 4a and Table 3). Scattering patterns, recorded at different concentrations for all samples, did not suggest any oligomerization or aggregation events. The Guinier plots are linear, and data at low angles did not indicate any aggregation.

The structure of apo MagD is reminiscent of that of Type I bacterial macroglobulins<sup>11,13,14,22</sup>. Indeed, when comparing the MagD diffusion curve to those of *E. coli* A2M (ECAM; PDB 5A42)<sup>13</sup> or *S. enterica* A2M (Sa-A2M; PDB 4U48)<sup>11</sup>, which were calculated from their structures using CRY SOL<sup>23</sup> (Fig. 4c), it is clear that the three diffusion curves fit well at small angles, indicating similar overall dimensions. At higher angles, the fits are less good, and could be related to different relative positions of the two N-terminal domains that appear to be flexible when comparing ECAM and Sa-A2M. We note that the  $R_g$  value measured here for MagD is slightly larger than the one measured previously<sup>15</sup>.

The Guinier analyses show an increase in the radii of gyration ( $R_g$ ) value when comparing MagD and the binary complexes (Fig. 4a inset and Table 3). Slightly larger dimensions for the complexes are corroborated by the values for  $R_g$  and calculated from the  $p(r)$  distributions curves. The maximum particle dimension ( $D_{max}$ ) and  $R_g$  values for all bipartite complexes, with  $D_{max}$  values ranging from 19.3 nm (MagF:MagD) to 20.1 nm (MagA:MagD) and  $R_g$  values ranging from 5.7 to 5.9 nm were higher than those for native MagD ( $D_{max}$ = 17.6 nm,  $R_g$ =5.2 nm) (Table 3). Thus, the modification in  $D_{max}$  and  $R_g$  values, as well as the change in the shape of the  $p(r)$

curve (Fig. 4b), indicate that there is an increase in measured dimensions when MagD binds to any of its partners.

SAXS experiments were complemented by SEC and Dynamic Light Scattering (DLS) measurements. The comparative analysis of  $R_g$  values obtained from SAXS experiments and  $R_h$  values calculated from analytical SEC and DLS showed the consistency of these data, which pointed to a slight increase of MagD dimensions in the presence of its partners (Table 3).

To characterize the stability of the Mag complexes, we monitored the thermal unfolding of the samples using circular dichroism. Scans were performed in the 260 nm – 200 nm range every 1 °C between 20 °C and 110 °C (Fig. 5). Thermal denaturation measurements showed that MagD conserves its secondary structure up to 95 °C, after which it unfolds rapidly. Thermal stability is improved when MagD is complexed to one of its partners. MagA:MagD and MagF:MagD samples still displayed secondary structure even at 110 °C. Interestingly, the MagB:MagD complex displayed the highest stability, conserving a constant minima at 216 nm even at 110 °C. These data suggested that MagA, MagF, and MagB stabilize the structure of MagD, with MagB displaying the highest capacity for complex stabilization.

### **MagB plays a key role in complex stabilization in a cellular context**

We have previously shown that the deletion of the whole *mag* operon (encompassing *magABCDEF*) had a dramatic effect on MagD, influencing its localization, stability and cleavage from the full-length, 165 kDa form to a 100 kDa form <sup>15</sup>. To confirm the key role of MagB identified by our *in vitro* assays and to delineate the specific role of each of the other Mag proteins, we individually deleted each gene from the *mag* operon and investigated the fate of

MagD by Western blotting using anti-MagD antibodies (Fig. 6a). Deletions of *magA*, *magC* and *magF* had no pronounced effect on MagD, since we could detect the protein in its two forms (165 and 100 kDa) in similar ratio/quantities, albeit with higher amounts of the full-length form in  $\Delta magA$ . This result is probably related to the increased stability levels of the whole RmsA-regulated mRNA in the strain carrying the *magA* deletion. However, the absence of MagB and of MagE greatly influenced the amount of MagD; only a barely detectable amount of the non-cleaved 165 kDa form could be visualized in the *magB* deleted strain. Importantly, the 100 kDa form was undetectable. This indicates that MagB could play a direct role in MagD stabilization and could be involved in its cleavage to the 100 kDa form. MagB expression *in trans* in a  $\Delta magB$  mutant restored the presence of the two forms. Interestingly, expression of MagD *in trans* in a  $\Delta magB$  background resulted in higher quantities of MagD but with prominent degradation (Fig. 6b), an observation that was also made for MagD in the  $\Delta OP$  background <sup>15</sup>

It is of note that in a mutant lacking *magE*, additional forms of higher molecular mass were detected. Our previous work suggested that MagE is cytoplasmic and does not associate stably with the Mag complex <sup>15</sup>. Therefore, MagE could be involved in cleavage of the signal peptide from MagD, allowing its translocation from the cytosol to the periplasm. The higher forms of MagD could thus correspond to its unprocessed, full-length form still harboring the 21 residue signal peptide, as well as degradation products.

### **The inner membrane localization of MagD and its cleavage are determined by MagB**

When full-length MagD was expressed *in trans* in a strain where the entire *mag* operon was knocked out (*P. aeruginosa*  $\Delta OP$ ), it lost its inner membrane localization <sup>15</sup>. Since MagB is the

only protein encoded by the Mag operon harboring a predicted transmembrane domain (amino-acids 26-48) and it plays an important role in MagD stabilization in both *in vitro* and *in vivo* assays, we investigated if it could play a direct role in MagD localization. We thus performed localization studies of MagD in a  $\Delta magB$  strain with or without MagB supplemented *in trans*. To that aim, *P. aeruginosa* total membranes and periplasm were separated and immunoblotted using anti-MagD antibodies. As shown in Fig. 6c, in the strain deleted for *magB*, the majority of full-length (165 kDa) MagD was found in the bacterial periplasm, while expression *in trans* of MagB restored its membrane localization. Moreover, the 100 kDa form could be readily detected in the complemented strain. These results show that MagB dictates the inner-membrane localization of the Mag complex, which directly or indirectly results in MagD processing into a 100 kDa form. In the same manner, we isolated membranes and periplasm in a  $\Delta magB$  strain overexpressing *magD in trans*; we found a fraction of full length MagD in membranes and again a fraction of the protein in the periplasm. Degraded forms could be observed in both bacterial compartments. These results suggest that all Mag proteins must be co-expressed from the same operon in similar amounts for optimal complex formation, possibly due to a highly regulated partner association/localization mechanism.

### **MagB is a key member of a higher ordered Mag complex**

As mentioned above, MagB, when expressed alone, is largely localized to inclusion bodies, but a small amount of soluble protein could be isolated and purified. To further investigate the role of MagB in Mag complex formation, we incubated purified MagB with MagA:MagD and MagF:MagD as well as MagD alone and performed AUC measurements (Fig. 7). The MagB sedimentation profile showed a major peak at  $s_{20,w}$  of 3.3 S, corresponding to the monomeric form

of the protein (not shown). Upon incubation of MagB with MagA:MagD, the sedimentation peak of the binary complex shifted from an  $s_{20,w}$  value of 6.6 S to 7.3 S (Fig. 7c), indicating the formation of a stable tripartite complex. Similarly, incubation of MagB with MagF:MagD also yielded a shift in the complex sedimentation peak from  $s_{20,w}$  of 6.5 S to 7.1 S (Fig. 7d). These results demonstrate that MagB is able to stably interact with MagD once it is already in complex with either MagA or MagF, forming the ternary complexes MagB:MagA:MagD and MagB:MagF:MagD. This also indicates that the binding sites for MagB, MagA, and MagF on the surface of MagD do not overlap.

## DISCUSSION

A2Ms are key proteins of the eukaryotic innate immune system, and the identification of bacterial genes encoding A2M-like proteins suggested that bacteria could also employ macroglobulin-like molecules in infectious or colonization processes <sup>7</sup>. The hallmark of A2M action is a CXEQ thioester motif, buried deep within the structure in order to protect it from hydrolysis, which becomes activated once the target protease cleaves the bait region, thus becoming covalently trapped <sup>3</sup>. The identification of bacterial A2M-like proteins that harbor bait regions but not CXEQ motifs (Type II A2Ms) put forth the question of the activity, and biological role, of such molecules. It is of interest that Type II A2Ms are often encoded in a six-gene operon, a situation which is quite distinct from that of Type I molecules (CXEQ-carrying), which are encoded in an operon that co-expresses the peptidoglycan synthase PBP1c.

We had previously structurally and functionally characterized a Type I A2M, Sa-A2M, which, in absence of a protease substrate, guarantees the stability of its thioester site through the

action of a “lock”. Once the protease-A2M reaction has taken place, Sa-A2M is cleaved into two products (102 kDa and 77 kDa), with the protease remaining covalently associated to the smallest form. An Sa-A2M mutant in which the thioester was inactivated was unable to trap the target protease <sup>11</sup>. The Type II A2M characterized in the present work (MagD) does not carry a thioester region, and yet upon incubation with a specific protease (in this case, TEV), the bait region was cleaved and the protease was stably trapped, as shown by gel filtration, N-terminal sequencing, and mass spectrometry experiments (Fig. 2). The TEV protease cleavage of MagD resulted in the generation of two products: 91.2 kDa (N-terminal) and 74.0 kDa (C-terminal). It is of note that despite the large excess of TEV, MagD was not fully cleaved, whether in its apoform or in the presence of MagA, MagB and MagF respectively (data not shown). This could indicate that the Mag complex must be fully assembled, with the presence of all partners, in order for full activation to be achieved. Thus, similarly to Sa-A2M and its “locked” conformation, MagD could possess an “inhibited” conformation where the bait region is not completely accessible. This assumption is supported by the observation that *in vivo*, MagD can be cleaved to a 100 kDa form only under specific conditions, i.e., in the presence of MagB. This suggests that Type II A2Ms have somehow evolved to be more highly regulated than their Type I counterparts in protease-recognition and trapping activities, a fact which is potentially linked to the circumstances in which they are expressed (i.e., during infection or colonization processes <sup>16-18</sup>).

Limited proteolysis experiments performed with MagD indicated that in addition to the bait region, MagD was cleaved between Tyr163 and Asp164, as well as Lys198 and Leu199. These first 199 residues, which are potentially flexible and thus more easily accessible to proteases, correspond to the two initial MG domains of the Type I homologs SaA2M and ECAM, whose structures indicated high flexibility for this region <sup>11,13,14,22</sup>. In ECAM, these domains have

been suggested as being implicated in its anchoring to the inner membrane <sup>19</sup>. MagD, however, does not carry a specific lipobox region or a predicted transmembrane domain; nevertheless, it associates with the inner bacterial membrane, and its presence is necessary for stability of the entire Mag complex in bacterial cells <sup>15</sup>. Here, we show that it is the 589-residue MagB that is specifically responsible for associating MagD, and thus the entire Mag complex, to the inner membrane. In addition, MagB plays a key role in structural stabilization of the complex, as seen in our CD results (Figs. 6 and S3).

MagB is able to associate to binary complexes MagA:MagD and MagF:MagD, comforting the idea that the binding sites for the partner proteins are not overlapping on MagD. Unfortunately, due to solubility issues regarding MagA and MagF, we were not able to test if these isolated molecules could simultaneously bind to the isolated MagB:MagD binary complex. However, the identification of stable interactions between MagA, MagB, MagD and MagF clearly indicate the formation of ternary complexes, with a potential for formation of higher order complexes. Independent of the stoichiometry of the studied complexes, MagB plays a clear, central role. This could also be observed in experiments performed directly on *P. aeruginosa* cells (Fig. 6). We show that MagB is essential for the cleavage of the full-length 165 kDa form to a 100 kDa form, previously suggested as representing a potential direct or indirect activation process <sup>15</sup>. Interestingly, the deletion of *magE* seems to prevent MagD from being processed. It is thus conceivable that MagE could play the role of chaperone in order to facilitate MagD's transport across the inner membrane and/or processing by a signal peptidase. Fig. 8 depicts a model for Mag complex formation that summarizes these results.

The question remains, however, as to why bacteria need to carry a rudimentary immune system with two types of macroglobulins, large, multi-domain molecules. The Type II macroglobulin, characterized in this work, also requires association to additional proteins on the cell membrane for optimal functioning and stabilization (Fig. 8), and generation of such an assembly is potentially energetically costly for the bacterial cell. It is of note that Mag complexes are also highly stable, with different Mag partners remaining associated even when MagD is cleaved to its 100 kDa form (Fig. 8). The widespread presence of these genes in pathogens and colonizers, as well as the link that has been identified with diminished virulence and the Type VI secretion system, indicate that bacterial macroglobulins could play key roles in fitness during infection, antimicrobial warfare, and/or colonization. In *P. aeruginosa*, it is conceivable that the Mag complex participates in defense of the bacterial periplasm during these processes, with MagD playing the role of protease entrapment and other Mag proteins providing stabilization and/or regulation for the complex.

## MATERIALS AND METHODS

### Cloning and protein purification

The *magD* gene was cloned into the pETDuet-1 vector for protein overexpression in *Escherichia coli* BL21 Star in such a way that the final expressed product would carry a hexahistidine sequence at its N-terminus, in lieu of the first 37 amino acids (corresponding to the signal peptide and lipobox). Bacteria were grown in LB medium containing 100 µg/mL of ampicillin at 37°C. At mid-exponential growth (OD<sub>600</sub> 0.6-0.8), 0.5 mM of IPTG were added to induce expression during 4h at 30°C. The cells were harvested by centrifugation at 5,500 rpm for 20 min at 4°C. The cell pellet was resuspended in lysis buffer (50 mM HEPES pH 7.5, 300 mM NaCl and 20 mM imidazole). A commercial mixture of protease inhibitors (SIGMAFAST™, Sigma-Aldrich) was added to the suspension, which was then sonicated, and the cell lysate was centrifuged at 20,000 *g* for 45 min at 4°C. The supernatant was filtered (0.20 µm) and loaded onto a Ni<sup>2+</sup>-NTA column equilibrated in lysis buffer. After extensive washing, the His<sub>6</sub>-tagged protein was eluted with a gradient of imidazole to 300 mM. The eluate was concentrated and injected onto a size exclusion chromatography column (Superdex S200 16/60, GE Healthcare) equilibrated in 25 mM HEPES pH 7.5, 100 mM NaCl. The purification was performed at 4°C on an HPLC ÄKTA Purifier (GE Healthcare). The purified His<sub>6</sub>-tagged protein was concentrated by ultrafiltration (Vivaspin).

The synthetic *magA*, *magB*, *magC*, *magE* and *magF* genes (Genscript) were cloned into pET28a. The sequence corresponding to the N-terminal signal peptides was replaced by a hexahistidine tag sequence. In the case of *magB*, the predicted transmembrane helix was also deleted from the sequence. Co-expression of Mag complexes was carried out by transforming *E. coli* BL21

Star cells with both pETDuet-1-*magD* and pET28a-*mag* plasmids expressing any of the other Mag proteins. Bacteria were grown in LB medium containing 100µg/mL ampicillin and 50µg/mL kanamycin at 37°C. At mid-exponential growth ( $OD_{600}$  0.6-0.8), 0.2mM of IPTG were added to induce expression overnight at 22°C. The cells were harvested by centrifugation at 5,500rpm for 20 min at 4°C and complexes were purified using the same purification protocol as described above for MagD.

### **MagD mutagenesis and TEV reaction**

The MagD bait region sequence ANRSERG (comprising the residues 847-853) was converted into the ENLYFQG sequence, which is recognized by Tobacco Etch Virus (TEV) protease, by site-directed mutagenesis using primers designed with the NEBaseChanger tool (<http://nebasechanger.neb.com/>). Briefly, primers were phosphorylated and used for amplification. The reaction was then incubated with DpnI (Thermo/Fermentas) to eliminate the template and subsequently purified from an agarose gel. The final product was then ligated and transformed into MACH1-T1R competent cells, and clones were confirmed by sequencing. MagD was incubated with a large excess (a molar ratio of 1:2) of TEV protease in a buffer containing 25 mM HEPES pH 7.5, 100 mM NaCl, 1mM DTT and 0.5 mM EDTA overnight at 4°C. Samples were injected onto an analytical size exclusion column (Superdex S200 10/30) and analyzed by 12.5% SDS-PAGE.

## **Dynamic Light Scattering**

Measurements of all sample solutions were conducted using a Protein Solutions DynaPro DLS system (Wyatt). Protein samples ranging from 0.5mg/mL to 1mg/mL were measured in duplicate at 20°C. One measurement corresponded to 20 acquisitions of 5 seconds.

## **Circular Dichroism**

Thermal unfolding was executed monitoring CD signal from 260 to 200 nm from 20°C to 110°C with a temperature rate of 1°C/min. Measurements were performed on a Jasco J-810 Spectropolarimeter with Pelletier control using 1mm Quartz cuvettes (Hellma) with a scan speed of 50 nm/min, 3 accumulations, and a response time of 4 seconds. Protein samples were tested at a concentration of 0.5mg/ml in a buffer consisting of 10 mM HEPES pH7.5 and 40 mM NaCl (protein buffer diluted 2.5 fold in water). Signals are reported as raw ellipticity and all the spectra were corrected for solvent contribution.

## **Analytical ultracentrifugation**

Sedimentation velocity experiments were performed in a Beckman Coulter Optima™ XL-A (Beckman) ultracentrifuge at 20°C. Samples were centrifuged at 35,000 rpm with absorbance monitoring at 280nm. Protein concentrations ranged from 0.25 to 1.0 mg/mL and samples were prepared in 25 mM HEPES pH 7.5 and 100 mM NaCl (density 1.0043 g/mL and viscosity 1.029 cp). Experiments involving apo MagB (shown in Fig. 7) were performed with samples obtained in

buffer containing 25 mM HEPES pH 7.5 and 100 mM NaCl supplemented with 5% glycerol where buffer density and viscosity values employed (but not measured, and perhaps imprecise) corresponded to 1.016 g/mL and 1.156 cp, respectively. The partial specific volume  $v$  was computed as 0.734 ml/g (MagD, MagA:MagD, MagB:MagD, MagF:MagD). Consecutive scans were automatically recorded at regular intervals and analyzed with Sedfit <sup>24</sup> using the continuous size distribution  $c(s)$  analysis method to determine  $s$ - values. Sedfit was also employed to fit a frictional ratio that was combined to the  $s$ -value in order to generate experimental molar masses, and sedimentation coefficients were corrected to  $s_{20w}$ .

### **Small angle X-ray scattering**

SAXS data were recorded at the Brazilian Synchrotron Light Laboratory (LNLS) on the SAXS1 beamline equipped with a Pilatus 300 k detector using a wavelength of 1.54 Å and a 903 mm sample-to-detector distance. The  $s$ -range extended from 0.1 nm<sup>-1</sup> to 2.8 nm<sup>-1</sup>. Protein samples were prepared in concentrations of 2 to 6 mg/mL in 25 mM HEPES pH7.5, 100 mM NaCl, 5% glycerol and 1mM DTT. Measurements were carried out using a 1.5 mm capillary cell, with a sample holder temperature kept constant at 10 °C. Scattering patterns for protein samples and buffers were collected alternatively with exposure times of 100 s. Data reduction included averaging of individual curves with FIT2D <sup>25</sup>. The radius of gyration,  $R_g$ , was estimated using the Guinier approximation  $I(s) = I(0) \exp(-(s^2 R_g^2)/3)$ , valid for small angles ( $sR_g < 1.3$ ), PRIMUS <sup>26</sup>. GNOM <sup>21</sup> was used to obtain the distance distribution function,  $p(r)$ , and maximum intramolecular distance.

The experimental curve of the MagD data was compared with the calculated scattering curves of the structures of the *S. enterica* and *E. coli* A2M (PDB codes 4U48 and 5A42, respectively) using CRY SOL <sup>23</sup>. In real space, the structures were superimposed with the *ab initio* models of MagD with SUPCOMB <sup>27</sup>.

## **Bacterial growth and genetic constructs**

Bacterial culture grown in LB medium overnight were diluted to an optical density measured at 600nm (OD<sub>600</sub>) of 0.15 and incubated further at 37°C to reach OD<sub>600</sub> of 1.5. *Pseudomonas aeruginosa* PA01 wild type and  $\Delta magD$  and  $\Delta operon$  mutants were described previously <sup>15</sup>. All DNA fragments to obtain  $\Delta magA$ ,  $\Delta magB$ ,  $\Delta magC$ ,  $\Delta magE$  and  $\Delta magF$  strains were synthesized and cloned in pUC57 by Genescript. In all cases, the ATG and TGA codons were conserved and upstream and downstream flanking regions were between 400 to 500 nucleotides. All sequences harbor *EcoRI* and *HindIII* restriction sites at their 5' and 3' ends, respectively. Final sizes of the gene to be inactivated were 15 nucleotides ( $\Delta magA$ ), 31 nucleotides ( $\Delta magB$ ), 18 nucleotides ( $\Delta magC$ ), 27 nucleotides ( $\Delta magE$ ) and 12 nucleotides ( $\Delta magF$ ). Fragments were cloned in pEXG2 plasmid <sup>28</sup> using *EcoRI* and *HindIII* restriction sites. pEXG2 vectors were introduced into *P. aeruginosa* PA01 by conjugation using pRK2013 as a helper plasmid and selection on sucrose, as described <sup>29</sup>. For the complementation experiment, a *magB* gene including 19 nucleotides upstream of ATG and the ribosomal binding site and *EcoRI/SacI* restriction sites at the respective 5' and 3' ends was synthesized by Genscript. Then *magB* fragment was cloned into a pminiCTX-1 derivative plasmid pSW196 containing the arabinose-inducible promoter pBAD <sup>30</sup>. Plasmids pSW196 harboring *magB* or *magD* <sup>15</sup> were introduced in *P. aeruginosa* by conjugation <sup>29</sup>. When needed cultures were grown in the presence

of 0.5 % arabinose. All bacterial strains, plasmids and primers used in this work are described in Table 4.

### **Fractionation of *Pseudomonas aeruginosa***

For analysis of total bacterial extracts, overnight cultures were diluted to an OD<sub>600nm</sub> of 0.15 AU and cultivated at 37°C, 300 rpm until they reached an OD<sub>600nm</sub> of 1.5 AU. Cultures were concentrated 10-fold by centrifugation, resuspended directly in SDS-PAGE loading buffer (62 mM Tris-HCl pH 6.8, 2% SDS, 5% β-mercaptoethanol) and incubated 10min at 100°C. Fractionation of bacterial cells was performed using exponential grown cultures (OD<sub>600</sub> of 1). The pellet equivalent to 20.10<sup>9</sup> bacteria was resuspended in 1ml Buffer M (20 mM Tris-HCl pH 8.0, 200 mM MgCl<sub>2</sub> containing Protease Inhibitor Cocktail - PIC, Roche) with 0.5 mg/ml lysozyme and incubated 15 min at 4 °C, under gentle rotation. The periplasmic fraction was obtained after centrifugation at 8,000 g for 15 min at 4°C. After one wash with buffer A the pellet was resuspended in buffer A (20 mM Tris-HCl pH 8.0, 20 mM MgCl<sub>2</sub>, PIC Roche) and disrupted by sonication (VibraCell 75185, 5 min, 5 sec on/5 sec off, 40% power). Unbroken bacteria were eliminated by centrifugation at 8000 g for 15 min. Then supernatant was ultracentrifuged at 200,000 g, 45 min at 4 °C to obtain the cytosolic fraction in the supernatant and the total membrane fraction in the pellet. All samples were diluted in SDS-PAGE denaturing buffer and heated 10 min at 100 °C before loading onto SDS-PAGE.

### **Immunoblot analyses**

Proteins were separated on SDS-PAGE (Criterion 8-16% TGX precast gel Biorad or 10% polyacrylamide gel) and transferred onto a PVDF membrane (Hybond LFP-Polyvinylidene

Difluoride, GE Healthcare) by 0.3 A electrotransfer in 20% ethanol Laemmli buffer (20 mM Tris pH 8.3, 192 mM glycine, 0.1 % SDS). Membranes were blocked with 5% nonfat dry milk in PBS buffer containing 0.1% Tween 20. Dilutions of primary polyclonal antibodies were as follows: anti-MagD <sup>15</sup> 1:40,000, anti-EF-Tu (Hycult Biotech HM6010) 1:20,000, anti-DsbA (a kind gift from R. Voulhoux, Marseille, France) 1:2,000 and anti-TagQ <sup>31</sup> 1:10,000 in PBS-Tween buffer. Incubations were performed overnight at 4°C. Secondary antibodies (anti rabbit-HRP, anti mouse-HRP, Sigma) were incubated for 1 hour at room temperature. Detection was performed using the Luminata Classico HRP-Substrate (Millipore).

### **Mass spectrometry and N-terminal sequencing**

Experiments were performed using the platforms of the Partnership for Structural Biology. For N-terminal sequencing, samples were transferred from a SDS-PAGE gel to a PVDF membrane. After staining, bands of interest were excised and subsequently injected into a Procise 492 sequencer (Applied Biosystems), and analyzed by Edman degradation. Protein samples for mass spectrometry were prepared in 25 mM HEPES pH 7.5, 300 mM NaCl. 8 uL of samples a concentration of 10 uM were injected into an ESI Q-TOF mass spectrometer from Waters (Ultima).

## REFERENCES

- 1 Rehman, A. A., Ahsan, H. & Kahn, F. H. Alpha-2-macroglobulin: a physiological guardian. *Cell. Physiol.* **228**, 1665-1675. (2012).
- 2 Armstrong, P. B. The contribution of proteinase inhibitors to immune defense. *Trends Immunol.* **22**, 47-52. (2001).
- 3 Armstrong, P. B. Proteases and protease inhibitors: a balance of activities in host-pathogen interaction. *Immunobiology* **211**, 263-281. (2006).
- 4 Meyer, C., Hinrichs, W. & Hahn, U. Human  $\alpha$ 2-macroglobulin- another variation on the Venus Flytrap. *Chemie Int. Ed.* **51**, 5045-5047. (2012).
- 5 Marrero, A. *et al.* The crystal structure of human  $\alpha$ 2-macroglobulin reveals a unique molecular cage. *Angew. Chem. Int. Ed. Engl.* **51**, 3340-3344. (2012).
- 6 Janssen, B. J. *et al.* Structures of complement component C3 provide insights into the function and evolution of immunity. *Nature* **437**, 505-511. (2005).
- 7 Budd, A., Blandin, S., Levashina, E. & Gibson, T. J. Bacterial  $\alpha$ 2-macroglobulins: colonization factors acquired by horizontal gene transfer from the metazoan genome? *Genome Biol.* **5**, R38 (2004).
- 8 Schiffer, G. & Holtje, J. V. Cloning and characterization of PBP 1C, a third member of the multimodular class A penicillin-binding proteins of escherichia coli. *J.Biol.Chem.* **274**, 32031-32039 (1999).
- 9 Höltje, J. V. Growth of the stress-bearing and shape-maintaining murein sacculus of *Escherichia coli*. *Microbiol. Mol. Biol. Rev.* **62**, 181-203 (1998).
- 10 Mattei, P.-J., Neves, D. & Dessen, A. Bridging cell wall biosynthesis and bacterial morphogenesis. *Curr. Opin. Struct. Biol.* **20**, 749-766. (2010).
- 11 Wong, S. G. & Dessen, A. Structure of a bacterial  $\alpha$ 2-macroglobulin reveals mimicry of eukaryotic innate immunity. *Nature Comm.* **5**, 4917. (2014).
- 12 Janssen, B. J. C., Christodoulidou, A., McCarthy, A., Lambris, J. D. & Gros, P. Structure of C3b reveals conformational changes that underlie complement activity. *Nature* **444**, 213-216. (2006).
- 13 Garcia-Ferrer, I. *et al.* Structural and functional insights into *Escherichia coli*  $\alpha$ 2-macroglobulin endopeptidase snap-trap inhibition. *Proc. Natl. Acad. Sci. USA* **112**, 8290-8295. (2015).
- 14 Fyfe, C. D. *et al.* Structure of the protease-cleaved *Escherichia coli*  $\alpha$ -2-macroglobulin reveals a putative mechanism of conformational activation for protease entrapment. *Acta Cryst. D* **D71**, 1478-1486. (2015).

- 15 Robert-Genthon, M. *et al.* Unique features of a *Pseudomonas aeruginosa*  $\alpha$ 2-macroglobulin homolog. *MBio* **4**, e00309-00313. (2013).
- 16 Brencic, A. & Lory, S. Determination of the regulon and identification of novel mRNA targets of *Pseudomonas aeruginosa* RsmA. *Mol. Microbiol.* **72**, 612-632. (2009).
- 17 Marden, J. N. *et al.* An unusual CsrA family member operates in series with RsmA to amplify posttranscriptional responses in *Pseudomonas aeruginosa*. *Proc. Natl. Acad. Sci. USA* **110**, 15055-15060. (2013).
- 18 Potvin, E. *et al.* In vivo functional genomics of *Pseudomonas aeruginosa* for high-throughput screening of new virulence factors and antibacterial targets. *Environ. Microbiol.* **5**, 1294-1308. (2003).
- 19 Doan, N. & Gettins, G. W. Alpha-macroglobulins are present in some Gram-negative bacteria: characterization of the alpha2-macroglobulin from *Escherichia coli*. *J. Biol. Chem.* **283**, 28747-28756. (2008).
- 20 Brown, P. H. & Schuck, P. A new adaptive grid-size algorithm for the simulation of sedimentation velocity profiles in analytical ultracentrifugation. *Comput. Phys. Commun.* **178**, 105-120. (2008).
- 21 Svergun, D. I. Restoring low resolution structure of biological macromolecules from solution scattering using simulated annealing. *Biophys J* **76**, 2879-2886 (1999).
- 22 Neves, D. *et al.* Conformational states of a bacterial  $\alpha$ 2-macroglobulin resemble those of human complement C3. *PLoS One* **7**, e35384. (2012).
- 23 Svergun, D., Barberato, C. & Koch, M. H. J. CRY SOL - A program to evaluate X-ray solution scattering of biological macromolecules from atomic coordinates. *J. Appl. Cryst.* **28**, 768-773. (1995).
- 24 Schuck, P. Size distribution analysis of macromolecules by sedimentation velocity ultracentrifugation and Lamm equation modeling. *Biophys. J.* **78**, 1606-1619. (2000).
- 25 Hammersley, A. P. FIT2D: An introduction and overview. *ESRF Internal Report ESRF97HA02T* (1997).
- 26 Konarev, P. V., Volkov, V. V., Sokolova, A. V., Koch, M. H. J. & Svergun, D. I. PRIMUS: a Windows PC-based system for small-angle scattering data analysis. *J. Appl. Cryst.* **36**, 1277-1282. (2003).
- 27 Kosin, M. & Svergun, D. Automated matching of high- and low-resolution structural models *J. Appl. Cryst.* **34**, 33-41. (2001).
- 28 Riesch, A., Vallet-Gely, I., Dove, S. L. & Mekalanos, J. J. ExsE, a secreted regulator of type III secretion genes in *Pseudomonas aeruginosa*. *Proc. Natl. Acad. Sci. USA* **102**, 8006-8011. (2005).
- 29 Hmelo, L. R. *et al.* Precision-engineering the *Pseudomonas aeruginosa* genome with two-step allelic exchange. *Nat. Protoc.* **10**, 1820-1841. (2015).

- 30 Baynham, P. J., Ramsey, D. M., Gvozdyev, B. V., Cordonnier, E. M. & Wozniak, D. J. The *Pseudomonas aeruginosa* ribbon-helix-helix DNA-binding protein AlgZ (AmrZ) controls twitching motility and biogenesis of type IV pili. *J. Bacteriol.* **188**, 132-140. (2006).
- 31 Casabona, M. G. *et al.* An ABC transporter and an outer membrane lipoprotein participate in posttranslational activation of type VI secretion in *Pseudomonas aeruginosa*. *Environ. Microbiol.* **15**, 471-486. (2013).

## **ACKNOWLEDGEMENTS**

This work was supported by the Laboratoire International Associé BACWALL and by grants 11/52067-6 and 2013/01962-0 from FAPESP (Fundação de Amparo à Pesquisa do Estado de São Paulo). This work used the platforms of the Grenoble Instruct-ERIC Center (ISBG: UMS 3518 CNRS-CEA-UGA-EMBL) with support from FRISBI (ANR-10-INSB-05-02) and GRAL (ANR-10-LABX-49-01) within the Grenoble Partnership for Structural Biology (PSB). We thank the Biosciences National Laboratory (LNBio) and the Synchrotron Light Laboratory (LNLS) at the Brazilian Center for Research in Energy and Materials (CNPEM), for access to all facilities (LPP, LEC and the D01B-SAXS1 beamline). We especially thank Juliana Fattori for technical assistance at LEC and Florian Meneau for access to and assistance with SAXS data collection. Figure 5 was generated by using the PyMOL Molecular Graphics System, Version 1.8 Schrödinger, LLC.

## **AUTHOR CONTRIBUTIONS**

SZ carried out all purifications, and performed SAXS, AUC, and CD experiments. MRG and VJ performed microbiology experiments on *mag* mutants. DMT generated Mag expression constructs, and MN participated in experiments with MagD-TB. CB and CE analyzed SAXS and AUC data. IA and AD conceived the project and analyzed results. AD and SZ wrote the manuscript.

## **ADDITIONAL INFORMATION**

The authors declare no competing financial interests.

## FIGURE LEGENDS

### Figure 1: Schematic diagram of MagD, its partners, and its genomic environment

(A) Scheme of MagD (Type II) compared to Sa-A2M from *Salmonella enterica* (Type I). Both macroglobulins carry bait regions, but only SaA2M displays the conserved CXEQ motif required for the covalent bonding of proteases. (B) Genetic organization of *magD* within the six-gene Mag operon: *magA*, *magB*, *magC*, *magD*, *magE* and *magF*. (C) Schematic of all Mag proteins encoded by the *mag* operon. SS, signal sequence; MG, macroglobulin; TMH, predicted transmembrane helix; TED, thioester domain

### Figure 2: MagD displays macroglobulin-like protease trapping activity

(A) Incubation of MagD-TB with TEV followed by gel filtration on a Superdex 200 10/30 column leads to the appearance of a peak that contains four bands, as shown on the gel (B): uncleaved MagD-TB, two forms of MagD-TB cleaved at the bait region, and TEV. Positions of molecular mass markers are indicated on the left. The gel includes only lanes of interest for analysis of the result. (C) Schematic of the reaction that occurs upon MagD-TB recognition by TEV.

### Figure 3: Sedimentation velocity of MagD and Mag binary complexes

(A) (Upper panel) Fitting of experimental sedimentation profiles of MagD using Sedfit and its residual (lower panel) (B) Results of the  $c(s)$  analysis for MagD (apoform), MagA:MagD (C), MagB:MagD (D), MagF:MagD (E) complexes. In (B), since the proportion of dimer does not increase with concentration, it probably does not result from a thermodynamic equilibrium. Samples were studied at 0.25, 0.5 and 1mg/ml, at 20°C with a rotor velocity of 35,000 rpm and an absorbance monitoring at 280 nm.

#### **Figure 4: Small angle X-Ray Scattering of MagD and Mag binary complexes**

(A) Experimental data: scattering curves are presented in the form  $\log I$  versus  $s$  ( $\text{nm}^{-1}$ ) where  $I$  is the measured scattered intensity and  $s$  is the scattering angle. Scattering data for MagD in native form (blue), in complex with MagA (green), MagB (orange) and MagF (magenta) were recorded at concentrations of 2 mg/mL for MagA:MagD and 6 mg/mL for the others. The inset presents the Guinier plot. Curves were normalized to have a  $I(0) = 1$ . (B) Pair-distance distribution function  $p(r)$  of the same data. (C) Measured scattering curve of MagD (solid blue) compared to the calculated scattering curves of *S. enterica* (dotted green, PDB 4U48,  $\text{Chi}^2=20.5$ ) and *E. coli* (dashed red, PDB 5A42) A2M, calculated with Crysol.

#### **Figure 5: Thermal unfolding of MagD and Mag binary complexes**

CD spectra were recorded from 260 to 200 nm using a temperature ramp of 20°C to 110°C and using an increment rate of 1°C/min. Protein samples were tested at 0.5 mg/ml, in a buffer containing 10 mM HEPES pH7.5 and 40 mM NaCl. For clarity, only spectra recorded at 20, 30, 40, 50, 60, 70, 80, 90, 95, 100 and 110°C are presented.

#### **Figure 6: MagD stability and cleavage are affected in mutants lacking MagB and MagE**

(A) Crude extracts of *P. aeruginosa* PAO1 (WT) or knock-out strains lacking indicated proteins were run on SDS-PAGE and immune-developed with polyclonal anti-MagD antibodies. The  $\Delta\text{op}$  mutant<sup>15</sup> that lacks the entire *mag* operon was used as control. In the wild-type background MagD appears as 165 kDa native and 100 kDa cleaved forms. The 100 kDa form is absent in  $\Delta\text{magB}$  and  $\Delta\text{magC}$  backgrounds. An additional higher molecular weight form observed in  $\Delta\text{magE}$  could correspond to unprocessed MagD still containing the signal peptide (\*). (B) Crude extracts

of indicated strains lacking MagB ( $\Delta magB$ ) or expressing *magB* or *magD* in trans were analyzed as in (A). (C) Bacteria were further fractionated into membranes and periplasm showing that MagB governs macroglobulin membrane localization and cleavage to the 100 kDa form. Note the presence of 165 kDa form of MagD exclusively in the periplasm of the *magB* mutant. This form is subject to rapid degradation as visualized by products of smaller sizes in the  $\Delta magB::magD$  strain. In the  $\Delta magB::magB$  strain, membrane localization was restored and MagD appears as 165 kDa and 100 kDa forms, similarly to wild-type. EFTu, DsbA and TagQ antibodies were used as loading controls for whole bacterial extracts, periplasm and membrane samples, respectively. Gels have had lanes selected/cropped for clarity.

### **Figure 7: Sedimentation velocity of ternary Mag complexes**

(A) (Upper panel) Fit of experimental curves of MagD + MagB sedimentation using Sedfit and its residual (lower panel). Results of the  $c(s)$  analysis for (B) MagD + MagB, (C) MagA:MagD + MagB, (D) MagF:MagD + MagB. Samples were studied at 0.5 mg/ml, at 20°C with a rotor velocity of 35,000 rpm and monitoring the absorbance at 280 nm. The buffer included 5% glycerol. Note that addition of MagB to the MagA:MagD sample causes disappearance of the shoulder at approximately 7 S, suggesting stabilization of a unique ternary form.

**Figure 8: Model of Mag complex formation on the bacterial periplasm.** MagB plays a key role in the stabilization of the complex; MagD can bind to MagA and MagF in both of its forms (165 and 100 kDa). MagE is potentially involved in cleavage of the signal peptide of MagD. IM, inner membrane; OM, outer membrane.

**Table 1: Mass spectrometry analyses of MagD/TEV incubation experiment**

Band (Fig. 2b)	Expected mass (Da)	Observed mass (Da)	Mass deviation (Da)	Identification
1	165,232.78	165,241.69	8.2	MagD (2-1495), full-length
2	91,231.90	91,234.90	2.9	MagD (2-821) N-terminal fragment
3	74,018.90	74,020.88	1.9	MagD (882- 1495) C-terminal fragment
4	28,556.42	28,556.55	0.24	TEV protease

**Table 2: Mass of Mag complexes obtained from analytical ultracentrifugation**

Sample	Theoretical mass (approx. kDa)	$s_{20,w}$ value	Fitted mass (kDa)
MagD	165	7.8 S +/- 0.5 S 10.3 S +/- 0.6 S	160 +/- 18 246 +/- 28 (a)
MagA:MagD	192	8.7 S +/- 0.6 S	192 +/- 16
MagB:MagD	225	8.4 S +/- 0.3 S	212 +/- 3
MagF:MagD	191	8.3 S +/- 0.3 S	189 +/- 18

(a) fitted globally

**Table 3: Data collection and structural parameters of the Mag complexes obtained using SAXS. Rh and Rg values obtained from SEC and DLS were also included for comparative purposes.**

	MagD	MagA:MagD	MagB:MagD	MagF:MagD
<b>Data collection parameters</b>				
Instrument	LNLS-SAXS1 beamline			
Beam geometry	Pinhole geometry, Pilatus 300k			
Wavelength (Å)	1.544			
s range (nm)	0.068 – 2.8			
Exposure time (sec)	100			
Temperature (°C)	10			
Concentration range (mg/mL)	2 - 6			
<b>Structural parameters <sup>1</sup></b>				
$R_g$ (nm) (from Guinier)	5.0 ± 0.1	5.8 ± 0.2	5.6 ± 0.1	5.3 ± 0.3
$R_g$ (nm) (from $P(r)$ )	5.2	5.9	5.9	5.7
$I(0)$ (cm <sup>-1</sup> )(from Guinier)	0.0018 ± 3.8 10 <sup>-6</sup>	0.00059 ± 3.1 10 <sup>-6</sup>	0.0019 ± 5.4 10 <sup>-6</sup>	0.0022 ± 6.4 10 <sup>-6</sup>
$D_{max}$ (nm)	17.6	20.1	19.8	19.3
Rh from SEC (nm)	5.1	5.3	5.2	5.2
Rh from DLS (nm); polydispersity (%)	5.1 (7.4)	5.3 (10.0)	5.2 (9.7)	5.2 (9.2)
<b>Software employed</b>				
Primary data reduction	FIT2d			
Data processing	PRIMUS/GNOM			

<sup>1</sup> Reported for the 6 mg/mL measurements, except for MagA:MagD, at 2 mg/mL

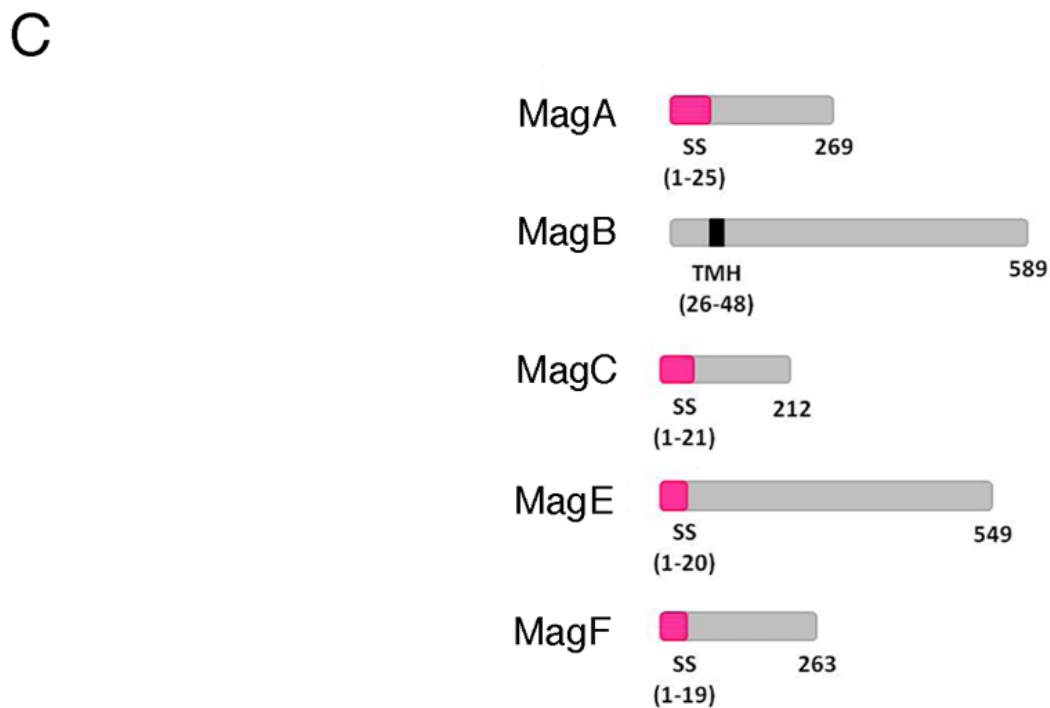
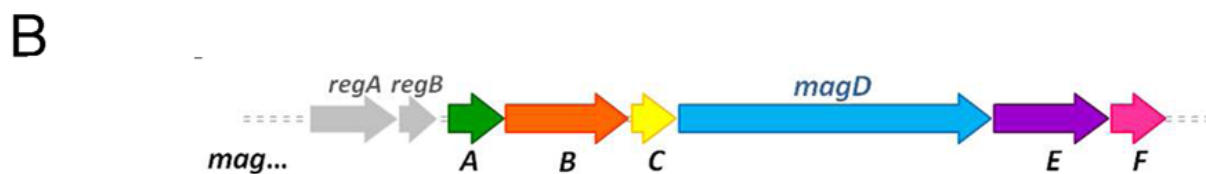
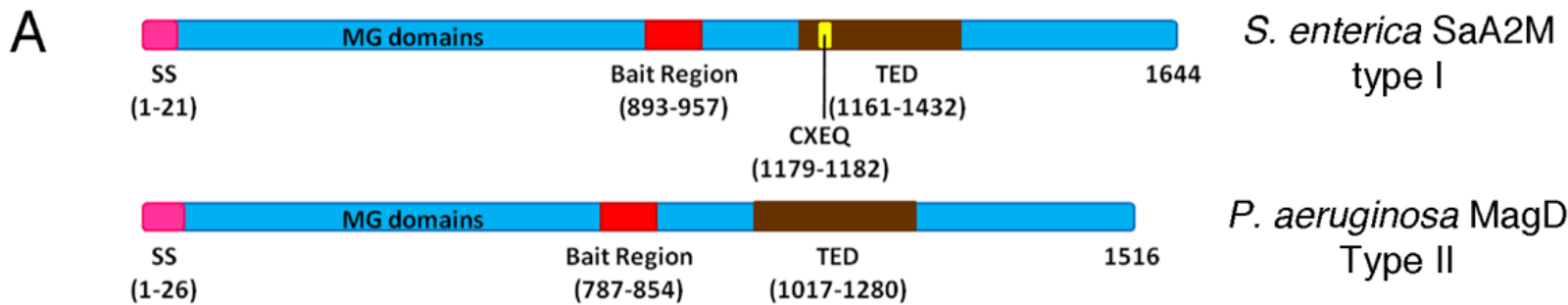
$D_{max}$  (nm) (+/-0.5 nm)

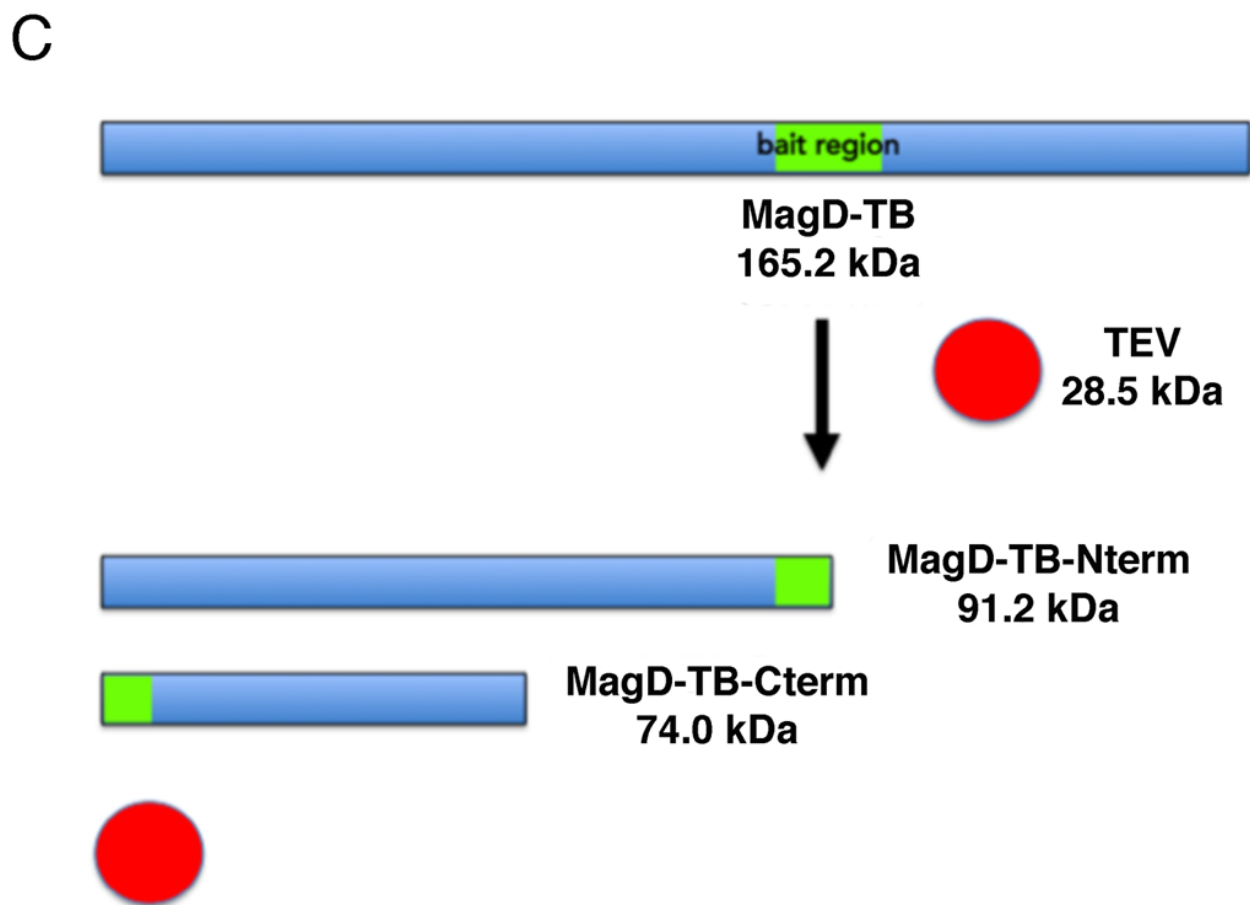
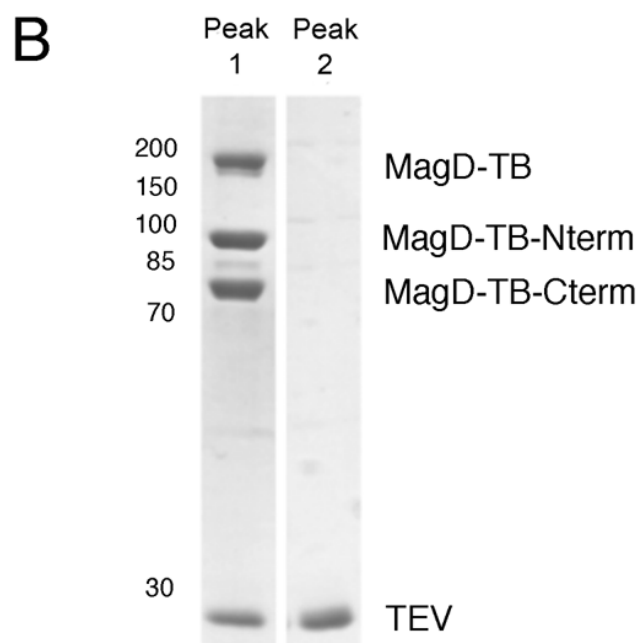
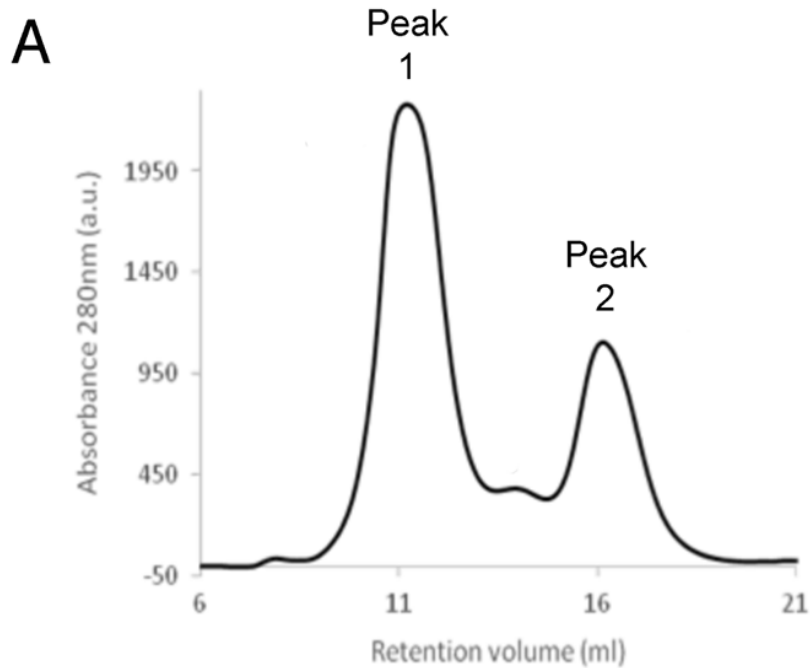
Rh from SEC (nm) (+/- 0.5 nm)

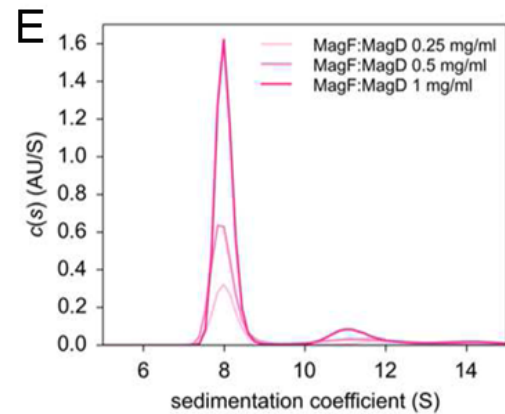
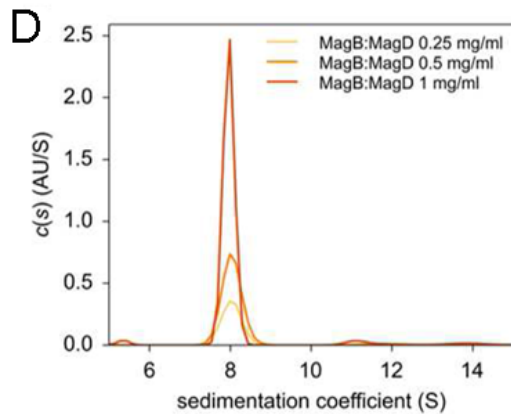
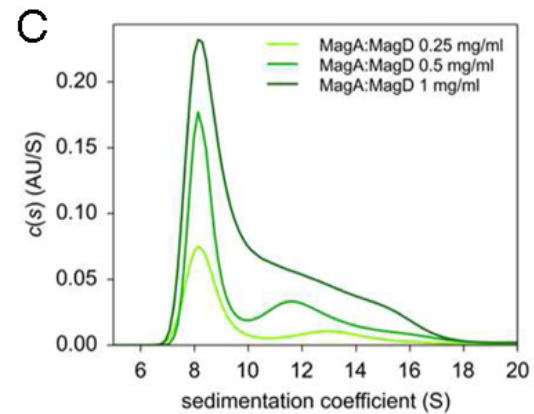
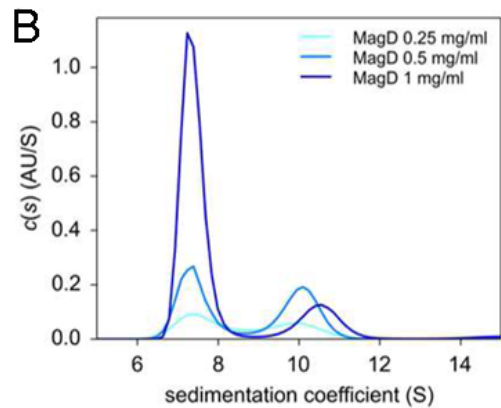
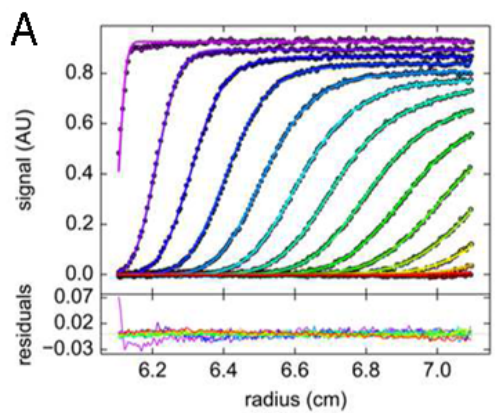
Rh from DLS (nm) (+/- 1 nm)

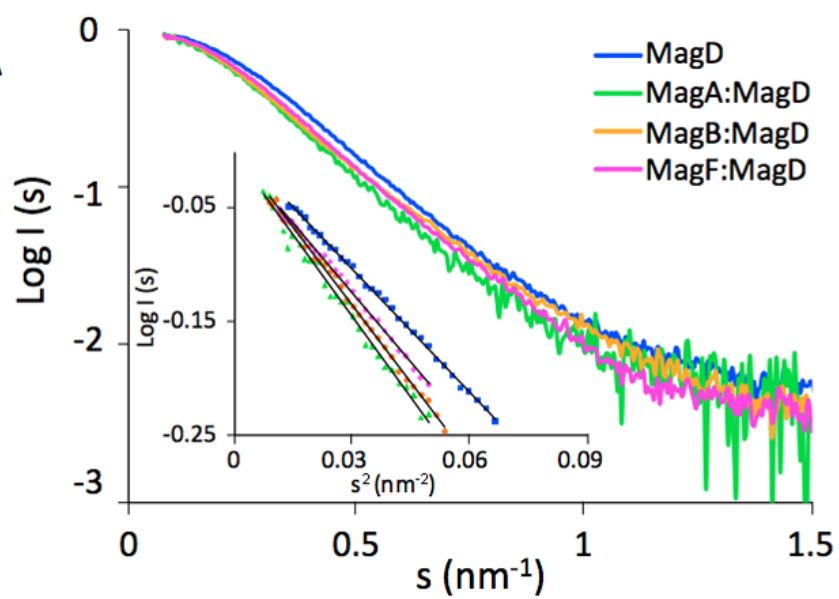
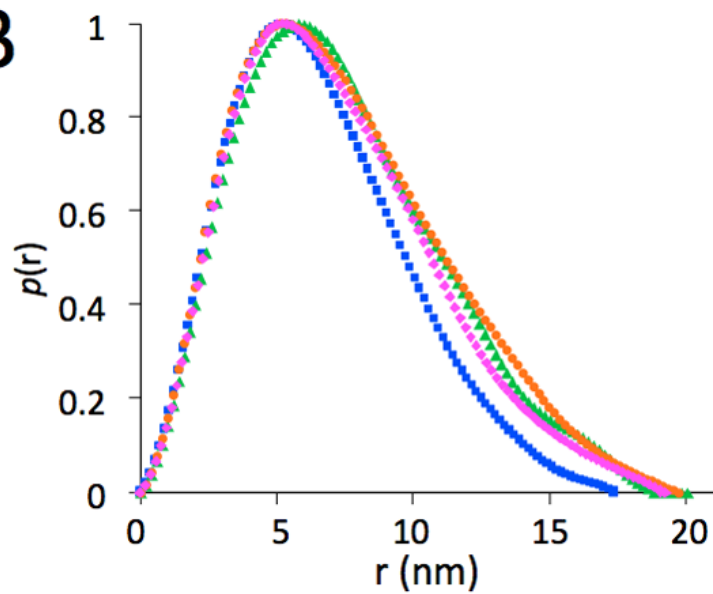
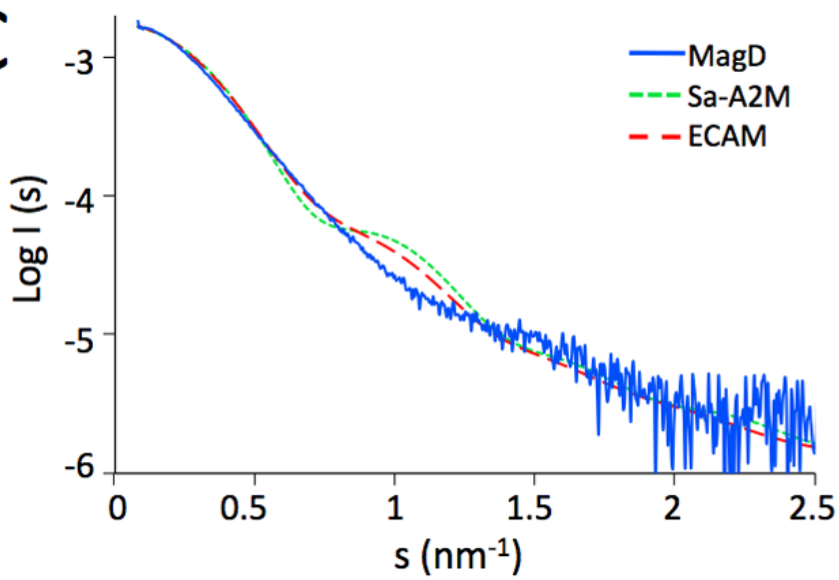
**Table 4: Strains, vectors and oligonucleotides used in this work**

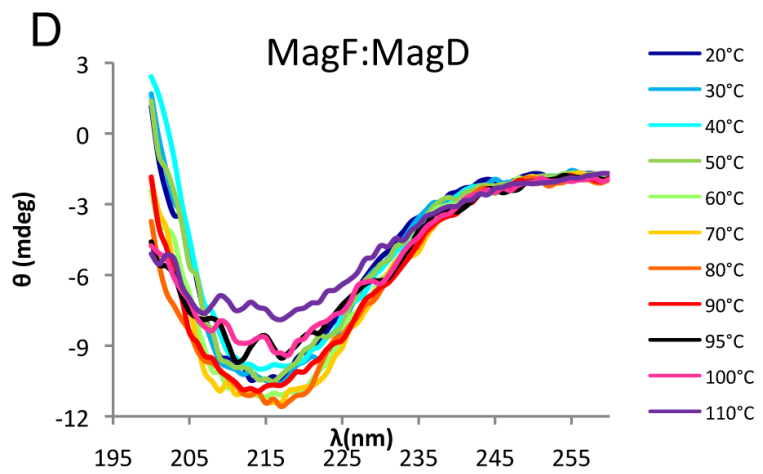
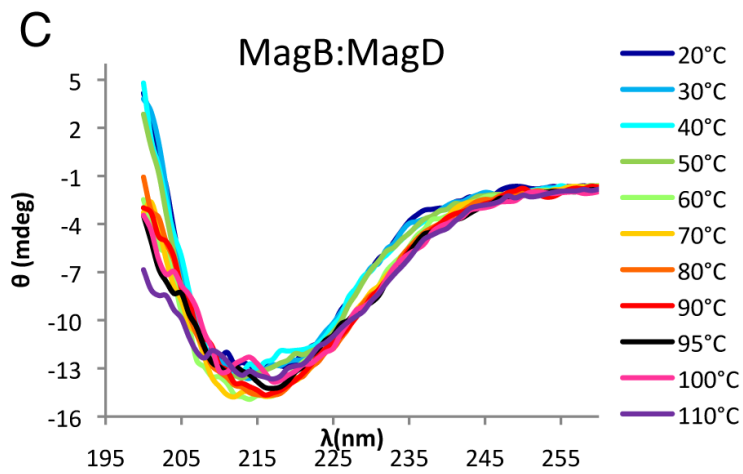
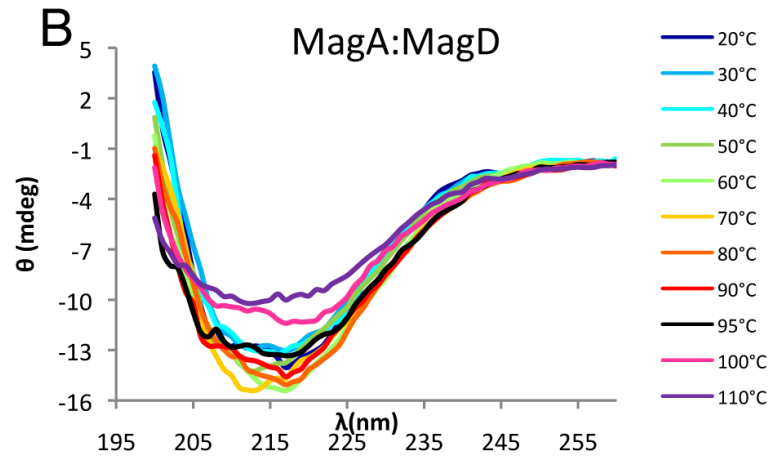
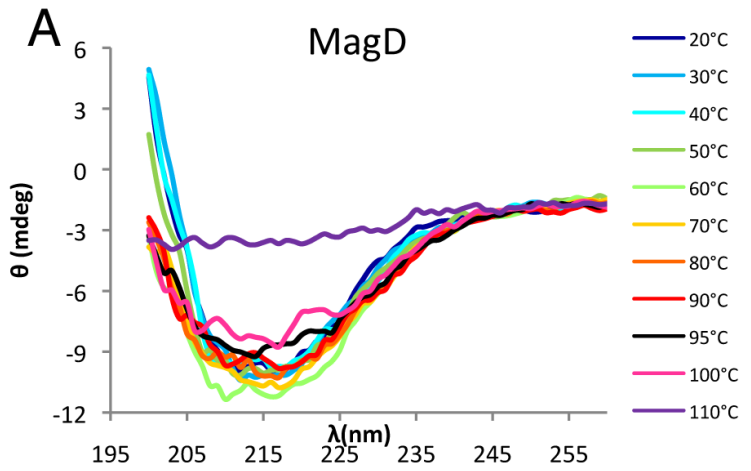
STRAINS	CHARACTERISTICS	ORIGIN OR REFERENCE
PA01	Sequenced laboratory strain	J.Mougous, USA
PA01 $\Delta$ <i>magA</i>	Internal deletion in PA4492 ( <i>magA</i> ) in PA01	This work
PA01 $\Delta$ <i>magB</i>	Internal deletion in PA4491 ( <i>magB</i> ) in PA01	This work
PA01 $\Delta$ <i>magC</i>	Internal deletion in PA4490 ( <i>magC</i> ) in PA01	This work
PA01 $\Delta$ <i>magD</i>	Internal deletion in PA4489 ( <i>magD</i> ) in PA01	Robert-Genthon et al.,2013
PA01 $\Delta$ <i>magE</i>	Internal deletion in PA4488 ( <i>magE</i> ) in PA01	This work
PA01 $\Delta$ <i>magF</i>	Internal deletion in PA4487 ( <i>magF</i> ) in PA01	This work
PA01 pEX100T_ $\Delta$ Op	Internal deletion of whole operon mag PA4492-PA4487	Robert-Genthon et al.,2013
E.coli Top10	Cloning strain	Invitrogen
E.coli pRK2013	E.coli with plasmid Helper for conjugaison	Addgene
PLASMIDS		
pUC57	Cloning vector, Amp <sup>R</sup>	Genescript
pCCI	Cloning vector, Cm <sup>R</sup>	Genescript
pEXG2	Plasmid for allelic exchange, <i>sacB</i> , Gm <sup>R</sup>	Rietsch et al, 2005
pEXG2- $\Delta$ <i>magA</i>	Plasmid containing <i>magA</i> deletion	This work
pEXG2- $\Delta$ <i>magB</i>	Plasmid containing <i>magB</i> deletion	This work
pEXG2- $\Delta$ <i>magC</i>	Plasmid containing <i>magC</i> deletion	This work
pEXG2- $\Delta$ <i>magE</i>	Plasmid containing <i>magE</i> deletion	This work
pEXG2- $\Delta$ <i>magF</i>	Plasmid containing <i>magF</i> deletion	This work
pEX100T	Mini-CTX1 based plasmid for allelic exchange, pBAD, Tc <sup>R</sup>	Baynham et al., 2006
pSW196- <i>magB</i> .RBS	Plasmid for <i>magB</i> .RBS (PA4491) gene complementation	This study
pSW196- <i>magD</i>	Plasmid for <i>magD</i> (PA4489) gene complementation	Robert-Genthon et al.,2013
PRIMERS	SEQUENCE 5'-3'	CHARACTERISTIC
F. <i>DmagA</i>	5' GTGGATTCGCACATTCGCGC	Verification <i>magA</i> deletion
R. <i>DmagA</i>	5' ACCTCGAGGATTCCTTCGGC	Verification <i>magA</i> deletion
F. <i>DmagB</i>	5' ACAGGACGTGATCACCGCGC	Verification <i>magB</i> deletion
R. <i>DmagB</i>	5' CGATGCGCACGAACCAGGC	Verification <i>magB</i> deletion
F. <i>DmagC</i>	5' GACACCCTCGACAAACGC	Verification <i>magC</i> deletion
R. <i>DmagC</i>	5' GCTTGAGGAACTCCAGCG	Verification <i>magC</i> deletion
F. <i>DmagE</i>	5' GCGTTCGAGTTCAAGGTCG	Verification <i>magE</i> deletion
R. <i>DmagE</i>	5' CCACCTTCAGTGGCATGC	Verification <i>magE</i> deletion
F. <i>DmagF</i>	5' CTGTATTCCTACAGGAACGCC	Verification <i>magF</i> deletion
R. <i>DmagF</i>	5' CGGTGCGCTGAACAACGGC	Verification <i>magF</i> deletion

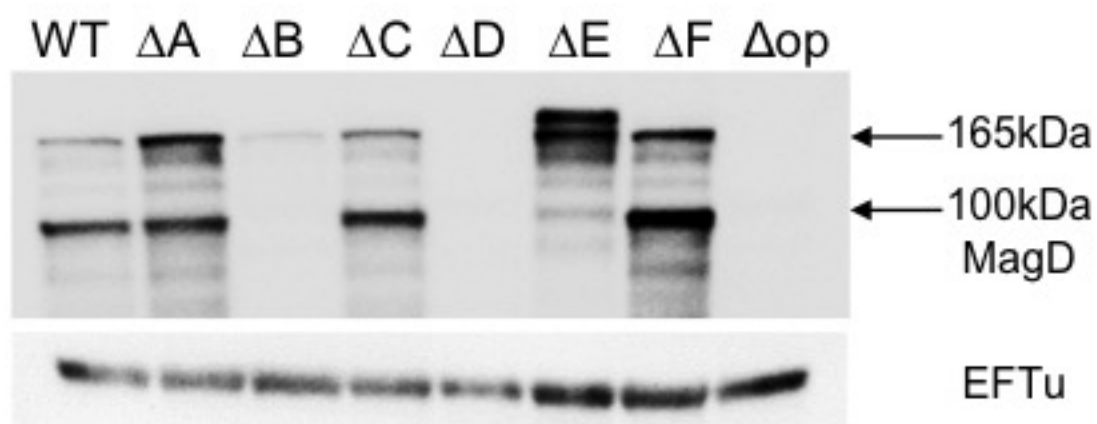
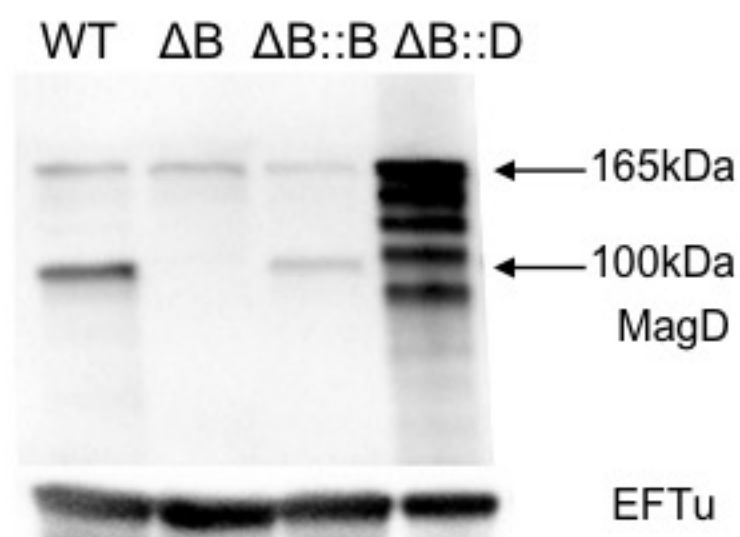






**A****B****C**



**A****B****C**